



University
of Glasgow

Pajek, Daniela (2013) Identifying chemokine receptors as plausible therapeutic targets in viral encephalitis. PhD

<http://theses.gla.ac.uk/4764/>

Copyright and moral rights for this thesis are retained by the author

A copy can be downloaded for personal non-commercial research or study, without prior permission or charge

This thesis cannot be reproduced or quoted extensively from without first obtaining permission in writing from the Author

The content must not be changed in any way or sold commercially in any format or medium without the formal permission of the Author

When referring to this work, full bibliographic details including the author, title, awarding institution and date of the thesis must be given.

Identifying chemokine receptors as plausible therapeutic targets in viral encephalitis

Daniela Pajek

(B.Sc, M.Res)

Submitted in fulfilment of the requirements for the degree
of Doctor of Philosophy

College of Medicine, Veterinary and Life Sciences

Institute of Infection, Immunity and Inflammation

University of Glasgow

September 2013

Abstract

Background: There are a large number of viruses spread by mosquitoes, many of which cause debilitating, often fatal, neurological disease such as acute encephalitis. In this study we have used two different neurotropic viruses: Semliki Forest virus (SFV), and West Nile virus (WNV), both of which can cause severe panencephalitis in the mouse. The influx of leukocytes into the infected tissues is mediated by chemokines and is believed to be important for virus clearance. To date, we have only limited insights into the precise nature of chemokine involvement, and an improved understanding of these important axes provides a new target for the development of novel therapies. **Hypothesis:** Based on previous studies investigating the role of chemokines during neuroinflammation it was hypothesised that chemokines and other cytokines are highly upregulated during viral encephalitis, and the blockade of selected chemokine receptors would lead to altered disease outcome. It was also hypothesised that chemokine receptors would present plausible targets for the treatment of viral encephalitis. **Results:** To test these hypotheses, the chemokine expression pattern and the kinetics of chemokine mediated leukocyte recruitment during viral encephalitis were analysed in unprecedented detail by TaqMan low density array, and flow cytometry, respectively, and key chemokine receptor were identified as therapeutic targets. Both SFV and WNV exhibited a similar pattern of chemokine upregulation, although WNV induced significantly higher fold expression. The key chemokines upregulated were CCL2, 3, 5, 7, CXCL9 and CXCL10. The upregulation of chemokines coincided with leukocyte influx into the CNS. After identifying the key chemokines upregulated during viral encephalitis, next a selected panel of chemokine receptor antagonists was utilized to evaluate the hierarchy and relative importance of distinct chemokine receptors for CNS leukocyte influx, viral clearance, neuropathogenesis and host survival. We identified the CXCR3 axis as being the key instigator of CNS inflammation in response to alphavirus infection, placing it at the top of a hierarchal cascade that is followed by CCR2 and CCR5. Critically, inhibition of both CXCR3 and CCR2 simultaneously, significantly improved host survival to otherwise lethal encephalitis. **Conclusion:** These data suggest that chemokine receptors represent plausible therapeutic targets for viral encephalitis.

Table of Contents

ABSTRACT	2
TABLE OF CONTENTS	3
LIST OF TABLES	7
LIST OF FIGURES	8
ACKNOWLEDGEMENTS	11
AUTHOR'S DECLARATION	13
LIST OF ABBREVIATIONS	14
CHAPTER 1	18
1.1 INNATE AND ADAPTIVE IMMUNITY	19
1.1.1 <i>Innate immunity</i>	19
1.1.1.1 Pattern-recognition receptors (PRRs)	20
1.1.1.2 Cells of the innate immune system.....	20
1.1.2 <i>Adaptive Immunity</i>	25
1.1.2.1 Cells of the adaptive immune system	26
1.1.3 <i>Cytokines during innate and adaptive immunity</i>	28
1.1.3.1 Interferon	28
1.1.3.2 Tumour necrosis factor (TNF).....	30
1.2 IMMUNE RESPONSES IN THE BRAIN	31
1.2.1 <i>Structure of the central nervous system</i>	32
1.2.2 <i>Cells of the CNS</i>	32
1.2.2.1 Neurons.....	33
1.2.2.2 Glia	33
1.2.3 <i>The blood-brain barrier and blood-cerebrospinal fluid barrier</i>	34
1.2.3.1 Blood-brain barrier.....	35
1.2.3.2 Blood-CSF barrier	36
1.2.4 <i>Immunosurveillance in the healthy brain</i>	37
1.2.5 <i>Immune responses in the virally infected brain</i>	38
1.3 CHEMOKINES AND THEIR RECEPTORS.....	41
1.3.1 <i>Nomenclature and classification of chemokines</i>	41
1.3.1.1 Homeostatic and inflammatory chemokines	45
1.3.2 <i>Chemokine receptors</i>	47
1.3.2.1 Chemokine receptor structure and classification	48
1.3.3 <i>Functions of chemokines and their receptors</i>	49
1.3.4 <i>The role of chemokine receptors in disease</i>	51
1.3.4.1 Human immunodeficiency virus (HIV).....	51
1.3.4.2 Multiple Sclerosis/EAE	53
1.3.5 <i>Methods of targeting the chemokine system</i>	53
1.3.5.1 Blockade of CCR2	54
1.3.5.2 Blockade of CCR5	55
1.3.5.3 Blockade of CXCR3	57
1.3.6 <i>The expression of chemokines in the CNS</i>	57
1.3.6.1 Constitutive chemokine expression in the healthy brain	58
1.3.6.2 Chemokine expression in the CNS during inflammation.....	58
1.4 VIRAL ENCEPHALITIS.....	61
1.4.1 <i>Alphaviruses</i>	63
1.4.1.1 Structure and replication of Alphaviruses.....	64
1.4.2 <i>Semliki Forest virus</i>	66
1.4.2.1 SFV strains	66
1.4.2.2 Restricted replication in the CNS	67
1.4.2.3 Immune responses to SFV and viral clearance.....	68
1.4.2.4 Demyelination	69
1.4.3 <i>West Nile virus (WNV)</i>	70
1.4.3.1 WNV replication	70

1.4.3.2	WNV infection of the CNS	71
1.4.3.3	Immune responses to WNV in the periphery and the CNS	72
1.5	THE ROLE OF CHEMOKINES IN THE PATHOGENESIS OF NEUROTROPIC VIRUSES	74
1.5.1	<i>Chemokine-mediated immune responses during WNV infection</i>	75
1.5.2	<i>Lymphocytic choriomeningitis virus infection</i>	77
1.5.3	<i>Mouse hepatitis virus infection</i>	79
1.6	THESIS AIMS	83
CHAPTER 2	85
2.1	GENERAL REAGENTS AND BUFFERS.....	86
2.2	MICE.....	87
2.3	VIRUSES.....	88
2.4	ANTIBODIES FOR FLOW CYTOMETRY	88
2.5	ANTIBODIES FOR IMMUNOHISTOCHEMISTRY (IHC)	90
2.6	PRIMERS FOR QUANTITATIVE (Q)PCR	92
2.7	INFECTION OF MICE WITH VIRUSES	92
2.8	TISSUE PROCESSING, EMBEDDING AND SECTIONING	96
2.8.1	<i>Tissue processing</i>	96
2.8.2	<i>Tissue embedding</i>	96
2.8.3	<i>Tissue sectioning</i>	97
2.9	HAEMATOXYLIN AND EOSIN STAINING	97
2.10	IMMUNOHISTOCHEMISTRY.....	98
2.10.1	<i>Indirect immunostaining method</i>	98
2.10.2	<i>Immunofluorescence double staining</i>	100
2.10.3	<i>Signal amplification using avidin/biotin complexes</i>	100
2.10.4	<i>Signal amplification using chain polymer-conjugated technology</i>	101
2.11	ISOLATION OF MONONUCLEAR CELLS FROM THE BRAIN.....	102
2.11.1	<i>Isolation of mononuclear cells using Myelin removal beads</i>	103
2.12	ISOLATION OF LYMPHOCYTES FROM SPLEEN	104
2.13	PROCESSING OF WHOLE BLOOD SAMPLES	104
2.14	FLOW CYTOMETRY.....	104
2.15	RNA EXTRACTION FROM TISSUE.....	105
2.15.1	<i>Measurement of RNA quality and degradation</i>	106
2.16	VIRAL RNA EXTRACTION FROM SERUM AND BRAIN	106
2.17	CDNA SYNTHESIS	107
2.17.1	<i>cDNA synthesis for TLDA and viral RNA samples</i>	107
2.18	QUANTITATIVE (Q)PCR	108
2.18.1	<i>Primer design</i>	108
2.18.2	<i>Generation of DNA standards for absolute quantitative QPCR</i>	109
2.18.3	<i>Calculation of the absolute copy numbers of standards</i>	110
2.18.4	<i>SYBR green QPCR</i>	111
2.18.5	<i>Normalization of QPCR data</i>	112
2.19	TAQMAN LOW-DENSITY ARRAY (TLDA)	112
2.20	MEASUREMENT OF CHEMOKINE LEVELS IN BRAINS AND SERUM OF VIRALLY INFECTED MICE USING ELISA	113
2.20.1	<i>Protein extraction from the brain</i>	113
2.20.2	<i>ELISA</i>	113
2.21	VIRUS PRODUCTION AND PURIFICATION	114
2.22	VIRUS PLAQUE ASSAY	115
2.23	ADMINISTRATION OF CHEMOKINE ANTAGONISTS	116
2.24	STATISTICAL ANALYSES	117
CHAPTER 3	118
3.1	INTRODUCTION AND AIMS.....	119
3.2	DETERMINATION OF VIRAL TITERS IN THE BLOOD AND BRAIN DURING SEMLIKI FOREST VIRUS INFECTION	120

3.3	NEUROPATHOLOGY DURING AVIRULENT AND VIRULENT SFV INFECTION	123
3.4	ASSESSMENT OF RNA QUALITY OF MOUSE BRAINS SAMPLES INFECTED WITH SFV STRAIN A7(74) OR L10	128
3.5	CHEMOKINE EXPRESSION DURING AVIRULENT INFECTION WITH SFV A7(74)	129
3.5.1	<i>CC-chemokine expression</i>	130
3.5.2	<i>CXC-chemokine expression</i>	132
3.5.3	<i>CX₃CL1 chemokine expression</i>	137
3.6	CHEMOKINE EXPRESSION DURING VIRULENT INFECTION WITH SFV L10.....	138
3.6.1	<i>CC-chemokine expression</i>	139
3.6.2	<i>CXC-chemokine expression</i>	141
3.6.3	<i>CX₃CL1- and XCL1-chemokine expression</i>	141
3.6.4	<i>Summary of chemokine expression resulting from avirulent and virulent SFV infection of the brain using strains A7(74) and L10</i>	143
3.7	EXPRESSION OF CYTOKINES AND GENES INVOLVED IN INNATE IMMUNE RESPONSES TO VIRAL INFECTION DURING SFV ENCEPHALITIS	146
3.7.1	<i>A7(74) infection</i>	146
3.7.2	<i>L10 infection</i>	148
3.7.3	<i>Expression of CD45 during A7(74) and L10 infection</i>	150
3.8	DISCUSSION AND SUMMARY	152
CHAPTER 4	158
4.1	INTRODUCTION AND AIMS.....	159
4.2	OPTIMISATION OF LEUKOCYTE ISOLATION FROM SFV INFECTED BRAINS.....	160
4.3	INCREASE OF CD45 ^{hi} CELLS WITHIN SFV A7(74) INFECTED BRAINS	162
4.4	NK-CELLS ARE ONE OF THE FIRST CELLS INFILTRATING THE BRAIN DURING SFV INFECTION.....	164
4.5	IDENTIFICATION OF MYELOID CELLS DURING SFV INFECTION.....	165
4.5.1	<i>Identification of residual neutrophils, and Ly6C^{hi} monocytes and Ly6C^{lo} cells in the brain during SFV infection</i>	167
4.6	IDENTIFICATION OF PLASMACYTOID DCs CELLS DURING SFV INFECTION.....	169
4.7	IDENTIFICATION OF T-CELLS IN SFV INFECTED BRAINS	172
4.7.1	<i>Phenotypic characterisation of T-cells in the brain</i>	173
4.8	ACCUMULATION OF B-CELLS IN THE BRAIN DURING LATER STAGES OF SFV INFECTION.....	177
4.9	LEUKOCYTE INFILTRATION INTO THE CNS DURING L10 INFECTION	180
4.9.1	<i>Identification of myeloid cells in L10 infected brains</i>	180
4.9.2	<i>Identification of T-cells and NK-cells in L10 infected brains</i>	181
4.10	DISCUSSION AND SUMMARY.....	183
CHAPTER 5	191
5.1	INTRODUCTION AND AIMS.....	192
5.2	DETERMINATION OF VIRAL TITERS IN THE BLOOD AND BRAIN DURING WEST NILE VIRUS INFECTION	193
5.3	HISTOLOGICAL ANALYSIS OF WNV INFECTED BRAINS	194
5.4	CHEMOKINE EXPRESSION DURING WNV INFECTION.....	195
5.4.1	<i>CC-chemokine expression</i>	196
5.4.2	<i>CXC-chemokine expression</i>	199
5.4.3	<i>CX₃CL1 and CXCR5 expression</i>	201
5.5	EXPRESSION OF CYTOKINES AND GENES INVOLVED IN INNATE IMMUNE RESPONSES TO VIRAL INFECTION WITH WNV	203
5.5.1	<i>Expression of CD45</i>	204
5.6	DISCUSSION AND SUMMARY	205
CHAPTER 6	210
6.1	INTRODUCTION AND AIMS.....	211
6.2	CHARACTERISATION OF THE ROLE OF CCR2 DURING VIRAL ENCEPHALITIS	212
6.2.1	<i>Identification of monocytes in the blood during early stages of SFV infection</i>	212
6.2.2	<i>Inhibition of CCR2 leads to the reduction of leukocyte accumulation in the CNS during SFV A7(74) infection</i>	216

6.2.2.1	T-cells and NK-cells entering the CNS during CCR2 blockade of SFV infected mice.....	217
6.2.2.2	Myeloid cells	219
6.2.2.3	Effect of CCR2 blocker on blood monocytes during SFV infection.....	220
6.2.3	<i>Chemokine expression levels in the CNS of mice with genetic or pharmacological blockade of CCR2.....</i>	<i>224</i>
6.2.4	<i>The role of CCR2 for the pathogenesis of virulent infection of the brain with SFV strain L10</i>	<i>225</i>
6.3	CHARACTERISATION OF THE ROLE OF CCR5 DURING VIRAL ENCEPHALITIS	226
6.3.1	<i>Antagonism of CCR5 during SFV infection using Maraviroc.....</i>	<i>226</i>
6.3.2	<i>Antagonism of CCR5 during SFV infection using DAPTA</i>	<i>228</i>
6.3.3	<i>Chemokine expression levels in the CNS of SFV infected mice treated with the CCR5 blocker DAPTA.....</i>	<i>232</i>
6.4	CHARACTERISATION OF THE ROLE OF CXCR3 DURING VIRAL ENCEPHALITIS	233
6.4.1	<i>The effect of CXCR3 blockade on leukocyte infiltration into the CNS of SFV A7(74) infected mice.....</i>	<i>233</i>
6.4.2	<i>Chemokine expression levels.....</i>	<i>237</i>
6.4.3	<i>Effects of blocking CXCR3 on mice infected with the virulent strain L10</i>	<i>239</i>
6.5	DISCUSSION AND SUMMARY	240
CHAPTER 7	247
7.1	INTRODUCTION	248
7.2	IDENTIFICATION OF CHEMOKINE EXPRESSION PATTERNS AND DETERMINATION OF LEUKOCYTE RECRUITMENT INTO THE CNS DURING VIRAL ENCEPHALITIS.....	249
7.3	CYTOKINE EXPRESSION PATTERNS DURING SFV AND WNV INFECTION	254
7.4	THE ROLE OF CHEMOKINE ANTAGONISTS DURING THE PATHOGENESIS OF SFV AND WNV INFECTION OF THE CNS	257
7.5	CONCLUSIONS.....	262
7.6	FUTURE DIRECTIONS	263
APPENDIX	265
REFERENCES	276

List of Tables

TABLE 1.1.	SYSTEMATIC NOMENCLATURE OF CHEMOKINES	44
TABLE 1.2.	MEDICALLY IMPORTANT NEUROTROPIC VIRUSES.....	62
TABLE 2.1	LIST OF ANTIBODIES AND STREPTAVIDIN CONJUGATES USED FOR STAINING CELLS FOR FLOW CYTOMETRY	89
TABLE 2.2	PURIFIED PRIMARY MONOCLONAL AND POLYCLONAL ANTIBODIES USED FOR IMMUNOHISTOCHEMISTRY	90
TABLE 2.3	SECONDARY ANTIBODIES USED FOR IMMUNOHISTOCHEMISTRY	91
TABLE 2.4	SERUM AND REAGENTS USED FOR IMMUNOHISTOCHEMISTRY	91
TABLE 2.5	FORWARD AND REVERSE PRIMERS USED FOR QPCR. ALL PRIMERS ARE IN THE 5'-3' ORIENTATION.....	93
TABLE 2.6	QPCR PRIMER SEQUENCES FOR DETECTING VIRAL GENE TARGETS	94
TABLE 2.7	STANDARD PRIMER SEQUENCES TO DETECT VIRAL GENE TARGETS.....	94
TABLE 2.8	STANDARD PRIMERS USED TO DETECT SPECIFIC TARGET GENE.....	95
TABLE 4.1	FOLD INCREASES OF LEUKOCYTES WITHIN SFV INFECTED BRAINS RELATIVE TO HEALTHY CONTROL MOUSE BRAINS	163

List of Figures

FIGURE 1.1	DIFFERENTIATION OF HEMATOPOIETIC CELLS	21
FIGURE 1.2	THE BLOOD BRAIN BARRIER.....	35
FIGURE 1.3	THE BLOOD-CSF BARRIER.....	36
FIGURE 1.4	CIRCULATION OF CSF IN THE BRAIN AND DRAINAGE OF ANTIGENS AND CEREBRAL INTERSTITIAL FLUID INTO CERVICAL LYMPH NODES.....	38
FIGURE 1.5	CHEMOKINE SUBFAMILIES	42
FIGURE 1.6	LEUKOCYTE MIGRATION ACROSS THE ENDOTHELIUM INTO THE TISSUE.....	50
FIGURE 1.7	STRUCTURE OF THE ALPHAVIRUS GENOME	65
FIGURE 1.8	LIFE CYCLE OF ALPHAVIRUSES	65
FIGURE 1.9	GENOME OF WEST NILE VIRUS.....	71
FIGURE 2.1.	INDIRECT IMMUNOSTAINING USING TWO DIFFERENT ANTIBODIES.	100
	THE PRIMARY ANTIBODY (BLUE) BINDS TO ANTIGEN (AG). THE SECONDARY (RED) ANTIBODY DETECTS THE PRIMARY ANTIBODY AND IS SPECIES SPECIFIC, RAISED AGAINST THE CORRESPONDING IGG.	100
FIGURE 2.2.	CHAIN POLYMER-CONJUGATED TECHNOLOGY (ENVISION SYSTEM)	102
FIGURE 3.1	DETERMINING THE DOSE OF INITIAL VIRUS CONCENTRATION OF L10 FOR INITIATING LETHAL INFECTION OF MICE	121
FIGURE 3.2	VIRAL TITERS IN THE PLASMA OF MICE INFECTED WITH SFV STRAIN A7(74) OR L10.....	122
FIGURE 3.3	VIRAL TITER IN THE BRAINS OF MICE INFECTED WITH SFV STRAIN A7(74) OR L10	123
FIGURE 3.4	SFV NSP3 STAINING WITHIN MOUSE BRAINS FOLLOWING INFECTION WITH A7(74)	125
FIGURE 3.5	NEUROPATHOLOGICAL CHANGES IN MICE FOLLOWING INFECTION WITH SFV USING THE VIRULENT STRAIN L10.....	126
FIGURE 3.6	SFV NSP3 STAINING WITHIN L10 INFECTED MOUSE BRAINS	127
FIGURE 3.7	ASSESSMENT OF RNA QUALITY ISOLATED FROM MOUSE BRAINS INFECTED WITH SFV STRAIN A7(74)	128
FIGURE 3.8	ASSESSMENT OF RNA QUALITY ISOLATED FROM L10 INFECTED MOUSE BRAINS.....	129
FIGURE 3.9	CC-CHEMOKINE EXPRESSION DURING VIRAL INFECTION OF THE BRAIN WITH SFV A7(74).....	130
FIGURE 3.10	VALIDATION OF TLDA RESULTS BY QPCR FOR THE GENES CCL2 AND CCL5 DURING SFV INFECTION OF THE BRAIN WITH A7(74)	131
FIGURE 3.11	IDENTIFICATION OF CXC-CHEMOKINES UPREGULATED DURING VIRAL INFECTION OF THE BRAIN WITH SFV A7(74).....	134
FIGURE 3.12	VALIDATION OF CXCL9 EXPRESSION BY QPCR AND CONCENTRATION OF CXCL9 IN THE PLASMA DURING SFV INFECTION.....	135
FIGURE 3.13	VALIDATION OF TLDA RESULTS BY QPCR FOR CXCL10 AND CXCL1 EXPRESSION DURING SFV INFECTION OF THE BRAIN WITH STRAIN A7(74)	136
FIGURE 3.14	EXPRESSION OF THE CHEMOKINE RECEPTOR CXCR5 IN SFV A7(74) INFECTED BRAINS OVER TIME.....	137
FIGURE 3.15	VALIDATION OF CX ₃ CL1 EXPRESSION DURING SFV A7(74) INFECTION	137
FIGURE 3.16	IDENTIFICATION OF THE CC-CHEMOKINE EXPRESSION PROFILE DURING VIRAL ENCEPHALITIS AT DIFFERENT STAGES OF DISEASE SEVERITY	140
FIGURE 3.17	IDENTIFICATION OF THE CXC-CHEMOKINE EXPRESSION PROFILE DURING VIRAL ENCEPHALITIS AT DIFFERENT STAGES OF DISEASE SEVERITY.....	142
FIGURE 3.18	EXPRESSION OF CX ₃ CL1 AND XCL1 DURING L10 INFECTION OF THE BRAIN.....	143
FIGURE 3.19	COMPARISON OF CHEMOKINE EXPRESSION BETWEEN AVIRULENT AND VIRULENT INFECTION OF THE BRAIN.....	145
FIGURE 3.20	EXPRESSION OF GENES INVOLVED IN INNATE IMMUNITY DURING VIRAL BRAIN INFECTION WITH SFV A7(74)..	147
FIGURE 3.21	EXPRESSION OF GENES INVOLVED IN INNATE IMMUNITY DURING VIRAL BRAIN INFECTION WITH SFV L10.....	149
FIGURE 3.22	EXPRESSION OF CD45 DURING VIRAL INFECTION OF THE BRAIN WITH SFV	151
FIGURE 3.23	EXPRESSION OF CXCL10 AND CCL2 IN SFV INFECTED BRAINS COMPARED TO VIRAL TITER	153
FIGURE 4.1.	ISOLATION OF LEUKOCYTES FROM SFV INFECTED BRAINS USING MYELIN REMOVAL BEADS OR DENSITY GRADIENTS	162
FIGURE 4.2.	IDENTIFICATION OF CD45 ^{HI} LEUKOCYTES IN THE BRAIN	164
FIGURE 4.3.	NK-CELLS ENTER THE BRAIN EARLY DURING SFV INFECTION.....	166
FIGURE 4.4.	IDENTIFICATION OF MYELOID CELLS ENTERING THE BRAIN DURING SFV INFECTION	167
FIGURE 4.5.	IDENTIFICATION OF MONOCYTES, MACROPHAGES AND NEUTROPHILS IN THE BRAIN DURING SFV INFECTION....	170
FIGURE 4.6.	IMMUNOHISTOCHEMICAL STAINING FOR MACROPHAGES WITHIN THE CNS OF INFECTED MICE.....	171
FIGURE 4.7.	IDENTIFICATION OF PLASMACYTOID DCs IN SFV INFECTED MURINE BRAINS	172
FIGURE 4.8.	ACCUMULATION OF CD3 ⁺ T-CELLS IN THE BRAIN DURING SFV INFECTION	175
FIGURE 4.9.	PHENOTYPIC CHARACTERIZATION OF T-CELLS FROM THE BRAINS OF SFV INFECTED MICE	176
FIGURE 4.10.	B-CELLS ENTER THE BRAINS OF MICE LATE DURING ACUTE ENCEPHALITIC INFECTION WITH SFV	178
FIGURE 4.11.	DOUBLE STAINING OF B-CELLS AND T-CELLS IN SFV INFECTED BRAINS	179

FIGURE 4.12.	INFILTRATION OF CD45 ^{HI} CELLS AND ACCUMULATION OF MYELOID CELLS IN THE BRAINS OF MICE INFECTED WITH THE VIRULENT STRAIN L10.....	182
FIGURE 4.13.	ACCUMULATION OF T-CELLS AND NK-CELLS IN THE BRAINS OF MICE INFECTED WITH THE VIRULENT STRAIN L10	183
FIGURE 4.14.	EXPRESSION OF CXCL10 AND CCL2 COMPARED WITH CD45 INFLUX INTO SFV INFECTED MOUSE BRAINS ...	185
FIGURE 5.1	VIRAL TITERS IN THE BLOOD AND BRAIN OF WNV INFECTED MICE.....	193
FIGURE 5.2	PERIVASCULAR CUFFINGS FORMING AROUND BLOOD VESSELS DURING WNV INFECTION	194
FIGURE 5.3	STAINING FOR VIRAL PROTEIN IN WNV INFECTED MOUSE BRAINS.....	195
FIGURE 5.4	ASSESSMENT OF RNA QUALITY, ISOLATED FROM WNV INFECTION BRAINS	196
FIGURE 5.5	IDENTIFICATION OF CC-CHEMOKINE EXPRESSION PATTERNS DURING WNV INFECTION WITH STRAIN NY99	198
FIGURE 5.6	VALIDATION OF CCL2 AND CCL5 EXPRESSION BY QPCR DURING WNV INFECTION.....	198
FIGURE 5.7	IDENTIFICATION OF CXC CHEMOKINE EXPRESSION PATTERNS DURING WNV INFECTION WITH STRAIN NY99....	200
FIGURE 5.8	VALIDATION OF CXCL1, CXCL2 AND CXCL10 EXPRESSION BY QPCR	201
FIGURE 5.9	EXPRESSION OF CX ₃ CL1 DURING WNV INFECTION RELATIVE TO AN UNINFECTED HEALTHY MOUSE BRAIN BY TLDA	202
FIGURE 5.10	THE EXPRESSION OF CXCR5 IN WNV INFECTED BRAINS.....	202
FIGURE 5.11	EXPRESSION OF CYTOKINES AND GENES INVOLVED IN INNATE IMMUNE RESPONSES DURING WNV INFECTION OF THE BRAIN.....	204
FIGURE 5.12	EXPRESSION OF IFN- β AND IFN- γ IN WNV INFECTED BRAINS BY QPCR	204
FIGURE 5.13	ABSOLUTE AND RELATIVE EXPRESSION OF CD45 DURING WNV INFECTION OF THE CNS.....	205
FIGURE 6.1	VIRAL TITERS IN THE SERUM OF SFV A7(74) INFECTED MICE	213
FIGURE 6.2	IDENTIFICATION OF MYELOID CELLS SUBSETS IN THE BLOOD DURING SFV INFECTION.....	215
FIGURE 6.3	REDUCTION OF LEUKOCYTE INFILTRATION INTO THE CNS DURING SFV INFECTION IN CCR2 DEFICIENT MICE OR MICE TREATED WITH CCR2 BLOCKER.....	216
FIGURE 6.4	REDUCTION OF CD3 ⁺ T-CELLS AND NK-CELLS WITHIN THE BRAINS OF SFV INFECTED MICE IN CCR2 DEFICIENT OR CCR2 BLOCKER TREATED MICE	218
FIGURE 6.5	IDENTIFICATION OF MYELOID CELLS IN THE CNS DURING SFV INFECTION OF CCR2 DEFICIENT MICE AND MICE TREATED WITH CCR2 BLOCKER.....	221
FIGURE 6.6	EXPRESSION OF CCR2 ON CD45 ^{HI} CELLS IN THE BRAIN OF SFV INFECTED MICE IN CCR2 DEFICIENT AND CCR2 BLOCKER TREATED MICE	222
FIGURE 6.7	IDENTIFICATION OF MYELOID SUBSETS IN THE BLOOD OF MICE TREATED WITH THE CCR2 BLOCKER RS504393	223
FIGURE 6.8	EXPRESSION OF CCL2 IN THE CNS OF CCR2 DEFICIENT MICE OR MICE TREATED WITH THE CCR2 BLOCKER	224
FIGURE 6.9	SURVIVAL OF CCR2 DEFICIENT MICE INFECTED WITH THE VIRULENT SFV STRAIN L10	226
FIGURE 6.10	IDENTIFICATION OF CD45 ^{HI} , CD3 ⁺ T-CELLS AND NK-CELLS IN SFV INFECTED MICE TREATED WITH THE CCR5 BLOCKER MARAVIROC	227
FIGURE 6.11	IDENTIFICATION OF MYELOID CELLS IN THE BRAIN OF SFV INFECTED MICE TREATED WITH THE CCR5 BLOCKER MARAVIROC.....	228
FIGURE 6.12	IDENTIFICATION OF CD45 ^{HI} AND CCR5 ⁺ CELLS IN THE BRAINS OF SFV INFECTED MICE TREATED WITH THE CCR5 BLOCKER DAPTA, AND DETERMINATION OF VIRAL TITERS	230
FIGURE 6.13	IDENTIFICATION OF CD3 ⁺ T-CELLS AND NK-CELLS IN THE BRAIN OF SFV INFECTED MICE TREATED WITH THE CCR5 BLOCKER DAPTA	231
FIGURE 6.14	IDENTIFICATION OF MYELOID CELLS IN THE BRAINS OF SFV INFECTED MICE TREATED WITH THE CCR5 BLOCKER DAPTA.....	232
FIGURE 6.15	IDENTIFICATION OF CD45 ^{HI} CELLS IN THE BRAINS OF SFV INFECTED MICE TREATED WITH THE CXCR3 BLOCKER COMPOUND 21, AND DETERMINATION OF VIRAL TITERS.....	234
FIGURE 6.16	REDUCTION OF T-CELLS SUBSETS WITHIN THE CNS OF SFV INFECTED MICE TREATED WITH THE CXCR3 BLOCKER COMPOUND 21.....	236
FIGURE 6.17	IDENTIFICATION OF MYELOID AND NK-CELLS IN THE BRAINS OF SFV INFECTED MICE TREATED WITH THE CXCR3 BLOCKER COMPOUND 21	237
FIGURE 6.18	COMPARISON OF CXC-CHEMOKINE EXPRESSION PATTERN IN UNTREATED AND CXCR3 BLOCKER TREATED MICE, INFECTED WITH SFV STRAIN A7(74)	238
FIGURE 6.19	SURVIVAL OF MICE INFECTED WITH SFV STRAIN L10, AND TREATED WITH CHEMOKINE BLOCKERS	240
FIGURE 7.1.	KINETICS OF LEUKOCYTE ENTRY DURING SFV INFECTION	252
FIGURE 7.2.	THE ROLE OF CHEMOKINE RECEPTOR ANTAGONISTS DURING SFV INFECTION	261
APPENDIX 1.	GENES SELECTED FOR TAQMAN LOW DENSITY ARRAY (TLDA)	268
APPENDIX 2.	RNA QUALITY MEASUREMENTS FROM SFV A7(74) AND L10, AND WNV SAMPLES	270
APPENDIX 3.	COMPARISON OF GENE EXPRESSION IN THE CNS OF SFV A7/74 AND L10 INFECTED MICE.....	271
APPENDIX 4.	CHEMOKINE AND CYTOKINE EXPRESSION LEVELS IN THE CNS OF MICE WITH GENETIC OR PHARMACOLOGICAL BLOCKAGE OF CCR2.....	273
APPENDIX 5.	CHEMOKINE AND CYTOKINE EXPRESSION LEVELS IN THE CNS OF MICE AFTER PHARMACOLOGICAL BLOCKAGE OF	

APPENDIX 6. CCR5.....274
CHEMOKINE AND CYTOKINE EXPRESSION LEVELS IN THE CNS OF MICE AFTER PHARMACOLOGICAL BLOCKAGE OF
CXCR3.....275

Acknowledgements

First, I would like to thank in particular my supervisor Gerry Graham for all his support and encouragement throughout the years. When I had any doubts about science you always managed to motivate me again (yes, the biscuits you gave me helped), and you made me feel confident that I could do this! I also appreciate how quickly you read my thesis and for all the constructive feedback I received from you.

Next I would give a BIG thanks to my friend and lab mentor Clive McKimmie. Words can't even express how grateful I am for all your support throughout these years and the invaluable advice I got from you. I would not have made it without you!

I would also like to thank my advisors Allan Mowat and Tom Evans for all the guidance throughout my project. In particular thanks to Allan for taking your time and helping me with my FACS analysis and reading some of my thesis chapters. Your comments were very helpful! I would also like to thank Rob Nibbs and Chris Linington for reading parts of my thesis. Your comments were also very constructive. To John Fazakerley and his group, thanks for providing me with virus, and advising me at the beginning of my PhD. Thanks to Alain Kohl and Esther Schnettler for helping me to grow virus. Also thanks to Tony Fooks, Nick Johnson and Karen Mansfield for collaborating with me and providing me with samples.

I appreciate all the help I got from Colin Nixon regarding immunohistochemistry. Before, IHC seemed like a daunting task but your knowledge and kind help made it all possible and I finally got it to work. I also would like to acknowledge the help I got from Debbie Dewar for showing me how to dissect mouse brains. This leads me to the beloved animal house.... Thanks to Colin, Tony, Dennis and all the other staff at the animal house for all your help with the animal work, and the many injections I had to do.

I would also like to extend my thanks to the Wellcome Trust 4-year PhD program, and Darren Monckton, Olwyn Byron and Bill Cushley for guiding me especially through my first year here in Glasgow.

Most importantly I would also like to thank every member of the Chemokine Research Group (CRG) for all your help in the lab, all the good laughs I had over the years, teaching me Scottish (I am almost able to communicate with taxi drivers now) and for the fun tea times and lunch breaks. It was a pleasure to come to work every day and I must say I will miss you guys. In particular I would like to thank Michelle for teaching me FACS and being such a great friend and listener through all the years. I still remember our Saturday routine of Pilates and coffee afterwards. Thanks also to Alastair for teaching me TLDA analysis, Jenny for advising me how to do staining and how to use chemokine blockers, Kenny for patiently helping me with immunohistochemistry at the beginning of my PhD, and Carolyn for teaching me how to mush up brains. What fun!

Thanks also to all my friends who motivated me throughout my PhD. You helped me to stay sane! Kave, Clive, Michelle, Helen, Lenka, Hulya, Mark Williams and Isabelle, you all became great friends over the years. Big thanks!

Last but not least, thanks to my best friend Veronika for being there for me day and night. Most importantly thanks to Martin, now my husband, for being there for me. Words can't describe how grateful I am to have you in my life. Also a big thanks to my parents and sister for supporting me and believing in me. Without you none of this would have been possible.

תודה לכולם

Author's declaration

I declare that, except where explicit reference is made to the contribution of others, that this thesis is the result of my own work and has not been submitted for any other degree at the University of Glasgow or any other institution.

Signature:

Printed name: Daniela Pajek

List of abbreviations

A

Ab	antibody
ADAM	a disintegrin and metalloproteinase
AIDS	acquired immunodeficiency syndrome
ANOVA	analysis of variance
APC	antigen presenting cell
ATP	adenosine-5'-triphosphate

B

BBB	blood-brain-barrier
BCR	B-cell receptor
BSA	bovine serum albumin
bp	base pair

C

CCL	CC-chemokine ligand
CCR	CC-chemokine receptor
CCRL1	CC-chemokine receptor like 1
CD	cluster of differentiation
cDC	conventional dendritic cell
cDNA	complementary DNA
CHIKV	chikungunya virus
CMV	cytomegalovirus
CNS	central nervous system
CPE	choroid plexus epithelial

CpG	non-methylated CG dinucleotide
CSF	cerebrospinal fluid
Ct	threshold cycle
CXCL	CXC-chemokine ligand
CXCR	CXC-chemokine receptor
CX ₃ CL	CX ₃ C-chemokine ligand
CX ₃ CR	CX ₃ C-chemokine receptor
Cy	cyanine

D

DAB	3,3'-diaminobenzidine
DAMPs	damage associated molecular pattern
DAPI	4',6-diamidino-2-phenylindole dilactate
DAPTA	D-ala-peptide T-amide
DARC	Duffy antigen/receptor for chemokine
DC	dendritic cells
DMSO	dimethyl sulfoxide
DNA	deoxyribonucleic acid
DPX	dibutyl phthalate xylene
dsRNA	double-stranded RNA

E

EAE	experimental autoimmune encephalomyelitis
EDTA	ethylenediaminetetraacetic acid
EEV	Eastern equine encephalitis virus
Eif3f	eukaryotic translation initiation factor 3
ELISA	enzyme-linked immunosorbent assay

F		HMGB1	high-mobility group box 1 protein
FACS	fluorescence activated cell sorting	HRP	horseradish peroxidase
FCS	fetal calf serum	HSP	heat shock protein
FDA	food and drug administration	I	
FITC	fluorescein isothiocyanate	ICAM	intercellular adhesion molecule
FSC	forward scatter	IC ₅₀	inhibitory concentration 50
G		Ig	immunoglobulin
Glu	glutamine	IFN	interferon
GMEM	Glasgow modified minimum essential medium	IHC	immunohistochemistry
GPCR	G-protein coupled receptor	IL	interleukin
gp120	glycoprotein120	int	intermediate
GTP	guanosin-5'-triphosphate	i.p.	intraperitoneal
H		IRF	interferon regulatory factor
h	human	ISG	interferon stimulated gene
hi	high	i.v.	intravenous
HBSS	Hank's balanced salt solution	J	
HCl	hydrochloric acid	JEV	Japanese encephalitis virus
H&E	Haematoxylin and Eosin	JHMV	JHM strain of mouse hepatitis virus
HHV	human herpes virus	K	
HIV	human immunodeficiency virus	KSHV	Kaposi's sarcoma associated herpesvirus
HIER	heat induced epitope retrieval	L	
		LC	Langerhans cell
		LCMV	lymphocytic choriomeningitis virus
		l	litre
		lo	low
		LPS	lipopolysaccharide
		M	
		m	mouse
		M	molar
		μg	microgram
		μl	microliter

ml	millilitre	PBSA	phosphate buffer saline with bovine serum albumin
μ M	micro molar	PCR	polymerase chain reaction
MBP	myelin basic protein	pDC	plasmacytoid dendritic cells
MDA	melanoma differentiation associated	PE	R-phycoerythrin
MHC	major histocompatibility complex	PECAM	platelet endothelial cell adhesion molecule
MMP	matrix metalloproteinase	PEG	polyethylene glycol
MHV	mouse hepatitis virus	PerCp	peridinin-chlorophyll-protein
MOI	multiplicity of infection	PFA	paraformaldehyde
mRNA	messenger RNA	PFU	plaque forming unit
MS	multiple sclerosis	PGE	prostaglandin E
MW	molecular weight	PID	post infection day
Mx	myxovirus-resistance	PKR	protein kinase R
N		PLP	proteolipid protein
N	normality/normal concentration	PRR	pattern recognition receptor
NBCS	new borne calf serum	Q	
NG2	neuron-glia 2	QPCR	quantitative polymerase chain reaction
NK	natural killer	R	
NKp	natural killer protein	RA	rheumatoid arthritis
nM	nano molar	RIN	RNA integrity number
NO	nitric oxide	RIG	retinoic acid inducible gene
nsp	non-structural protein	RLR	RIG-I like receptor
NY99	New York 99	RNA	ribonucleic acid
O		ROS	reactive oxygen species
OAS	oligoadenylate synthetase	RPMI	Roswell Park Memorial Institute 1640 medium
OD	optical density	RQ	relative quantification
P		RRV	Ross-River virus
p	probability	RSAD	radical-S-adenosyl-methionine domain containing
PAMPS	pathogen associated molecular pattern	RT	reverse transcriptase
PBS	phosphate buffered saline		

S

s.c.	subcutaneous
SCID	severe combined immunodeficiency
SD	standard deviation
SDF	stromal derived factor
SEM	standard error of the mean
SFV	Semliki Forest virus
SINV	Sindbis virus
SSC	side scatter
ssRNA	single-stranded RNA

T

TBST	tris-buffered sodium Tween
TBP	TATA-binding protein
TCR	T-cell receptor
T _{CM}	central memory T-cell
TE	tris EDTA
T _{FH}	follicular helper T-cell
Th	T-helper
TGF- β	transforming growth factor
TLDA	TaqMan low density array
TNF	tumor necrosis factor
TNE	tris sodium EDTA
TNFR	tumor necrosis factor receptor
TLR	toll-like receptor
T _{reg}	regulatory T-cell
TRITC	tetramethyl rhodamine isothiocyanate

V

VB	VioBlue
VCAM	vascular cell adhesion molecule
VEEV	Venezuelan equine encephalitis virus

W

WEEV	Western equine encephalitis
WNV	West Nile virus
WT	wild type

X

XCL	XC-chemokine ligand
XCR	XC-chemokine receptor

Z

ZAP	zinc antiviral protein
-----	------------------------

Chapter 1

General Introduction

1.1 Innate and adaptive immunity

The immune system is important for the protection of the host from infectious agents, tissue injury and harmful substances like toxins. To achieve this the immune system has to recognize the presence of pathogens, contain the spread of infection and eliminate the infectious agent from the body. Following this, the immune response must be regulated in order to prevent allergy and autoimmunity. Finally, to build up a protective and strong immune response against any subsequent reinfection, the immune system must be capable of generating an immunological memory by producing highly specific antibodies that can persist life long in the host. The immune response can be divided into two categories: innate and adaptive immune responses. Both systems are capable of discriminating between 'self' and 'non self' (1, 2).

In this introduction I will give a brief overview of the immune system in general before specifically discussing immune responses in the CNS. I will then describe the role of chemokines and their receptors in the CNS, and discuss Semliki Forest virus and West Nile virus as models of viral encephalitis. These two pathogens, and in particular Semliki Forest virus, form the focus of my thesis. Finally, I will discuss what is currently known in the field about the role of chemokines in the pathogenesis of viral encephalitis.

1.1.1 Innate immunity

The innate immunity is an important first line of defense, occurs within minutes after infection and is capable of containing the spread of an infection and eliminating the pathogen. There are two phases of innate immune responses: the immediate innate immune response (0-4 hours after infection), followed by the early induced innate immune response (4-96 hours after infection) (3, 4).

To infect a host, a pathogen must first overcome the epithelial surfaces which provide a physical barrier against infectious agents. These epithelial surfaces are also able to produce a variety of antimicrobial enzymes, such as lysozymes, or antimicrobial peptides such as defensins, cathelicidin and histatin (5, 6). Lysozyme is a glycosidase and digests bacterial cell walls. Antimicrobial peptides are able to lyse bacterial cell walls. Another system of immediate host defence

is the complement system (7-9). This system is comprised of 30 soluble plasma proteins that act as pattern-recognition receptors and bind directly to pathogens and target them for lysis or phagocytosis by immune cells.

The early induced innate immune response is initiated after the pathogen has passed the epithelial barrier and activated the complement system. Cells of the innate immune system such as phagocytes, mast cells and natural killer (NK) cells recognize characteristic components of pathogens called pathogen-associated molecular patterns (PAMPS) or damage-associated molecular patterns (DAMPS) via pattern-recognition receptors (PRRs) (10, 11). The activation of PRRs leads to the release of pro-inflammatory cytokines which initiate inflammation and trigger an adaptive immune response in order to specifically target the invading pathogen. Furthermore phagocytes are pivotal for the direct killing of the infectious agent and release antimicrobial peptides and enzymes that are toxic to microbes (12).

1.1.1.1 Pattern-recognition receptors (PRRs)

PAMPS and DAMPS can be recognized by germ line encoded PRRs which can be soluble, membrane bound or cytoplasmic. PAMPS are highly conserved structures among microbes such as highly repetitive cell membrane components of bacteria (lipoteichoic acids, lipopolysaccharide) and fungi (β -glucan), unmethylated repeats of dinucleotide CpG, viral nucleic acid (double stranded or single stranded RNA) and other microbial structures (10). DAMPS are non-infectious, endogenous, molecules that are sequestered from the cytoplasm of dying cells due to cellular stress, toxic injury or hypoxia. Prototypical DAMPS are high-mobility group box 1 proteins (HMGB1), heat shock proteins (HSPs), adenosine 5-triphosphate (ATP), uric acid or hyaluronan (13). PRRs are expressed by all cells of the innate immune system but in particular by 'professional' immune cells such as macrophages and dendritic cells.

1.1.1.2 Cells of the innate immune system

Leukocytes are white blood cells and are pivotal for innate and adaptive immunity. Their role during viral encephalitis is not yet clear, as leukocytes can be either detrimental or beneficial for the pathogenesis of this disease (14). Leukocytes originate in the bone marrow and are derived from pluripotent

hematopoietic stem cells. These pluripotent hematopoietic stem cells give rise to two progenitors: lymphoid and myeloid progenitor cells. While lymphoid progenitor cells give rise to B-cells, T-cells and NK-cells, myeloid progenitor cells give rise to granulocytes, monocytes, macrophages, mast cells and dendritic cells (Fig. 1.1). Cells of the innate immune system comprise granulocytes, monocytes, macrophages, DCs and NK-cells. Phagocytes are a group of innate immune cells which are specialised in the uptake of pathogens and apoptotic particles and are therefore important for viral clearance during infection. Professional phagocytes are comprised of monocytes, macrophages, DCs and granulocytes. Other non-professional phagocytes such as endothelial or epithelial cells are also capable of phagocytosis.

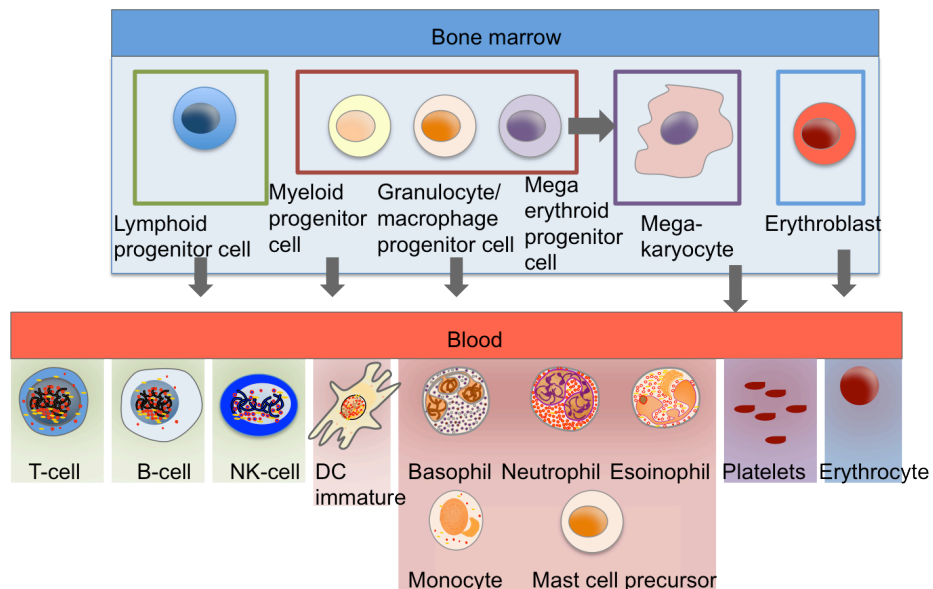


Figure 1.1 Differentiation of hematopoietic cells

Pluripotent stem cells differentiate into either lymphoid or myeloid progenitor cells. Lymphoid progenitor cells give rise to B-cells, T-cells and NK-cells. Myeloid progenitor cells give rise to immature DCs, and granulocyte/macrophage or megakaryocyte/erythrocyte progenitor cells which differentiate further into megakaryocytes or erythrocytes. Granulocytes, mast cells and monocytes are derived from granulocyte/macrophage progenitor cells. Adapted from (15).

Granulocytes

Granulocytes contain dense granules in their cytoplasm. There are three types of granulocytes which can be distinguished by different staining properties of the granules using haematoxylin and eosin staining: neutrophils (stain pink), eosinophils (stain red) and basophils (stain blue). Generally granulocytes exhibit a relatively short life span and are terminally differentiated cells. Eosinophils

and basophils will not be discussed as part of this thesis and are reviewed elsewhere (16, 17).

Neutrophils are the most abundant white blood cell in the blood of humans and mice. During infection the number of neutrophils increases enormously and they are one of the first leukocytes recruited to the inflamed tissue, although this might be different in the CNS. Activation of neutrophils will result in degranulation, secretion of cytokines and receptor-mediated phagocytosis of the pathogen. There are three types of granules in the cytoplasm of neutrophils: azurophilic or primary granules, specific or secondary granules, and gelatinase or tertiary granules (18). The granules contain a plethora of antimicrobial proteins that are toxic to the pathogen. While azurophilic granules are the largest granules and contain myeloperoxidase, the other granules are myeloperoxidase negative. The granules show varying propensities for mobilisation. For instance, azurophilic granules are the most difficult to mobilise whereas tertiary granules are more readily released into the cytoplasm (19).

Monocytes

Monocytes are generated in the bone marrow and are released into the blood upon expression of the chemokine receptor CCR2. Depending on the context, monocytes can differentiate further into tissue macrophages, microglia or DCs (20). Monocytes are important for immunosurveillance in the blood and are capable of replenishing tissue macrophages or DC populations in the steady state. They also play a pivotal role during infection and inflammation where they exert antimicrobial activities (21, 22). During viral brain infections, monocytes play a critical role in the initiation of immune responses and antigen presentation of viral particles and differentiate into brain macrophages or microglia (23). This will be discussed in detail later. Murine monocytes can be divided into two different subsets on the basis of specific surface markers including Ly6C, CD62L, CCR2 and CX₃CR1 (24). Monocytes that are Ly6C^{hi}, CD62L⁺, CCR2⁺ and CX₃CR1^{lo} are referred to as ‘inflammatory’ or Ly6C^{hi} monocytes. These Ly6C^{hi} monocytes have a propensity to rapidly migrate to sites of infection and inflammation, and within the tissue they preferentially differentiate into macrophages or DCs that produce pro-inflammatory cytokines and antimicrobial proteins (25). Ly6C^{hi} monocytes can downregulate the

expression of Ly6C and it has been suggested that they can become Ly6C^{lo} monocytes (21).

The second subset of monocytes circulating in the blood is characterised as Ly6C^{lo}, CD62L⁻, CCR2⁻ and CX₃CR1^{hi} and often referred to as 'resident' or Ly6C^{lo} monocytes. These Ly6C^{lo} monocytes circulate in the blood and migrate along luminal surfaces of the vascular endothelium. Since Ly6C^{lo} monocytes preferentially circulate in the blood in steady state it has been proposed that these monocytes patrol the blood vessels and may play important roles in scavenging dead cells, oxidised lipids and pathogens (26). Furthermore, in response to tissue damage or infection, these Ly6C^{lo} monocytes can rapidly extravasate into the inflamed tissue and become the main source of inflammatory monocytes during very early stages of inflammatory immune responses (26).

Macrophages

Macrophages are large tissue resident cells, present in almost every tissue of the body. Macrophages contain phagocytic granules and are highly efficient in removing cellular debris, apoptotic cells and pathogens. Upon detection of DAMPS or PAMPS, macrophages can become activated via PRRs, leading to changes in their morphology and physiology. It has been suggested that activated macrophages can be divided into three different subsets depending on their activation phenotype: classically activated macrophages (M1), alternatively activated macrophages (M2), and regulatory macrophages which will not be discussed here (27-29).

Classically activated macrophages, or M1 macrophages are mostly derived from 'inflammatory' monocytes. These macrophages become activated after recognizing PAMPS or DAMPS and initiate the production of tumor necrosis factor (TNF). Furthermore the presence of IFN- γ , produced by NK-cells and T-helper (Th) cells in response to infection, can induce an M1 phenotype. Classically activated macrophages produce nitric oxide (NO) and reactive oxygen species (ROS) for antimicrobial defence (30, 31). In addition to that, M1 macrophages also produce inflammatory cytokines including TNF, IL-11, IL-6, IL-12, IL-23, IL-27, chemokines such as CXCL9 and CXCL10, and matrix-metalloproteinases

(MMPs) for the degradation of extracellular matrix. Due to the upregulation of major histocompatibility (MHC) class II molecules on their cell surface, macrophages can also act as antigen presenting cells (APCs), bridging innate and adaptive immunity (28).

Alternatively activated macrophages or M2 macrophages are important during parasitic infections and allergies, and promote wound healing (32). M2 macrophages are activated in the presence of IL-4 and IL-13 which is produced by granulocytes, mast cells and Th2 cells (1). Compared to M1 macrophages, M2 macrophages produce low levels of inflammatory cytokines and high levels of IL-10 and transforming growth factor (TGF)- β .

Macrophages show a high degree of plasticity, which allows them to perform different specific functions in response to environmental cues. This means that during pathological processes, macrophages are capable of switching their phenotype and adapting rapidly to a new environment. However, this plasticity makes it complicated to assign one specific phenotype to macrophages (28). For instance in the brain, macrophages become microglia, and are indistinguishable from these cells based on the markers available for flow cytometry. These microglia are then important during viral brain infections (4, 33).

Dendritic cells (DCs)

DCs, CD11c⁺MHC-II⁺ cells, are 'professional' antigen presenting cells, which means that they can ingest foreign particles by phagocytosis and present the antigen on the surface to lymphoid cells, such as T-cells. Therefore DCs form a crucial link between the innate and adaptive immune system. In comparison to macrophages, which are specialised in destroying pathogens, DCs are specialised in presenting antigens (34). DCs are derived from myeloid progenitor cells and most of the DCs exit the bone marrow as immature DCs (7). DCs are an extremely heterogeneous cell population and it is difficult to categorize them but DCs can be broadly divided into steady state conventional DCs and non-conventional DCs including plasmacytoid DCs (pDCs) and monocyte derived DCs, although this is controversial as it has been shown that most DCs are derived from specific precursors in the bone marrow (21, 35, 36). pDCs are a major source of type-I interferon, and are therefore important during viral infections.

Natural killer cells (NK-cells)

NK-cells are derived from lymphoid progenitor cells and circulate in the blood after exiting the bone marrow. NK-cells are known for their ability to kill virus or bacteria infected cells and certain tumour cells, and are therefore important during infection (37). Their exact role during viral encephalitis is not yet understood, and there are sparse data investigating their role during brain infection.

NK cells are filled with cytotoxic granules that can be released after binding the target cell. The cytotoxic granules contain perforin which forms pores through the target cell wall, granzyme (a serine protease) which induces apoptosis, and granulysin that is cytolytic. Furthermore upon activation NK-cells can produce large amounts of IFN- γ and also other pro-inflammatory cytokines such as TNF, and chemokines including CCL3, CCL4 and CCL5 (38, 39).

NK-cell activation is tightly regulated by the expression of inhibiting and activating receptors on their surface. Inhibiting receptors usually bind to MHC class I molecules. The balance of inhibiting and activating receptors determines the activation status of NK-cells. The lack of MHC-I in combination with other activating receptors such as IFN- α , IFN- β or IL-12 leads to NK-cell activation (37, 40).

1.1.2 Adaptive Immunity

If a pathogen is able to overcome innate immunity, the adaptive immune response is induced, which is able to specifically recognize the antigen and eliminate it. Adaptive immunity is induced late during infection and needs approximately at least four days to generate activated effector lymphocytes from naïve T- and B-cells. Adaptive immunity uses somatic gene rearrangement to produce antigen specific receptors which means that these receptors are encoded in different gene segments that are then assembled to form T- and B-cell receptor genes (41). This system allows the host to produce an enormous variety of different antigen specific receptors.

1.1.2.1 *Cells of the adaptive immune system*

Lymphocytes are cells of the adaptive immune system and can be divided into T- and B-cells. Both cells are derived from lymphoid progenitor cells in the bone marrow. While B-cells mature in the bone marrow, T-cells need to migrate to the thymus for maturation. Lymphocytes that have not yet encountered an antigen are specified as naïve lymphocytes. Upon activation of naïve lymphocytes they become activated and turn into effector lymphocytes (41).

T-cells

T-cells are divided into different groups based on the expression of their lineage markers and functional activities. There are two distinct T-cell lineages known as CD4⁺ and CD8⁺ cells. On the basis of functional activity, T-cells can be divided into three groups: naïve, effector and memory T-cells. All T-cells have a T-cell receptor (TCR) which can bind to peptide antigen presented on MHC molecules on the surface of antigen presenting cells. The TCR assembles with the CD3 surface molecule and forms the T-cell receptor complex (42). T-cells have been shown to be important during viral encephalitis and their role in this context will be discussed in chapter 1.5. A brief overview of different subsets of T-cells will be presented here.

CD4⁺ T helper cells are specialized in producing cytokines that can stimulate other immune effector cells or that can be toxic to the target cell. Furthermore CD4⁺ T-cells are also pivotal in providing help to B-cells for the production of high-affinity antibodies. The CD4 co-receptor recognizes only peptides bound on MHC-II molecules. These peptides are mostly derived from intracellular vesicles through phagocytosis or endocytosis and presented on APCs. There are at least six different effector types within the CD4⁺ T-cell population: Th1, Th2, Th9, Th17, T_{reg} and T_{FH}. Depending on the cytokine expression, activated naïve CD4⁺ T-cells can differentiate into different types of effector cells (43). In the presence of IL-12 and IFN- γ , T-cells preferentially differentiate into Th1 cells which mainly develop following bacterial or viral infections. Th1 cells mainly release the cytokines IL-2, IFN- γ and TNF- β (lymphotoxin). These cytokines in turn activate macrophages which then kill the invading pathogen. The expression of IL-4 favours the development of Th2 cells. Signature cytokines produced by

Th2 cells are IL-4, IL-5 and IL-13, which activate eosinophils, mast cells and plasma cells. Th2 cells control predominantly parasitic infections and play a role during allergies (44). A balance between Th1 and Th2 response decides on pathogen growth and immunopathology. In the context of viral encephalitis, the main focus is on Th1 cells, which have been shown to be important for the pathogenesis of viral infections in the CNS (45).

Cytotoxic CD8⁺ T-cells are particularly important in viral infections, are specialized in the direct lysis of the pathogen or infected/malignant cell, and produce few cytokines. Kristensen *et al.* have shown that LCMV-specific CD8⁺ T-cells produce IFN- γ , TNF and inflammatory chemokines such as CCL3, CCL4 and CCL5 (46). Viral clearance by CD8⁺ T-cells has also been implicated in demyelination in the CNS, suggesting a pathogenic role of these cells during brain infection (47). The CD8 co-receptor selectively recognizes peptides bound to MHC-I molecules. MHC-I molecules are expressed on most cells of the body and present antigens derived from proteins within the cytoplasm. This means that CD8⁺ T-cells are able to detect virally infected cells and kill them through lysis using their cytotoxic granules. Many CD8⁺ T-cells do not need additional co-stimulatory signals after binding to MHC-I molecules. However during most viral infections CD8⁺ T-cells require additional help from CD4⁺ T-cells for their activation. This additional help prevents inadvertent activation of CD8⁺ T-cells, because cytotoxic granules would be destructive to many cells (48).

B-cells

B-cells are also able to present antigen to T-cells, produce cytokines, exert suppressive functions through the secretion of IL-10, and can differentiate into either antibody producing plasma cells or memory B-cells. After antigen binding via the B-cell receptor (BCR) B-cells become activated, proliferate and differentiate into either plasma cells, which are terminally differentiated cells that secrete antibodies, or memory cells. The process of secretion of antibodies into blood or extracellular fluids is also known as humoral immunity (49, 50).

The secreted antibodies protect the host against pathogens in three different ways: neutralization, opsonisation and complement activation, which all lead to phagocytosis by macrophages and other cells. On the basis of the constant

region, antibodies can be divided into five immunoglobulin classes: IgM, IgD, IgG, IgE and IgA. The IgG isotype is the most abundant antibody and has shown to be important during Semliki Forest virus (SFV) infection. Amor *et al.* have shown that SCID mice, lacking serum antiviral antibodies and infected with Semliki Forest virus develop high viremia and persistent CNS infection. After transfer of IgM, viremia was cleared, and in the presence of high titer IgG, the virus was cleared from the blood and CNS, suggesting that antibodies are essential for viral clearance (51).

1.1.3 Cytokines during innate and adaptive immunity

Cytokines are small proteins with a low molecular weight. Various cells in the host secrete them during innate and adaptive immunity in response to activating stimuli. Once secreted, they can act in an autocrine (affecting the same cell), paracrine (affecting adjacent cells) or endocrine manner (affecting distant cells). All cytokines have different biological effects on different target cells (pleiotropic). One of their main roles is to orchestrate innate and adaptive immune responses by activating and recruiting leukocytes to the site of inflammation (52). Interferons have been shown to be particularly important during virus infections and have been a focus in virology for a long time (53, 54). Interferons exert immediate antiviral effects and are able to bridge the innate with the adaptive immune system (55). TNF is important for the initiation of inflammation during viral infection. In my analysis I have focussed specifically on the expression of these two cytokines during viral encephalitis, although other important cytokines playing a role during infection were also measured.

1.1.3.1 *Interferon*

Interferon was discovered in 1957 by Isaacs and Lindenmann and they termed it interferon because this molecule was capable of interfering with viral replication (56). Interferon can be produced by almost all cells in the body in response to pathogen recognition, and plays a crucial role in the regulation of the activity of cells of the innate and adaptive immune system. The interferon family can be divided into three different groups: Type-I, type-II and type-III interferon.

Type-I interferon

The group of type-I interferon is comprised of seven different classes: IFN- α (12 subtypes), IFN- β , IFN- δ , IFN- ϵ , IFN- κ , IFN- τ and IFN- ω (57). All of these IFNs exist in humans with the exception of IFN- δ and IFN- τ which only exist in pigs and cattle (58, 59). Type-I interferon is usually not constitutively expressed in steady state, but is typically induced by PRRs after the recognition of pathogens such as viruses. One of the best characterised type-I interferons is IFN- α , predominantly expressed by leukocytes, and IFN- β particularly expressed by fibroblasts and endothelial cells (60). All type-I interferons bind to the IFN $\alpha\beta$ receptor expressed on a variety of cells. IFN- β and IFN- $\alpha 4$ are immediately produced in response to interferon regulatory factor (IRF3) activation (61). The expression of IFN- β and IFN- $\alpha 4$ leads to the activation of IRF7 which in turn activates transcription of the full spectrum of IFNs (62, 63). The expression of type-I interferon induces the expression of interferon stimulated genes (ISGs) which are responsible for the antiviral and immunomodulatory effect of IFNs (64). The lack of type-I interferon during viral infection rapidly leads to death of infected mice (65, 66). Furthermore the expression of type-I interferon leads to the upregulation of MHC-II molecules on adjacent cells, which results in the activation of other immune cells.

Type-II interferon

This class of IFN consists of only one member, IFN- γ . This IFN is structurally unrelated to type-I IFNs and binds to a different receptor known as the IFN- γ receptor (IFNGR). Although IFN- γ is also important for immediate antiviral activities like type-I interferon, IFN- γ is mainly expressed during later stages of infection and is therefore particularly important during adaptive immune responses including Th1 development and B-cell isotype switching to IgG2a (66, 67). Only certain cells such as NK-cells and Th1 CD4⁺ and CD8⁺ T-cells produce IFN- γ . NK-cells are the major source of IFN- γ during innate immune responses while Th1 CD4⁺ and CD8⁺ T-cells are the major sources of IFN- γ during adaptive immune responses (68). IFN- γ also leads to the upregulation of MHC-I and MHC-II expression which leads to the activation of CD8⁺ and CD4⁺ T-cells, respectively (69). Thus, IFN- γ has important immunomodulatory functions during infection

and inflammation and its ability to coordinate the transition from innate to adaptive immunity makes type-II interferon distinguishable from other IFNs.

Interferon stimulated genes (ISGs)

Many viral infections trigger the production of interferon which results in the production of specific ISGs that exert antiviral effector functions and target the viral life cycle (70). There are approximately 2000 genes that can be regulated by type-I IFNs but only a few of these (<40) ISGs have so far been shown to play a role during viral infection (70). Little is known of the role of ISGs during viral encephalitis. ISGs can have various effector functions and form a diverse and overlapping network (71). Each virus induces a unique 'ISG profile' where some ISGs are very potent and others are only moderate virus inhibitors (72, 73). One of the best characterized ISGs is the double stranded (ds) RNA activated protein kinase R (PKR), also known as 'eukaryotic translation initiation factor 2-alpha kinase 2' (EIF2AK2). PKR inhibits virus replication and production of virion progeny and initiates apoptosis (74). It has been shown that other ISGs such as 2'-5' oligoadenylate synthetases (OAS) and RNase L are also activated by dsRNA and lead to the degradation of viral mRNA through activated endoribonucleases (75, 76). The myxovirus-resistance (Mx) proteins are IFN-inducible GTPases that inhibit trafficking or activity of viral polymerase (77). Mx proteins particularly bind to negative stranded RNA viruses such as bunyaviruses and influenza virus (78). Viperin, also known as radical-SAM-domain- containing-2 (RSAD2) protein, has been shown to promote IFN production by upregulating TLR7 and TLR9 signalling pathways and to prevent the egress of influenza virus A from host cells (79). Another ISG, which promotes interferon production, is the zinc antiviral protein (ZAP) that is encoded by the gene ZC3HAV1. ZAP preferentially inhibits retroviruses, filoviruses and alphaviruses, and is initially induced by binding to modified 5' RNA ends (27, 29, 80). Due to the potency of ISGs to interfere in viral replication, some viruses have evolved strategies to downregulate or block ISG activities and enhance viral replication, subsequently leading to a survival advantage (81, 82).

1.1.3.2 *Tumour necrosis factor (TNF)*

The TNF family consists of cytokines which have important functions in innate and adaptive immunity. TNF- α , also known as cachectin, is one of the best-

characterized cytokine within the TNF family. TNF- α is mainly secreted by macrophages but can also be secreted by T-cells and NK-cells (83). TNF- α binds to two types of TNF receptors (TNFR): TNFR-I expressed on the plasma membrane of many cells with the exception of erythrocytes, and TNFR-II which is predominantly expressed on lymphocytes (84). If TNF binds to its cognate receptor a signalling cascade is initiated which ultimately results in apoptosis (85). During local infection, TNF leads to the upregulation of vascular adhesion molecules on the endothelium which promotes the interaction of circulating leukocytes with the vascular endothelium and extravasation of leukocytes into the inflamed tissue. This process is particularly important for the compromise of the intact blood-brain barrier during CNS infections, discussed in detail later.

In regard to viral encephalitis, Chen *et al.* have shown that during Japanese encephalitis virus infection (JEV) TNF- α is secreted in the infected CNS by activated microglia. This process triggers the expression of inflammatory chemokines such as CCL5 by activating astrocytes, and leads subsequently to the infiltration of immune cells into the CNS (86). In another study using TNF deficient mice in a model of West Nile virus (WNV) infection, it was shown that TNF- α protects mice against lethal WNV infection by promoting the infiltration of leukocytes into the CNS (87). In agreement with this, Zhang *et al.* have demonstrated that TNF expression by neurons during WNV infection diminishes CXCL10 induced death of neuronal cells (88).

1.2 Immune responses in the brain

In the mammalian body, the central nervous system (CNS) is very complex and comprises a sophisticated network of neurons and glial cells, which will be discussed in further detail in 1.2.2. Basic functions such as regulation of body temperature, sleep or hunger, orientation and coordination of movements as well as higher functions such as memory, cognition and intellect are all controlled by the CNS and render the brain one of the most vital organs. From an immunological point of view the CNS is considered to be an immunoprivileged site due to the following features: lack of antigen presenting cells, low expression of MHC-I and MHC-II, lack of lymphatic vessels within the brain, absence of resident DCs, blood-brain barrier (BBB) and blood-cerebrospinal fluid barrier that restricts the number of leukocytes circulating through the CNS (89).

Despite the immunoprivilege of the brain it is now recognised that this is not absolute, and therefore the brain is still subject to immunosurveillance. The BBB and cerebrospinal fluid-brain barrier constitute a pivotal part of the protection of the brain, and they will be discussed in further detail in section 1.2.3. If the BBB is compromised due to infection or inflammation in the CNS, immune cells are able to infiltrate the brain and cause damage in the CNS, resulting in profound neurological deficits (90). Therefore immune responses in the brain must be highly regulated to prevent inadvertent CNS damage.

1.2.1 Structure of the central nervous system

The CNS consists of the brain and the spinal cord, which are protected by the skull or vertebral column, respectively. Underneath these, three layers of membranes surround the brain and are called collectively the meninges. The outermost membrane of the meninges is the dura mater and consists of a tough and fibrous coat. The intermediate membrane is the arachnoid mater and is a collagenous structure, and the innermost membrane or pia mater is a thin membrane attached to the surface of the brain and spinal cord. The gap between the arachnoid and pia mater is known as the subarachnoid space and is filled with cerebrospinal fluid. Some of the blood vessels supplying the brain run partially in the subarachnoid space (91).

The brain itself can be divided into three parts: the forebrain, the midbrain and the hindbrain. Additionally the brain consists of two hemispheres, or halves, which are linked through fibres of the corpus callosum. To maximize the surface area of the cerebral hemisphere the surface is folded into ridges (gyri) and furrows (sulci) (92). The brain also contains a system of interlinked cavities filled with cerebrospinal fluid (CSF) that constitute the ventricular system. This system is comprised of the lateral ventricles (one in each cerebral hemisphere), third ventricle, cerebral aqueduct and the fourth ventricle. Each ventricle contains a choroid plexus where CSF is produced and secreted (93).

1.2.2 Cells of the CNS

The cells of the CNS can be broadly categorized into two groups: neurons and neuroglial cells or glia. Neurons are highly specialised cells in the nervous system

and are pivotal for the relay of information. The information within neurons is coded by changes in electrical energy. Glia are the most abundant cell type in the CNS and support neural function rather than processing information like neurons (94).

1.2.2.1 *Neurons*

Neurons consist of three main structures: the cell body, the dendrites and the axon. The cell body contains a nucleus and many organelles and inclusions including Nissl granules which consist of endoplasmic reticulum. The dendrites are important for receiving information from other neurons and passing information on to axons which transfer messages to other neurons via a specialised region known as the synapse or nerve terminal (95). Many neurons are unique in their shape, function and location within the CNS and it is difficult to divide each neuron into specific groups. After development most neurons are terminally differentiated and do not replicate although limited neurogenesis occurs in the hippocampus. Therefore neurons must be particularly protected from damage and tissue injury (96).

1.2.2.2 *Glia*

Glia can be divided into macroglia or microglia. Macroglia are comprised of astrocytes, oligodendrocytes and NG2 cells which will not be discussed here and are reviewed by Nishiyama *et al.* (94, 97). Astrocytes are the most abundant type of glia and have a stellate morphology. They play important roles in synapse formation, modulation of synaptic connectivity, energy metabolism, axonal outgrowth and maintenance of the BBB. Astrocytes generate signals that are chemical rather than electrical. They are able to produce a variety of chemokines and pro-inflammatory cytokines in response to infection or inflammation, which will be discussed in further detail in chapter 1.3.6. Upon activation astrocytes start proliferating, change their morphology and increase their size (98).

Oligodendrocytes are myelin-producing cells in the CNS and surround the axons of neurons. Myelin is a lipid-rich membrane and consists of glycosphingolipids and cholesterol. Furthermore myelin also contains myelin basic proteins (MBP)

and proteolipid protein (PLP) (99). Each oligodendrocyte wraps the axon with myelin which allows fast transmission of information between neurons over long distances. Viral infection with Semliki Forest virus leads to the destruction of oligodendrocytes and results in viral demyelination (47). This will be discussed further in section 1.4.2.4.

Microglia are the only immune cells of the CNS and express many of the common macrophage markers such as CD45, CD11b, F4/80, MHC-I and MHC-II, but expression of these markers is low compared to macrophages. Resident microglia, or parenchymal microglia, originate from embryonic progenitor cells in the yolk sac (100). These microglia can be distinguished from macrophages based on the low expression of CD45, MHC-I and MHC-II molecules. The other types of microglia found in the brain are derived from blood monocytes and are located in very specific areas of the brain. These microglia are indistinguishable from macrophages and are often referred to as perivascular, meningeal or choroid plexus macrophages (101). Both types of microglia are important for the recognition of pathogens, phagocytosis, antigen presentation, repair and protection of neurons. The function of microglia can be either protective or detrimental depending on the signal that the microglia receive from the environment (102). Upon activation microglia can kill neurons directly or indirectly through the release of pro-inflammatory cytokines which promote the influx of leukocytes into the CNS (103-105). Previous studies have shown that West Nile virus infection of the CNS results in an increase of activated microglia during infection, and that these cells are important for initiating immune responses in the brain after entry of virus by releasing inflammatory cytokines and removing infected neurons or glial cells (23, 106). In general microglia are very sensitive to changes in their environment and subsequently several regulatory mechanisms need to be in place to prevent inadvertent activation of microglia and subsequent tissue damage (107).

1.2.3 The blood-brain barrier and blood-cerebrospinal fluid barrier

The blood-brain barrier (BBB) and blood-cerebrospinal fluid (blood-CSF) barrier are physical barriers to prevent the entrance of toxic molecules and pathogens

into the CNS, and maintain homeostasis within the brain tissue necessary for the delicate function of neurons and glial cells.

1.2.3.1 Blood-brain barrier

The BBB is composed of cerebral micro-vascular endothelial cells which are surrounded by the endothelial basement membrane, pericytes, located within the perivascular space, and astrocytic endfoot processes which constitute the 'glia limitans' (Fig. 1.2) (108). Microglia and neurons contribute further to the stability of the BBB (109). The cerebral endothelial cells are characterised by the lack of transendothelial fenestration, low pinocytosis and presence of tight junctions (110, 111). The endothelial cells are additionally covered with the basement membrane which is composed of extracellular matrix proteins such as collagen and laminin (112) (Fig. 1.2).

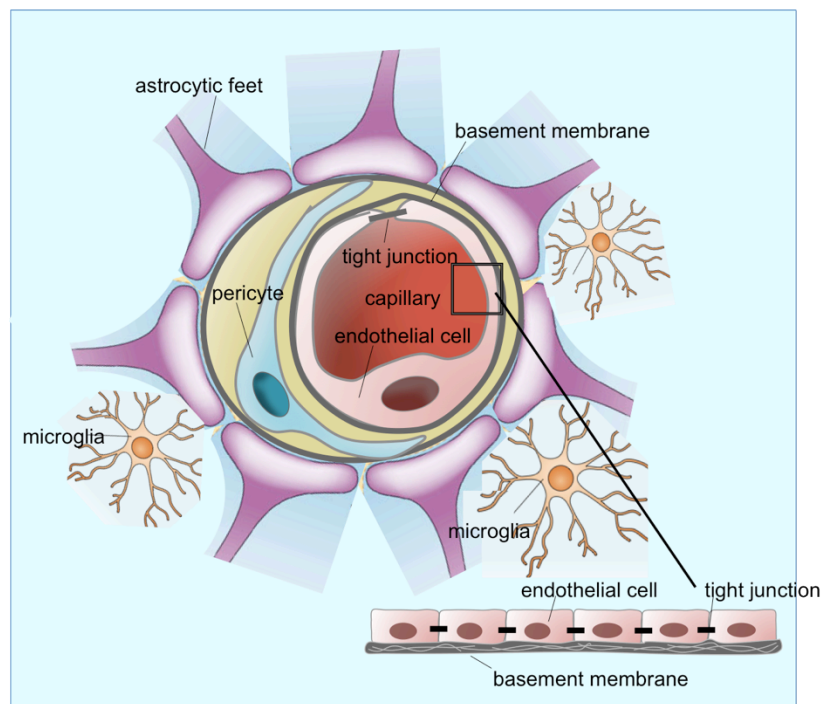


Figure 1.2 The blood brain barrier

Cerebral endothelial cells of capillaries contain tight junctions to prevent entry of molecules and leukocytes into the brain parenchyma. Endothelial cells are surrounded by the basement membrane. The perivascular space is localised between the endothelium and glia limitans and contains pericytes and perivascular macrophages. The glia limitans consists of a parenchymal basement membrane and astrocytic end feet processes. The BBB is further surrounded by microglia which are important immune cells of the CNS. Adapted from (113).

Endothelial cells are the first point of entry for many neurotropic viruses before they can spread within the CNS parenchyma. Therefore the BBB is an important

barrier during viral infections of the brain and protects the brain from entry of viruses and other substances, which could damage the brain tissue. Small lipophilic molecules, and gaseous molecules such as O_2 and CO_2 , can diffuse freely across the lipid membrane of the BBB (114). In general hydrophilic molecules are restricted from crossing the BBB unless they bind to a specific carrier transporter molecule (115). The transport of large hydrophilic molecules, ions or proteins across the BBB is mediated via transporter proteins such as glucose and amino acid carriers and sodium pumps.

1.2.3.2 Blood-CSF barrier

The blood-CSF barrier is located in the ventricles where CSF is generated by secretory cells within the choroid plexus epithelium (CPE) (116). The choroid plexus consists of a highly vascularized and fenestrated endothelium allowing the migration of leukocytes across the capillary endothelial wall into the interstitial space (stroma). The stroma is lined with CPE which is derived from the adjacent ependyma covering the ventricles. The CPE contains tight junctions and forms the actual blood-CSF barrier which allows transportation of only small molecules across the barrier similar to the BBB (Fig. 1.3). The CSF circulates from the ventricles through the subarachnoid space of the brain and spinal cord and is reabsorbed into the blood via venous sinuses in the arachnoid membrane (93). How CSF carries antigens into the cervical lymph nodes will be discussed in further detail in the following section.

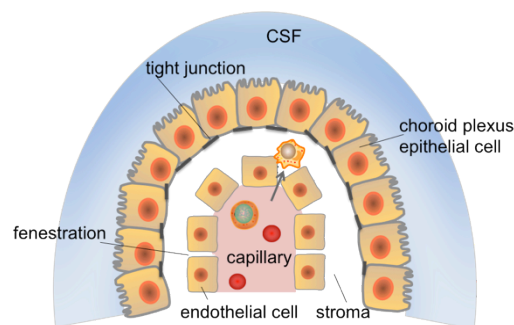


Figure 1.3 The blood-CSF barrier

The choroid plexus is localized in the ventricles and comprises the blood-CSF barrier. The cerebral capillaries in the ventricles consist of a fenestrated endothelium allowing leukocytes to enter the stroma of the choroid plexus. The choroid plexus epithelium consists of a basement membrane and tight junctions which prevent entry of leukocytes into the CSF. Furthermore choroid plexus epithelial cells produce CSF which circulates in the subarachnoid space throughout the brain and spinal cord.

1.2.4 Immunosurveillance in the healthy brain

Even though the CNS is considered as ‘immune-sheltered’, pathogens are capable of entering the brain under certain circumstances and can cause damage to delicate neurons and glial cells. In the normal healthy CNS, microglia constantly sample their environment for the presence of antigens and contribute in this way to immunosurveillance in the CNS. Resident microglia, derived from embryonic progenitor cells, are the only immune cells of the CNS which are localised in the brain parenchyma (100). Other immune cells of the CNS are located outside the parenchyma and include meningeal macrophages in the meninges, choroid plexus macrophages and Kolmer’s epiplexus cells in the choroid plexus parenchyma and perivascular macrophages in the perivascular spaces of the brain parenchyma. These cells are also considered to be microglia, as they reside in the brain in steady state, but compared to other microglia, they are of myeloid origin (117).

Compared to the periphery, cerebral APCs do not leave the CNS but soluble antigen present in the CSF or interstitial fluid of the brain can be transported to the deep cervical lymph nodes where it is presented to naive T-cells (118). CSF carrying the antigen drains across the cribriform plate and is transported alongside olfactory rootlets to the nasal mucosa from where it is drained into afferent lymphatic vessels to the deep cervical lymph node (Fig. 1.4). Thus, CSF can act as an equivalent of lymph, although less efficiently (116).

In the healthy brain the CSF appears to be the only location where leukocytes traffic in and out of the CNS, although only a few leukocytes are able to do that. All other parts of the brain parenchyma are devoid of leukocytes in steady state. In the healthy CSF 90% of infiltrating leukocytes are memory T-cells, 5% B-cells and 5% monocytes (93). Granulocytes and DCs seem to be absent from the CNS. T-cells found in the CSF are mainly CD4⁺ central memory T-cells (T_{CM}) (89, 119). These T_{CM} enter the CSF via the choroid plexus through the interaction of CCR7, expressed on T_{CM}, with CCL19, expressed on CPE cells. Additionally T_{CM} also express L-selectin and ICAM1 which interacts with CPE cells, facilitating trafficking of T_{CM} into the CSF (120, 121). T_{CM} are the main leukocytes carrying out immune surveillance in the CSF, and are the most abundant leukocytes within the healthy CSF (119). If T_{CM} recognise their antigen, they become

activated, acquire effector functions and initiate neuroinflammation. Additionally with the progression of neuroinflammation, for instance during viral infection of the brain, leukocyte infiltration becomes more evident across the CSF barrier, and ultimately leukocytes are able to cross the BBB due to the break down of the BBB as discussed in further detail in section 1.2.5. In the brain parenchyma only activated T-cells are able to cross the endothelial barrier. This is based on studies by Wekerle *et al.* who have demonstrated that radioactively labelled encephalitogenic T-cells in Lewis rats are capable of crossing the BBB whereas resting T-cells cannot cross this barrier (122). In the absence of the appropriate antigen, activated T-cells and T_{CM} leave the CNS or die.

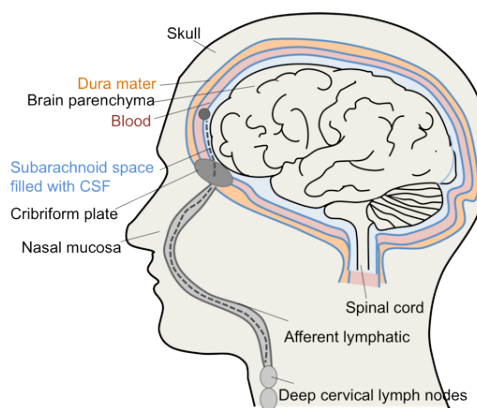


Figure 1.4 Circulation of CSF in the brain and drainage of antigens and cerebral interstitial fluid into cervical lymph nodes

The CSF circulates in the subarachnoid space of the meninges throughout the brain and spinal cord. Antigen and interstitial fluid from the brain parenchyma can drain into afferent lymphatics via the cribriform plate and nasal mucosa, from where they are carried into deep cervical lymph nodes. In the cervical lymph nodes antigen is finally presented to T-cells. Adapted from (93).

1.2.5 Immune responses in the virally infected brain

Virus infections of the CNS can lead to devastating neurological symptoms that may result in death of the host. Immune responses in the host have to be balanced without damaging delicate and mostly non-renewable neurons. Therefore immune responses during viral encephalitis need to be tightly controlled to prevent damage by inflammatory and cytotoxic cells (123). Mouse models of viral encephalitis inform us about the consequences of immune responses in the brain. Well-characterised mouse models to study viral infection of neurons include West Nile virus (WNV), Semliki Forest virus (SFV) and lymphocytic choriomeningitis virus (LCMV) (123). In this thesis SFV and WNV

were used as models of infection. Other well-characterised mouse models of glial infection include mouse hepatitis virus (MHV). These models of viral encephalitis will be discussed in depth in sections 1.4 and 1.5.

In general, immune responses to viral brain infection can be divided into three phases: innate immune responses of the CNS characterised by virus recognition and production of inflammatory cytokines, adaptive immune responses characterised by infiltration of leukocytes, followed by regulation of immune responses and viral clearance.

During innate immune responses interferons exert antiviral effects and are able to slow down virus spread within the CNS as it has been shown that type-I IFN deficient mice succumbed earlier, and were unable to control viral spread (124). Damaged or stressed neurons produce many chemokines and cytokines, which in turn activate astrocytes and microglia, and therefore this process initiates neuroinflammation (125). Some of the cytokines and chemokines produced by neurons during viral encephalitis are IFN- γ , IFN- β , IL-6 and CX₃CL1 (126, 127). Activated astrocytes and microglia are a major source of cytokines and chemokines during infection within the CNS, and these include TNF, IL-1 β , IL-2, CCL2, CCL4, CCL5, CCL7 and CXCL10 (128-130). Furthermore activated microglia upregulate their MHC-I and MHC-II expression for subsequent antigen presentation. In response to CNS infection endothelial cells of the BBB start upregulating adhesion molecules, allowing leukocytes to enter the perivascular space of the BBB. During infection additional enzymes, known as matrix-metalloproteinases (MMPs), are produced by myeloid cells which are able to degrade components of the second barrier, the glia limitans (131, 132). Once the glia limitans is broken down, leukocytes are able to infiltrate the brain parenchyma.

The second phase of the immune response to CNS infection comprises the recruitment of leukocytes into the brain in response to inflammatory chemokines and cytokines produced by activated neuronal and glial cells. Depending on the virus, the pathogen can enter the brain either through the BBB, blood-CSF barrier or blood-subarachnoid membrane barrier (133). Although priming of T-cells can occur in the brain through viral antigens presented on the surface of activated microglia, T-cells are usually primed in secondary lymphoid tissues

outside the CNS (134-136). Viral infections of the CNS are initiated in the gut, respiratory tract or in the skin, after the bite of a mosquito. In support of this, a study by Stevenson *et al.* has shown that the inoculation of virus directly into the brain parenchyma, which lacks immunological activity, elicits minimal or no immune response, confirming that immune responses to neurotropic viruses usually start outside the CNS (137).

Studies of lethal LCMV infection in mice demonstrated that neutrophils rapidly enter the brain, and this was associated with more severe disease outcome (138). However the role of neutrophils within the CNS is contentious and it is not yet clear when and how neutrophils enter the brain. The other leukocyte subset entering the brain during early stages of viral encephalitis are NK-cells. NK-cells have been shown to be able to target damaged neurons during very early stages of experimental autoimmune encephalomyelitis (EAE) (139). However there are very sparse data examining the role of NK-cells during brain infection, and therefore the implication of NK-cell infiltration into the brain remains unclear. T-cells, and in particular CD8⁺ T-cells, infiltrate the brain during the adaptive immune response (140, 141). Studies have demonstrated that the blockade of T-cell entry into virally infected brains of T-cell deficient mice often results in higher viral loads and increased mortality rates of mice. However the role of T-cell during viral encephalitis depends on the type of virus infection. B-cells arrive relatively late in the CNS during viral encephalitis, and these cells release antibodies predominantly of the IgA or IgG subclass (142). Antibodies have been shown to be pivotal in clearing viruses from infected neurons whereas T-cell mediated responses are more important for clearance of virus from glial cells. The reason for this is not yet clear.

The last phase of an immune responses to a viral brain infection consists of virus clearance by producing neutralizing antibodies and downregulating inflammatory immune responses. Gangliosides produced by neurons have been shown to inhibit MHC expression by astrocytes, and inhibit IL-2 mediated T-cell proliferation (142, 143).

In summary, immune responses in the brain can be both beneficial or detrimental depending on the extent of activation and timing during infection, and there are many contradictory studies which make a final conclusion difficult

(144-146). Despite the mostly beneficial role of the innate immune responses during early stages of viral infection to control spread of the pathogen within the CNS, the large-scale influx of leukocytes for a prolonged time can cause profound damage to neurons and glial cells if the reaction is excessive or inappropriate.

1.3 Chemokines and their receptors

Chemokines are pivotal for pathological and physiological processes in the body, orchestrating recruitment and positioning of leukocytes in tissue (147). The chemokine superfamily exists only in vertebrates and comprises a large number of ligands and receptors. Many ligand and receptor genes form clusters in the genome, which suggests a rapid evolution of chemokines and their receptors (148). Inflammatory ligands and receptors are highly promiscuous due to the fact that a ligand is able to bind up to three different receptors and receptors can bind many different ligands. Therefore the chemokine network is a highly complex system. Chemokines and receptors can be divided into different categories based on their structure or function and this will be discussed in more detail in this chapter.

1.3.1 Nomenclature and classification of chemokines

Chemokines are small chemotactic cytokines (8-12 kDa) that have a characteristic structure and are able to direct leukocytes to specific sites in the body during inflammation or homeostasis (149). The characteristic structure of chemokines is the presence of four conserved cysteine residues, although XC chemokines lack two of the cysteines (Figure 1.5). The first cysteine residue is connected with the third, and the second residue with the fourth via disulphide bonds. There are approximately 45 chemokines in most mammals (47 in humans) (150). Some chemokines exist only in one species and complicate orthologous relationships between humans and mice. This is probably due to different evolutionary pressures on mice and humans by pathogens (148). Most chemokines are secreted as soluble proteins but there are two chemokines, CXCL16 and CX₃CL1 that are membrane bound. The discovery of chemokines happened relatively quickly and initially chemokines were named according to their function. However the more chemokines were discovered the more

confusing the naming system became. In 1999 it was decided to develop a new nomenclature system, and it was suggested to divide chemokines into four families based on the position of the first two cysteine residues at the N-terminus: CC, CXC, XC and CX₃C (Fig. 1.5). Additionally chemokines were numbered within each family according to the date of discovery of the gene encoding the chemokine (147). A list of all chemokines and their corresponding chemokine receptors can be found in Table 1.1.

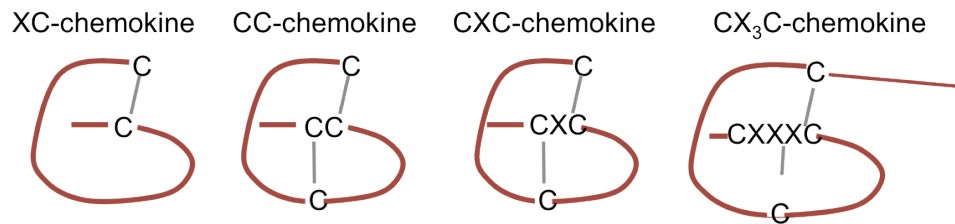


Figure 1.5 Chemokine subfamilies

Chemokines are divided into four subfamilies based on the position of conserved cysteine residues (C) and number of other amino acids (X) between the N-terminal cysteines.

CC-chemokines

The CC-chemokine family consists of approximately 28 members (CCL1-CCL28) and is the biggest group within the chemokine family. The CC-chemokines are also known as β -chemokines. Some of these CC-chemokines exist in humans and not in mice, such as CCL13 to CCL16, whereas some chemokines such as CCL6, CCL9, CCL10 and CCL12 exist only in mice and not in humans (150). Furthermore some chemokines exist as isoforms such as CCL3 and CCL3L1 or CCL4 and CCL4L1, which have slightly different functions and exhibit a different affinity to their cognate receptor (151). Not all isoforms occur in one individual, and this shows that the chemokine system contains a high degree of 'redundancy'. The characteristic of the CC-chemokine family is that the first two cysteine residues at the N-terminus are directly next to each other. Many of the CC-chemokines play an important role in leukocyte migration during inflammation (147). The expression of CC-chemokines specifically in the CNS during viral encephalitis shall be discussed later.

CXC-chemokines

The CXC-chemokine family consists of 17 members and they are also referred to as α -chemokines. The first two cysteine residues in CXC-chemokines are not

adjacent to each other but separated by one amino acid designated as X. Hence these chemokines are called CXC-chemokines. Similar to CC-chemokines, some CXC-chemokines exist in humans such as CXCL6 and CXCL8, but not in mice whereas CXCL15 exists only in mice and not in humans. Many CXC-chemokines have been shown to play an important role during angiogenesis (152). In the context of viral encephalitis CXCL9 and CXCL10 have been shown to be highly upregulated during LCMV and WNV infection (153, 154).

XC-chemokines

XC-chemokines lack the first and third cysteine residue and are also known as γ -chemokines or lymphotactin (Figure 1.5). The XC-chemokine family consists of only two members, XCL1 and XCL2, although XCL2 exists in humans but not in mice. XC-chemokines are expressed on T-cells, NK-cells and NKT-cells during infection. The appropriate receptor XCR1 is expressed by a subpopulation of dendritic cells. Furthermore XCL1 and its receptor are constitutively expressed in the thymus where they are important for the establishment of self tolerance and play regulatory roles (155).

CX₃C-chemokine

The CX₃C chemokine family is also referred to as δ -chemokine family. This family only consists of one member known as CX₃CL1, or fractalkine. CX₃CL1 contains three amino acids between the first two cysteine residues at the N-terminus (Figure 1.5). This chemokine is membrane bound but can be cleaved into a soluble chemokine by specific proteases which are members of the ADAM (a disintegrin and metalloproteinase) family (156). Membrane bound CX₃CL1 is highly expressed on endothelial and smooth muscle cells in the periphery. In the CNS CX₃CL1 is highly expressed by neurons, and after cleavage, the soluble chemokine signals to the receptor expressed on microglia. CX₃CL1 binding to microglia inhibits neurotoxic effector functions of microglia. If the CX₃CL1-CX₃CR1 axis is disrupted it can lead to the initiation of degenerative CNS diseases such as Alzheimer's or Parkinson's (157, 158).

Table 1.1. Systematic nomenclature of chemokines

Chemokines and their receptors are listed according to their systematic nomenclature. Chemokines which only occur in humans or mice are indicated with (h) or (m) respectively, preceding the systematic name. Chemokines predominantly involved in homeostatic processes are highlighted in blue, inflammatory chemokines in red and dual-function chemokines in green. Unknown chemokine functions are not highlighted and left blank.

CC-chemokine subfamily

Systematic name	Alternative name	Chemokine receptor
CCL1	I-309, TCA-3	CCR8
CCL2	MCP-1, JE, MACF	CCR2
CCL3	MIP-1 α S, MIP1-1 α	CCR1, CCR5
hCCL3L1	MIP-1 α P, MIP-1 α	CCR1, CCR3, CCR5
CCL4	MIP-1 β	CCR5
hCCL4L1	MIP-1 β	CCR5
CCL5	RANTES	CCR1, CCR3, CCR5
mCCL6	C10, MRP-1	CCR1
CCL7	MCP-3, MARC	CCR1, CCR2, CCR3, CCR5
CCL8	MCP-2	hCCR2, hCCR3, mCCR8
mCCL9	MIP-1 γ , MRP-1, CCF18	CCR1
mCCL10	MIP1 γ , MRP-1, CCF18	CCR1
CCL11	Eotaxin	CCR3, CCR5, (CXCR3 antagonistic)
mCCL12	MCP-5	CCR2
hCCL13	MCP-4	CCR2, CCR3
hCCL14	HCC-1	CCR1
hCCL15	HCC-2, Lkn-1, MIP-1 δ	CCR1, CCR3
hCCL16	HCC-4, LEC, LCC-1	CCR1, CCR2, (CCR5 antagonistic)
CCL17	TARC	CCR4
hCCL18	DC-CK1, PARC	PITPNM3, (CCL3 antagonistic)
CCL19	ELC, MIP-3, exodus-3	CCR7
CCL20	MIP-3 α , LARC, exodus-1	CCR6
CCL21	SLC, 6Ckine, exodus-2	CCR7
CCL22	MDC, STCP-1, ABCD-1	CCR4
hCCL23	MPIF-1	CCR1
CCL24	Eotaxin-2, MPIF-2	CCR3
CCL25	TECK	CCR9
hCCL26	Eotaxin-3	CCR3, CX ₃ CR1 and CCR1, CCR2, (CCR5 antagonistic)
CCL27	C-TACK, PESKY, Eskine	CCR10
CCL28	MEC	CCR3, CCR10

CX₃C-chemokine subfamily

Systematic name	Alternative name	Chemokine receptor
CX ₃ CL1	Fractalkine, Neurotactin	CX ₃ CR1

CXC-chemokine subfamily

Systematic name	Alternative name	Chemokine receptor
CXCL1	GRO α , KC	CXCR1, CXCR2
CXCL2	GRO β , MIP-2	CXCR2
CXCL3	GRO γ , DCIP-1	CXCR2
CXCL4	PF4	hCXCR3B
CXCL5	ENA-78, mGCP-2, LIX	CXCR2
hCXCL6	GCP-2	CXCR1, CXCR2
CXCL7	NAP-2	CXCR2
hCXCL8	IL-8	CXCR1, CXCR2
CXCL9	Mig	CXCR3, (CCR3 antagonistic)
CXCL10	IP-10	CXCR3, (CCR3 antagonistic)
CXCL11	I-TAC	CXCR3, CXCR7, (CCR3 antagonistic)
CXCL12	SDF-1	CXCR4, CXCR7
CXCL13	BCA-1, BLC	CXCR5
CXCL14	BRAK, Bolekine	unknown
mCXCL15	Lungkine, WECH	unknown
CXCL16	SCYB16, SR-PSOX	CXCR6

XC-chemokine subfamily

Systematic name	Alternative name	Chemokine receptor
XCL1	Lymphotactin, SCM-1 α	XCR1
hXCL2	SCM-1 β	XCR1

1.3.1.1 Homeostatic and inflammatory chemokines

Chemokines can be categorized into groups not only structurally but also based on their function. The two biggest functional groups are homeostatic and inflammatory chemokines. However the classification into homeostatic and inflammatory chemokines is not always that clear and some homeostatic chemokines can be expressed under inflammatory conditions and vice versa. Chemokines that can display both homeostatic and inflammatory functions are also referred to as dual-function chemokines (159). A list of homeostatic, inflammatory and dual-function chemokines is found in Table 1.1.

Homeostatic chemokines

Homeostatic chemokines are constitutively expressed at specific sites in the body including lymphoid organs, skin, gut and other organs (160). These chemokines play an important role for the basal trafficking of leukocytes under homeostasis. Thus they are important for the development of lymphocytes and the lymphoid organs and regulate the movement and localization of T-cells and DCs (161). The genes for homeostatic chemokines are often located outside the large CXC and CC chemokine chromosomal clusters and are often well conserved between species. Homeostatic chemokines are considered evolutionally ancient compared to inflammatory chemokines. Members of homeostatic chemokines include the 'primordial' chemokine CXCL12, also known as stromal derived factor (SDF), which is one of the most ancient chemokines (160). CXCL12 has been shown to be important for the movement of stem cells during development, homing of stem cells to the bone marrow and the maintenance of stem cells in the bone marrow (162, 163). Other homeostatic chemokines include the mucosal chemokines CCL25 and CCL28, the skin homing associated chemokines CCL17 and CCL27 and the chemokines involved in lymph node homing CCL19 and CCL21 (159).

Inflammatory chemokines

Inflammatory chemokines are predominantly expressed under inflammatory conditions in the body and are important for the recruitment of leukocytes to sites of infection or inflammation. Therefore these chemokines are important during viral infections. The genes for inflammatory chemokines are often clustered in the chromosome, such as CCL1-5 on chromosome 17, and CXCL1-11 on chromosome 4 (150). The clustering of inflammatory chemokines in the chromosome suggests that they rapidly evolved in response to new pathogens that threatened the survival of the host (148). CCL1-5 attract a whole range of leukocytes including monocytes/macrophages and T-cells. CXCL1-8 are important for the recruitment of neutrophils and CXCL9-11 often play a role in the attraction of T-cells. However chemokines are highly promiscuous, can bind to many different chemokine receptors and therefore attract various different leukocytes depending on the context and location of inflammation. For instance CCL5 has been shown to bind to three different receptors, CCR1, CCR3 and

CCR5, recruit many different cells and is highly inducible. Generally inflammatory chemokines bind to many different receptors compared to homeostatic chemokines which usually bind only to one or two receptors (164).

Dual-function chemokines

This group of chemokines can have both homeostatic and inflammatory functions. Members of the dual-function chemokines include CCL2, CCL11, CCL17, CCL20, CCL22, CX₃CL1 and both members of the XC family. CCL2 has been shown to be important for the exit of Ly6C^{hi} monocytes from the bone marrow in steady state, but is also important for the recruitment of 'inflammatory' monocytes into inflamed tissue (25, 160).

1.3.2 Chemokine receptors

Chemokine receptors are G-protein coupled receptors (GPCRs) containing a seven transmembrane spanning domain. Chemokine receptor genes are also clustered in the chromosome similar to chemokine ligands and many receptors can be found on the human chromosome 3, suggesting a rapid evolution of these genes through gene duplication, although other chromosomes also contain genes for chemokine receptors. Compared to ligands, chemokine receptors are well conserved between species, including mice and humans (148). Chemokine receptors are categorized into the same structural families (CC, CXC, XC and CX₃C) as their ligands and are also numbered (159). Altogether there are 18 chemokine receptors and four atypical chemokine receptors. The chemokine receptors can again be subdivided functionally into inflammatory and homeostatic chemokine receptors. Generally inflammatory chemokine receptors tend to bind many ligands (160). For instance, CCR3 binds up to 14 ligands, CCR1 binds up to 10 different ligands and CCR5 is capable of binding up to 7 different chemokines. In comparison homeostatic chemokine receptors typically bind one or two chemokine ligands.

Chemokines and their receptors also play an important role during viral infection. In response to this some viruses have developed different strategies to evade the immune system. Alcami and Lira have demonstrated that many DNA viruses are capable of producing their own chemokine and chemokine receptor homologues which mimic chemokines and their receptors in the host (165). For instance, the human herpes virus (HHV)-6 encodes the chemokine receptor U51

which downregulates the transcription of CCL5. The cytomegalovirus (CMV) produces the chemokine receptor US28 which can modify the chemokine environment and deplete CC-chemokines from the site of infection (166). Virally encoded chemokines can also act as antagonists for chemokine receptor. For instance Yamin *et al.* have shown that the virally encoded chemokine vMIP-II of Kaposi's sarcoma associated herpesvirus (KSHV) is capable of binding to two distinct chemokine receptors, CX₃CR1 and CCR5. Both chemokine receptors are expressed on naïve and activated NK-cells. Hence the antagonism of both receptors by vMIP-II has been shown to inhibit the migration of NK-cells during infection, and therefore the virus is able to escape the attack by NK-cells (167). Thus, chemokines play an important role during viral infection and have put evolutionary pressure on viruses to evade the immune system.

1.3.2.1 Chemokine receptor structure and classification

All chemokine receptors have an approximate length of 350 amino acids and consist of an extracellular acidic N-terminus and an intracellular C-terminus. Generally the N-terminus is important for binding chemokines whereas the C-terminus regulates downstream signalling events. Furthermore chemokine receptors contain three extracellular and three intracellular loops which are involved in chemokine binding and signal transduction, respectively (149). The second intracellular loop contains the conserved DRYLAIV motif and plays an important role in the coupling of G-proteins to the receptor (168, 169).

There are four different chemokine receptor families: CCR, CXCR, XCR and CX₃CR. The CC-chemokine receptor family consists of 10 members (CCR1-10) and the CXC-family is comprised of six receptors (CXCR1-6) (160). CXCR7 is considered as an atypical chemokine receptor. There is one XCR receptor (XCR1), binding XCL1 and hXCL2, that is expressed not only on neutrophils, T-cells, NK-cells and B-cells but also on a subset of dendritic cells (155). The chemokine receptor CX₃CR1 is expressed on 'inflammatory' monocytes, macrophages and microglia (170). Atypical chemokines receptors are characterized by the seeming absence of signalling after ligand binding compared to typical chemokine receptors, defined by the International Union of Pharmacologists (IUPHAR) (150, 171). Subsequently the atypical chemokine receptors have not been assigned a systematic chemokine receptor

nomenclature, and it has been suggested to categorize them as chemokine-binding proteins (160, 172).

There is little knowledge about the role of chemokine receptors during viral encephalitis but to date three receptors have been reported to be pivotal during viral encephalitis using different models of infections such as West Nile, lymphocytic choriomeningitis and mouse hepatitis virus (128, 173, 174). These chemokine receptors identified were: CXCR3, CCR2 and CCR5.

1.3.3 Functions of chemokines and their receptors

Chemokines are important during inflammatory and homeostatic conditions in the body and regulate leukocyte migration, hematopoiesis, angiogenesis, embryonic organ formation, lymphoid development and metastasis. One of the main roles of chemokines is the orchestration of leukocyte migration to specific sites in the body. During infection this process becomes crucial for pathogen removal and repair of damaged tissues. Therefore as one of my aims the kinetics of leukocyte infiltration during viral encephalitis will be investigated. The process of leukocyte migration into the inflamed tissue will be briefly discussed here. The role of chemokines in other contexts is beyond the scope of this work and is well reviewed in many scientific publications (175-177).

The migration of leukocytes to sites of infection or inflammation is a multi-step process and involves essentially four steps: rolling of leukocytes via selectins, tight binding of leukocytes to the endothelium via chemokine mediated integrin activation, diapedesis and migration of leukocytes to the inflamed site within the tissue (Fig. 1.6) (178).

In the first step the endothelium becomes activated in response to cytokines (TNF, IL-1 β), lipopolysaccharide (LPS) or histamine leading to the rapid mobilisation of P-selectins from Weibel-Palade bodies (secretory storage granules in the endothelium) and platelet granules. Shortly after P-selectin mobilisation, E-selectin expression is transcriptionally upregulated by endothelial cells in response to cytokines. Selectins bind to carbohydrate structures on the surface of leukocytes including P-selectin glycoprotein 1 (PSGL-1) or sialyl-Lewis^x which binds preferentially to E-selectin (179). The binding of

selectins to ligands leads to the reversible binding of leukocytes to the endothelium and rolling of leukocytes along the surface due to the shear flow of the blood (180).

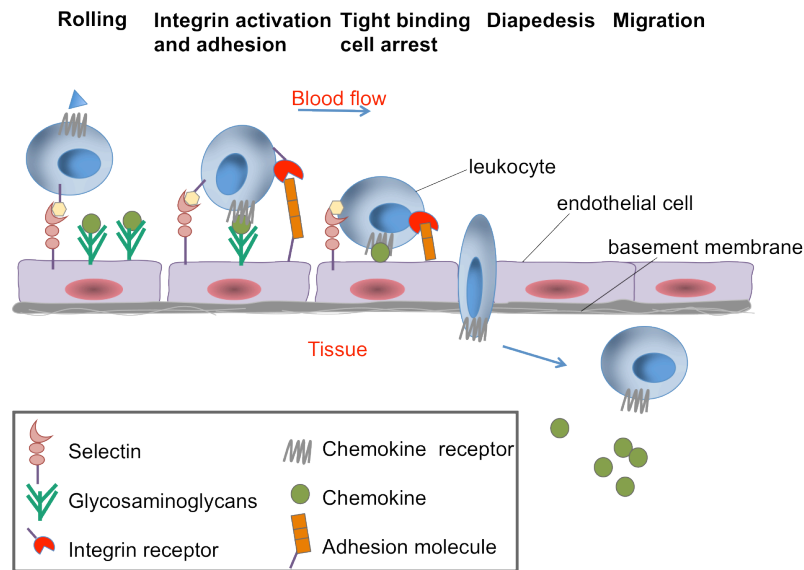


Figure 1.6 Leukocyte migration across the endothelium into the tissue

During the first step, leukocytes roll along the endothelium mediated by selectin binding. Chemokine receptors expressed on the surface of leukocytes bind to chemokines bound on glycosaminoglycans and this process leads to conformational changes and activation of integrin. In the subsequent step, leukocytes become firmly attached to the endothelium and this process allows diapedesis across the endothelial membrane. Once the leukocyte has entered the tissue, cells migrate to sites of infection mediated by chemokines. Adapted from Handel *et al.* (181).

In the second step the rolling leukocyte binds to immobilised chemokines on the surface of the endothelium, which activates chemokine receptors to initiate a signalling cascade. During this process integrin is activated through conformational changes and binds to cell-adhesion molecules and extracellular matrix including fibronectin, laminin and collagen. Integrins consist of two transmembrane proteins known as α - and β -subchains which form a heterodimer. There are 18 α - and 8 β -subchains which can form 24 heterodimers (180, 182). Intracellular adhesion molecules (ICAMs) are mostly expressed on activated endothelium with the exception of ICAM-2. Once integrin is activated and binds to its ligand, leukocytes become tightly bound to the endothelium which leads to the arrest of the rolling leukocytes (183).

In the third step leukocytes transmigrate through the endothelium and the whole process is referred to as diapedesis. The leukocytes can migrate into the tissue either transcellularly where leukocytes extravasate through the endothelial cell

directly, or paracellularly where leukocytes migrate through the junctions of endothelial cells (184). In order to penetrate the basal membrane of the endothelium, many cells express matrix metalloproteinase enzymes (185). In the CNS, leukocytes mainly cross the BBB via transcellular transport, due to tight junctions of the cerebral endothelium (114, 121). In the fourth and final step leukocytes migrate to the site of infection where they elicit their effector functions (186).

1.3.4 The role of chemokine receptors in disease

Chemokines are central in regulating leukocyte trafficking during infectious diseases such as viral, bacterial or parasitic infections, and during chronic and autoimmune diseases. Whereas chemokine-mediated leukocyte entry is mostly beneficial during acute inflammation or infection, chemokines can be detrimental during chronic infections such as rheumatoid arthritis, cancer and multiple sclerosis (MS) or experimental autoimmune encephalomyelitis (EAE). Thus, chemokines and their receptors are implicated in the pathogenesis of many diseases, and this highlights the importance of targeting chemokine receptors for therapy or prevention of disease. The specific role of chemokines during viral encephalitis, which is the focus of my thesis, will be discussed in further detail in chapter 1.5. However, to illustrate the importance of chemokines in disease, prominent examples of chemokine-mediated diseases such as HIV and MS/EAE will be briefly discussed here. The involvement of chemokines in many other diseases such as cancer will not be addressed here and are reviewed by Balkwill, Raman and Gerard *et al.*

1.3.4.1 *Human immunodeficiency virus (HIV)*

HIV is a retrovirus and was isolated from patient samples for the first time in 1983. HIV has been shown to cause acquired immunodeficiency syndrome (AIDS) in the host with the progression of the disease (187). HIV infects cells through the interaction of the viral envelope glycoprotein 120 (gp120) with the host cellular surface receptor CD4 in conjunction with the co-receptors CCR5 or CXCR4 (188, 189). HIV-1 variants that use only CCR5 as co-receptor are referred to as R5, and those which use CXCR4 are referred to as X4. If both co-receptors, CCR5 and CXCR4, can be used by the virus for cell entry, HIV variants are

considered to be dual tropic and are known as R5/X4. CCR5 and CXCR4 are differentially expressed on the surface of leukocytes and therefore HIV-variants target different cells. During early stages of infection R5 tropic viruses dominate and are preferentially transmitted to other hosts (190). X4 tropic HIV-1 variants are found predominantly during later stages of infection and are associated with the decline of CD4⁺ T-cells and development of AIDS (191, 192). The presence of many CCR5 binding chemokine ligands, expressed by other cells, has shown to slow down disease progression, as the ligands for CCR5 bind to the receptor and therefore block binding sites of gp120 to CCR5 (193, 194).

A loss-of function mutation in the CCR5 gene due to the deletion of 32 base pairs in the gene encoding CCR5 is designated as CCR5 Δ 32 mutation, and occurs naturally in some humans (195). Humans homozygous for this mutation are resistant to HIV because this mutation prevents the expression of functional CCR5 needed for cell entry of HIV. Approximately 1% of the whole Caucasian population of European origin are homozygous for the CCR5 Δ 32 mutation, and the occurrence of this mutation varies with the geographical region and can be as high as 16% within northern European populations (196). Based on these findings CCR5 became a focus of research for the prevention and treatment of HIV, although blockade of CCR5 is only effective in individuals infected with the R5 tropic strain. The CCR5 Δ 32 mutation does not seem to cause any adverse effects in healthy humans carrying this mutation, but it has been shown recently that the people carrying this mutation might be more susceptible to severe forms of WNV characterised by panencephalitis, which is a life threatening condition (197). In 2007 the Food and Drug Administration (FDA) has approved the use of the CCR5 blocker known as Maraviroc for the treatment of HIV (198, 199). General caution has to be taken when Maraviroc treated patients become infected with WNV. Maraviroc and other chemokine blockers used in this thesis will be briefly discussed in the following section.

The CXCR4 inhibitor, known as AMD3100, is also efficient in blocking HIV entry, but during clinical trials it was discovered that AMD3100 leads to the mobilisation of stem cells from the bone marrow into the blood (200, 201). Therefore this drug was later approved under the name Plerixafor or Mozobil, for the mobilisation of stem cells for the subsequent autologous transplantation of

stem cells in patients with leukemia such as non-Hodgkin's lymphoma or multiple myeloma (202).

1.3.4.2 *Multiple Sclerosis/EAE*

Multiple sclerosis (MS) is an autoimmune disease in humans characterised by demyelination of axons, axonal loss and gliosis, leading to paralysis. The onset of the disease can be progressive or relapsing, characterised by remyelination and amelioration of disease. The most commonly and best-characterised mouse model of MS is EAE, which is induced by myelin specific Th1 and Th17 cells produced after immunisation of mice with myelin oligodendrocytes glycoprotein (MOG) in combination with adjuvant containing bacterial components. The symptoms of EAE in mice are similar to MS and are characterised by the large influx of inflammatory leukocytes, including myeloid cells and lymphoid cells, into the CNS. As a model, EAE plays a major role in the identification and characterisation of key aspects of neuroinflammation and immune-mediated tissue damage of the brain. Based on EAE studies three therapeutics for MS have been tested and validated in this model and were approved for the treatment of MS. Thus, EAE is a valuable model for studying immune responses in the brain, and many aspects of neuroinflammation are derived from these studies.

Chemokines play an important role during EAE and MS, influencing the pathogenesis of the disease. This will be discussed in depth in 1.3.6.2. In brief, CCR1, CCR2, CCR5 and CXCR3 ligands are highly upregulated in the brain of MS patients and in EAE mice (203, 204). CXCR3 and CXCL10 deficient mice showed both increased susceptibility to EAE, suggesting that chemokine receptors play a role in the pathogenesis of the disease (205). In contrast to this CCR1, CCR2 and CCR6 deficient mice display an increased resistance to EAE characterised by delayed disease onset (206).

1.3.5 **Methods of targeting the chemokine system**

The chemokine system is highly complex with complicated binding patterns of chemokines and their receptors, and many studies have described the chemokine system as promiscuous or 'redundant', although Schall and Proudfoot have proposed the idea that this might not be entirely true (207). In recent years

chemokine receptors have been identified as possible targets for the treatment of various diseases such as HIV, MS and rheumatoid arthritis (198, 208). However a successful chemokine target for the treatment of viral encephalitis has not yet been identified and I attempted to explore this as part of this thesis.

There are various possibilities how to antagonise the chemokine system such as the use of small molecule antagonists, modified chemokines or antibodies against a specific receptor(209). For instance it has been demonstrated during EAE that the use of the CCR1 inhibitor (BX 741) in mice has a similar effect to that of CCR1^{-/-} mice suggesting that the antagonist is highly efficient and specific in blocking CCR1 (210). However, the design of new anti-chemokine compounds has been proven difficult, not only because of the redundancy of the chemokine system, but also because mouse chemokines and chemokine receptors are to some degree structurally different to the human counterpart or exist only in the mouse but not in humans, or vice versa.

Another way to study the role of chemokines is to generate ‘knock out’ mice, deficient of a specific chemokine receptor gene. Most studies, including studies of viral encephalitis, have used this approach to examine the role of chemokines and their receptors in the pathogenesis of the disease. However one disadvantage of using gene deficient mice is that blockade of the chemokine receptor is absolute and cannot be modulated or varied with the disease progression. In contrast to this, using small molecule inhibitors allows adjustment of timing and dose during disease. Therefore in this thesis small molecule antagonists were selected over gene deficient mice to investigate the role of chemokine receptors during viral encephalitis, and this is the first time that these blockers were used in the context of viral brain infections. The role of the chemokine receptors CCR2, CCR5 and CXCR3 are a key focus point in my thesis, and therefore I will briefly introduce these receptors and the appropriate antagonists I have used for my studies.

1.3.5.1 Blockade of CCR2

CCR2 has been shown to be predominantly expressed on the surface of Ly6C^{hi} monocytes (98%), DCs, and also on other leukocytes such as NK-cells, neutrophils

and 2-15% of T-cells, although this is regarded as controversial (25, 211, 212). CCR2 plays an important role during homeostatic and inflammatory processes. Studies using CCR2 deficient mice have shown that this receptor is implicated in the exit of monocytes from the bone marrow (213). Therefore CCR2^{-/-} mice display severe monocytopenia which renders these mice more susceptible to certain infection such as bacterial infection with *Listeria monocytogenes* or viral infection with WNV (25, 214). However the lack of CCR2 can also be beneficial, as some studies using EAE as model of neuroinflammation have shown that CCR2^{-/-} mice are less susceptible to the development of EAE (215).

To block the function of CCR2 during viral encephalitis the CCR2 blocker RS504393 was used, which is a small molecule inhibitor. RS504393 is a spiropiperidine compound, identified after a high throughput screening of many chemical compounds (216). This compound has been shown to block the receptor by occupying a binding site within the CCR2 protein that includes the acidic residue Glu²⁹¹. The specificity of the antagonist to bind CCR2 is 700-fold higher than for CCR1, and therefore RS504393 is considered to be a highly selective CCR2 antagonist. Furuichi *et al.* have shown that RS504393 blocks CCR2 binding in a dose dependent manner within 20 minutes after administration in a model of ischemia reperfusion injury in the kidney of mice (217). Additionally another study by Kitagawa *et al.* has shown that RS504393 was efficient in blocking CCR2 in a similar fashion to CCR2^{-/-} mice in a model of progressive fibrosis of the kidney of mice, confirming, again, the efficiency of CCR2 inhibition by RS504393 (218). The compound RS504393 has a short half life and therefore the drug has to be administered to mice twice daily (217).

1.3.5.2 Blockade of CCR5

CCR5 has been shown to be highly expressed (>90%) on the surface of murine NK-cells but is only weakly expressed on human NK-cells (212). Additionally CCR5 expression in mice can also be found on 3-10% of CD4⁺ and 10-40% of CD8⁺ T-cells, but is only weakly expressed on monocytes. CCR5 has become the focus of HIV research as people carrying the natural CCR5 Δ 32 mutation on both alleles are resistant to HIV infection, and heterozygous carriers exhibit partial resistance to HIV (195). In addition to this, CCR5 is also implicated in many other inflammatory diseases and infections. For instance CCR5 deficient mice are more

susceptible to parasitic infections such as *Listeria monocytogenes* or *Toxoplasma gondii* (219, 220). Contrary to this, CCR5 deficient mice show increased tolerance to LPS and reduced ulceration in a model of colitis using dextrane sulphate (219, 221).

Two CCR5 blockers were used in this thesis: Maraviroc and DAPTA. Both drugs have been shown to be efficient in blocking CCR5. Maraviroc is an approved CCR5 inhibitor for the treatment of HIV. It was synthesised by a multi-step process by Pfizer, and this compound belongs to the group of imidazopyridine (198). Dorr *et al.* have shown that Maraviroc is an allosteric inhibitor, which binds to CCR5 in a non-competitive way, suggesting that the binding site of Maraviroc is different from chemokine ligands or HIV glycoprotein (gp120) binding sites (198). In addition to this Maraviroc does not only inhibit binding of other ligands to CCR5 but also inhibits signalling through CCR5. Maraviroc has a high potency of inhibiting gp120 protein binding to CCR5 and therefore acts antiviral. Many different HIV-1 R5 tropic isolates were used and tested for the efficiency of Maraviroc in inhibiting CCR5 binding. Dorr *et al.* have shown that Maraviroc works efficiently in all R5 tropic patient samples, including samples from patients resistant to antiretroviral medication (198). All clinical trials have so far shown that Maraviroc is a safe drug, which is orally bioavailable, and has no severe side effects. Maraviroc was also tested in rats and dogs, where it was found to be safe. The drug is 30% absorbed from the gut and can be detected in the blood within 1.5 hours post treatment in dogs (198, 222).

The other CCR5 inhibitor D-Ala₁-peptide T-amide (DAPTA) is a synthetic peptide which consists of 8 amino acids (185-192) of the gp120 V2 region of the envelope of HIV, and is characterised by a high threonine content (ASTTTNYT) (223). This small non-toxic peptide binds competitively to the CCR5 region and inhibits binding of gp120 and chemokine ligands to CCR5. Furthermore it was shown that DAPTA is 34-180 times more potent in inhibiting CCR5 than Maraviroc, and makes DAPTA a very potent CCR5 inhibitor (224). Based on studies by Polianova *et al.* the drug is administered to mice i.v. once daily, and levels of DAPTA can be detected within the blood and the CSF 30-60 min and 90-145 min, respectively, suggesting that DAPTA is capable of passing the CSF-brain barrier (223, 224). In support of this, Rosi *et al.* have shown that DAPTA attenuates neuroinflammation in rats after chronic LPS injection into the brain by inhibiting

CCR5 expression by microglia and astrocytes (225). This effect is also accompanied by a reduction of TNF and IL-1 secretion by activated glial cells.

1.3.5.3 *Blockade of CXCR3*

CXCR3 has been shown to be predominantly expressed on activated CD4⁺ and CD8⁺ T-cells (226). Expression of CXCR3 could also be found on few NK-cells and B-cells although at very low levels (227). No expression of CXCR3 was detected on neutrophils, eosinophils and monocytes.

CXCR3 plays an important role during various inflammatory diseases such as MS, psoriasis, rheumatoid arthritis, and also during infection (228-231). There are a few studies using CXCR3 deficient mice in mouse models of viral encephalitis using MHV, WNV or LCMV, although this will be discussed in more depth in chapter 1.5. Due to the important role of CXCR3 during many inflammatory and infectious diseases, research has recently also focussed on developing CXCR3 antagonists although only few are currently available.

Here the CXCR3 antagonist, known as compound 21 was used. It is a imidazo-pyrazine derivative synthesised by Amgen and has been shown to be a small molecule antagonist binding specifically to CXCR3 (232). This compound inhibits binding of appropriate ligands CXCL9, CXCL10 and CXCL11 to CXCR3, and Du *et al.* have shown that compound 21 was potent in binding CXCL10 in *in-vitro* assays (232). In addition to this the efficacy of compound 21 was also evaluated in mice using a bleomycin induced lung inflammation model. In this model, compound 21 significantly reduced the infiltration of leukocytes into the inflamed lung, suggesting that this antagonist is potent in blocking CXCR3 (232). Compound 21 is administered s.c. once daily, and reaches stable levels in the plasma of mice.

1.3.6 **The expression of chemokines in the CNS**

Neurons and glial cells are sensitive post-mitotic cells that need a certain environment for survival and optimal functioning. Therefore chemokines that attract leukocytes from the periphery must be carefully regulated in the brain to prevent the inadvertent recruitment of immune cells from the periphery into the CNS.

1.3.6.1 *Constitutive chemokine expression in the healthy brain*

In principal, neurons, glial cells and vascular endothelial cells of the capillaries can produce chemokines in the CNS. To date, there is little data about chemokine expression in the CNS during homeostasis because most of the research is focussed on inflammatory conditions in the brain. Chemokines in the healthy brain play an important role during the development of the CNS and some chemokines are retained in the adult brain. In the adult brain, chemokines play important roles during neurogenesis, neuron-glia and glia-glia communication networks, can have neuro-hormonal properties and act as neurotransmitter (233). Many studies have reported that the chemokines CXCL12 and CX₃CL1 are constitutively expressed in the healthy brain (170, 234). CXCL12, and its corresponding chemokine receptor CXCR4, are highly expressed in the brain during development. The main source of CXCL12 is neurons. CXCL12 is important for the directional migration of neuronal progenitor cells to different areas of the brain (235). Soluble CX₃CL1 is ubiquitously produced in the brain by neurons, and signals to CX₃CR1 expressed on microglia. (236). Additionally it has been reported that the inflammatory chemokine CCL2 is also expressed in the healthy CNS of adult rats, although at low levels. For example, Purkinje neurons in the cerebellum and the dentate gyrus in the hippocampus have been shown to produce CCL2 in steady state (233, 237).

Some chemokines such as CCL3 and CCL5 and the CXC chemokine CXCL8 are transiently expressed in the CNS during embryogenesis which suggests that they may be important for the development of organs and migration of neuronal and glial cells (238). The chemokine receptors expressed in the adult rat brain are CCR1, CXCR4, CXCR2 and CX₃CR1. CCR1 is expressed on neurons in the cerebellum, CXCR4 on neurons and glial cells except oligodendrocytes and CXCR2 on oligodendrocytes. CX₃CR1 has been detected on microglia and macrophages in the meninges and choroid plexus (239, 240).

1.3.6.2 *Chemokine expression in the CNS during inflammation*

The recruitment of leukocytes into the CNS is a complex process and involves a variety of chemokines and cytokines. Blocking of chemokines and their receptors in various animal models has been shown to change leukocyte infiltrates within

the CNS. In all models of neuroinflammation, or infection, specific types of leukocytes enter the brain in response to chemokines, and this either contributes to pathogenesis or not. Only few studies have investigated the role of chemokines and their receptors during viral encephalitis, and these will be discussed in further detail in section 1.5. However studies of EAE informed us of the basic mechanism of neuroinflammation and helped us to understand the role of chemokine-mediated leukocyte entry into the CNS, which occurs in the brain not only during EAE, but also during viral encephalitis.

In EAE the following chemokines were expressed in the brain: CCL2, CCL3, CCL4, CCL5, CCL20, CXCL1, CXCL8, CXCL9 and CXCL10. Most of the chemokines detected during EAE are inflammatory chemokines. The spatial and temporal expression patterns of these chemokine varies during the disease and complicate matters even further (241-243). For example CCL2, CXCL1 and CXCL10 are mainly expressed by astrocytes, and have often been associated with acute phases of EAE, whereas CCL2 and CCL20 have often been found in the relapsing phase (241). Chemokine receptors are also expressed during inflammation in the brain, including CCR1, CCR2, CCR5, CCR6, CXCR1, CXCR2 and CXCR3. Receptors and chemokines can be expressed by neurons, glial cells and infiltrating leukocytes (244). The main source of chemokines during neuroinflammation are astrocytes and microglia (241). To investigate the exact role of chemokines in relation to leukocyte recruitment and disease outcome, knock out models have been used for most studies.

A large number of leukocytes infiltrating the brain of mice with EAE are monocytes which can develop into microglia once they enter the inflamed brain (139). It has been suggested that the CCL2-CCR2 axis is pivotal for the entry of monocytes into the brain. A study by Mildner *et al.* has demonstrated that in CCR2 deficient mice, intravenously injected with adoptively transferred CCR2⁺ Ly6C^{hi} cells, CCR2⁺ monocytes preferentially and rapidly traffic into the brain (33). However CCR2⁻ monocytes could not be detected in the inflamed brain of CCR2 deficient mice, which suggests that monocyte entry into the brain is CCR2 dependent. Furthermore in other EAE studies, CCR2 deficient mice showed delayed disease onset, milder forms of EAE, reduced demyelination and reduced numbers of monocytes entering into the CNS (215). This suggests that CCR2^{-/-} mice are less susceptible to EAE. However, it has been shown that the large

reduction of monocytes leads to increased infiltration of neutrophils into the brain as a compensatory mechanism. In support of this, Grainger *et al.* have recently demonstrated that CCR2 deficient mice develop a severe pathology in the gut during *Toxoplasma gondii* infection characterised by increased influx and activation of neutrophils, expressing many inflammatory cytokines (245). The authors have shown that ‘inflammatory’ monocytes control the pathogenic potential and activation of neutrophils by secreting prostaglandin E₂ (PGE₂). Thus in the absence of monocytes, neutrophils are highly activated and recruited to the inflamed tissue.

CCR1 deficient mice exhibit delayed disease onset and reduced severity of EAE due to impaired trafficking of monocytes and macrophages to the brain (246). In another study using CX₃CR1 deficient mice it has been observed that the severity of EAE increases due to impaired trafficking of NK-cells to the brain. NK-cells express CX₃CR1 on their surface and play an important role in regulating EAE severity (170). In contrast to CCR2, CCR1 and CX₃CR1, CCR5 deficient mice have not exhibited any noticeable changes in EAE susceptibility and disease severity (247). Thus, CCR5 appears to play only a minor role in the pathogenesis of EAE.

The CCR6-CCL20 axis has been shown to be important for the initiation of EAE (206). CCR6 is expressed on the surface of specific regulatory T-cells and Th17 cells (248, 249). In the CNS epithelial cells of the choroid plexus constitutively express CCL20. Using CCR6 deficient mice Reboldi *et al.* have shown that these mice are highly resistant to EAE, and that T-cell infiltration into the CNS occurs in two waves during EAE (206). The first wave of cells entering the brain is CCR6⁺Th17 cells, which infiltrate the brain most likely through the choroid plexus of the CSF-brain barrier. The entry of Th17 cells is indispensable for the entry of the second wave of T-cells comprised of Th17 and Th1 cells, which enter the CNS through activated parenchymal postcapillary venules of the BBB. This is consistent with studies by Kivisäkk *et al.*, who have demonstrated that T-cells first accumulate in the meninges and subarachnoid space and subsequently appear in the brain parenchyma (250). Thus, the CCR6-CCL20 axis is pivotal for the initiation of neuroinflammation in mice and humans and controls immune surveillance of the CNS.

Studies investigating the role of CXCR3 during EAE have produced contrasting results with regard to disease outcome. Liu *et al.* have demonstrated that CXCR3 deficient mice display more severe neurological symptoms during EAE, while T-cell accumulation in the brain is not altered compared to wild type mice (251). The same result was obtained in another study by Muller *et al.*, who have shown that CXCR3^{-/-} mice have widespread lesions throughout the CNS and similar numbers of T-cells in the brain compared to WT mice (252). Thus, CXCR3 seems to have a beneficial role during EAE. In contrast to this, other studies have demonstrated that blocking CXCR3 in mice lead to a milder onset of EAE and decreasing numbers of T-cells within the CNS. Hence, CXCR3 appears to be pathological in these studies of EAE (253, 254). The exact role of CXCR3 during neuroinflammation remains unclear and will be a focus in my studies, using a mouse model of viral encephalitis as described later.

Taken together, neuroinflammation results in the upregulation of many chemokines and cytokines which are able to modify leukocyte entry into the CNS. Thus, chemokines may potentially be good candidates for the development of new drug therapies for currently untreatable CNS diseases. However the complexity of the chemokine network makes this a challenging task and more studies are required to elucidate the exact dynamics of chemokines and their role in leukocyte attraction into the CNS.

1.4 Viral encephalitis

Viral encephalitis is an inflammation of the brain caused by viruses. If the infection of the brain involves areas such as meninges or spinal cord it is referred to as meningoencephalitis or encephalomyelitis, respectively. Meningitis is the most common form of viral CNS infection. Viral encephalitis is a relatively rare condition but can cause life threatening or fatal disease in the host depending on the affected brain area. According to the WHO there are annually 50,000 cases of Japanese encephalitis worldwide with a mortality rate of around 30-60% (255). Viruses which have an ability to infect cells of the CNS are referred to as neurotropic viruses. A list of medically important neurotropic viruses is shown in Table 1.2.

Table 1.2. Medically important neurotropic viruses

DNA viruses are highlighted in blue, RNA virus in red and retroviruses in green

Virus	Target cell	Geographical distribution
DNA viruses		
Herpes simplex virus	Neurons	Worldwide
Cytomegalovirus	Neurons	Worldwide
Adenovirus	Neurons, ependyma	Worldwide
RNA viruses		
Poliovirus	Motor neurons	India, Africa
Japanese encephalitis virus	Neurons	Asia, Australia
West Nile virus	Neurons	Europe, Africa, Americas
Rabies	Neurons	Europe, Asia, Africa, Americas
Equine encephalitis virus (Western, Eastern, Venezuelan)	Neurons	Americas
Mumps	Meninges, ependyma	Worldwide
Retroviruses		
HIV	Microglia	Worldwide
Human T-lymphotropic virus I	Astrocytes	Japan, Caribbean

Viruses can enter the CNS through various routes: direct entry through the BBB or blood-CSF barrier or by transport along axons of peripheral or olfactory nerves (256). The entry of virus across the BBB is more complex compared to entry via the blood-CSF barrier due to the intrinsic properties of the endothelium of the BBB. Generally viruses can cross the BBB or blood-CSF barrier directly by transcytosis or by infecting endothelial, meningeal or CPE cells, but can also be passively transported into the perivascular space of microvessels via migrating leukocytes. This mechanism is also known as the ‘Trojan-horse’ mechanism (123).

Viral encephalitides that are transmitted to vertebrate hosts by blood feeding arthropods, such as mosquitoes or ticks, are collectively named arboviruses (257). Three major virus families are part of arboviruses: alphaviruses, flaviviruses and bunyaviruses. Due to global warming and increased travelling between different countries, arboviral encephalitides have spread to many parts of the world, and have therefore become an increasing concern for humans. A recent example is the outbreak of West Nile virus in the Americas in 1999 (258).

Arbovirus infections make up almost 30% of all emerging infectious diseases in the last decade (259). Despite the fact that arboviral encephalitides are relatively rare they can cause severe and permanent neurological symptoms that can result in death. For instance the mortality rates in humans for JEV infection is 30-60%, for Eastern equine encephalitis infections 50-70%, for Western equine encephalitis 3-7% and for West Nile virus infection 10% amongst human neuroinvasive WNV cases (260, 261). Currently there are hardly any vaccines available for these life-threatening virus infections and more research is necessary to explore potential therapeutics.

There are several animal models available that are mostly low-risk to work with, providing us with the opportunity to enhance our knowledge of viral infections of the CNS. Semliki Forest virus (SFV), West Nile virus (WNV), lymphocytic choriomeningitis virus (LCMV) and mouse hepatitis virus (MHV) are amongst the most extensively studied mouse models of viral encephalitis and will be discussed in further detail in the following sections. As part of this thesis the main focus will be on Semliki Forest virus, belonging to genus alphaviruses, and this virus will be discussed in depth in the following sections.

1.4.1 Alphaviruses

The virus family *Togaviridae* consists of two genera: *Alphavirus* and *Rubivirus*. The genus *Alphavirus* consists of approximately 30 members, which can generally be divided into two groups based on their geographical distribution: Old World and New World viruses. Both groups contain medically important viruses that can cause a febrile illness accompanied by rash, joint pains or encephalitis which can be lethal in human and animal hosts (262). Alphaviruses are arboviruses and cycle naturally between the arthropod vector and the vertebrate host (263). Humans are usually dead-end hosts. Furthermore alphaviruses are geographically widely distributed with the exception of Antarctica. The incidence of infections in humans is generally low but regional outbreaks occur from time to time. A recent example in the past years is the large outbreak of chikungunya (CHIKV) in 2005-2006 in the region of the Indian Ocean (264). Due to climate changes alphaviruses spread more readily to new areas and become endemic there (265, 266).

Alphaviruses can be further divided into seven antigenically different complexes. Old World viruses possess a wide geographical distribution and usually cause arthralgia and rash, whereas New World viruses appear to be geographically confined to the Americas and typically cause encephalitis. Members of the Old World virus group include SFV, chikungunya (CHIKV), Ross River virus (RRV) and Sindbis virus (SINV) (262). The New World virus group consists of the Venezuelan equine encephalitis virus (VEEV), Eastern equine encephalitis virus (EEEV) and Western equine encephalitis virus (WEEV), with EEE being the most virulent equine encephalitis virus (267). Most of the New World viruses and a few of the Old World viruses such as SINV and SFV often cause encephalitis. However the severity of encephalitis is much higher among New World virus infections including EEEV, WEEV and VEEV (268-270). Good animal models, such as SFV, provide us with important insights into the pathogenesis of viral encephalitis and enable the development of new drugs.

1.4.1.1 *Structure and replication of Alphaviruses*

Alphaviruses are enveloped, spherical, single stranded (ss) positive RNA viruses, have a genome of approximately 12 kb which acts directly as messenger RNA (mRNA) (262). The genome consists of two open reading frames and encodes four non-structural proteins (nsP1-nsP4) close to the 5' end and five structural proteins near the 3' end of the genome (Figure 1.7). The first reading frame codes for the non-structural proteins which are necessary for viral replication and transcription, whereas the structural proteins are required for viral capsid and envelope production (262, 271, 272). The production of structural proteins is under the control of the subgenomic promoter which is activated during later stages of viral replication and leads to high levels of expression of subgenomic RNA. The two major structural proteins are E1 and E2, which form heterodimers on the envelope surface. Recently the structure of the alphavirus envelope has been unveiled and shows that the envelope consists of 80 spikes, each spike containing three E1/E2 heterodimers (273, 274). The E1 protein is important for membrane fusion and E2 initiates receptor binding (275-277).

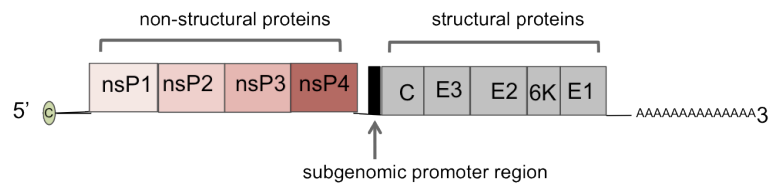


Figure 1.7 Structure of the alphavirus genome

The genome is comprised of non-structural and structural genes. The structural genes are regulated from the subgenomic promoter. Furthermore the genome consists of a methylated cap at the 5' end and a polyadenylated 3' end.

The exact cellular receptors for cellular entry by alphaviruses remain unclear but some studies have reported MHC-I, laminin receptors and glycosaminoglycans as possible receptors for alphaviruses (278-280). After fusion with the cell membrane, alphaviruses are taken up into endosomal vesicles. The pH changes inside the vesicles trigger conformational changes in the viral envelope proteins and lead to fusion of the envelope with the endosomal membrane of the host (281, 282). Subsequently the virus is released into the cytoplasm of the cell where it initiates viral replication. Following viral replication the viral proteins assemble and are packed into immature virions. In the next step virions bud from the cell membrane to release mature virions (Fig. 1.8) (283).

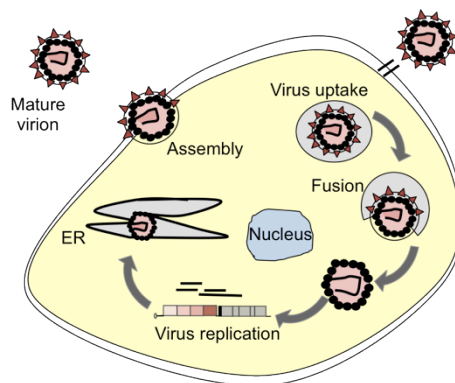


Figure 1.8 Life cycle of alphaviruses

Virus binds to a cellular receptor and is taken up into the cell inside via endocytosis. Depending on the pH, the virus envelope fuses with the endosome vesicle membrane, and virions are released into the cytoplasm. In the next step, viral RNA is directly translated into non-structural and later structural proteins. Parts of the structural polyprotein translocate into the endoplasmic reticulum (ER) where protein modifications and processing takes place. Structural and non-structural proteins finally assemble into immature virions which bud from the cell membrane of the host. Mature virions are released from the cell surface. Adapted from (262).

1.4.2 Semliki Forest virus

Semliki Forest virus (SFV) is a neuroinvasive low-risk pathogen, and is extensively used as model of viral encephalitis and demyelination. SFV was originally isolated in 1942 from a pool of female mosquitoes in the Semliki valley in Uganda (284). SFV is capable of infecting humans and animals including horses, monkeys, mice, rats, guinea pigs, rabbits and voles (285-287). However the natural host of SFV in the wild remains unknown. SFV occurs naturally throughout Africa and human outbreaks have been reported in 1987 in the Central African Republic where 23 patients showed symptoms of febrile illness, myalgia, arthralgia and headaches (288). The virus has been isolated from *Aedes aegypti* and *Aedes africanus* but also occurs in *Culex* and *Anopheles* species (288). To date, there is only one documented case of SFV induced death from 1978. This report has shown that a scientist working with the virulent Osterrieth strain suddenly developed meningoencephalomyelitis accompanied with neurological symptoms. The virus was isolated from the brain, CSF and spinal cord of the patient and a high viral titre was observed in the CNS tissue (289). It remains unknown why this patient became infected with SFV but it has been suggested that the patient might have been immunosuppressed, and would therefore have been more susceptible to virulent SFV infection (289). Although this is the only documented case of death in a human caused by SFV, seroconversion in laboratory workers can be commonly detected (289).

1.4.2.1 SFV strains

SFV can be divided into virulent and avirulent strains. Generally the categorisation of viruses into virulent and avirulent is utilised to describe the pathogenicity of a virus. Virulent virus strains have the ability of causing a lethal disease in the host, and are capable of replicating within the host and overcoming protective immune responses. Avirulent virus strains do not usually cause illness in the host and are asymptomatic (290). However, depending on the immune status of the host avirulent viruses can cause disease and virulent strains can cause mild disease in the host. Thus, the classification of viruses into virulent and avirulent strains is not always that clear. The virulent strains of SFV include L10, V13, Osterrieth and the prototype strain, and the avirulent strains are comprised of A8, A7, A7(74) and MRS MP192/7 (257, 286, 291). The best-

examined strains of SFV so far are L10, A7 and A7(74). The SFV strain L10 originates from the first SFV isolates from Uganda and was passaged eight times intracerebrally through adult mouse brains and two times through baby mouse brains (286). The avirulent strain A7(74) was derived from a pool of mosquitoes (original strain AR2066) in 1959 in Mozambique and was passaged seven times through neonatal mouse brains (292).

All strains of SFV are neurotropic but only virulent strains cause severe panencephalitis in mice within 5-7 days after infection. Avirulent strains usually only cause demyelination in the adult mouse that can last up to one month post infection and cause lethal encephalitis only in the developing mouse or in neonates. The age-dependent virulence and demyelination will be briefly discussed in sections 1.4.2.2 and 1.4.2.4. It was documented that SFV in the periphery infects a variety of cells that includes fibroblasts and skeletal, smooth and cardiac muscles. In the brain, all strains of SFV infect predominantly neurons and oligodendrocytes, and rarely endothelial, meningeal, ependymal and choroid plexus cells of the CNS (293, 294). Determinants of virulence are mainly located in the non-structural proteins of SFV and in particular in the nsp3 gene. The nsp3 gene of avirulent viruses contain a deletion of 21 nucleotides and an opal termination codon. However other mutations within the genome have been identified and it has been shown that all mutations act synergistically with regard to virulence (295-297).

1.4.2.2 *Restricted replication in the CNS*

Virulence of A7(74) has been reported to be age-dependent in mice. All mice up to 14 days of age die due to severe panencephalitis, similar to virulent infection with L10 (298). From post natal day 16 onwards all mice survive, and the replication of SFV seems to be restricted to certain areas of the brain in perivascular foci (299). No budding and mature virions are detectable in the brains of adult mice infected with A7(74). Characteristics of avirulent infections of adult mouse brains are: low replication of virus, absence of virus budding and accumulation of viral capsid proteins in form of aggregates within infected cells. (51, 298, 300). The difference in virulence between neonatal mice and adult mice is not due to defects or immaturity of the immune response but is dependent on the maturity of the CNS (298, 301). Oliver *et al.* have shown that

neonatal mice still undergo synaptogenesis, axonogenesis, gliogenesis and myelination (299, 302). With the maturation of the brain they have shown that neurons shut down their metabolic processes, including smooth membrane production, and become refractory to apoptosis. A study by Scallan *et al.* have demonstrated that these gold compounds, administered intraperitoneally to SFV A7(74) infected mice, induce full replication of avirulent SFV in neurons of adult mice (303). Thus, there is substantial evidence that an avirulent infection with SFV can be converted into a virulent infection characterised by high virus replication and spread throughout the brain (304). This process appears to be dependent on the differentiation status of neurons.

1.4.2.3 *Immune responses to SFV and viral clearance*

After intraperitoneal infection of mice, viral titres of SFV are cleared from the blood within four days post infection. Between days four and ten the BBB becomes leaky and allows the migration and entry of leukocytes into the CNS. (294, 305). Viral RNA can be detected in the CNS as early as three days post infection and infectious virus particles are cleared from the brain by day eight, although viral RNA can persist in the CNS for much longer (306). In the brain, SFV is recognized by PRRs expressed on the surface of neurons and glial cells. This initiates the production of TNF- α , type-I and type-II interferon and several interleukins that include IL-1 β (307).

Leukocytes enter the brain between days three and four when the BBB is permeable. However the kinetics of leukocyte entry has not yet been determined for SFV infection, and this is one of the aims in this thesis. Studies using severely B- and T-cell deficient mice have shown that these mice are unable to clear viral infection (51). Furthermore, IFN seems to play a crucial role in disease severity as mice which lack functional type-I interferon succumb to infection within 48 hours post infection (308, 309). Thus, the immune response is necessary to control viral replication. However, leukocytes, and in particular CD8⁺ T-cells, can also play a pathogenic role during SFV infection of the brain. Subak-Sharpe *et al.* have demonstrated that the depletion of CD8⁺ T-cells results in the reduction of demyelination suggesting a pathogenic role of these cells (310).

IgM antibodies are important for viral clearance from the blood, whereas IgG is capable of clearing viral antigens from the blood and brain. Nu/nu mice which are deficient in T-cells but produce IgM, control viremia but have a persistent CNS infection (311). SCID mice, which are deficient in B- and T-cells and produce no immunoglobulins, have a persistent infection of SFV in the blood and brain. However, transfer of IgG sera from wild type mice into SCID mice resulted in viral clearance within and outside the CNS, suggesting that IgG is important for the clearance of SFV (51). This highlights the role of antibodies during SFV infection.

T-cells also play an important role during SFV infection of the CNS. It has been demonstrated that depletion of CD8⁺ T-cells results in an enormous reduction in demyelination. This suggests that CD8⁺ T-cells are important for the elimination of infected oligodendrocytes. Further studies are required to confirm this hypothesis (308, 310). Depletion of CD4⁺ T-cells has led to the reduction of neuroinflammation (310). However the depletion of both CD4⁺ and CD8⁺ T-cells has significantly affected viral titres. Therefore it is most likely that T-cells play mostly pathogenic roles during viral encephalitis, characterised by demyelination and tissue damage of the brain as shown by Fazakerley *et al.* (312, 313). Histological analysis has shown that perivascular cuffs form around cerebral microvessels and peak after seven days post infection with SFV (307). MHC-I⁺ cells, cluster around sites of infection in the CNS. The expression of MHC-I and -II are both upregulated on activated microglia and astrocytes (307).

1.4.2.4 *Demyelination*

After SFV infection with the avirulent strain, the immune response eventually results in demyelination, starting approximately 14 days post infection (47, 312). Demyelination is most likely driven by pathogenic T-cell responses, and in particular by CD8⁺ T-cells, as mentioned before. A study has shown that by post infection day 20-30 most of the lesions in the brains of BALB/c mice are repaired due to various remyelination processes. In SJL mice, it has been shown that remyelination takes much longer, and lesions persist in the brain for up to 12 months (314). Infection with the virulent strain of SFV, such as L10, does not result in demyelination because mice die before immune-mediated

demyelination processes start and therefore this process is seemingly obscured by death (267, 315).

1.4.3 West Nile virus (WNV)

WNV is a spherical and enveloped positive single stranded (ss) RNA virus with a genome size of approximately 11 kb (316). WNV belongs to the family *Flaviridae*, genus *Flavivirus* and is primarily transmitted by mosquitoes including *Culex* species and sometimes *Aedes albopictus* or *Aedes vexans* (317). Within the genus *Flavivirus*, WNV belongs to the Japanese encephalitis serogroup (316). WNV was originally isolated from a patient with febrile illness in the West Nile district in Uganda in 1937 (318, 319). Cases of WNV infection have since been reported from other regions in Africa, Middle East, Asia and Australia (320, 321). In 1999 WNV caused an outbreak in North America starting in New York city, and over the years WNV has spread all over the Americas and has become endemic there (258, 322, 323).

In humans 70-80% of WNV infections are asymptomatic (324). The incubation period is usually between 2 and 14 days and symptoms of WNV infection can generally be divided into either a mild febrile illness accompanied with headache, pains, myalgia and arthralgia, or into a neuroinvasive syndrome that includes symptoms like paralysis, meningitis and encephalitis. Of all symptomatic patients approximately 1% develop either encephalitis (60%) or meningitis (40%) that can result in death (261). This usually concerns immune-compromised patients and the elderly (174, 325). The American East coast strain, designated as NY99, is highly neuroinvasive, leads to severe forms of encephalitis in mouse models and has been extensively studied over time in respect of pathogenesis (326, 327).

1.4.3.1 WNV replication

The 11 kb genome consists of one open reading frame that is translated into one polyprotein which is then cleaved by enzymes into three structural proteins (C, prM and E) and seven non-structural proteins known as NS1, NS2A, NS2B, NS3, NS4A, NS4B and NS5) (Figure 1.9). The structural proteins are important for

capsid and envelope production of the virus and the non-structural proteins are necessary for the replication process (316, 328, 329).

WNV enters the cell by binding to an unknown cell receptor and is taken up into endosomes. The pH inside the endosomes becomes more acidic over time and finally triggers the fusion of virus with the membrane of the endosome which results in uncoating of the virus. The virus replicates in the cytoplasm and the (+) ssRNA genome is directly translated into protein. After production of structural proteins the virions assemble to mature virions and exit the cell via exocytosis (316, 330, 331).

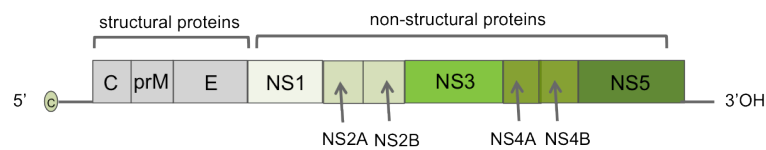


Figure 1.9 Genome of West Nile virus

The genome of West Nile contains a methylated cap at the 5' end but no polyadenylated 3' end. The genome is comprised of structural and non-structural genes which are directly translated from the RNA genome. Adapted from (316).

1.4.3.2 WNV infection of the CNS

Infection of the CNS with WNV occurs within 5 days post infection can lead to meningitis, encephalitis or acute flaccid paralysis depending on which area of the CNS is affected. WNV can enter the CNS through three different routes: haematogenous route via BBB or blood-CSF barrier, retrograde axonal transport route via peripheral nerves and the olfactory route via infection of olfactory neurons to the olfactory bulb (129, 332, 333). WNV can cross the BBB or blood-CSF barrier through passive transport through the endothelial or choroid plexus cells or through direct infection of these cells (334, 335). The other possibility of crossing the BBB is through extravasation of infected leukocytes across the activated endothelium. (336, 337). The endothelium becomes activated in the presence of high levels of inflammatory cytokines that include TNF- α , or after activation of matrix-metalloproteinases (326, 338).

WNV primarily infects neurons and, only in rare cases, glial and cerebral endothelial cells of capillaries. Infection of neurons can lead to apoptosis or

necrosis of the cell. The injury and subsequent damage of neurons can be directly induced through the virus or can be a consequence of immune responses in the CNS (326, 339). In either case, WNV infection of the CNS leads to the activation of microglia and to the infiltration of leukocytes into the perivascular space and into the brain parenchyma. High numbers of macrophages, CD4⁺ and CD8⁺ T-cells and plasma cells have been observed during WNV encephalitis. Viral brain lesions due to neuronal damage and loss, are predominantly found in the hippocampus, brain stem, cortex, thalamus spinal cord and cerebellum (340, 341). Dying neurons can release inflammatory chemokines and cytokines such as CXCL10, IL1- β and TNF which can have detrimental effects on adjacent neurons that are uninfected and subsequently lead to neuronal loss (88, 342).

1.4.3.3 *Immune responses to WNV in the periphery and the CNS*

Immune responses are crucial for viral clearance, but must be tightly controlled in the brain to prevent neuronal damage and loss. Severely immune-compromised mice show high viral loads and persistent infection of the CNS, highlighting the importance of cell-mediated immune responses in the brain (343). After initial infection with WNV, nucleic acid can be detected by PRRs at the site of infection which initiates the production of pro-inflammatory cytokines, chemokines and type-I interferons. Type-I interferons are key players in innate immunity and can be produced by many cells during infection. Mice deficient for the IFN- α/β receptor exhibited increased viral replication, widespread infection and rapid CNS invasion, which subsequently results in earlier death (344).

Macrophages and DCs can be infected with WNV and are amongst the first cells involved in the recognition of WNV and antigen presentation outside the CNS (337, 345). Depletion of macrophages during WNV infection results in higher viremia and a 50% increase in mortality in mice, accompanied with enhanced neuroinvasiveness of WNV (346). Furthermore monocytes, which are precursors of macrophages, are also important for viral clearance from the periphery and clearance of virus from the CNS (214). This function is dependent on the expression of CCR2. The role of chemokine receptor will be further discussed in section 1.5.

NK-cells and γ/δ T-cells both produce IFN- γ which is important for the dissemination of WNV. (347). However, only γ/δ T-cell deficient mice, but not NK-cell deficient mice, have displayed increased lethality, higher viral loads in peripheral tissues and more rapid dissemination of WNV in the CNS (348, 349). These studies have suggested that γ/δ T-cells are the main producers of IFN- γ . IFN- γ has direct antiviral activities and is primarily required for early innate immune responses in order to reduce viral spread in the periphery and neuroinvasion (347). Neutrophils have been shown to play a dual role during WNV. Bai *et al.* have shown that neutrophil depletion prior to WNV infection leads to reduced viral loads and increased survival whereas depletion after viral infection leads to increased viremia and enhanced mortality (350). Therefore the timing during infection is crucial and determines what role neutrophils play during WNV infection. During early stages of infection neutrophils are infected by WNV and contribute to the viral dissemination but during later stages of infection neutrophils are beneficial and contribute to viral clearance (350).

B-cell deficient mice die due to persistent infection of the CNS and high viral titres in the blood and brain (351). Similar to SFV studies Diamond *et al.* have shown that the early transfer of IgM limits viremia and prevents dissemination into the CNS (352). T-cells are one of the key players during WNV infection. Depletion of CD4⁺ and CD8⁺ T-cells leads to persistent infection of the brain and enhanced neuronal loss and damage (140, 141, 348). CD8⁺ T-cells are important for viral clearance from the brain but excessive CD8⁺ T-cell responses lead to neuropathology associated with loss and damage of uninfected neurons (353). Thus, CD8⁺ T-cell responses can be either beneficial or detrimental to CNS infection depending on the extent of viral infection and CD8⁺ T-cell accumulation in the brain. CD4⁺ T-cells also play important roles during WNV infection similar to SFV infection. Mice deficient in CD4⁺ T-cells exhibit higher mortality rates and viral titres in the CNS (141). CD4⁺ T-cells are important for providing help by priming B-cells and maintaining CD8⁺ T-cell responses. Finally T_{regs} seem to influence disease severity during WNV infection. Patients with a low number of T_{regs} were more likely to develop symptoms whereas patients with normal or increased levels of T_{regs} usually did not develop symptoms during WNV infection (354). Further studies are required to elicit their role during WNV pathogenesis.

1.5 The role of chemokines in the pathogenesis of neurotropic viruses

Encephalitis caused by neurotropic viruses is characterized by the activation of glial cells and neurons, increased permeability of the BBB and blood-CSF barrier, activation of vascular cerebral endothelium and, most importantly, by the large infiltration of leukocytes from the periphery into the perivascular space of capillaries or into the brain parenchyma (355). Several ‘knock out’ mouse models, deficient for CCR2, CCR5 and CXCR3, have shown that chemokines are pivotal in attracting leukocytes to sites of inflammation for viral clearance. However large influx of leukocytes into the CNS of virally infected mice is associated with pathology in the brain and can cause loss, and damage, of neurons and glial cells (356).

Chemokines are induced in a highly specific manner during viral infection and orchestrate leukocyte infiltration into the CNS with the goal of removing infected cells and clearing the virus from the brain with minimal neurological damage to the brain. A clear chemokine expression pattern during viral brain infection has not yet been established (357). The chemokines expressed during viral encephalitis can be very distinct between different pathogens, and depend on virus strains and host factors including age and immune status of the host. Thus, the differential chemokine expression during viral infection highlights the complexity of the chemokine-mediated immune responses, and as part of this thesis I aim to conduct a thorough chemokine expression analysis during SFV and WNV infection.

Some mouse models have examined cell-mediated immunity during viral encephalitis but the involvement of chemokines in these immune processes is still not fully understood and shall be analysed as part of this thesis. Amongst the best-characterised mouse models with regard to chemokine-mediated immune responses in the CNS during viral encephalitis are WNV, LCMV and MHV, although these studies have not comprehensively investigated the role of chemokines. Instead, the authors of these studies have selected a few chemokines and investigated their role using gene deficient mice. Small molecule antagonists have not been used in this context. The current knowledge

of the role of chemokines during WNV, LCMV and MHV encephalitis will be briefly introduced here and will build the basis for this thesis.

1.5.1 Chemokine-mediated immune responses during WNV infection

WNV infection of the CNS leads to the high expression of CCR2 (CCL2, CCL7 and CCL12), CCR5 (CCL3, CCL4 and CCL5) and CXCR3 (CXCL9 and CXCL10) ligands (153, 173, 358, 359). In particular CXCL10 and CCL5 have been shown to be highly expressed in WNV infected brains. Neurons appear to be the main source of chemokines but also astrocytes and microglia are able to express considerable amounts of chemokines such as CXCL10, CCL2 and CCL5 (360). The cellular infiltrate within the CNS during WNV infection of mice consists mainly of T-cells, NK-cells, monocytes and neutrophils (173). In humans the infiltrate is slightly different from mice and consists mainly of CD8⁺ T-cells and to a less extent CD4⁺ T-cells and B-cells. The T-cells are mainly found in the brain parenchyma and perivascular space. NK-cells and monocytes are mostly confined to the perivascular space (153, 361).

Murine CCR5 is expressed on activated T-cells, NK-cells, activated microglia and a few monocytes (212). CCR5 seems to play a crucial role in the pathogenesis of WNV infection and is critical for survival (173, 362). A study conducted by Glass *et al.* has shown that CCR5 deficient mice cannot control viral loads in the CNS, have reduced numbers of CD4⁺ and CD8⁺ T-cells, NK-cells and macrophages entering the brain, which cumulatively results in rapid death and 100% lethality (173). However, mice can be rescued from this phenotype after adoptive transfer of CCR5⁺ splenocytes from wild type mice into CCR5^{-/-} mice, and the survival rate after WNV infection can be restored to a similar level compared to that in infected wild type mice (173). The extent of viral clearance in the periphery has not been affected in CCR5^{-/-} mice and therefore a CNS specific role of CCR5 has been suggested.

In humans a mutation in the CCR5 gene, referred to as CCR5 Δ 32 mutation, leads to complete loss of function of CCR5 and is found in up to 1% of the Caucasian population. Humans who are homozygous for the mutation are naturally resistant to HIV infection (197). A few studies have shown that humans with the CCR5 Δ 32

mutation are more susceptible to symptomatic WNV disease, often associated with the development of meningitis or encephalitis (173, 361). Based on these studies it has been suggested that CCR5 is a crucial determinant of WNV severity. Later, these data were contradicted by two other studies that have shown that the CCR5 Δ 32 mutation does not correlate with symptomatic WNV infections (363, 364). Thus, the exact role of CCR5 during viral encephalitis remains unclear.

CXCR3 is mainly expressed on T-cells and binds to CXCL9, CXCL10 or CXCL11. CXCL10 is one of the most highly upregulated chemokines during WNV infection and is primarily expressed by neurons very early during infection (153). CXCL10 deficient mice exhibit a significant reduction in CD8⁺ T-cells, higher viral titres in the brain and enhanced mortality. However it should be noted that the effect of CXCL10 on the pathogenesis is specific to the CNS because viral titres and clearance of WNV in peripheral tissues have not been shown to be different from wild type infected mice (153). Thus, these data suggest a specific role for CXCL10 in the recruitment of CD8⁺ T-cells into the CNS, which results in reduced viral titres and mortality.

CCR2 is mainly found on 'inflammatory' monocytes and binds to CCL2, CCL7 and CCL12 expressed in the inflamed brain (173, 214). A large number of these 'inflammatory' monocytes enter the brain during WNV infection and it has been suggested that they give rise to microglia and perivascular macrophages (106). The role of monocytes in WNV infection has been shown to be protective, or pathogenic, depending on the route of virus administration. In the intranasal model, monocytes appear to be pathogenic and reduce survival, whilst in the intraperitoneal model monocyte entry into the CNS leads to an increase in survival and decreased viral titres (106, 346). Lim *et al.* have demonstrated that CCR2 deficient mice infected intraperitoneally with WNV die earlier and have enhanced viral titres in the CNS, suggesting a protective role of CCR2 (214). However the authors have suggested that CCR2 is not directly involved in monocyte trafficking to the CNS but is rather important for the egress of monocytes from the bone marrow. Thus, the monocytopenia observed in CCR2^{-/-} mice leads to the subsequent enormous reduction of monocytes accumulating in the brain and is independent of the ability of monocytes to traffic into the brain.

Furthermore Lim *et al.* have shown that adoptively transferred CCR2⁺ but not CCR2⁻ monocytes from wild type mice are capable of entering the CNS (214). This study suggests that CCR2 is critical for monocytosis and leads to the subsequent accumulation of monocytes in the brain where they play a protective role during WNV infection. Based on these data the role of CCR2 is not yet fully understood.

CXCR4 is expressed on T-cells, NK-cells, neutrophils and many other leukocytes. CXCR4 is one of the 'primordial' chemokine receptors and depletion of CXCR4 in mouse embryos is lethal (365). The ligand CXCL12 is expressed by endothelial cells of cerebral microvessels and retains CXCR4⁺ leukocytes in the perivascular space and prevents the crossing of leukocytes into the brain parenchyma. McCandless *et al.* have shown that blocking CXCR4, with the blocker AMD3100, increases infiltration of CD8⁺ T-cells into the brain parenchyma and leads to enhanced viral clearance (366). This leads to a better disease outcome and enhanced survival in WNV infected mice. Thus, blocking CXCR4 may be a potential way of treating acute viral encephalitis in the future.

1.5.2 Lymphocytic choriomeningitis virus infection

Lymphocytic choriomeningitis virus (LCMV) belongs to the family *Arenaviridae* and infects mice in nature. Intracranial injection of mice with LCMV leads to meningoencephalitis 6-8 days later resulting in death. The cellular infiltrate of LCMV in the CNS consists of macrophages, high numbers of CD8⁺ T-cells and only few CD4⁺ T-cells (320, 367, 368). T-cells have been shown to play a pathogenic role during LCMV infection and appear in the brain five days post infection. Most of the CD8⁺ T-cell deficient mice have been shown to survive fatal i.c. injection with LCMV. Additionally athymic nude mice, which are severely deficient in T-cells, do not develop symptoms after LCMV infection (369, 370). Asensio and Campbell have conducted a study investigating chemokine expression during LCMV infection (128). They have observed that chemokines are upregulated as early as three days post infection. CXCL10 is the most highly upregulated chemokine in the CNS followed by CCL5, CCL2, CCL4 and CCL7. With the progression of the disease, chemokines are further upregulated and additional chemokines such as lymphotactin, CXCL16, CXCL2 and CCL3 are produced. It is worth noting that the expression of chemokines in the CNS is comparable to that

of peripheral tissues. CXCL10 has been shown to be produced mainly by resident cells of the brain including choroid plexus and meningeal cells.

Furthermore Asensio and Campbell have investigated whether nude mice which are resistant to LCMV infection show altered chemokine expression patterns in the infected brain (128). No changes in chemokine expression have been detected in nude mice compared to healthy control mice, despite high viral titres in the brain (371). Thus, it has become evident that T-cell responses during LCMV are pathogenic and the presence of virus is not enough to alter chemokine expression in the CNS. Other factors such as type-I or type-II IFN, or TNF- α , have been suggested as possible candidates for the initiation of chemokine expression (372, 373). It has been reported that IFN- γ deficient mice upregulate chemokines to a certain extent but that the magnitude of expression was much lower compared to WT mice suggesting only a weak modulating function of IFN- γ (128).

Several chemokine receptor 'knock out' mice have been used to investigate the role of chemokines during LCMV infection. CCL3, CCR5, CCR1 and CCR2 deficient mice all succumb to the disease and do not display a changed phenotype compared to WT mice (319, 374). Additionally the reduced infiltration of macrophages into the CNS in CCR1 and CCR2 knock out mice suggests that these receptors play a minor role in the attraction of macrophages and monocytes into the CNS (320).

Studies using CXCR3 and CXCL10 deficient mice have both shown enhanced survival during LCMV infection with a marked reduction of CD8⁺ T-cell infiltration into the CNS (322, 323). Thus, CD8⁺ T-cells play a detrimental role in the pathogenesis of LCMV infection. Adoptive transfer of CXCR3⁺ CD8⁺ T-cells into CXCR3^{-/-} mice results in a reversal of the phenotype and mice succumb to the disease. The generation of effector T-cells in the spleen of CXCR3^{-/-} and CXCL10^{-/-} mice is unaffected and CD8⁺ T-cells are still capable of trafficking into the CSF but with reduced efficiency. However the infiltration of CD8⁺ T-cells into the brain parenchyma in the absence of CXCR3 or CXCL10 is impaired (322, 323). This suggests that the CXCL10-CXCR3 axis is important for rapid positioning of T-cells within virally infected brain parenchyma, although other chemokines

appear to be involved in attracting a few CD8⁺ T-cells into the brain. Infiltration of CD8⁺ T-cells into the brain parenchyma, and other important parts of the brain, is crucial for the outcome of LCMV infection. The other CXCR3 ligands (CXCL9 and CXCL11) have not shown any compensatory effect for CXCL10 and therefore CXCL10 appears to be the major player in the attraction of CD8⁺ T-cells into the CNS (322). In contrast to these studies, WNV studies have shown that CXCR3 is beneficial for the pathogenesis of WNV infection, by attracting T-cells into the brain (375).

1.5.3 Mouse hepatitis virus infection

Another well-studied model of viral encephalitis is mouse hepatitis virus (MHV) which belongs to the family of *Coronaviridae*. MHV is a positive ssRNA virus that can cause acute encephalomyelitis leading to death, or demyelination, in surviving mice (376). The outcome of MHV infection depends on the virus strain and route of virus inoculation. The neurotropic strain, JHMV, induces lethal encephalitis in mice and is characterised by a cellular infiltrate consisting mainly of macrophages and neutrophils. Hence, CCL2 and CXCL2 are highly expressed during JHMV infection, similar to WNV or LCMV infection. In comparison to JHMV, the neuroattenuated strain RA59 causes mild encephalitis which is cleared by day 7. The chemokine profile is different in these mice expressing mainly CXCL9 and CXCL10 (174). MHV infects glial cells including astrocytes, microglia and oligodendrocytes.

Clearance of virus from astrocytes and microglia depends on the action of CD8⁺ T-cells by releasing perforin, and clearance from oligodendrocytes depends on IFN- γ (326, 377). In response to acute viral infection of the CNS, primarily CD4⁺ T-cells, CD8⁺ T-cells, NK-cells and macrophages enter the brain (330). Lane *et al.* have investigated the role of T-cells. They have shown that CD4^{-/-} and CD8^{-/-} mice have reduced demyelination, fewer leukocytes accumulating in the brain and increased viral titres, associated with higher mortality. In particular CD4^{-/-} mice infected with MHV display reduced neuroinflammation and reduced levels of CCL5. Thus, CD4⁺ T-cells regulate neuroinflammation and extent of demyelination. This study is in agreement with WNV studies where similar results were found. However T-cell deficient mice exhibit higher survival and milder

symptoms during LCMV infection. Thus, the role of T-cells in the pathogenesis of viral encephalitis differs with the pathogen.

The reduced expression of CCL5 during MHV infection has been shown to reduce macrophage numbers in the inflamed CNS which in turn might explain the reduction in demyelination (326). This has also been shown in studies using SFV as model of infection as discussed before (378). Infection of severely immunocompromised mice does not lead to demyelination despite higher viral titres in the CNS compared to wild type mice and highlights the importance of the immune system in the pathogenesis of MHV infection (328, 329). The role of NK-cells infiltrating the CNS during MHV infection is not yet clear. However Trifilo *et al.* have shown that NK-cells might be important for viral clearance within the CNS of mice during MHV infection, due to the secretion of IFN- γ from these cells (379). Generally data about the contributions of NK-cells to antiviral immunity within the CNS are sparse and need to be determined in detail.

CXCL10 is upregulated very early during infection and can be detected in the brain within 24h post infection (129). CXCL10 has been shown to co-localise with MHV infected areas in the brain and the primary source of CXCL10 in the CNS has been identified as astrocytes even though microglia also produce this chemokine (129). Dufour *et al.* have reported that CXCL10^{-/-} mice display reduced T-cell numbers in the CNS, reduced demyelination, lower IFN- γ levels and higher viral titres in the CNS, associated with higher mortality (380). This suggests that CXCL10 is important for the attraction of CXCR3⁺ T-cells into the CNS for viral clearance. Stiles *et al.* have then tested the hypothesis whether the loss of CXCL10 also leads to impaired effector T-cell generation (381). They have found that the generation of effector T-cells was not impaired in CXCL10 deficient mice infected with MHV, and they have confirmed that the role of CXCL10 during MHV encephalitis is only important for trafficking of T-cells into the CNS. In subsequent experiments Stiles *et al.* have investigated the role of CXCR3 during MHV infection by using CXCL10 neutralising antibodies or CXCR3 neutralising antiserum (381). The authors have demonstrated that the blockade of CXCR3 resulted only in a modest decrease of CD4⁺ T-cell numbers within the CNS while the number of CD8⁺ T-cells was unaffected. Additionally viral titers in the brain were not altered, and survival was similar to untreated MHV-infected mice. The

reason for this discrepancy between receptor or ligand blocking during MHV infection remains unclear.

Other chemokines reported to be upregulated during MHV infection are CCL2, CCL3, CCL4, CCL5, CCL7 and CXCL2 (129). The expression of CCR1, CCR2, CCR5 and CXCR3 have also been found in the brain during infection. CCR2 deficient mice exhibit reduced T-cell and macrophages numbers accumulating in the brain and uncontrolled high viral titres, resulting in 100% mortality ten days post infection (334). Thus, CCR2 is an important chemokine receptor during MHV pathogenesis and is required for T-cell, and macrophage, entry into the CNS.

CCR5 has been shown to be dispensable for the entry of CD8⁺ T-cells into the CNS but is important for antiviral activities of CD8⁺ T-cells using CCR5 deficient mice infected with MHV (1, 326, 382). In addition to this Glass *et al.* have shown that CCR5 is highly expressed by macrophages and microglia, and the infection of CCR5 deficient mice with MHV resulted in a significant reduction of macrophages entering the CNS (382). This reduction was furthermore shown to be associated with reduced demyelination. Thus, the authors have suggested that CCR5 is involved in demyelination by allowing macrophages to enter the brain during MHV infection, and it is these cells which aggravate demyelinating processes within the CNS of these mice. These studies are in contrast to WNV studies where CCR5 is important and is indispensable for T-cells trafficking into the CNS, suggesting that CCR5 plays differential roles during viral encephalitis depending on the virus model used (173).

Murine neutrophils express primarily CXCR2 and bind to CXCL1, CXCL2 and CXCL5. Neutrophils play a role in the breakdown of the BBB, and in this way these cells facilitate the entry of other leukocytes into the brain. During MHV infection neutrophils seem to play a protective role. Blocking of CXCR2 with an antibody almost completely blocks entry of neutrophils into the brain and leads to decreased MMP9 activity, reduced BBB permeability and higher viral titres. Subsequently all mice rapidly succumb to MHV infection (340, 383). Thus, CXCR2 plays an important role in neutrophil attraction which is indispensable for survival of the host during MHV infection. However, during WNV studies Bai *et al.* have shown that neutrophils can play beneficial or detrimental roles in the

pathogenesis of WNV infection, depending on the timing of neutrophil depletion (350).

In summary, the existing data on the role of chemokines during viral encephalitis have made it clear that chemokines may play differential roles during encephalitis, depending on the virus used for infection. It is not yet clear what role chemokines play during alphavirus infections. Additionally the analysis of chemokine expression during viral encephalitis has not been thoroughly analysed so far and it is possible that other chemokines might play important roles during brain infection. This will be addressed as part of my thesis.

1.6 Thesis aims

As discussed in the general introduction, chemokines are important regulators of leukocyte trafficking in the body. The healthy CNS contains few leukocytes which exert immunosurveillance of the brain to enable fast detection in response to pathogens invading the CNS. Leukocytes within the brain can be either beneficial or detrimental to the host depending on the virus and strain used. Although mouse models of viral encephalitis such as WNV have been well described, a thorough picture of chemokine expression and chemokine-mediated leukocyte influx during viral encephalitis has not yet been established. In particular, there are sparse data on chemokine expression and their role in leukocyte recruitment for alphavirus encephalitides. Developing a deeper understanding of these key aspects of the encephalitic process is central to the ability to therapeutically manipulate it.

Based on previous studies presented in chapter 1.5 it was hypothesized that chemokines are highly upregulated during viral encephalitis and lead to leukocyte infiltration into the CNS. *Therefore the main aim of this thesis is to define the form and magnitude of chemokine expression and kinetics of leukocyte entry during viral encephalitis, using SFV as model of infection.* Furthermore it has been demonstrated for some encephalitic viruses, such as WNV, that chemokine receptors can play a pivotal role in the pathogenesis of the infection. *Therefore in addition to this, a further aim is to define the role of key chemokine receptors during viral encephalitis to identify relevant therapeutic targets for the treatment of viral CNS infections.*

In chapter 3 of this thesis I set out to perform a thorough analysis of chemokine expression during avirulent and virulent infection with SFV, identifying key chemokines upregulated in the brain during viral encephalitis.

In chapter 4 the kinetics of distinct leukocyte subsets entering the CNS during viral encephalitis will be investigated and interpreted in the context of chemokine expression during SFV infection.

In chapter 5 a thorough analysis of chemokine expression in the CNS during lethal WNV infection will be conducted and compared to the expression of chemokines in the brain in response to SFV infection.

In chapter 6 the role of key chemokine receptors during viral encephalitis will be determined using specific pharmacological chemokine receptor antagonists. This is the first time such pharmacological blockers are used in the context of viral encephalitis.

Chapter 2

Materials and Methods

2.1 General reagents and buffers

Plastics: All plastics used for experiments were purchased from Corning (Loughborough, UK) and Gibco (Invitrogen, Paisley, UK) unless indicated otherwise. 1.5 ml microcentrifuge tubes were purchased from Eppendorf (Stevenage, UK). QPCR plates were purchased from Starlab (Milton Keynes, UK)

Tips: All tips were filter tips and purchased from Starlab.

1% acid alcohol: 1% concentrated Hydrochloric acid (HCl) was added to 100 ml of 70% Ethanol

Citrate buffer (0.1 M): 2.1 g citric acid monohydrate (Sigma, Poole, Dorset, UK) and 700 ml distilled water adjusted to pH6 using 2 M NaOH. Water was added again to make up a total volume of 1ml of buffer.

Complete medium: RPMI1640, 10% heat inactivated fetal bovine calf serum, Penicillin (100 units/ml), Streptomycin (100 µg/ml) and L-Glutamine (2 mM) (Invitrogen, Paisley, UK).

DAB solution: 1 drop of buffer stock solution, 2 drops DAB stock and 1 drop of Hydrogen Peroxide stock (all from Vector laboratories, Peterborough, UK) were added to distilled water and made up to a final volume of 1 ml.

Digestion buffer: 9.6 ml 1x Hank's balanced salt solution (HBSS) and 250 µl HEPES buffer (Sigma) were mixed.

Eosin Y solution: 1% Eosin Y (Cell Path, Newtown, UK) was added to tap water

ELISA wash buffer: 1x PBS (Invitrogen) was mixed with 0.5% Tween 20 (Sigma)

FACS buffer: 500 ml Phosphate buffered saline (PBS) without Ca²⁺ and Mg²⁺ was mixed with 0.5% fetal calf serum (FCS) and 2 mM EDTA (all reagents from Invitrogen)

10% complete GMEM: 10% new borne calf serum (NBCS) and 10% Tryptose phase broth was added to GMEM solution (all from Invitrogen)

0.5% Hydrogen Peroxide in Methanol: 5 ml of 30% H₂O₂ was mixed with 295 ml of Methanol (both from Sigma)

4% Paraformaldehyde solution (PFA): 40 g of Paraformaldehyde powder (Sigma) were added to ~ 900 ml of heated (60°C) PBS and stir until powder dissolves. A few drops of 1N NaOH were added to raise the pH to 6.9. After PFA had dissolved, the solution was filtered and stored at -20°C for further use.

PBSA: 0.75 g bovine serum albumin (BSA) in 100 ml PBS (both from Invitrogen)

Rinsing buffer: 2 mM EDTA (Ambion, Paisley, UK) and 0.5% FCS (Sigma) were added to 1x HBSS (Gibco, Invitrogen)

Scott's tap water: 3.5 g sodium hydrogen carbonate and 20 g magnesium sulphate were added to 1 litre (l) of distilled water. Thymol (Sigma) was added to inhibit mould formation

Sucrose solution: 20g sucrose (Sigma) was dissolved in 100 ml 10x Tris-Sodium-EDTA buffer (TNE buffer)

TE buffer: 10 mM Tris (HCl) pH8 and 1 mM EDTA were mixed

10x TBST: To prepare 1 l 24.23 g Tris base (= 200 mM), 87.66 g NaCl (1.5 M) and 10 ml Tween[®] 20 (1%) were added to 800 ml of distilled water. The solution was adjusted to pH 7.6 using concentrated HCl and diluted 1:10 to obtain 1x TBST

10x TNE buffer: 15.76 g Tris (pH7.5), 3.7 g EDTA (5 mM) and 16.4 g NaCl (140 mM) were dissolved in a final volume of 200 ml distilled water.

2.2 Mice

For all studies unless stated otherwise, wild type mice C57BL/6 were purchased from Harlan laboratories (Bicester, UK) and were given one week to acclimatise before any experimental procedures. Age and sex matched wild type (WT) and D6 deficient mice on a C57BL/6J (F11) background strain were bred in house for direct comparison studies. CCR2-null mice on a C57BL/6 background were kindly provided by Prof. Nibbs and originally purchased from Jackson laboratories

(Maine, USA). Both in-house bred and purchased mice were maintained at the University of Glasgow Central Research Facility (CRF) under specific pathogen free conditions and used between 8 and 12 weeks of age for all studies. All procedures were carried out in accordance with the United Kingdom Home Office regulations under the authority of the appropriate project and personal license. The group size of mice, used in each experiment, was selected based on previous studies to obtain statistical significance in accordance with the animals (Scientific Procedures) Act 1986, which has at its centre the '3Rs' concept: replacement, refinement and reduction.

2.3 Viruses

Virus stocks for Semliki Forest virus strain A7(74) and L10 were kindly provided by Prof. John Fazakerley (The Pirbright Institute, Pirbright, UK) and kept at -80°C . Both strains of SFV were stored at a stock concentration of 10×10^{10} PFU/ml in PBSA. West Nile virus (WNV) strain NY99 was stored and kept at the containment level 3 laboratory at the Animal Health and Veterinary Laboratory Agencies (AHVLA, Surrey, UK).

2.4 Antibodies for flow cytometry

Monoclonal antibodies, used for flow cytometry, were labelled with either Biotin, VioBlue (VB), fluorescein isothiocyanate (FITC), R-phycoerythrin (PE), peridinin-chlorophyll-protein (PerCp), PE conjugated to cyanine 5.5 (PE-Cy5.5) or cyanine 7 (PE-Cy7), and allophycocyanin (APC) (Table 2.1). The antibodies against pDCA and CCR5 were biotinylated and therefore an additional incubation step with Streptavidin conjugated with the fluorochrome PE-Cy7 or APC was necessary for the detection of target cells. DRAQ7TM (Biostatus, Shepshed, UK), conjugated to APC-Cy7, is a fluorescent DNA dye, which was used to determine cell viability for all flow cytometry experiments. Cells infected with SFV L10 strain were fixed and the fixable Viability Dye eFluor 780 (eBioscience, Hatfield, UK) was used to determine cell viability.

Table 2.1 List of antibodies and Streptavidin conjugates used for staining cells for flow cytometry

Antibody	Clone	Isotype	Dilution	Source
CD3e	145-2C11	armenian hamster IgG	1:40	eBioscience
CD4	GK1.5	rat IgG2b	1:140	eBioscience
CD8a	53-6.7	rat IgG2a	1:100	Biolegend
CD11b	M1/70	rat IgG2b	1:100	eBioscience
CD11c	N418	armenian hamster IgG	1:200	eBioscience
CD19	1D3	rat IgG2a	1:140	BD Pharmingen
CD44	IM7	rat IgG2b	1:100	Biolegend
CD45	30-F11	rat IgG2b	1:100	BD Pharmingen
CD62L	MEL-14	rat IgG2a	1:140	eBioscience
CD183 (CXCR3)	CXCR3-173	armenian hamster IgG	1:100	eBioscience
CD192 (CCR2)	475301	rat IgG2b	1:10	R&D systems
CD194 (CCR4)	2G12	armenian hamster IgG	1:40	eBioscience
CD195 (CCR5)	HM-CCR5-7A4	armenian hamster IgG	1:20	eBioscience
CD335 (NKp46)	29A1.4	rat IgG2a	1:40	eBioscience
F4/80	BM8	rat IgG2a	1:100	eBioscience
Ly-6C	HK1.4	Rat IgG2c	1:80	eBioscience
Ly-6G	1A8	rat IgG2a	1:140	BD Pharmingen
NK1.1	PK136	mouse IgG2a	1:80	eBioscience
MHC-II (IA-IE)	M5/114.15.2	rat IgG2b	1:140	eBioscience
pDCA	JF05-1C2.4.1	rat IgG2b	1:10	Miltenyi
Streptavidin PE-Cy7			1:100	BD Pharmingen
Streptavidin APC			1:200	eBioscience

2.5 Antibodies for immunohistochemistry (IHC)

Purified monoclonal and polyclonal antibodies were used for formalin fixed and paraffin-embedded tissue sections. Antibodies to CCL2, Myeloperoxidase, NeuN and SFV nsp3 were polyclonal (Table 2.2).

Table 2.2 Purified primary monoclonal and polyclonal antibodies used for immunohistochemistry

Antibody	Clone	Isotype	Dilution	Source
CD3	SP7	rabbit IgG	1:100	Vector laboratories
CD45R/B220	RA3-6B2	rat IgG2a	1:500	Biolegend
CD49b	DX5	rat IgM	1:100	Biolegend
CCL2/JE/MCP-1	-	goat IgG	1:50	R&D systems
F4/80	Cl:A3-1	rat IgG2b	1:50	Serotec AbD
Gr1 (Ly-6C/Ly-6G)	RB-8C5	rat IgG2b	1:300	Biolegend
MAC-2	M3/38	rat IgG2a	1:500	Cedarlane
Myeloperoxidase	-	rabbit IgG	1:500	DAKO
NeuN	-	rabbit IgG	1:500	Millipore
SFV nsp3		rabbit IgG	1:500	kind gift from John Fazakerley (Pirbright Institute)

Purified antibodies were detected using secondary antibodies conjugated to either biotin, fluorescein isothiocyanate (FITC), tetramethyl rhodamine isothiocyanate (TRITC) (Table 2.3). All secondary antibodies were used at a concentration of 5-10 $\mu\text{g/ml}$. Biotinylated secondary antibodies were then visualised by adding either Fluorescein or Texas Red Avidin D (Vector laboratories, Peterborough, UK) at a concentration of 10 $\mu\text{g/ml}$. Primary polyclonal rabbit antibodies were detected using the DAKO EnVision kit (DAKO, Ely, UK) as per manufacturer's protocol. Reagents used for IHC are listed in Table 2.4.

Table 2.3 Secondary antibodies used for immunohistochemistry

Antibody	Dilution	Source
goat anti-rat IgG (H+L) Biotin	1:200	Vector laboratories
goat anti-rat IgM TRITC	1:200	Southern Biotech
goat anti-rabbit IgG (H+L) FITC	1:200	Southern Biotech
horse anti-goat IgG (H+L) Biotin	1:200	Vector laboratories
donkey anti-goat IgG (H+L) TRITC	1:200	Jackson Immuno Research laboratories

Table 2.4 Serum and reagents used for immunohistochemistry

Serum/Reagents	Source
goat serum	Vector laboratories
mouse serum	Invitrogen
normal horse serum	Vector laboratories
rabbit serum	Vector laboratories
Fluorescein Avidin D	Vector laboratories
DAB substrate kit for Peroxidase	Vector laboratories
DAKO EnVision System-HRP (DAB) kit	DAKO
DAKO Proteinase K	DAKO
DAKO REAL™ Antibody Diluent	DAKO
ImmEdge™ Pen	Vector laboratories
Texas Red Avidin D	Vector laboratories
Tris buffered saline and Tween 20	Thermo scientific
Vectashield® Hard Set Mounting Medium with DAPI	Vector laboratories
Vectastain <i>Elite</i> ABC kit	Vector laboratories
Vectastain Avidin/Biotin Block	Vector laboratories

2.6 Primers for quantitative (Q)PCR

All primers were synthesized by IDT (Leuven, Belgium) by standard DNA synthesis and desalted to remove small molecule impurities. Standard and QPCR primers (Tables 2.5-2.8) were resuspended in RNase free water to a concentration of 100 μM and then both, forward and reverse primers, were mixed 1:1 to obtain a final primer concentration of 50 μM . All primers in Tables 2.5-2.8 are shown in the 5'-3' orientation. Primers were designed using Primer3 software (Whitehead Institute for Biomedical Research, Massachusetts, USA) as described in section 2.18.1. All primers were stored at -20°C once resuspended in water.

2.7 Infection of mice with viruses

For all *in vivo* experiments using Semliki Forest virus strain A7(74) or L10, intraperitoneal injections were conducted using 0.1 ml PBSA containing 5×10^3 PFU SFV A7(74) or 2×10^5 PFU SFV L10. Mouse brains, spleens and serum were then collected at post infection days (PID) 3, 4, 5, 7 and 10.

Trained staff of Prof Tony Fooks's group at the Animal Health and Veterinary Laboratories Agency (AHVLA) carried out infections of mice with West Nile virus (WNV) in a containment level three laboratory. In brief, mice were anaesthetised with isoflurane and then inoculated intranasally with 10^5 PFU of WNV strain NY99 diluted in 50 μl serum-free Eagle's minimal essential medium (EMEM) (Sigma). Brain tissue was harvested at PID 2, 4 and 6 for further analysis.

Table 2.5 Forward and reverse primers used for QPCR. All primers are in the 5'-3' orientation.

Gene		Primer sequence	Product size	Accession number
CCBP2 (D6)	forward	TTCTCCCACTGCTGCTTCAC	93	NM_001276719.1
	reverse	TGCCATCTCAACATCACAGA		
CCL2	forward	CTACCTGCTGCTACTCATTCA	153	NM_011333.3
	reverse	CCATTCCTTCTTGGGGTCA		
CCL5	forward	CTGCTGCTTTGCCTACCTCT	124	NM_013653
	reverse	ACACACTTGGCGTTTCCTT		
CCR2	forward	TGTGGGACAGAGGAAGTGG	130	NM_009915
	reverse	GGAGGCAGAAAATAGCAGCA		
CD45	forward	CGCATCAGAAGGGGATAAAG	99	NM_001111316
	reverse	TCCAGCAAAGAGCAACAGAA		
CX3CL1	forward	TCCTTGTTCTCCTGGCTTT	125	NM_009142
	reverse	CGGTGTTGATGGTGATGGT		
CXCL1	forward	GCTTGCCTTGACCCTGAA	87	NM_008176
	reverse	TGTCTTCTTCTCCGTTACTTGG		
CXCL10	forward	GCTCAAGTGGCTGGGATG	111	NM_021274
	reverse	GAGGACAAGGAGGGTGTGG		
CXCR5	forward	CCTCTCCATCCACATCACCT	148	NM_007551.2
	reverse	AGTTTCCGCTTCGTTTTCT		
CXCR3	forward	AGTGCTTGCTCCTTGTAGT	129	NM_009910.2
	reverse	GGTGTGTCCTTGTGCTGA		
GAPDH	forward	CAGCAAGGACACTGAGCAAG	93	NM_001001303
	reverse	TATTATGGGGTCTGGGATG		
IFN-alpha 4	forward	GCAATGACCTCCATCAGCA	98	NM_010504
	reverse	GTATGTCCTCACAGCCAGCA		
IFN-beta 1	forward	CACAGCCCTCTCCATCAACT	152	NM_010510
	reverse	GCATCTTCTCCGTCATCTCC		
IFN gamma	forward	AGCAAGGCGAAAAAGGATG	66	NM_008337
	reverse	CTGGACCTGTGGGTTGTTG		
IL-6	forward	TTCCATCCAGTTGCCTTCTT	171	NM_031168
	reverse	ATTTCCACGATTTCCAGAG		
IL-10	forward	CAACATACTGCTAACCGACTCCT	105	NM_010548.1
	reverse	TGGGCATCACTTCTACCA		
TBP	forward	TGCTGTTGGTGATTGTTGGT	99	NM_013684
	reverse	AACTGGCTTGTGTGGGAAAG		

Table 2.6 QPCR primer sequences for detecting viral gene targets

Gene		Primer sequence	Product size	Accession number
SFV E1	forward	CGCATCACCTTCTTTTGTG	173	NC_003215
	reverse	CCAGACCACCCGAGATTTT		
SFV nsp3	forward	GCAAGAGGCAAACGAACAGA	205	NC_003215
	reverse	GGGAAAAGATGAGCAAACCA		
WNV NS1	forward	GAACTCGCCAACAACACCTT	105	DQ211652
	reverse	ACCAAATCCAAAATCCTCCAC		

Table 2.7 Standard primer sequences to detect viral gene targets

Gene		Primer sequence	Product size
SFV E1	forward	AAGTGAAGACAGCAGGTAAGGTG	446
	reverse	TATGAGTTGCCCCGAGTTTC	
SFV nsp3	forward	GCAATCCCTCAACCATCTATT	556
	reverse	CCTTCTCGCACTTACCTTCT	
WNV NS1	forward	TGGAAATTGGCTGGAAGG	200
	reverse	AGTTGTGTTGCTCTCTGACCT	

Table 2.8 Standard primers used to detect specific target gene.

Gene		Primer sequence	Product size
CCL2	forward	CACCAGCACCAGCCAACT	519
	reverse	GCATCACAGTCCGAGTCACA	
CCL5	forward	CCCTCACCATCATCCTCACT	280
	reverse	TCAGAATCAAGAAACCCTCTATCC	
CCR2	forward	AGGGGAGAGCAGAAGGCTAA	212
	reverse	CCCAGGAAGAGGTTGAGAGA	
CD45	forward	GGGTTGTTCTGTGCCTTGTT	294
	reverse	GCTGTCTTCCCTGGGCTTTATT	
CX3CL1	forward	CTGCTGCTGGCTGGTTAGA	473
	reverse	TTTACAGGTGGGGCACTTTG	
CXCL1	forward	CTGGGATTCACCTCAAGAACA	469
	reverse	CTTTTCGCACAACACCCTTC	
CXCL10	forward	ATCCCTGCGAGCCTATCC	524
	reverse	AAACTTAGAACTGACGAGCCT	
CXCR5	forward	TCGCTCTGCACAAGATCAAT	289
	reverse	TAGAGGAAACGGGAGGTGAA	
CXCR3	forward	TGGGGTCTCTGTCTGCTCTT	889
	reverse	TTTGCCCTCTCCCTCTTCTCA	
GAPDH	forward	TGTCTCCTGCGACTTCAA	341
	reverse	TGCAGCGAACTTTATTGATG	
IFN-alpha 4	forward	TGGCTAGGCTCTGTGCTTTC	595
	reverse	TCCAGAAAAGTCCTCTCC	
IFN-beta 1	forward	GGCTTCCATCATGAACAACA	399
	reverse	TCCCACGTCAATCTTTCCTC	
IFN gamma	forward	ATCTGGAGGAACTGGCAAAA	597
	reverse	AGATAACAACCCCGCAATCAC	
IL-6	forward	TCCAGAAACCGCTATGAAGT	370
	reverse	CTCCAGAAGACCAGAGGAAA	
IL-10	forward	ATGCTGCCTGCTCTTACTGAC	414
	reverse	TCACTCTTCACCTGCTCCACT	

2.8 Tissue processing, embedding and sectioning

2.8.1 Tissue processing

SFV infected mice were euthanized in a carbon dioxide chamber and then perfused with 20 ml of cold PBS (Invitrogen). The brains were then removed from the skull and hemisected sagittally at the midsagittal plane into two halves. One half brain was immediately transferred into RNA later (Sigma) for gene expression analysis and stored at 4°C for up to 5 days. The other half brain was fixed in 4% paraformaldehyde (PFA) in 0.1 M PBS at 4°C for 24 hours for immunohistochemical analysis. For flow cytometry studies half brains were kept in Hank's balanced salt solution (HBSS, Invitrogen). Fixed brains were then dehydrated using an automated tissue processor (Shandon Citadel 1000, Thermo Scientific, Loughborough, UK). For this, tissue sections were immersed in increasing concentrations of ethanol until dehydration was complete and then immersed in xylene before the tissue was finally infiltrated with the embedding medium paraffin wax (see details below).

1. 70% Ethanol	1 hour
2. 90% Ethanol	1 hour
3. 95% Ethanol	1 hour
4. 100% Ethanol	1x 1 hour, 1x 2 hours, 1x 2.5 hours
5. Xylene	2x 1 hour and 1x 1.5 hours
6. Molten paraffin wax	2x 4 hours at 60-65°C

2.8.2 Tissue embedding

After processing the tissue in the automated tissue processor, the samples were then placed into metal moulds and embedded in paraffin wax blocks (Histocenter 3, Thermo Scientific). The blocks were then cooled on an integral cold plate for several hours until the wax was set hard and stored at room temperature until sectioning.

2.8.3 Tissue sectioning

Paraffin blocks were placed on crushed ice to harden the wax for better sectioning. Then, the brain sections were cut sagittally into 6-8 μm thick sections from lateral to medial on a microtome (Shandon Finesse 325, Thermo Scientific). Cut sections were floated onto a warm water bath set at 40°C to smooth out any creases and then lifted out onto charged poly-L-lysine coated glass slides (VWR, Lutterworth, UK). Next, the slides were placed on a histology hot plate (Raymond A Lamb Hotplate, Thermo Scientific) set at 55°C to allow the sections to dry for 1 hour. Once the sections were dried, slides were stored at room temperature until needed for staining.

2.9 Haematoxylin and Eosin staining

For basic histological examination of tissue, Haematoxylin and Eosin (H&E) staining was performed. Haematoxylin is a basic dye that forms a complex with metal cations like aluminium. The positively charged complex then reacts with negatively charged and basophilic cell components like nucleic acid in the nucleus and stains the nucleus blue as a result. Eosin is an acidic dye and is negatively charged. Subsequently it reacts with positively charged, acidophilic components of the cell like cytoplasm, intra- and extracellular matrix proteins and erythrocytes. The stain appears pink as a result. At the beginning of the H&E staining, paraffin sections were first deparaffinized and then rehydrated by immersing slides in decreasing ethanol concentrations to prepare the tissue for the staining with water-soluble dyes. The steps are detailed below:

- | | |
|-----------------|----------|
| 1. Xylene | 2x 3 min |
| 2. 100% Ethanol | 2x 3min |
| 3. 95% Ethanol | 2x 3min |
| 4. 90% Ethanol | 3 min |
| 5. 70% Ethanol | 3 min |

The sections were then rinsed in running tap water for 3 min and stained with Harris Haematoxylin (Cell Path, Newtown, UK) for 5 min. Excess stain was

masking of the epitope of interest. Heat induced epitope retrieval (HIER) was used to reverse epitope masking and restore primary antibody binding capacity. For all immunohistochemical studies, 10 mM sodium citrate buffer at pH 6 was used except for staining using the primary antibody F4/80. In this case Proteinase K (DAKO) was used as a method of antigen retrieval instead of citrate buffer. For this, sections were incubated for 10 min at room temperature with Proteinase K and then briefly washed with TBST before proceeding to the next step. For antigen retrieval with citrate buffer, slides were transferred from water into hot (95°C) citrate buffer and boiled for 8 min on full power in the microwave. The slides were allowed to cool in the buffer and then briefly washed for 1 min with 1x Tris-buffered saline with 0.01% Tween 20 (TBST, Thermo Scientific). Brain sections were circled using the hydrophobic wax pen ImmEdge (DAKO).

When biotinylated antibodies and streptavidin HRP were used, endogenous peroxidase activity was inhibited with 0.5% hydrogen peroxide (Sigma) in methanol for 30 min. Sections were then blocked with 20% horse serum containing 4 drops of Avidin block/ml (Vector laboratories). Next the blocking serum was quickly tapped off and primary antibody (see Table 2.2) was diluted in DAKO antibody diluent containing 2.5% normal horse serum, 2.5% mouse serum and 4 drops of Biotin block/ml (Vector laboratories) were added to each section, and incubated overnight at 4°C. The working concentration of primary antibodies was between 1-5 µg/ml unless stated otherwise.

On the next day sections were incubated for 30 min at room temperature with either biotinylated or fluorochrome conjugated secondary antibody raised against the corresponding IgG (Table 2.3). Both types of secondary antibodies were used at a working concentration of 5-10 µg/ml. The fluorophore label was visualised directly on the microscope after mounting sections with Vectashield hard-set medium containing DAPI (Vector laboratories). A fluorescent microscope Axio Imager M2 (Carl Zeiss, Oberkochen, Germany) with Axiovision 4.8 software (Carl Zeiss, Germany) was used for immunofluorescence microscopy. The biotin label was detected using streptavidin conjugated with a fluorophore like Fluorescein Avidin D or Texas Red Avidin D (Table 2.4). Fluorescein or Texas Red Avidin D were used at a concentration of 10 µg/ml and

diluted in PBS at pH 8. The slides were incubated for 40 min at room temperature before mounting the section with Vectashield hard-set mounting medium.

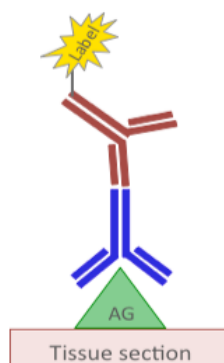


Figure 2.1. Indirect immunostaining using two different antibodies.

The primary antibody (blue) binds to antigen (AG). The secondary (red) antibody detects the primary antibody and is species specific, raised against the corresponding IgG.

2.10.2 Immunofluorescence double staining

For the detection of two antigens in paraffin fixed brain sections, an indirect staining method was used as described above. Primary antibodies raised in two different species were detected using fluorescently labelled secondary species specific antibodies. The staining was performed using both antibodies simultaneously. For antibodies raised in the same species the FITC antibody labelling kit was used to conjugate one of the primary antibodies directly to a fluorophore.

2.10.3 Signal amplification using avidin/biotin complexes

To enhance the sensitivity of low-density antigens (<10K molecules/cell) a signal amplification system was used. The ABC method is a patented procedure called the 'preformed complex' method developed by Vector laboratories. This method is based on high affinity of streptavidin for biotin. One mole avidin binds four moles of biotin. In the ABC method a preformed complex between avidin and biotin was added to biotinylated secondary antibodies using the Vectorstain *Elite* ABC kit according to the manufacturer's instructions. Unoccupied biotin binding sites of the preformed avidin/biotin complex bind to the biotinylated secondary

antibody. This results in more enzyme attachment to the target than is possible using enzyme or fluorochrome labelled secondary antibodies alone.

After incubation of slides with biotinylated secondary antibody, the sections were incubated with the avidin/biotin complex for 30 min before proceeding to the next step. The preformed complex was conjugated to HRP which was then visualised in the next step by adding 3,3'-diaminobenzidine (DAB) substrate to the samples. The sections were incubated for 3 min and the enzymatic reaction stopped with tap water. After washing the slides in tap water, all sections were then dehydrated through a series of increasing alcohol concentrations, as described in chapter 2.10, and mounted with mounting medium DPX (Leica Biosystems). Finally coverslips were carefully mounted on the DPX covered tissue sections and slides were allowed to dry for at least 1 hour before visualisation on the microscope.

2.10.4 Signal amplification using chain polymer-conjugated technology

A more potent amplification method is the chain polymer-conjugated technology (EnVision System) developed by DAKO cytometry (Fig. 2.2). This method is based on the use of an enzyme (HRP) labelled 'spine' molecule dextran. This molecule can bind up to ten molecules of antibody. Since this method does not use avidin and biotin, nonspecific background staining was eliminated. In this study three antibodies, CD3, Myeloperoxidase and SFV nsp3 viral protein, were detected using this method. All three antibodies were raised in rabbit. The HRP labelled polymer was detected using a 3,3'-diaminobenzidine (DAB) substrate-chromogen which resulted in red/brown coloured staining of target cells. The detailed protocol is depicted below:

1. Deparaffinize section in Xylene and rehydrate slides as detailed above through a series of decreasing Ethanol concentrations.
2. TBST wash 5 min
3. Antigen retrieval with Citrate buffer pH 6 for 8 min (see 2.10)
4. TBST wash 5 min
5. Peroxidase block 5 min

6. TBST wash 5 min
7. primary antibody 45 min at room temperature
8. TBST wash 5 min
9. secondary antibody from kit 40 min at room temperature
10. TBST wash 5 min
11. DAB up to 3 min until staining visible
12. stop DAB reaction with tap water and dehydrate tissue sections as described above.

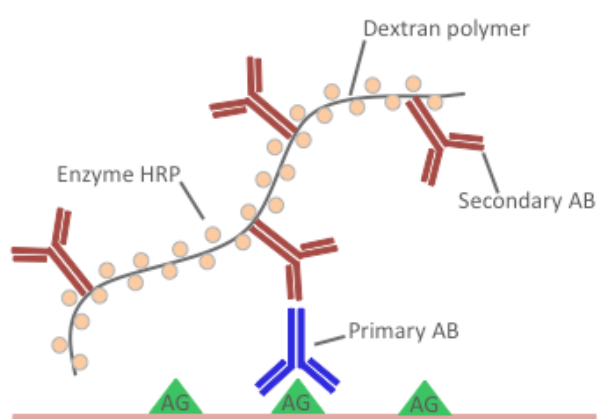


Figure 2.2. Chain polymer-conjugated technology (EnVision System)

2.11 Isolation of mononuclear cells from the brain

Half mouse brains from infected and healthy control mice were obtained as described in 2.8.1 and directly placed into ice-cold HBSS buffer. The brains were then finely minced with a scalpel and digested shaking on the Thermomixer Comfort (Eppendorf, Cambridge, UK) for 60 min at 37°C. Up to two brains were digested in 10 ml of digestion buffer containing 5U/ml DNase I (Sigma) and 0.08 Wunsch units/ml Liberase TM research grade (Roche, Welwyn Garden City, UK). The digestion reaction was quenched with rinsing buffer containing 0.5% fetal calf serum (FCS) and the homogenized brains were passed through a 70 µm nylon cell strainer (BD Biosciences, Oxford, UK) to remove large tissue debris.

The residual brain tissue that did not pass through was then mashed through the cell strainer with the back end of the plunger of a 5 ml syringe (BD Biosciences).

The brain cell suspension was then spun down twice at 300 g for 5 min at 4°C and the cell pellet was resuspended in Percoll (Sigma) and 1x HBSS to obtain 5-7 ml of 30% (v/v) Percoll solution. After thorough mixing, the 30% Percoll cell suspension was underlayered with 5 ml of 70% (v/v) Percoll in 1x HBSS. The tubes were spun at 2000 g for 20 min at room temperature and leukocytes from the 70%/30% interphase were collected and washed twice at 300 g for 5 min at 4°C with rinsing buffer before resuspending cells in ice cold FACS buffer. Cells were then counted using a haemocytometer and cell viability determined using 0.4% Trypan blue solution (Sigma). For flow cytometry, pooled cells were resuspended at a concentration of 5×10^5 - 2×10^6 cells/ml in 100 μ l FACS buffer.

2.11.1 Isolation of mononuclear cells using Myelin removal beads

As an alternative to the Percoll based method, mononuclear cells were isolated from mouse brains using the neural tissue dissociation kit with papain (Miltenyi, Bisley, UK) in combination with Myelin removal beads II (Miltenyi) according to the manufacturer's instructions. In brief, brain tissue (up to 400 mg) was transferred into C-tubes (Miltenyi) and dissociated with a mix of enzyme solutions using the automated gentleMACS dissociator (Miltenyi), filtered through a 40 μ m nylon cell strainer (BD Biosciences) and resuspended in 2 ml of FACS buffer. The brains were washed once more at 300 g for 5 min and then resuspended in 1.8 ml of FACS buffer. Following this, 200 μ l Myelin removal beads II (Miltenyi) were added to each brain sample and incubated for 20 min at 4°C. Next, cells were washed by adding 10x the labelling volume of FACS buffer (20 ml) and spun down at 300 g for 10 min. The supernatant was discarded and cells were resuspended in 2 ml FACS buffer. Depletion of magnetic labelled Myelin was performed on the autoMACS® Pro Separator (Miltenyi). After priming the instrument, tubes containing the sample were placed in row A, tubes containing the negative fraction in row B and tubes containing the positive fraction (labelled Myelin) in row C. For depletion the program 'Deplete S' was chosen on the machine and ran until the whole sample was processed. The negative fraction was used for further antibody labelling for flow cytometry. The positive fraction containing the Myelin was discarded.

2.12 Isolation of lymphocytes from spleen

Spleens from mice were placed directly into ice-cold PBS for further processing. The spleens were transferred to a petri dish and splenocytes collected by cutting the spleen with a scalpel into half and squeezing cells out of the tissue with the back end of a plunger from a 5 ml syringe. Cells and spleen tissue fragments were then mashed through a 70 μm cell strainer (BD Biosciences), washed twice with RPMI (Sigma) and spun down at 300g for 5 min at 4°C. The cell pellet was treated with 2 ml of red cell lysis buffer (Miltenyi) for 10 min at room temperature. The cells were then spun down at 300g for 5 min and the pellet was checked visually for any remaining red cell debris. If the pellet still looked red, cells were treated once more with the red cell lysis buffer. Cells were finally resuspended in 1 ml FACS buffer and viable cells determined by staining with Trypan blue (Sigma) and then counted with a haemocytometer (Hawksley, Lansing, UK). Cells were resuspended at a final concentration of 3×10^6 cells/ml and kept on ice for further use.

2.13 Processing of whole blood samples

Blood was taken from mice by cardiac puncture and treated immediately with 2 mM EDTA to prevent blood clotting. The blood was then spun down at 300 g for 5 min and the supernatant (= plasma) was transferred to a fresh tube and frozen at -80°C for further analysis. If leukocytes were isolated from whole blood, the samples were treated with 2 ml red cell lysis buffer (Miltenyi) for 3 min at room temperature. Cells were spun down at 300 g for 5 min and resuspended in FACS buffer for flow cytometry analysis.

2.14 Flow cytometry

All flow cytometry studies were performed using 12x75 mm polystyrene tubes (BD Falcon). The resuspended cells ($0.5 - 2 \times 10^6$ cells/tube) were incubated with Fc-receptor blocking reagent (Miltenyi) at a dilution of 1:20 for 10 min at 4°C to prevent non-specific binding through the Fc-receptor on antibodies. Cells were washed once with FACS buffer at 300 g for 5 min and then incubated with primary antibody (see Table 2.1) at a tested concentration for 15-20 min at 4°C

in the dark. Next, cells were washed twice with FACS buffer at 300g for 5 min each.

For the use of biotinylated antibodies a further 10 min incubation step with fluorescently labelled streptavidin (Table 2.1) was necessary. Cells were resuspended in a final volume of 100 μl of FACS buffer for the final analyses. Shortly before data acquisition on the flow cytometer all samples were stained with 1 μl of DRAQ7 (Biostatus) to discriminate dead cells from viable cells. All data were acquired using a MACSQuant flow cytometer (Miltenyi) and analysed using FlowJo software (Tree Star Inc., Ashland, USA). Appropriate isotype and fluorescence minus one (FMO) controls were included in all studies. For brain samples a total of 5×10^5 cells were counted in each sample.

2.15 RNA extraction from tissue

Harvested mouse brains were stabilized in RNA later (Sigma) up to 5 days, to prevent RNA degradation. Each half brain was removed from RNA later and placed into a 2 ml microcentrifuge tube containing 1 ml of Trizol® reagent (Invitrogen). A 5 mm stainless steel bead (Qiagen, Manchester, UK) was added to each sample and brains were homogenized through high speed shaking at 50 Hz for 10 min using the TissueLyser LT machine (Qiagen). After homogenisation the samples were incubated for 5 min at room temperature to allow complete dissociation of tissue. Next, 0.2 ml of chloroform per 1 ml of Trizol was added to each sample which was then immediately shaken vigorously by hand.

Samples were incubated for 2-3 min at room temperature and then centrifuged at 12 000 g for 15 min at 4°C for phase separation. Following this, three layers were formed: an upper aqueous layer containing RNA, an interphase/middle layer containing DNA and a lower red phenol-chloroform phase containing protein. Only the upper RNA containing aqueous layer was carefully transferred into a fresh 1.5 ml tube without disturbing the middle layer. Following this, an equal volume (approximately 550 μl) of 70% ethanol was added to each RNA sample (approximately 550 μl) to precipitate RNA. After mixing the samples by vortexing, total RNA was 'cleaned' up using the PureLink™ RNA Mini kit (Ambion, Life technologies), which can purify a maximum of 1 mg of RNA. The RNA was bound, washed and eluted using Spin Cartridge columns according to the

manufacturer's guidelines. Genomic DNA contamination was eliminated by performing an 'on column' DNase treatment with the PureLink® DNase. The DNase mixture (80 µl), containing 8 µl DNase reaction buffer, 10 µl DNase at a concentration of 3U/µl and 64 µl RNase free water, was added to each sample and incubated for 15 min at room temperature for ideal DNA digestion. Following this, the spin cartridge was washed with wash buffer I and II and eluted in 50 µl RNase free water. The final concentration of RNA was quantified using the NanoDrop 2000 spectrophotometer (Thermo Scientific) using 1 µl of RNA. RNase free water was used as a reference and to 'blank' the NanoDrop. The stock RNA was stored at -80°C until further use.

2.15.1 Measurement of RNA quality and degradation

RNA quality was determined using the Agilent 2100 Bioanalyser (Agilent Technologies, Cheshire, UK). With the Agilent RNA 6000 Nano kit (Agilent) a total of 25-500 ng/µl can be analysed. All West Nile virus infected RNA samples, used for TLDA, had a concentration of 194-430 ng/µl and all SFV infected RNA samples were diluted 1:10 with RNase free water to reach a concentration of 100-200 ng/µl. The RNA quantity was determined and the RNA integrity number (RIN) calculated. The obtained RIN value allowed a numerical assessment of the RNA integrity and therefore a low RIN (<5) was considered as degraded RNA and a high RIN (>7) was considered as good quality RNA. RIN values of >8 were considered as high quality RNA (no degradation visible) and were used for subsequent TLDA analysis. In these samples two ribosomal RNA peaks, 18S and 28S, were visible when analysing the electropherogram.

2.16 Viral RNA extraction from serum and brain

Serum and brain RNA samples from SFV infected mice were thawed. Viral RNA was extracted from brain and serum using the QIAamp viral RNA Mini kit (Qiagen). Carrier RNA was prepared at a concentration of 1 µg/ul in buffer AVE and aliquots were stored at -20°C. 2 µl of carrier RNA/AVE mix and 560 µl AVL buffer were used per 80-100 µl serum or brain sample. RNA was extracted according to the manufacturer's guidelines and eluted in a final volume of 30 µl AVE buffer. Viral RNA was stored at -80°C and thawed only once.

2.17 cDNA synthesis

Three different cDNA kits were used for the generation of cDNA from RNA samples. In early experiments the Quantitect Reverse transcription kit (Qiagen) was used. This kit consists of two steps: a genomic wipe-out step and the reverse transcription step using a mixture of random and oligo-dT primers according to the manufacturer's instructions. In later experiments the Precision™ nanoscript Reverse Transcription kit (Primer design Ltd., Southampton, UK) was used to transcribe a total of 0.5-2 µg of RNA following the manufacturer's guidelines. In the first step, the annealing step, RNase free water, oligo-dT and random nonamer primers were both added to each RNA sample to make up a final volume of 10 µl. The RNA was denatured in the PCR machine at 65°C for 5 min and then immediately cooled to 4°C until the master mix was added for the second step, the extension step. The master mix was made up as following:

- nanoScript 10x buffer 2 µl
- dNTP mix 10 mM each 1 µl
- DTT 100 mM 2 µl
- nanoScript enzyme 1 µl
- RNase free water 4 µl

For the -RT control addition of nanoScript enzyme was omitted. 10 µl of master mix was added to each sample on ice and samples then run on the PCR machine at the following conditions: 25°C for 5 min, 55°C for 20 min and 75°C for 15 min for heat inactivation. The cDNA samples (20 µl) were diluted with RNase free water 1:5, if total RNA was less than 3 µg, or 1:10, if total RNA used was more than 3µg. All cDNA samples were stored at -20°C until use.

2.17.1 cDNA synthesis for TLDA and viral RNA samples

For TaqMan low-density arrays (TLDA), cDNA was synthesized using the High-capacity RNA-to-cDNA kit (Applied Biosystems, Invitrogen) according to the manufacturer's protocol. For all TLDA studies 1 µg of total RNA was used for the cDNA synthesis. A total volume of 20 µl cDNA per sample was stored undiluted at -20°C until use for TLDA studies. Viral RNA was also transcribed into cDNA using

the High-capacity RNA-to-cDNA kit (Applied Biosystems, Invitrogen). For this, 9 μ l RNA and no RNase free water was used to set up the cDNA reaction. Undiluted cDNA was then diluted 1:10 for all samples and stored at -20°C .

2.18 Quantitative (Q)PCR

Quantitative polymerase chain reaction (QPCR) or real time PCR is a method to assess quantitatively the number of transcripts in a sample by generating a standard curve and normalizing samples to a housekeeping gene, which has a high and stable expression in all tissues/cells. In all studies TATA-binding protein (TBP) was used as a housekeeping gene unless stated otherwise. The QPCR used in all studies is based on the SYBR Green method. SYBR green is a fluorescent DNA binding dye that binds double stranded DNA. Once SYBR green binds to DNA it emits a fluorescent signal that is directly proportional to the amount of transcript present in the tested sample.

2.18.1 Primer design

A set of ‘inner’ primers (QPCR primers) was designed to detect the gene of interest in the sample by QPCR using SYBR green (Tables 2.5 and 2.6). The set of ‘outer’ primers were required for the generation of specific PCR products that act as standard templates and contain binding sites for the inner primers (Table 2.7 and 2.8).

All oligonucleotide primers were designed using Primer 3 software (available online at <http://frodo.wi.mit.edu/>). Primers were designed according to the following criteria:

1. 18-23 base pair (bp) in length
2. 40-65% GC content
3. T_m (melting temperature of primers) between 59.5°C - 61°C (60°C ideal)
4. Maximum self complementarity = 2 and maximum 3’ self complementarity = 1
5. Amplicon size for QPCR <150 bp
6. no more than 4 G or C in a row

If no primers were suggested by the Primer3 software using the above-mentioned parameters, the maximum self complementarity was increased from 2 to 3 and the T_m was reduced to 59°C or the conditions were further relaxed until ‘inner’ primer pairs were suggested. The maximum 3’ self complementarity was not altered and remained 1 for all the primers designed. Outer primers were designed to amplify a region of the gene of interest where ‘inner’ primers could bind. Therefore similar parameters as shown above were used for the design of ‘outer’ primers but a higher self complementarity and a bigger product size of more than 150 bp was allowed. To ensure specificity of primers, they were analysed using the BLAST analysis tool (<http://blast.ncbi.nlm.nih.gov/Blast.cgi>).

2.18.2 Generation of DNA standards for absolute quantitative QPCR

The generation of standard curves are necessary for quantifying the levels of gene expression of the unknown sample. Therefore a PCR product was generated by standard PCR using the ‘outer’ primer set (Tables 2.7 and 2.8). The standard PCR was performed using a ready-made master mix called red PCR master mix (Roalab, Vh-bio, Gateshead, UK) containing 1.1x buffer, $MgCl_2$, 1mM dNTPs and Taq DNA polymerase. To set up the PCR reaction, 45 μ l of the Red PCR master mix, 4 μ l of cDNA and 1 μ l of primer mix (forward and reverse, 50 μ M) were added into small 0.2 ml PCR tubes. PCR was performed on the Veriti™ thermal cycler machine (Applied Biosystems) at the following cycling conditions:

1. 95°C	2 min	
2. 95°C	30 seconds	} x 35 cycles
3. 55°C*	30 seconds	
4. 68°C	1 min	
5. 68°C	10 min	
6. 4°C	until stored at -20°C in freezer	

* The annealing temperature was varied depending on the calculated T_m of the primer pairs

The product generated was run on a 2% Agarose gel and visualized using ethidium bromide. A single band with a certain base pair size signifies that the

standard PCR product has been amplified and can be used as a standard template for QPCR analysis. The sample was then purified using the QIAquick PCR purification kit (Qiagen) according to the manufacturer's instruction and eluted in 30 μl of RNase free water. Next, the standards were 10 fold serially diluted. For the creation of a standard curve a range from 1×10^4 to 1×10^{10} fold dilution was used. All samples should lie within the range of the standard curve to prevent erroneous results. Each of the standard dilutions was used as a template for QPCR. For relative expression the absolute copy number of the sample was compared to the absolute copy number of control samples and expressed as fold change. Each dilution was given an arbitrary copy number such as 10^6 copies for a dilution of 1×10^6 .

2.18.3 Calculation of the absolute copy numbers of standards

The absolute level of transcripts of the standard can be calculated by measuring the optical density (OD) of the standard PCR products on a NanoDrop and by using a series of formulae:

1) *Calculate molecular weight (MW) of the standard (double stranded DNA):*

- Average molecular weight for a double stranded nucleotide= 660 Dalton
- **660 Daltons x length of the standard in bp = MW of standard**

2) *Calculate number of moles/ μl :*

- **Mass per μl /MW of DNA (=211,200) = Moles of standard/ μl**

3) *Convert Moles/ μl into copy number:*

- 1 mole = 6.023×10^{23} molecules (Avogadro's constant)
- **Avogadro's constant x Moles of standard/ μl = Total copies/ μl**

The number of total copies of standard/ μl was then used to calculate the number of copies at each dilution of standards. The standard curve is essential to extrapolate the copy number of the gene of interest.

2.18.4 SYBR green QPCR

Most QPCRs were performed using a 384 well plate containing a total of 10 μl of reaction volume. Each sample was analysed in triplicate on the QPCR machine.

First a master mix was prepared for all samples containing per well:

- 5 μl PerfeCTa SYBR green fast mix (Qanta Bioscience, Gaithersburg, MD, USA)
- 0.3 μl 'inner' primer mix (each primer mixed at 50 pmol/ μl) (Table 2.5 & 2.6)
- 4 μl nuclease free water (Ambion, Invitrogen)

The master mix (9 μl) and 1 μl sample or standard cDNA was added to each well and spun down briefly for 1 min at 200 g to ensure that all reagents are at the bottom of the well. On each plate a non-template control with 1 μl RNase free water instead of cDNA, and a -RT control was added to determine the level of contamination with RNA or genomic DNA respectively. The plate was then run on the 7900HT QPCR machine (Applied Biosystems). The general QPCR conditions were:

1. 94°C 10 min
 2. 94°C 3 s
 3. 60°C 30 s
- } x 40 cycles
4. Dissociation step/Melting curve

The melting curve is important to determine the specificity of the PCR primers. In some cases 96-well plates were used to analyse gene expression. In this case the amount of all reagents mentioned above were proportionally increased to reach a total volume of 20 μl per well. 96-well plates were run on the smaller 7500 fast QPCR machine at the same conditions as mentioned above. The SDS software automatically created a threshold level of fluorescence that indicated exponential PCR amplification. The cycle value (= Ct value) was determined by the software, which calculated at which cycle number each sample crossed this specific threshold level. Using the Ct values, the software then calculated the absolute copy number on the basis of the standard curve. To prevent errors and

to produce reliable results, the standard curve needed to have a coefficient of determination (R^2) of more than 0.97 and a slope of 3.3. The slope means that the PCR product was amplified by a factor of 10 every 3.3 cycles and implies that the reaction was 100% efficient. The formula for PCR efficiency is:

$$10^{(-1/\text{slope})} - 1$$

2.18.5 Normalization of QPCR data

The QPCR data obtained from all samples was then normalised using the housekeeping gene or 'reference' gene TBP. The housekeeping gene TBP is expressed in all cells. The amount of transcripts of the gene of interest can vary between samples due to RNA degradation, different amounts of RNA used in the cDNA synthesis or variations occurring during RNA extraction. The use of a housekeeping gene reduces this variation by normalizing samples. To calculate the absolute copy number of the sample, the estimated copy number of the target gene was divided through the copy number of the TBP gene. Since the values obtained were very low, all the samples were then multiplied by 10^4 or 10^5 , depending on how low the values were, and were denoted as copy number per 10^4 or 10^5 TBP.

2.19 TaqMan low-density array (TLDA)

TaqMan® low-density array microfluidic cards (Applied Biosystems) were designed using two different formats: 32 and 64 genes of interest. The TLDA plates containing 32 genes contained probes for 17 chemokines of which the majority are typically classified as inflammatory chemokines. Additionally the plate also contained probes for IL-1 β , TNF and type-I interferon which are inflammatory cytokines, and 3 anti-inflammatory cytokines (159). All chemokines and cytokines were selected based on publications investigating their role in inflammation in the mouse. The TLDA plate containing 64 genes contained probes for all murine chemokines with the exclusion of CCL10, CXCL4, CXCL7 and CXCL11 which have not been shown to be involved in viral inflammation. Additionally the plate also contained probes for 9, mostly inflammatory, cytokines, 4 pattern recognition factors, 2 transcriptions factors involved in the induction of interferon and 8 interferon inducible genes. These genes were, again, selected based on the literature of virus infection in mice infected with

WNV, Sinbis virus, LCMV, MHV, influenza and other viruses (71, 87, 359). Each TLDA plate contained two housekeeping genes, 18S, TBP and Eif3f, 18S for the 32- and 64 gene plates, respectively.

The Microfluidic card consisted of 384 wells which were preloaded with probes and primers for each gene (Appendix 1 A and B). Two or four samples were analysed per card containing 32 or 64 genes respectively and filled via a loading port. Into each loading port 100 µl reaction mix consisting of 2.5 µl cDNA (562 ng total RNA equivalent), 22.5 µl of RNase free water and 25 µl of 2× TaqMan Universal PCR Master Mix (Applied Biosystems) were added. The TaqMan array cards were run on a 7900HT fast real time machine for 40 cycles and data analysed using SDS 2.2 software and RQ Manager as per manufacturer's instructions (Applied Biosystems). The relative amount of each target gene mRNA, was double normalized to an endogenous reference gene (18S) and healthy control sample (uninfected mouse brain) using the formula $2^{-\Delta\Delta CT}$. On the TLDA plates containing 64 genes, the endogenous reference gene was Eif3f (eukaryotic translation initiation factor 3) because the Ct values of 18S were not consistent between samples.

2.20 Measurement of chemokine levels in brains and serum of virally infected mice using ELISA

2.20.1 Protein extraction from the brain

Protein was extracted from virally infected brains by placing half mouse brains into 1 ml of T-Per tissue protein extraction reagent (Thermo Scientific) containing one complete mini EDTA free (Roche) tablet. Next, 5 mm stainless steel beads (Qiagen) were added to each sample and the brains were homogenized on the TissueLyser Lt (Qiagen) for 10 min at 50 Hz. The homogenized brains were then spun down at 16 000 g for 15 min. The interphase layer was transferred into a new 2 ml tube and samples stored at -80°C until further use.

2.20.2 ELISA

To measure chemokine levels of CXCL9 in the serum and brain of SFV infected mice, an Enzyme Linked Immunosorbent Assay (ELISA) was performed according

to the manufacturer's instructions. 96 well microplates (Greiner Bio-One, Stonehouse, UK) were coated with 0.8 µg/ml capture antibody diluted in PBS and incubated overnight at 4°C. On the next day, plates were washed briefly with wash buffer containing 0.05% Tween® 20 in PBS (pH7.2-7.4), and then blocked with reagent diluent (R&D) containing 1% BSA in PBS for 1 hour at room temperature to prevent non-specific binding. In the meantime the standard solution was serially diluted 1:2 with reagent diluent seven times, starting from the top standard concentration at 1000 pg/ml. After blocking the plate, 100 µl of sample and standards were added to each well in duplicate and triplicate, respectively. The samples were diluted 1:2 and 1:5 with reagent diluent. The plate was covered and then incubated for two hours at room temperature.

Following incubation, the plates were washed two times with wash buffer and then incubated with 100 µl of detection antibody at 200 ng/ml for two hours at room temperature. After another two wash steps with wash buffer, the plates were then incubated with 100 µl of streptavidin-HRP (1:200 diluted) for 20 minutes in the dark. The plates were washed again twice and 100 µl of substrate solution (R&D), containing tetramethylbenzidine in water, was added to each well and incubated for 20 min at room temperature in the dark. The reaction was stopped using 50 µl of stop solution (2N H₂SO₄) (R&D Systems) and the plate was read on the Tecan Sunrise™ microplate reader (Tecan, Maennedorf, Switzerland) set to 450 nm to measure optical density (OD). The wavelength correction was set to 540 nm to correct possible optical imperfections in the plate. Data were analysed using Magellan™ software (Tecan).

2.21 Virus production and purification

First 2×10^7 baby hamster kidney (BHK) cells in 100 ml of 10% complete GMEM were infected with SFV strain L10 at a multiplicity of infection (MOI) of 0.1. The MOI is the average number of virus infecting each cell and can be calculated from the plaque forming units (PFU) as follows:

MOI= PFU of virus used for infection /number of cells

Choosing a low MOI to grow virus in BHK cells reduces the production of defective virus particles. After infection of BHK cells with SFV L10 cells were

grown for approximately 3-4 days until the cells looked detached and dead. The supernatant was taken off and kept at 4°C until further use.

Virus purification

The BHK supernatant containing the virus was taken from the cold room and equally divided between two 'buckets' and spun down at 2,000 rpm for 30 min at 4°C to remove large cellular debris. The supernatant was then transferred to a fresh bottle and 23 g/l sodium chloride (NaCl) and 70 g/l polyethylene glycol (PEG) were added.

The solution was then spun down at 8,000 rpm for 25 min to pull down PEG with attached virus. The supernatant was removed and the pellet was resuspended in 10 ml of GMEM (Gibco, Invitrogen) and transferred into the centrifuge tube. The resuspended virus was then underlayered with 12 ml of 20% sucrose solution in 10x TNE buffer until two distinct layers were visible and topped with GMEM to equal the weight in all centrifuge tubes. Ultracentrifuges are extremely weight sensitive and therefore all buckets and centrifuge tubes were weighed before centrifugation. The tubes were then centrifuged at 25,000 rpm for 90 min at 4°C on the L8-70M Ultracentrifuge (Beckman, High Wycombe, UK). After the virus has been pulled through the sucrose cushion and was stuck on the bottom of the tube, the medium and sucrose was poured off and the sides of the tubes were dried with a paper towel. Following this, 400 µl of 1x TNE buffer was added to the tube containing the virus and incubated for 2 hours on ice. The solution was gently stirred every 30 min. After incubation, the solution was transferred into 1.5 ml microcentrifuge tubes, frozen on dry ice and stored at -80°C until further use.

2.22 Virus plaque assay

On day one a 12-well plate was seeded with 3×10^5 BHK cells/well and 2 ml of 10% GMEM was added into each well. The plate was incubated overnight until cells were 80% confluent.

Next, a serial dilution at 1:2 of the virus stock starting from 1×10^{-2} until 1×10^{-10} was prepared, using PBSA for the dilution. Following this, the supernatant of

BHK cells was removed and 200 μ l of each dilution was added to each well in duplicate starting with the highest dilution (-2). The plate was incubated for 1 hour at 37°C and gently shaken every 15 min. In the meantime 1.2% Avicell in water and 2% minimum essential medium (MEM) (Sigma) with 2% FBS, 1% L-glutamine and HEPES buffer were prepared. Both solutions were mixed at a ratio of 1:1. After the incubation of the plates, the cells were covered with 3 ml of Avicell mix starting at the highest dilution. Once set, the plates were incubated at 37°C for at least three days.

On day four, 3 ml of 10% formaldehyde was added to each well and incubated for 1 hour at room temperature. The formaldehyde was then removed and each well was covered with 0.1% Toluidine blue solution and incubated for 30 min. The Toluidine blue was removed and the plate was gently washed with water and left to dry. After drying plates, the plaques were counted and the dilution with only 2-70 plaques visible and calculated as follows:

PFU/ml= average number of plaques (in duplicate)

amount of inoculum x dilution factor

2.23 Administration of chemokine antagonists

In this study four different chemokine antagonists were used (see below). The CCR2 (RS504393) and CCR5 (Maraviroc and DAPTA) blockers (Tocris Bioscience, Bristol, UK) and the CXCR3 blocker (compound 21) was a kind gift from Amgen Inc. (Thousand Oaks, CA, US).

The CCR2 blocker, called RS504393, can be dissolved in DMSO up to 10 mM. Therefore 10 mg of blocker was dissolved in 4 ml to reach a final concentration of 2.5mg/ml. Mice were dosed twice orally with 5 mg/kg/day in PBS by oral gavage in a volume of 300 μ l. The blocker was administered to mice between PID 3-7 during SFV infection. Brains and serum were harvested on post infection day PID 7 for flow cytometry analysis, QPCR and ELISA. Control mice were also infected with SFV but were given PBS and DMSO (6.6% DMSO solution) only without CCR2 blocker.

The CCR5 blocker Maraviroc was dissolved in 50% DMSO and PBS to a stock concentration of 10mg/ml. Mice were injected intraperitoneally (i.p) once daily

with 25 mg/kg/day of Maraviroc in PBS in a volume of 300 μ l. The blocker was administered from PID 3-7. On PID7 brains and serum were harvested for further analysis. Control mice were injected with 300 μ l of DMSO in PBS only at the same concentration as the treatment group. The other CCR5 blocker D-alanine peptide T-amide (DAPTA) was soluble to 1mg/ml in water. The mice were then injected subcutaneously (s.c) with 1 mg/kg once daily in a volume of 200 μ l water. The control mice were injected s.c with water only. The blocker was administered from PID 3 until PID 7 like Maraviroc.

Compound 21 (CXCR3 blocker) is a very organic compound and care had to be taken to dissolve the compound. First a stock solution was prepared by dissolving compound 21 in 100% DMSO to a concentration of 7.9 mg/ml. The stock solution was stored at -20°C for further use. 4 ml of the stock solution was then mixed with 2 ml of 50% PEG400 (Sigma) and 2 ml of water. The water was added very slowly to prevent the compound falling out of solution. Mice were injected s.c once daily at a concentration of 10 mg/kg. The treatment was administered to mice between PID 3-7 during SFV infection. Control mice were injected with DMSO, PEG400 and water only at the same concentration as the treatment group.

2.24 Statistical analyses

All data were analysed using the Prism 4 software (GraphPad, San Diego, CA, US). Results are shown as mean \pm standard deviation (SD) unless stated otherwise. To determine if data were normally distributed a normality test was performed using the D'Agostino and Pearson omnibus K2 or Shapiro-Wilks test. Normally distributed data were analysed using the unpaired two-tailed student's t-test if two groups were compared. If more than two groups were compared a One-way ANOVA or Two-way ANOVA was performed using the Tukey-Kramer, Bonferroni or Dunnett's post-test. If the data was nonparametric, a Mann-Whitney U test or Kruskal Wallis test with a Dunn's post test was performed. The figure legends indicate which statistical test was used for each graph. A p-value of <0.05 was considered as statistically significant and suggests that the null hypothesis can be rejected and the observed difference is not a consequence of random sampling. The sample size was determined based on previous studies.

Chapter 3

Characterization of chemokine and cytokine driven CNS responses in Semliki Forest virus infection

3.1 Introduction and aims

Neurons are post-mitotic and mainly non-regenerating cells within the CNS and need a delicate and finely balanced environment to elicit their appropriate function. As a consequence, immune responses in the brain must be tightly controlled to maintain homeostasis and subsequently the brain is considered to be an 'immune privileged' site (93, 122); MHC-I expression, antibodies, complement and pro-inflammatory cytokines are generally absent and there are no lymphatic vessels within the CNS. Additionally there is a low abundance of leukocytes detectable in the CSF, mainly memory T-cells. Despite the 'immune-privilege', resident and leukocyte derived microglia constantly exert immune-surveillance to protect the brain from invading pathogens (384).

Viruses are capable of invading the brain and often elicit life-threatening CNS immune responses characterised by breakdown of the BBB and consequent leukocyte infiltration into the brain. As discussed in the introduction, chemokines are essential for controlling the migration and positioning of leukocytes and only a few chemokines, such as CX₃CL1 and CXCL12, have been reported to be constitutively expressed in the healthy CNS (204). Viral infections of the CNS can trigger substantial chemokine expression by glia and neurons, although the function and relevance of chemokines in attracting antiviral leukocyte subsets into the CNS has yet to be fully elucidated (385, 386). A partial chemokine expression analysis in the virally infected CNS has only been conducted for LCMV and MHV infected mice but not in great detail (128, 129). In addition to that the expression of some of the inflammatory CC and CXC chemokines has also been investigated during WNV infection, and this is discussed in the introductory chapter 1.5 (197, 214). Depending on the virus or strain used, chemokine-mediated leukocyte influx into the infected CNS has been shown to be beneficial or detrimental for disease outcome (340, 356, 361). However to understand chemokine-mediated leukocyte migration into the CNS in greater detail, it was first necessary to establish a clearer picture of the expression of chemokines during viral encephalitis.

Therefore the main aim of this chapter was to identify, in unprecedented detail, the form and magnitude of chemotactic cues expressed by the virus-

infected brain. Developing a deeper understanding of this key aspect of the encephalitic process is central to our ability to therapeutically manipulate it.

Furthermore the expression of cytokines and antiviral genes in the brain is also very important for initiating innate immune responses in the CNS, to rapidly clear virus from this delicate tissue. *Therefore another aim was to identify cytokines and genes involved in innate immune responses during viral encephalitis.*

As a model of infection, Semliki Forest Virus (SFV) has been used for most of the studies in this thesis. The advantage of working with SFV is that it is a low-risk pathogen, which has been previously used in experimental systems *in vitro* and *in vivo*, to study the pathogenesis of neurotropic viruses (309, 378). SFV strains A7(74) and L10 have been used for all SFV studies, to determine whether varying degrees of virulence have an effect on the expression of chemokines and cytokines during viral encephalitis. The pathogenesis of viral encephalitis following infection with strain A7(74) has been well documented and is discussed in chapter 1.4 (293, 309, 378). However, symptoms arising during the virulent infection with L10 have not yet been documented. *In this chapter, I additionally set out to describe, for the first time, neuropathological symptoms developing during L10 infection of mice.*

3.2 Determination of viral titers in the blood and brain during Semliki Forest virus infection

Before defining levels of chemokine and cytokine expression in the brain during SFV infection, viral titers in the blood and brain were determined by QPCR, to test the efficiency of SFV as a model of viral encephalitis in C57BL/6 mice. Previous studies have reported that the blood brain barrier becomes leaky between days 4 and 10 after acute viral encephalitis (294, 305). Since the focus of this study was to analyse chemokine expression and leukocyte infiltration during acute viral encephalitis, mice were infected with an i.p. inoculum of 5×10^3 PFU with strains A7(74) or L10 as suggested by previous studies (298). While mice were successfully infected with A7(74) using this dose, L10 mice did not become ill as expected and previously described by Gates *et al.*, where BALB/c mice succumbed to the disease on PID 4 (387). Subsequently the

inoculation dose of L10 was increased to 5×10^4 and 2×10^5 PFU, and the majority of mice finally succumbed to lethal L10 infection between PID 5-6 using 2×10^5 PFU (Fig. 3.1). Blood and brain samples were collected from A7(74) infected mice on PID 3, 4, 5, 7 and 10 and compared to healthy control samples. During L10 infection samples were taken from mice on PID 4, when mice were still asymptomatic, and between PID 5-6, when mice were terminally ill and were subsequently euthanized according to the Home Office regulations.

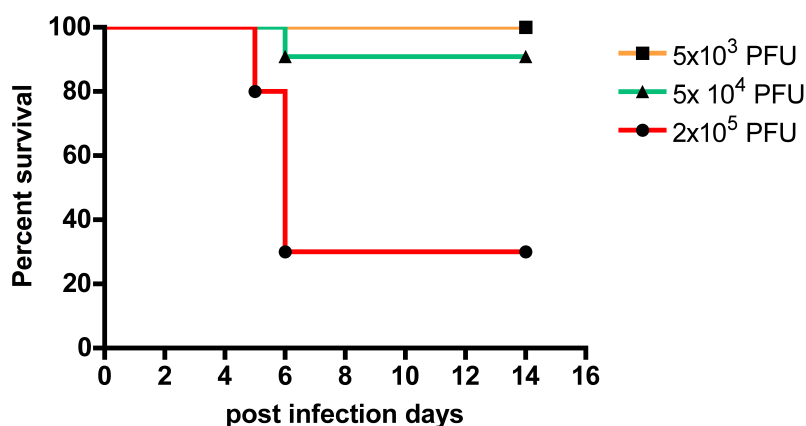


Figure 3.1 Determining the dose of initial virus concentration of L10 for initiating lethal infection of mice

Mice were infected with different doses of SFV strain L10 as indicated and survival was analysed. The experiment was terminated 14 days post infection. n=10 mice per group.

To determine viral titers in the blood, plasma samples were tested for the presence of viral transcripts, measuring the expression of E1, a viral capsid protein of SFV. During A7(74) infection, viral titers in the plasma reached high levels by PID 3 and slowly decreased over time (Fig. 3.2 A). By PID 7 the virus was almost cleared from the plasma. During L10 infection the viral titer in the plasma attained higher levels reaching almost 1×10^8 E1 copies/ml plasma. In comparison to avirulent infection with SFV, during L10 infection, virus was not cleared from the plasma and the titer remained elevated until mice died or were terminally ill (Fig. 3.2 B).

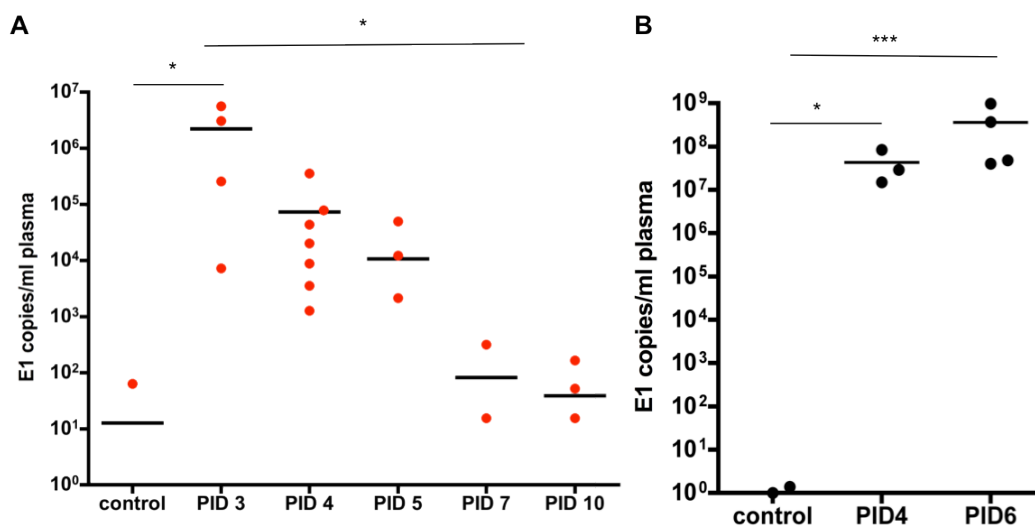


Figure 3.2 Viral titers in the plasma of mice infected with SFV strain A7(74) or L10

Mice were inoculated i.p. with 5000 or 2×10^6 PFU of SFV strain A7(74) or L10, respectively, and whole blood was collected on post infection day (PID) 3, 4, 5, 7 and 10. Viral gene transcripts for E1 in the plasma of mice were quantified by QPCR. (A) Viral titer in mice infected with strain A7(74) or (B) L10 with $n=4-7$ or $n=3-4$ mice, respectively, per time point. (Kruskal-Wallis test with Dunn's post test; * $p < 0.05$, *** $p < 0.001$)

In the brains of SFV A7(74) infected mice, viral copy numbers significantly increased over the time course of infection and seemed to peak on PID 7. On PID 10, a slight but not significant reduction in viral copy numbers was observed (Fig. 3.3 A). During L10 infection CNS viral E1 transcript levels were only slightly elevated on PID 4 but quickly increased to high levels by PID 5 or 6, when mice became terminally ill and had to be euthanized (Fig. 3.3 B).

Thus, these results demonstrate that SFV A7(74) is cleared from the blood while simultaneously replicating to a high titer within the CNS. In the brain, the number of viral transcripts of SFV reached maximal levels on PID 7. By PID 10 SFV titers slowly appeared to be decreasing. This is in line with findings from a previous study by Fazakerley *et al.*, where they have shown that SFV cannot be detected by day 8 using a virus plaque assay and by day 14 using in-situ hybridisation (298). In contrast, virus RNA during SFV L10 infection was not reduced with the progression of the disease in the blood or the brain, and mice succumbed a few days post infection.

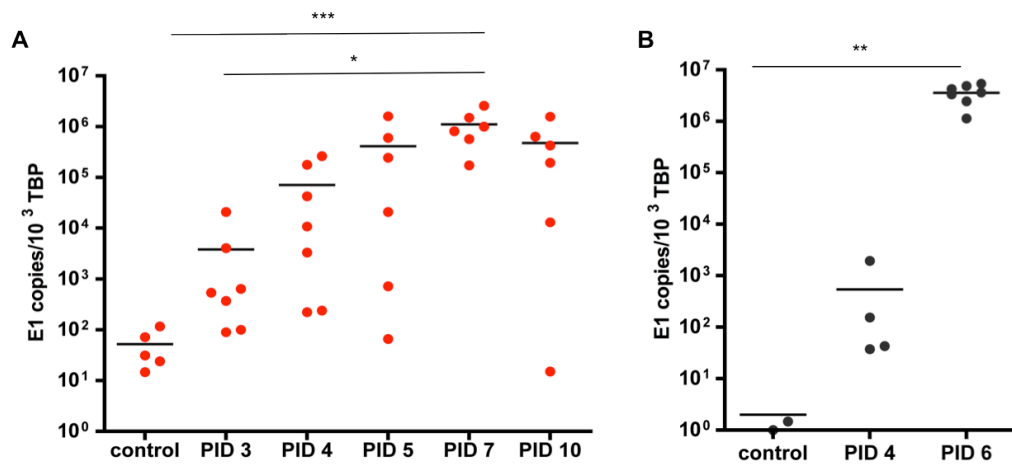


Figure 3.3 Viral titer in the brains of mice infected with SFV strain A7(74) or L10

Mice were inoculated with 5000 or 2×10^6 PFU of SFV A7(74) or L10, respectively, and brains were collected on post infection day (PID) 3, 4, 5, 7 and 10. Viral gene transcripts for E1 were assayed by QPCR, and absolute copy numbers calculated and normalized to TATA binding protein (TBP). Each sample was tested in triplicate. (A) E1 gene transcripts during A7(74) and (B) L10 infection with $n=6-7$ mice and $n=4-7$ mice, respectively, per time point. (Kruskal-Wallis test with Dunn's post test; * $p < 0.05$, ** $p < 0.01$, *** $p < 0.001$)

3.3 Neuropathology during avirulent and virulent SFV infection

Having investigated viral titers during infection with avirulent and virulent strains of SFV, in the next experiment mice were examined for pathological changes in the brain. Firstly, mice were infected with SFV A7(74) or L10, and brains were collected for immunohistochemistry. Brains were fixed in paraformaldehyde, processed and embedded in paraffin before being cut into 6 μm thick sections and stained for the viral non-structural protein 3 (nsp3).

Infection of mice with SFV A7(74) does not induce any overt signs of disease in mice, but staining for viral nsp3 in the brains of infected mice revealed many perivascular foci, particularly around the hippocampus, striatum and frontal cortex (Fig. 3.4 A-E). The shape of infected neurons appeared normal throughout infection. The cerebellum contained fewer infected cells compared to other parts of the brain, and, on the basis of cell morphology and localisation of these cells, infection within this part of the brain appeared to affect mostly Purkinje neurons (Fig. 3.4 E).

The clinical picture of disease in L10 infected mice has not been documented in previous studies, and will briefly be described here. All the mice appeared to be healthy on PID 4 with no signs of disease but on PID 5-6 mice developed a sudden onset of the disease, and mice succumbed rapidly thereafter within a few hours. The typical signs of prolonged illness usually observed in sick mice, such as ruffled fur and weight loss, were not observed during L10 infection. Due to the sudden onset of the disease, mice were monitored every four hours to check their health status. Once the mice became sick, they often displayed severe neurological defects ranging from hind- or forelimb paralysis (Fig. 3.5 A-C), seizures, loss of orientation (Fig. 3.5 D), ataxia. One mouse also developed narcoleptic behaviour in so far as this mouse would constantly fall asleep while being fully active during the waking state. The most common sign observed was hindlimb paralysis and only occasionally one of the other signs was observed. Histological examination of brains from terminally ill mice revealed extensive infection throughout the brain with perivascular foci and cuffings (Fig. 3.6 A-D).

Taken together, infection with A7(74) is asymptomatic in mice, whereas infection with L10 results in the development of a severe neurological disease, which is rapidly fatal to mice. During both infections, viral proteins could be detected within the brain by immunohistochemistry, showing widespread infection within the parenchyma although the distribution of perivascular foci and infected neurons was wider during L10 infection compared with A7(74). Previous studies have also shown that the spinal cord is affected by SFV infection, which would explain the development of paralysis in a large number of these mice (378).

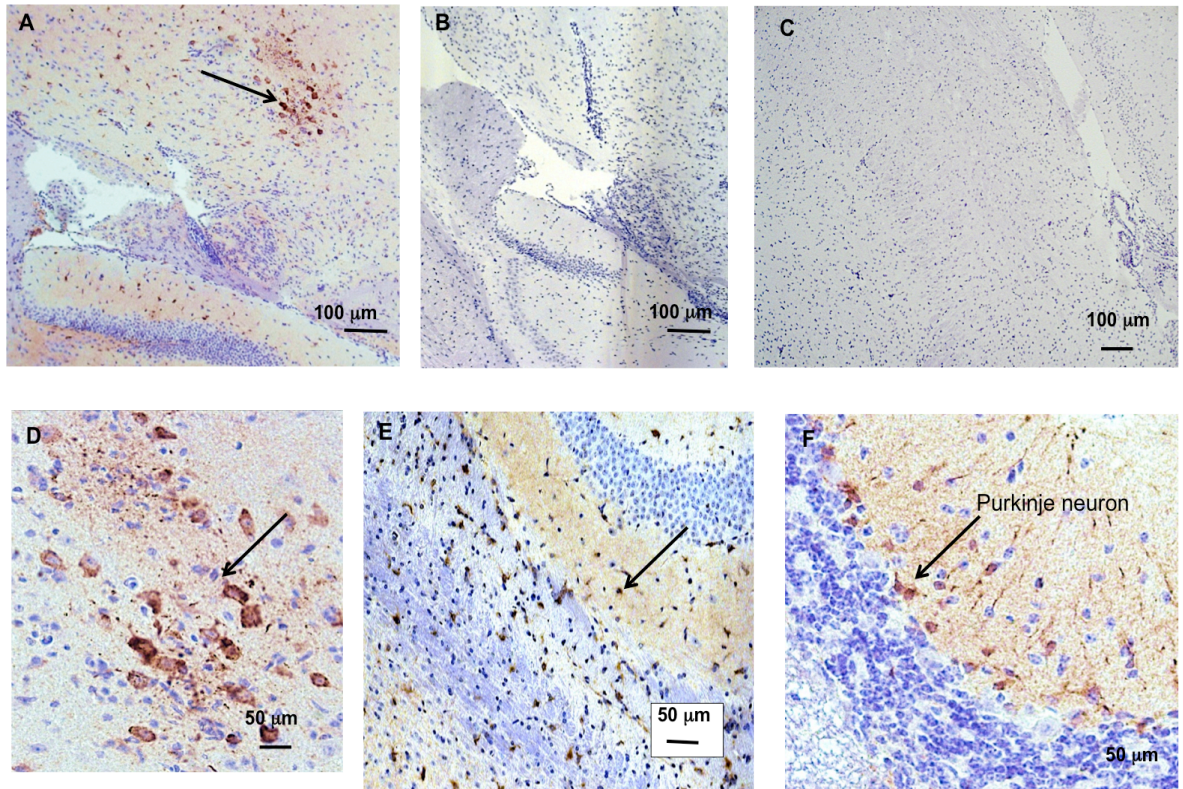


Figure 3.4 SFV nsp3 staining within mouse brains following infection with A7(74)

C57BL/6 mice were infected i.p. with SFV A7(74) and brains were harvested on day 7. The brains were fixed in formalin, embedded in paraffin and cut into 6 μm thick sections. Brain sections were stained with anti-mouse SFV nsp3 antibody using the DAKO Envision system. Viral protein was detected throughout the brain. (A) Perivascular foci of SFV within the limbic system, and (B) staining with the appropriate isotype control, both at 5x magnification. (C) Uninfected control brain stained for nsp3. Magnification 5x. (D) SFV infected neurons in the brain, magnification 40x. (E) Infected neuronal cells in the cerebellum and (F) in cortical areas of the brain. Both images were taken at 20x magnification. Images are representative of 7 mice per time point. Arrows indicate SFV infected neurons

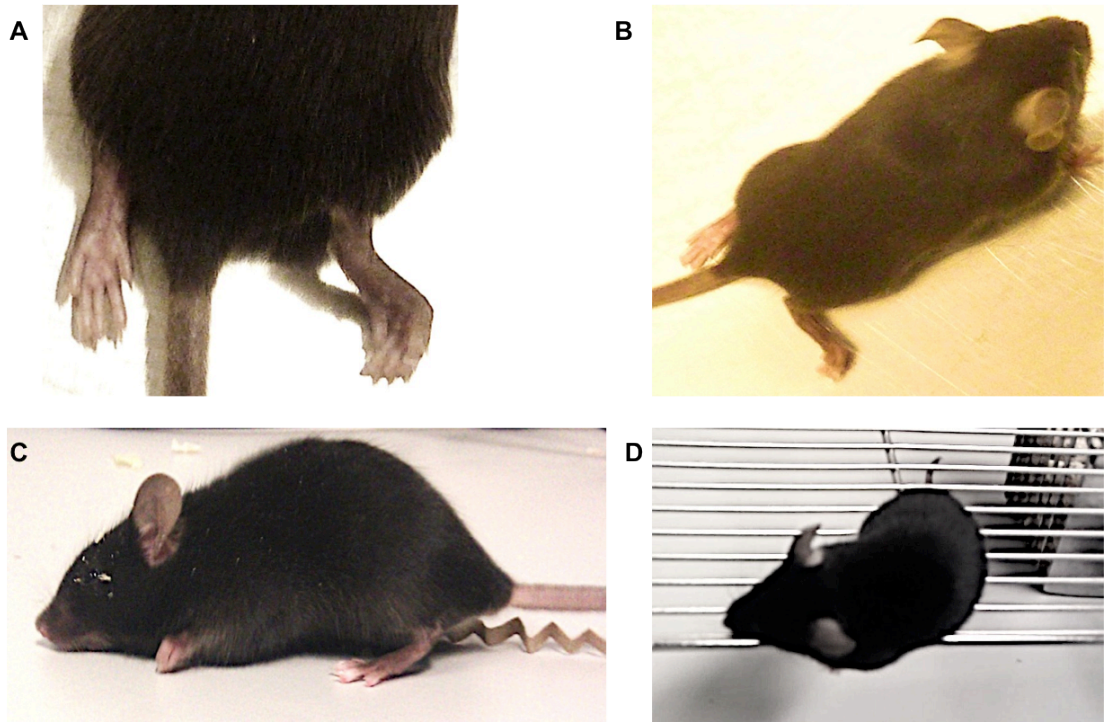


Figure 3.5 Neuropathological changes in mice following infection with SFV using the virulent strain L10

Mice were infected i.p. with SFV strain L10. Mice became ill between post infection days 5-6 and showed various neurological signs. (A) Mouse with complete or (B) partial hind limb paralysis. (C) Mouse with fore limb paralysis and (D) loss of orientation. Images are representative of 10 mice.

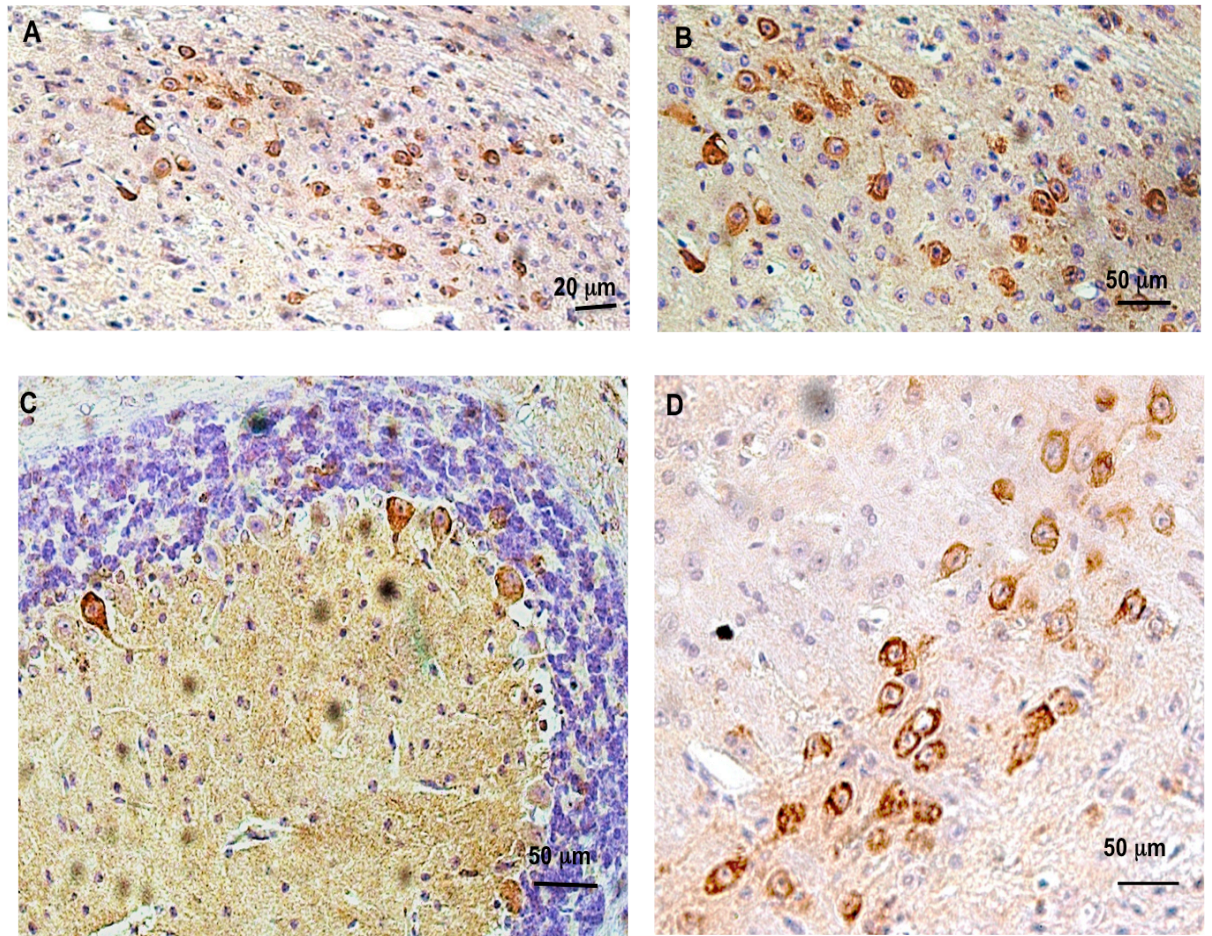


Figure 3.6 SFV nsp3 staining within L10 infected mouse brains

C57BL/6 mice were infected i.p. with SFV L10 and brains were harvested from terminally ill mice (PID5-6). The brains were formalin-fixed, embedded in paraffin and cut into 6 μm thick sections. Brain sections were stained with anti-mouse SFV nsp3 antibody using the DAKO EnVision system. Viral protein was detected throughout the brain. (A, B and D) Infected cells within the limbic system and (C) in the cerebellum. Magnification at 20x (A and C) and 40x (B and D).

3.4 Assessment of RNA quality of mouse brains samples infected with SFV strain A7(74) or L10

To test the brain samples from A7(74) or L10 infected mice by TLDA, the RNA quality was first assessed using the Agilent Bioanalyser. All RNA samples for chemokine expression analysis were of high quality displaying an RNA Integrity number (RIN) >8 (Fig. 3.7 and 3.8). The definition of the RIN value is explained in more detail in the Materials and Methods section 2.18.1. The electropherogram for each sample showed a distinct and clear 18S and 28S band, which, again, is an indicator of high quality RNA (Fig. 3.7 A and B, Fig. 3.8 A and B). RIN values for all A7(74) and L10 sample, analysed by TLDA, are shown in Appendix 2 A and B.

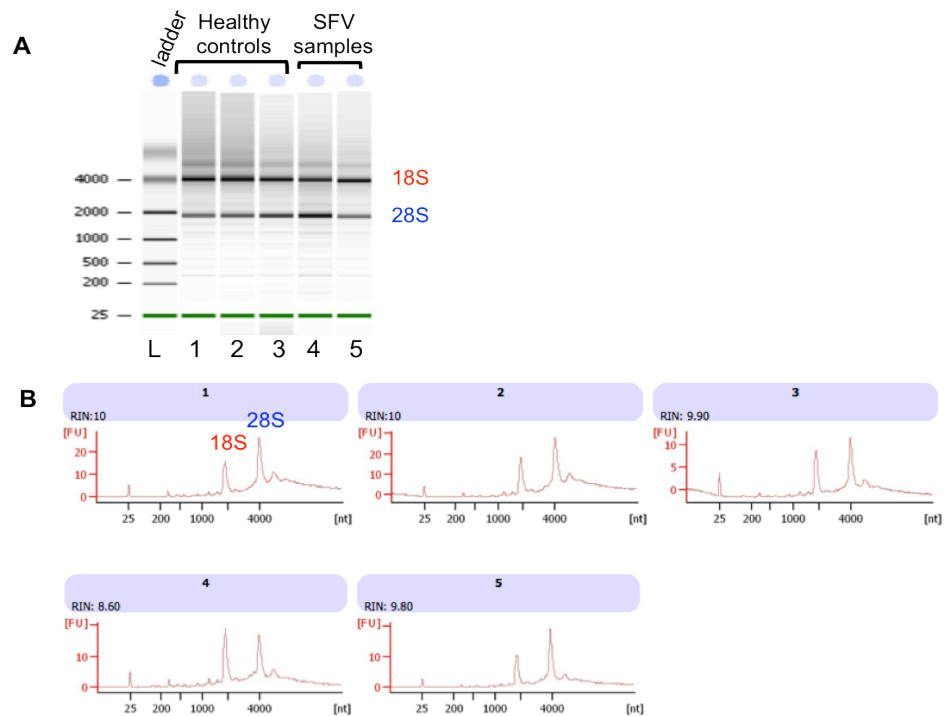


Figure 3.7 Assessment of RNA quality isolated from mouse brains infected with SFV strain A7(74)

Total RNA was isolated from healthy controls and SFV A7(74) infected brains over the time course of infection and the RNA quality was analysed using the Agilent Bioanalyser. (A) Representative gel-like image of total RNA isolated from murine brains. Lane L: size marker (nucleotides, nt); Lane 1-3: healthy control brains; Lane 4-5: brains from post infection day 3; The distinct ribosomal RNA bands 18S and 28S were observed for all samples. (B) Electropherograms are shown for all 5 samples. The x-axis represents the amplicon size (nt), while the y-axis represents fluorescence units (FU). The RNA integrity number (RIN) was calculated and is indicated on the left hand corner of each electropherogram. The larger 28S ribosomal peak closely follows the 18S peak. High RIN values, and distinct 18S and 28S ribosomal bands characterize high quality RNA.

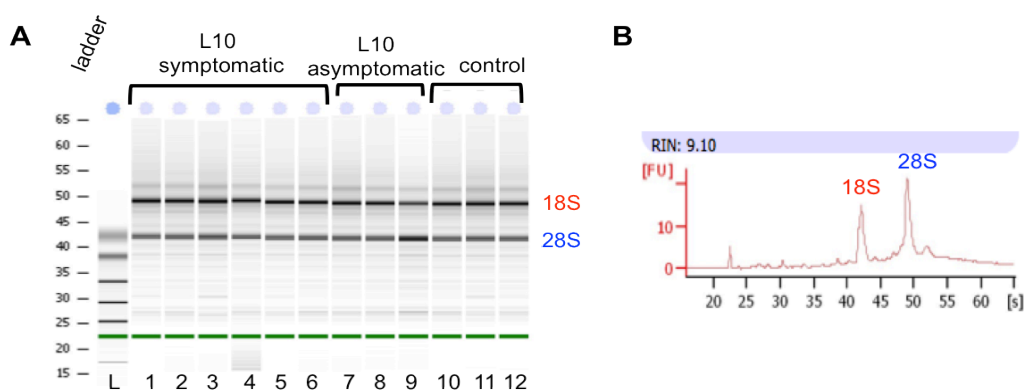


Figure 3.8 Assessment of RNA quality isolated from L10 infected mouse brains

Total RNA was isolated from healthy controls and SFV L10 infected brains over the time course of infection and the RNA quality was analysed using the Agilent Bioanalyser. (A) Representative gel-like image of isolated RNA. Lane L: size marker (nucleotides, nt); Lane 1-6: samples from terminally ill mice displaying several different neurological symptoms; Lane 7-9: samples from infected mice before the onset of symptoms; Lane 10-12: healthy uninfected control samples. Distinct ribosomal RNA bands 18S and 28S were observed for all samples. (B) Representative electropherogram showing the RNA profile of a high quality RNA sample. The x-axis represents the amplicon size (nt), while the y-axis represents fluorescence units (FU). The RNA integrity number (RIN) was calculated and is indicated on the left hand corner of each electropherogram.

3.5 Chemokine expression during avirulent infection with SFV A7(74)

Having determined viral titers in the brain and blood, and characterised neuropathological changes during avirulent and virulent infection with SFV, the next goal was to examine chemokine expression during infection with the avirulent strain A7(74) and virulent strain L10. To identify the chemokine expression profile during A7(74) infection, mice were infected with the virus for 10 days and brains were collected on PID 3, 4, 5, 7 and 10 to perform TaqMan low density array analysis (TLDA) and QPCR. For TLDA analysis, the microfluidic cards were first designed in the lab and finally manufactured by Applied Biosystems. A 384-well format was selected, containing 32 genes, including most inflammatory CC- and CXC- chemokines, CX₃CL1, XCL1, and a few inflammatory cytokines and innate immune response genes, known to play a role during viral infections. In Figure 3.9 and 3.11 only the most highly upregulated chemokines are shown. The fold change of other chemokines that are not or only minimally upregulated during SFV infection is presented in Appendix 3. TLDA results of cytokine and innate immune response gene expression are presented in section 3.7. Similar to chemokines only a limited number of cytokines is shown in Fig. 3.20. A detailed list of fold changes for each cytokine and other innate immune

genes is shown in Appendix 3. The table containing all genes selected for TLDA analysis of A7(74) samples is shown in Appendix 1A.

3.5.1 CC-chemokine expression

The results obtained from the TLDA analysis demonstrate that CCL2 and CCL5 were the most upregulated CC-chemokines (Fig. 3.9), both being upregulated by more than 100-fold during viral encephalitis compared with an uninfected healthy control brain. The maximal upregulation was reached 7-10 days post infection. mRNA levels for CCL3, CCL4, CCL7 and CCL8 were significantly (t-test; $p < 0.01$) upregulated on day 7, but the magnitude of expression was lower than that of CCL2 and CCL5. The expression of CCL11 was only minimally elevated during SFV infection (approximately 1.5-fold) compared with baseline but did not reach statistical significance. CCL20 was not up- or downregulated in response to viral infection and expression was similar to uninfected mouse brains (data not shown).

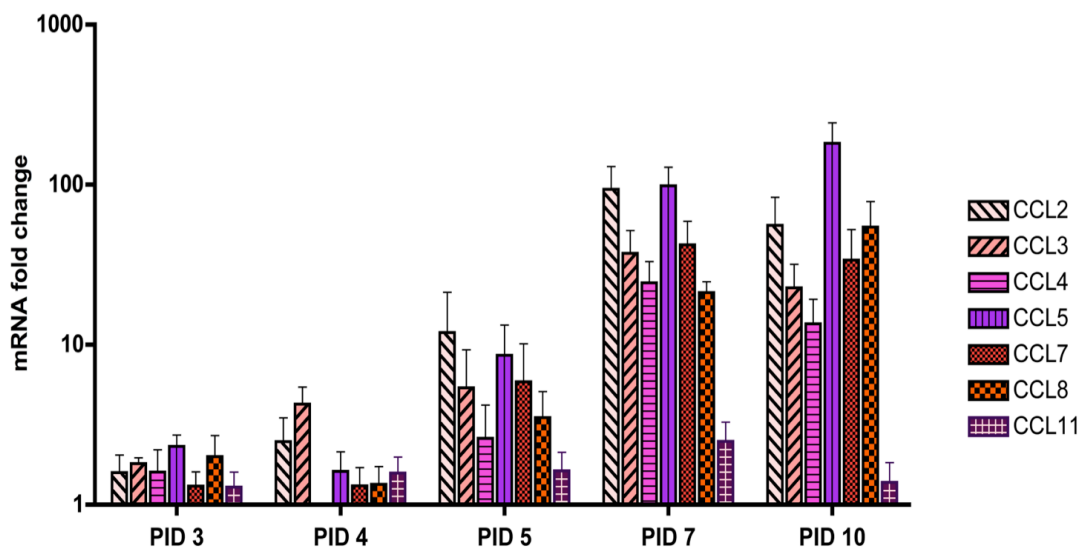


Figure 3.9 CC-chemokine expression during viral infection of the brain with SFV A7(74)

cdNA from high-quality RNA samples, isolated from infected mouse brains on post infection day (PID) 3, 4, 5, 7 and 10, was analysed for the expression levels of CC-chemokines using TLDA analysis. Samples from each time point ($n=4-5$ mice) were double normalized; firstly, to the housekeeping gene 18S and secondly, to an uninfected healthy control brain (mean relative quantification (RQ) value set to 1). The RQ values are depicted as mRNA fold changes, represented on the y-axis. Samples with a RQ values >1 signify upregulation of gene transcripts compared to the healthy control brain. Each sample was tested in triplicate. Data represent mean \pm SD

In general, the expression of all CC-chemokines on PID 3 and 4 was relatively similar to control brains (relative quantification (RQ) value =1). Most chemokines were maximally upregulated between PID 7 and 10, which coincided with high viral titers in the brain as illustrated in Fig. 3.3 A.

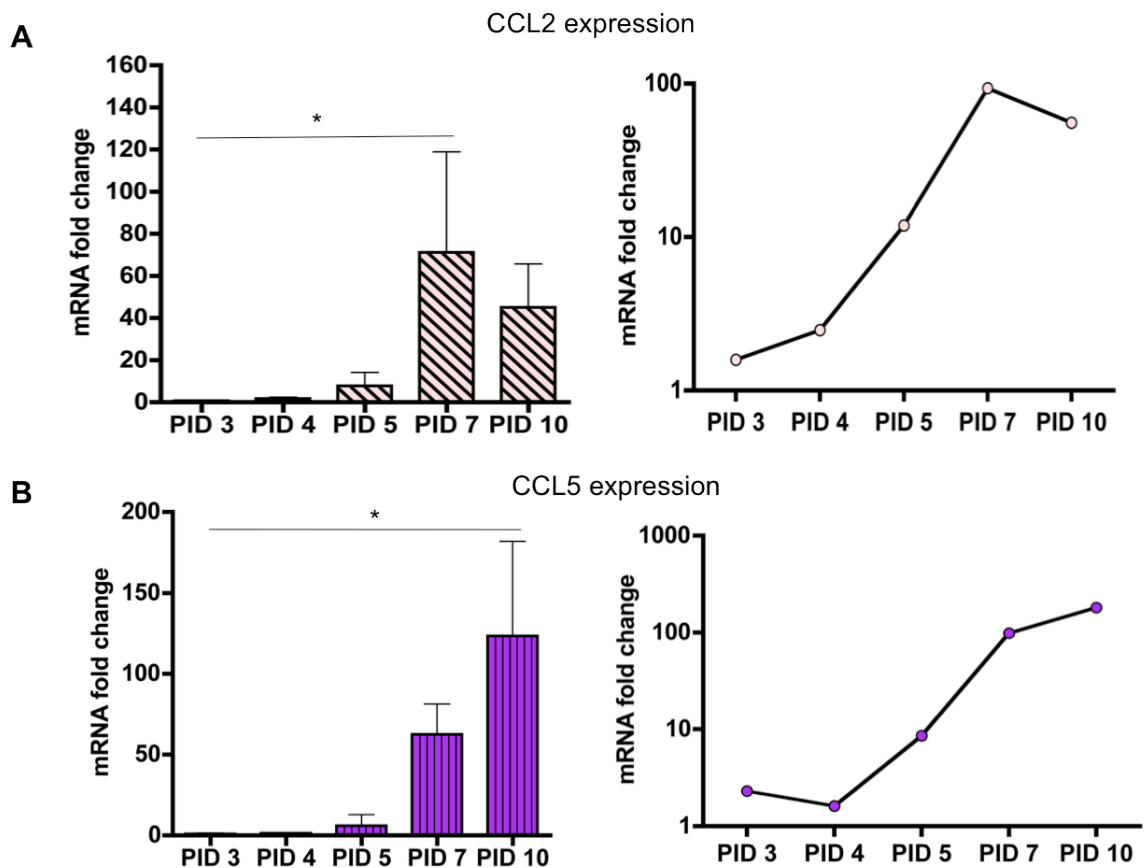


Figure 3.10 Validation of TLDA results by QPCR for the genes CCL2 and CCL5 during SFV infection of the brain with A7(74)

Two chemokines, CCL2 and CCL5, were highly upregulated during viral infection of the brain, and were validated by QPCR. The relative gene expression compared to uninfected control brains and normalised to TATA binding protein (TBP) is shown on the y-axis. (A) CCL2 expression by QPCR (left panel) and mRNA fold change compared to an uninfected control brain measured by TLDA (right panel). (B) CCL5 expression by QPCR (left panel) and fold changes evaluated by TLDA analysis (right panel). $n=3$ mice for QPCR and $n=4-5$ mice for TLDA analysis. Each sample was tested in triplicate. Data are presented as mean \pm SD. PID= post infection day (Kruskal-Wallis test with Dunn's post test; * $p<0.05$)

The expression of CCL2 and CCL5 was most upregulated during SFV A7(74) infection compared to healthy control. A QPCR analysis was performed to validate the CCL2 and CCL5 upregulation in infected brains. CCL2 expression was significantly ($p<0.05$) upregulated on PID 7 compared with controls, before

decreasing by PID 10 (Fig. 3.10 A). This decrease was not statistically significant. CCL5 expression was significantly ($p < 0.05$) upregulated by PID 10 compared to PID 3 samples (Fig. 3.10 B). Both results obtained by QPCR validate the TLDA results and confirm the strong upregulation of CCL2 and CCL5 expression in response to SFV A7(74) infection of the brain (Fig. 3.10).

3.5.2 CXC-chemokine expression

CXCL9 and CXCL10 were the most highly upregulated CXC-chemokines during A7(74) infection, increasing more than 300-fold and 500-fold, respectively, relative to a healthy uninfected control brain (Fig. 3.11 A). The maximal upregulation was obtained at 7 days post infection. The chemokine CXCL16 was also significantly upregulated during viral encephalitis, showing a 12-fold upregulation compared with healthy control mouse brains. CXCL1 was minimally elevated compared with baseline levels, but the mRNA fold change of CXCL1 over the time course of infection was not significantly altered ($p > 0.05$). The expression of the other CXC-chemokines CXCL2, CXCL3, CXCL5 were unchanged compared with healthy control brains, suggesting a minor involvement of these chemokines during SFV encephalitis.

The 'homeostatic' chemokine CXCL12 has been reported to play a role in the maintenance and homeostasis of the blood-brain barrier (388). Disruption of the polarised expression of CXCL12 on the BBB during neuroinflammation has been shown to promote leukocyte infiltration into the CNS (389). Therefore the expression of CXCL12 was also examined by TLDA. The results show that CXCL12 expression is downregulated in comparison to healthy control brains but this did not reach statistical significance ($p > 0.05$) (Fig. 3.11 B). In general, maximal upregulation of all CXC-chemokines was seen by PID 7. CXCL9 and CXCL10 were upregulated very early during infection, being 5-10 fold upregulated by PID 3, although this was not statistically significant (Fig. 3.11 A).

To examine, if the expression of the two major upregulated chemokines CXCL9 and CXCL10, and CXCL1 is reproducibly elevated during SFV A7(74) infection relative to healthy uninfected control brains, a QPCR analysis was performed to validate the results obtained through TLDA analysis. Levels of CXCL9 expression were significantly ($p < 0.05$) upregulated in the brain on PID 7, followed by a

decrease of expression on PID 10 (Fig. 3.12 A). CXCL9 protein levels were also significantly ($p<0.01$) upregulated in the blood on post infection day 5, and reached maximal levels at this time point (Fig. 3.12 B).

CXCL10 transcripts were also significantly upregulated in the brain on PID 7 ($p<0.01$) and 10 ($p<0.05$) compared to PID 3 samples (Fig. 3.13 A). CXCL1 was only minimally upregulated (<5 fold) in the brain during infection compared to an uninfected control brain using TLDA analysis. QPCR analysis confirmed that CXCL1 expression was not significantly different during avirulent infection compared with controls (Fig. 3.13 B).

CXCR5 is commonly known to be mainly expressed on B-cells and binds to the ligand CXCL13 (390). The expression of CXCR5 was measured by QPCR only since this chemokine receptor was not included on the TLDA plates. It was found that CXCR5 is significantly upregulated on PID 7 and 10 ($p<0.05$), suggesting the possibility of B-cell infiltration into the virally infected brains at these two time points (Fig. 3.14).

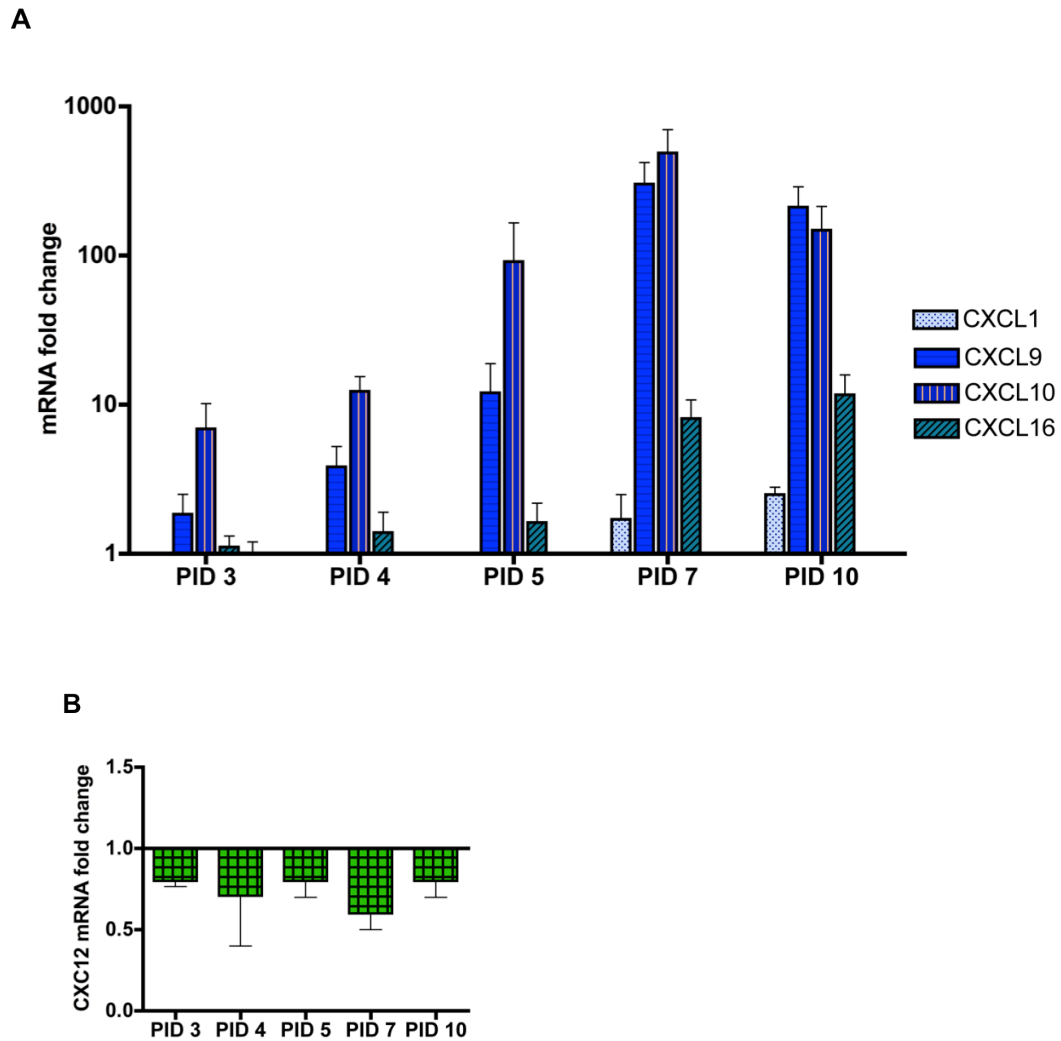


Figure 3.11 Identification of CXC-chemokines upregulated during viral infection of the brain with SFV A7(74)

RNA isolated from SFV infected brains was analysed for the expression of CXC chemokines by TLDA. Samples from each time point ($n=4-5$ mice) were double normalized; firstly, to the housekeeping gene 18S and secondly, to an uninfected healthy control brain (mean relative quantification (RQ) value set to 1). The y-axis represents fold changes of CXC chemokine expression compared to a healthy control brain. Samples with a RQ value >1 are upregulated, and RQ values <1 are downregulated compared to the uninfected control. (A) Upregulation of specific CXC-chemokines. (B) Fold change of CXCL12 over the time course of infection. Each sample was tested in triplicate. Data represent mean \pm SD. PID=post infection day (Kruskal-Wallis test; * $p<0.05$, ** $p<0.01$)

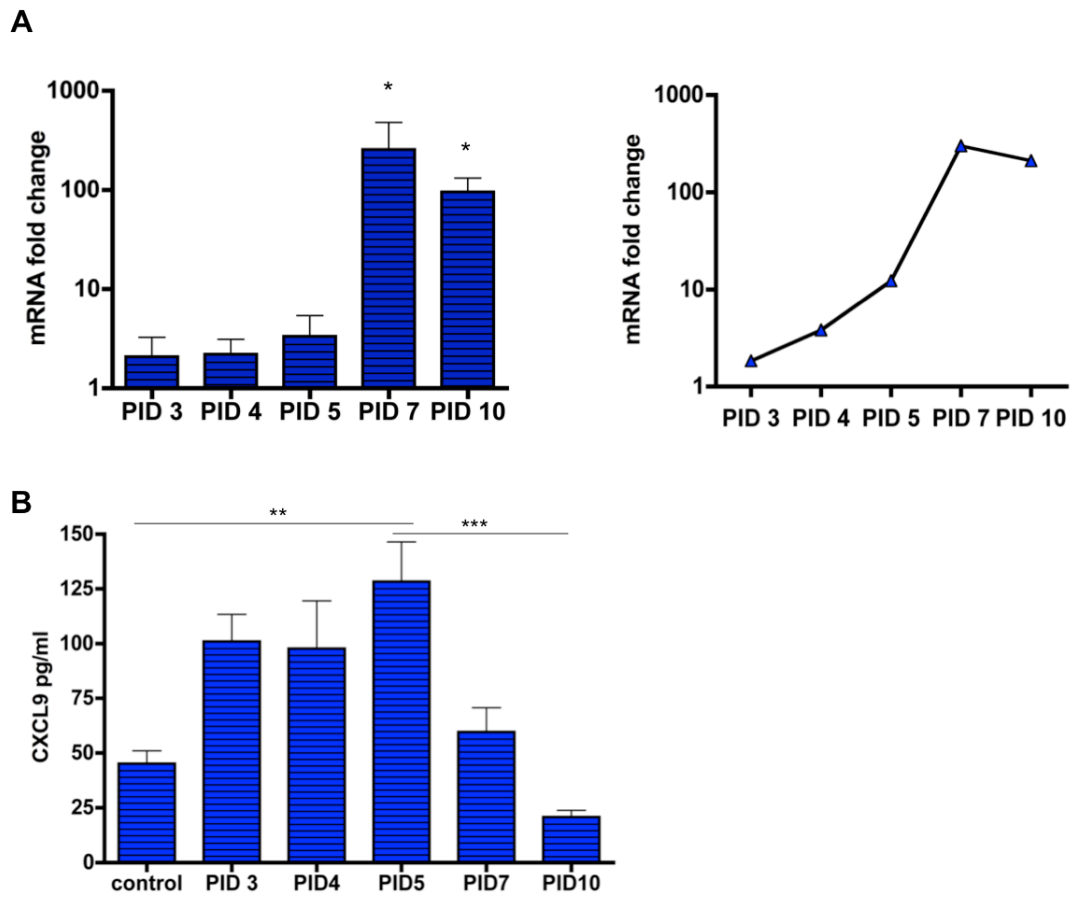


Figure 3.12 Validation of CXCL9 expression by QPCR and concentration of CXCL9 in the plasma during SFV infection

The relative expression of CXCL9 was validated by QPCR and compared to results obtained from TLDA analysis. (A) Relative expression of CXCL9 determined by QPCR (left panel) and fold increase of CXCL9 expression relative to an uninfected control brain measured by TLDA (right panel). Data represent mean \pm SD, $n=3$ mice for QPCR and $n=4-5$ mice for TLDA analysis. Each sample was tested in triplicate. (B) Concentration of CXCL9 measured by ELISA. The results are representative of 5 mice per time point. Each sample was tested in duplicate. PID=post infection day ((A) Kruskal-Wallis test with Dunn's post test and (B) One-way ANOVA with Tukey's post test; * $p<0.05$, *** $p<0.001$)

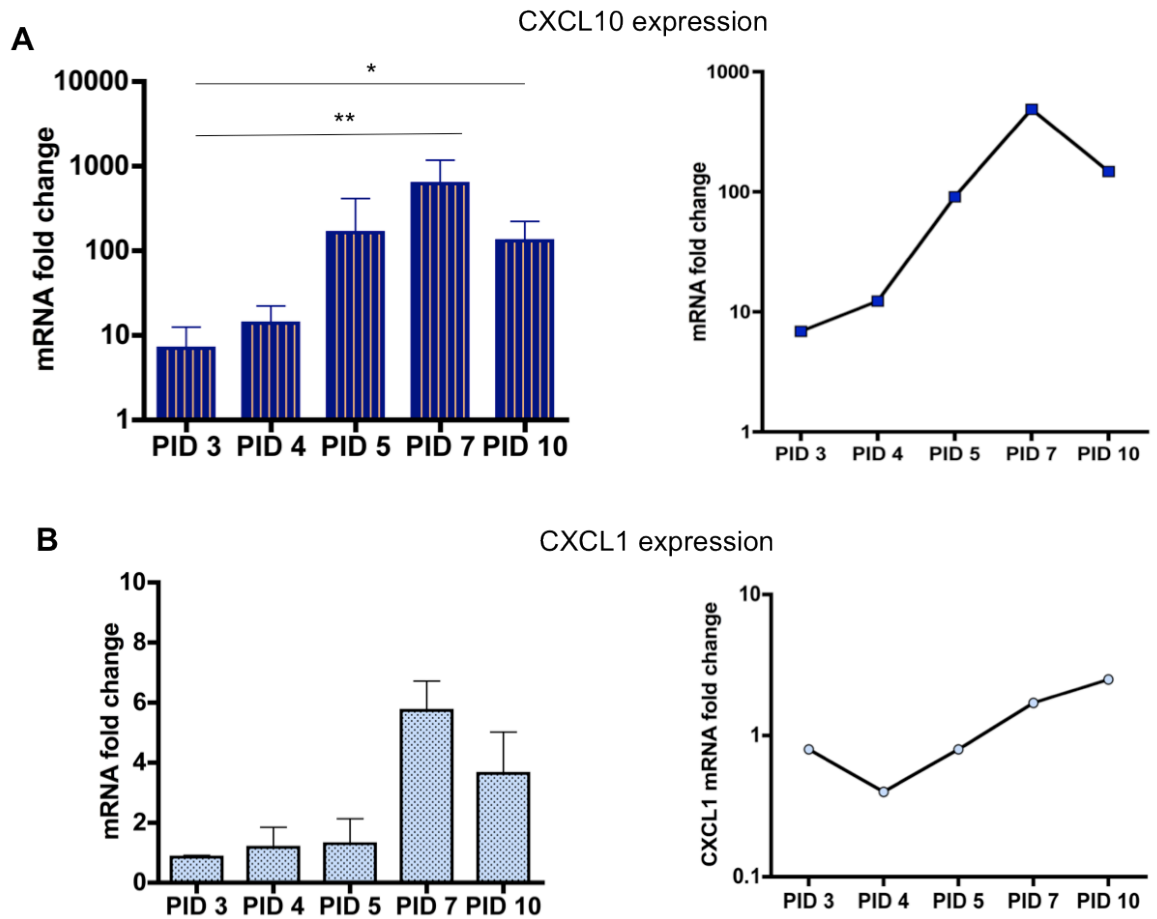


Figure 3.13 Validation of TLDA results by QPCR for CXCL10 and CXCL1 expression during SFV infection of the brain with strain A7(74)

The expression of CXCL10 and CXCL1 was validated by QPCR and compared to results obtained from TLDA analysis. (A) Relative expression of CXCL10 compared to uninfected controls determined by QPCR (left panel), and fold increase of CXCL10 expression relative to an uninfected control brain measured by TLDA (right panel). (B) Relative expression of CXCL1 determined by QPCR (left panel) and fold change evaluated by TLDA (right panel). Data are presented as mean \pm SD, $n=3$ mice for QPCR and $n=4-5$ mice for TLDA analysis. Each sample was tested in triplicate. ((A) Kruskal-Wallis test with Dunn's post test and (B) student's t-test; * $p<0.05$, ** $p<0.01$)

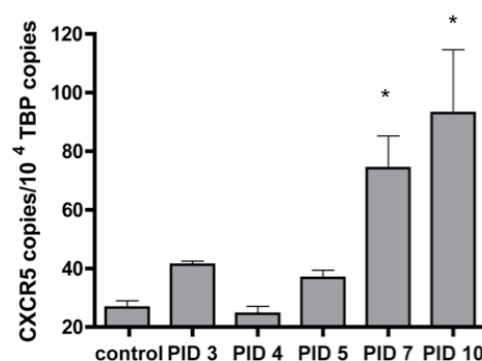


Figure 3.14 Expression of the chemokine receptor CXCR5 in SFV A7(74) infected brains over time

Absolute copy numbers of CXCR5 were measured by QPCR. Data were normalized to 1×10^4 copies of TATA binding protein (TBP). Data represent means \pm SD, $n=3$ mice per time point. PID= post infection day (Kruskal-Wallis test with Dunn's post test; * $p < 0.05$)

3.5.3 CX₃CL1 chemokine expression

CX₃CL1 is constitutively and highly expressed in the healthy CNS of mice. TLDA results reveal that the expression of CX₃CL1 was not significantly altered during viral infection with SFV A7(74) compared with healthy uninfected mouse brains (Fig. 3.15 B). Validation by QPCR confirmed this result (Fig. 3.15 A). Generally, CX₃CL1 is highly expressed in control and infected brain samples but there is no difference in expression between both groups during SFV driven viral encephalitis.

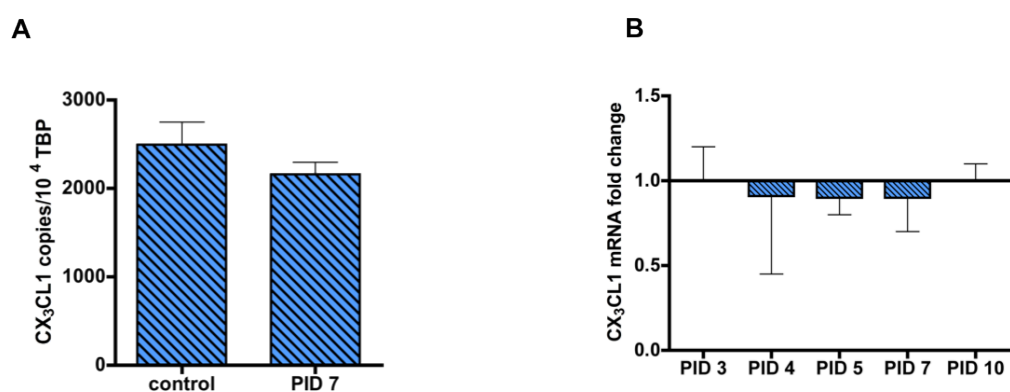


Figure 3.15 Validation of CX₃CL1 expression during SFV A7(74) infection

Absolute copy numbers were calculated for the expression of (A) CX₃CL1 and normalized to 1×10^4 copies of TATA binding protein (TBP). Samples from uninfected and infected mice from post infection day (PID) 7 were compared ($n=3-4$ mice). (B) The fold change of CX₃CL1 over the time course of infection is shown relative to the expression of an uninfected control brain (measured by TLDA analysis). Results are shown as mean \pm SD. (student's t-test; not significant)

Taken together, these results demonstrate that chemokines are selectively upregulated during SFV A7(74) infection. Some chemokines were highly upregulated, including CCL2, CCL5, CXCL9 and CXCL10. The expression of some chemokines, including CCL11, CXCL12 and CX₃CL1, was not significantly altered compared to uninfected healthy mouse brains, highlighting the differential expression of chemokines during viral encephalitis. Therefore, the expression profile of chemokines in the CNS, obtained during SFV infection, suggests that induction of chemokine expression after avirulent SFV infection is not a random process, but appears to be a relatively specific and selective process. I will next examine whether this is also the case during virulent infection with SFV using strain L10.

3.6 Chemokine expression during virulent infection with SFV L10

After inoculation of mice with L10, mice were monitored daily several times until the onset of neurological symptoms. As described above, mice became ill very suddenly and displayed severe neurological symptoms. To examine whether there is a difference in the magnitude and type of chemokines expressed before and after the onset of clinical signs, brains were collected from asymptomatic mice on PID 4 and from terminally ill mice, displaying severe neurological signs. The term asymptomatic was defined as the absence of any signs of illness or condition, and the term symptomatic was used for mice exhibiting signs of sickness. Signs of disease typically started between day 5 and 6 post infection. Once mice became severely ill, they were immediately euthanized in accordance with Home Office regulations.

After testing the RNA quality, samples were analysed by TLDA for the expression of chemokines, cytokines, interferon stimulated genes (ISGs), pattern recognition factors (PRRs) and genes involved in innate immune responses. I first designed the TLDA plates and these were then manufactured by Applied Biosystems. A 384-well format was selected containing 64 genes, including all CC-, CXC, XC and CX₃C chemokines, allowing a more comprehensive analysis of chemokines compared to section 3.5. A complete list of all 64 genes assayed by the second set of TLDA analyses is shown in Appendix 1 B.

3.6.1 CC-chemokine expression

TLDA analysis revealed that the expression levels of CCL2, CCL5 and CCL7 were more than 1000-fold upregulated following L10 infection, and the levels of CCL3, CCL4, CCL8 and CCL12 were approximately 100-600 fold upregulated relative to an uninfected healthy control mouse brain (RQ value set to 1) (Fig. 3.16 A). Chemokine expression CCL21-CCL28 was either downregulated or unchanged relative to the healthy controls (Fig. 3.16 B). When comparing asymptomatic and symptomatic mice, the magnitude of CC-chemokine expression was always more up- or downregulated in brains of terminally ill mice except for CCL26 (unchanged expression). There was a significant difference in expression between symptomatic and asymptomatic mice for CCL1-CCL5, CCL11, CCL24 and CCL27 (Fig. 3.16 A and B).

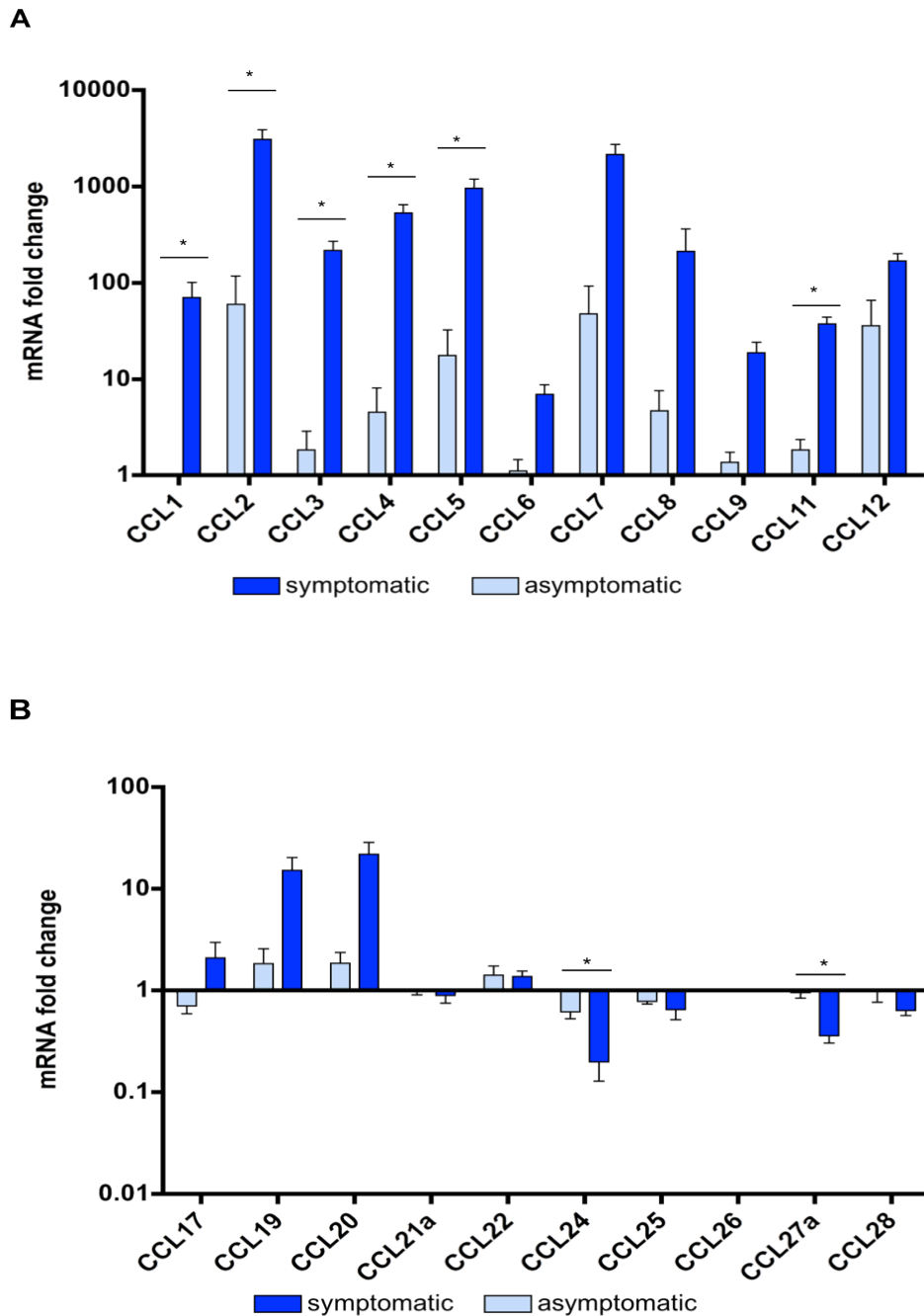


Figure 3.16 Identification of the CC-chemokine expression profile during viral encephalitis at different stages of disease severity

All mice were inoculated i.p. with L10, and RNA was isolated from infected brains shortly before the onset of symptoms and at the end stage of the disease (between PID 5-6). The expression of (A) CCL1-12 and (B) CCL17-CCL28 was measured by TLDA. All samples were normalized to an endogenous control *Eif3f* and calibrated against an uninfected control brain (relative quantification value (RQ) =1). The fold increases or decreases are depicted on the y-axis. Data are shown as mean \pm SD, $n=3-6$ mice per group. Each sample was tested in triplicate. (Student's t-test; * $p<0.05$)

3.6.2 CXC-chemokine expression

The biggest changes in CXC-chemokines were CXCL2, CXCL9 and CXCL10, which were more than 2000 fold upregulated (Fig. 3.17 A). The expression of CXCL1, CXCL3, CXCL13 and CXCL17 was approximately 100-300 fold upregulated during L10 infection. The expression of some chemokines such as CXCL5, CXCL12, CXCL14 and CXCL15 was not significantly altered and expression was similar to healthy control brains. The comparison between asymptomatic and symptomatic infection of mice revealed that the magnitude of expression was many fold higher during symptomatic infection. In particular, there was a significant difference in expression between asymptomatic and symptomatic mice for CXCL1-3, CXCL9, CXCL10 and CXCL16 (Fig. 3.17 A). For instance, CXCL10 expression in symptomatic mice was 2800 fold upregulated compared to baseline, whereas in asymptomatic mice, CXCL10 was only 88-fold upregulated compared to healthy control mice. This amounted to an approximately 30-fold difference between the two groups.

Validation by QPCR showed that the baseline level of CXCL10 expression in control mice is relatively high, with more than 100 mRNA copies per 1×10^4 TBP. The expression levels of CXCL10 in terminally ill mice were significantly increased compared to baseline levels with more than 10,000 copies per 1×10^4 TBP (Fig. 3.17 B). QPCR also confirmed the significant increase in CXCL1 expression levels compared to controls (Fig. 3.17 C).

3.6.3 CX₃CL1- and XCL1-chemokine expression

Due to the constitutive and high expression of CX₃CL1 in the brain, the expression of CX₃CL1 expression was also measured by TLDA. The results demonstrate that CX₃CL1 expression levels were not significantly altered during viral infection with L10 compared with healthy uninfected mouse brains (Fig. 3.18). The expression of the chemokine XCL1 was approximately 10-fold and 4-fold upregulated during symptomatic and asymptomatic infection with L10, respectively (Fig. 3.18). However this result was not statistically significant.

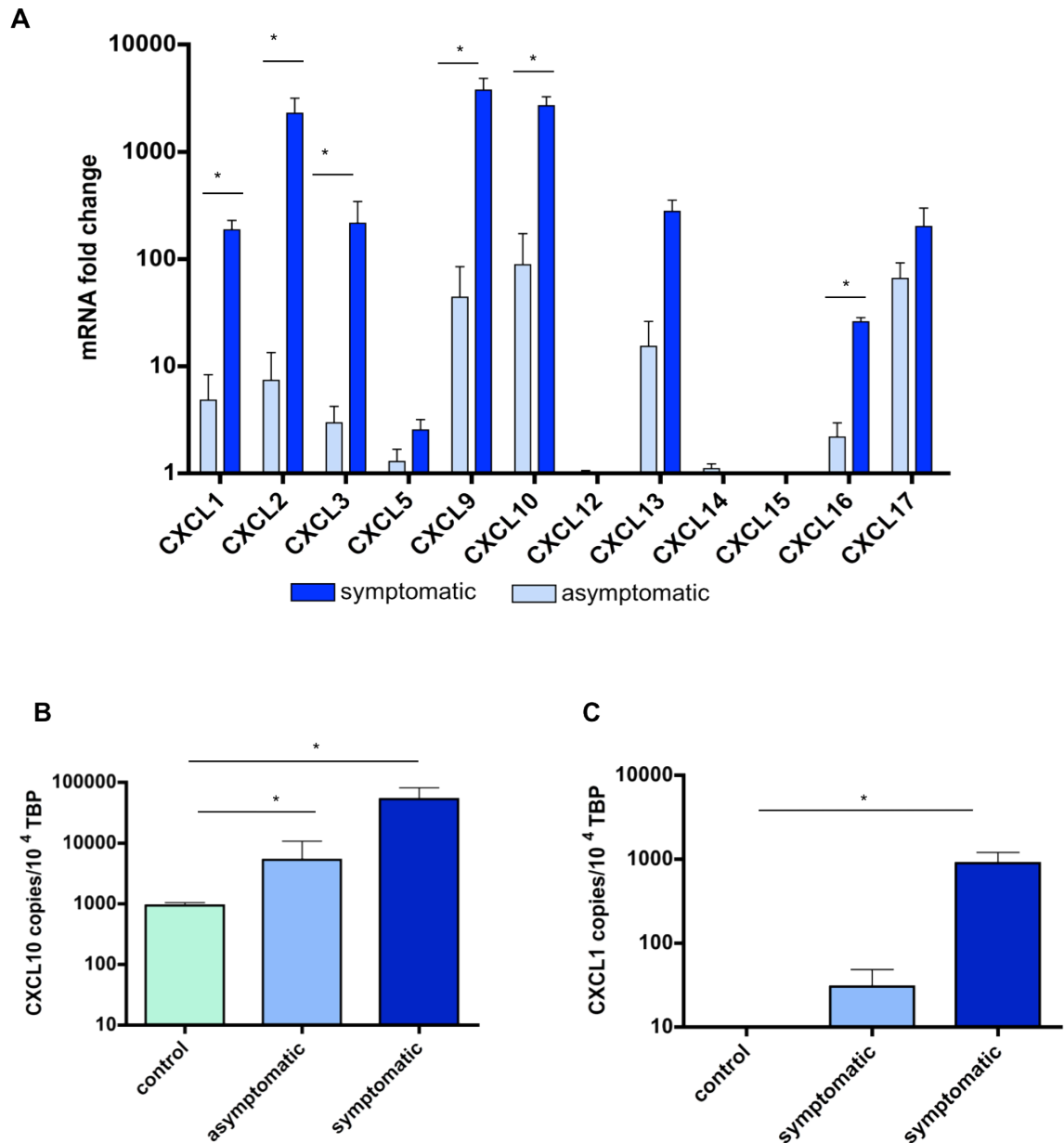


Figure 3.17 Identification of the CXC-chemokine expression profile during viral encephalitis at different stages of disease severity

All mice were inoculated i.p. with L10, and RNA was isolated from infected brains shortly before the onset of symptoms and at the end stage of the disease (between PID 5-6). (A) The expression of CXCL1-CXCL17 was measured by TLDA. All samples were normalized to an endogenous control *Eif3f* and calibrated against an uninfected control brain (relative quantification (RQ) value=1). The fold increases or decreases are depicted on the y-axis. Validation of (B) CXCL10 and (C) CXCL1 expression by QPCR. The copy numbers of each gene were normalized to TATA binding protein (TBP). All data are shown as mean \pm SD, $n=3-6$ mice per group. Each sample was tested in triplicate. (TLDA samples: Student's t-test; * $p<0.05$; QPCR samples: Kruskal-Wallis test; * $p<0.05$)

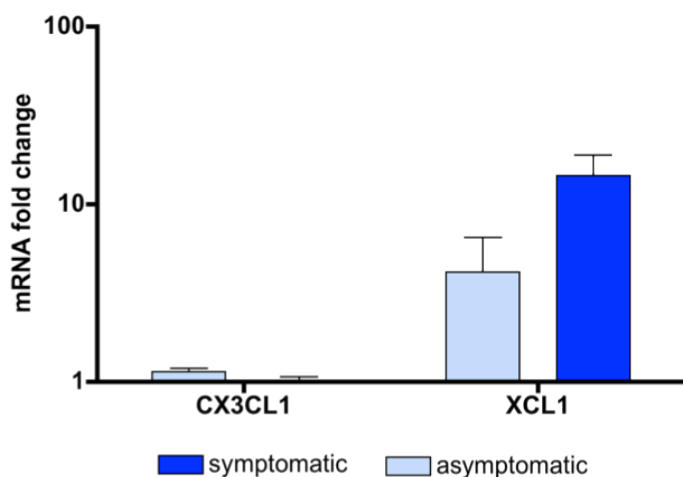


Figure 3.18 Expression of CX₃CL1 and XCL1 during L10 infection of the brain

All mice were inoculated i.p. with L10 and RNA was isolated from infected brains shortly before the onset of symptoms and at the end stage of the disease (between PID 5-6). The fold increase of CX₃CL1 and XCL1 expression relative to an uninfected control brain was measured by TLDA and normalized to an endogenous control Eif3f. Each sample was tested in triplicate and data are represented as mean \pm SD, n=3-6 mice/group.

3.6.4 Summary of chemokine expression resulting from avirulent and virulent SFV infection of the brain using strains A7(74) and L10

In order to determine the key chemokines upregulated during viral encephalitis with SFV, the chemokine patterns of CC- and CXC-chemokines during avirulent and virulent infection were compared although experiments were not performed simultaneously. A comparison of all gene fold changes in the CNS of SFV A7/74 and L10 infected mice are depicted in Appendix 3. The results, obtained by TLDA, showed that the expression pattern of CC- and CXC-chemokines was somewhat similar between A7(74) and L10 infection, but the magnitude of upregulation in L10 infected brains was generally much higher. For instance the most upregulated chemokine during A7(74) infection was CXCL10, with an approximate 500-fold upregulation of transcripts compared to an uninfected healthy control brain. During L10 infection, CXCL10 was 2800 fold upregulated, amounting to a 5.6-fold increase compared to A7(74) infected brains. A key difference between A7(74) and L10 infection is the high upregulation of CXCL1 and CXCL2 in L10 infected brains, which were not, or only minimally ($p > 0.05$), upregulated during avirulent infection with SFV. In general, there was a significant difference between A7(74) and L10 infection with regards to gene

expression levels of CCL2, CCL5, CXCL1, CXCL9 and CXCL10. All chemokines tested were many fold more strongly upregulated during L10 infection (Fig. 3.19 A and B).

Overall, the results in this chapter demonstrate that chemokines are selectively upregulated during CNS infection with SFV. The magnitude of expression is dependent on the virus strain and disease severity. Virulent infection of the brain induces a substantially more robust, comprehensive and rapid induction of chemokines than observed with the avirulent A7(74) strain. During L10 infection the chemokine expression varied with disease progression. Asymptomatic infection by L10 induced much weaker upregulation of chemokines. Key chemokines identified during SFV encephalitis were CCL2, CCL5, CXCL9 and CXCL10, which were all highly upregulated during infection. Additionally the expression of CCL20, CXCL1, CXCL2 and CXCL3 were only associated with symptomatic L10 encephalitis. CXCL1-CXCL3 are known to be chemoattractant for neutrophils. The implications of these results will be discussed in further detail in the discussion (section 3.8).

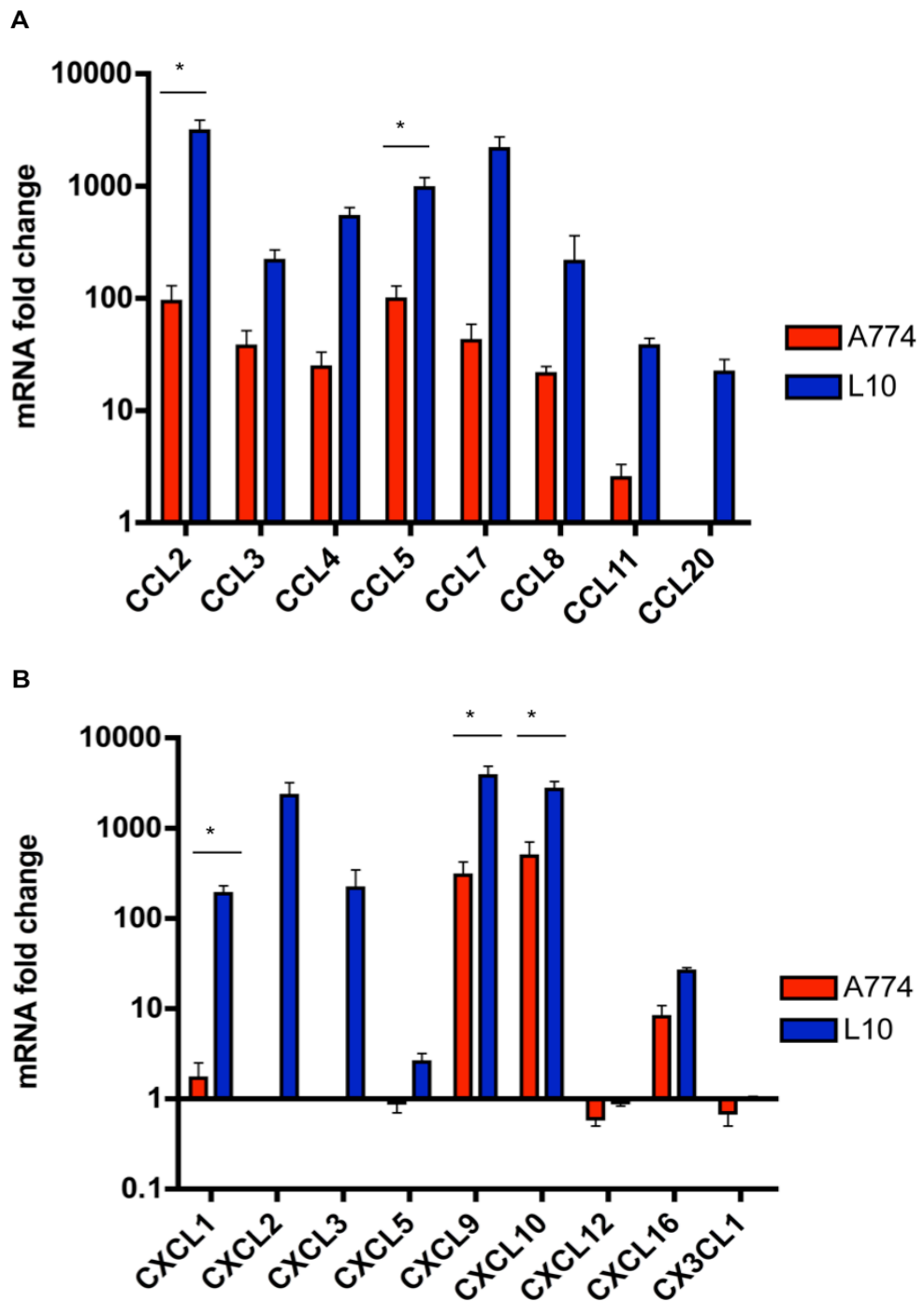


Figure 3.19 Comparison of chemokine expression between avirulent and virulent infection of the brain

Mice were infected with SFV using the strain A7(74) or L10. Mouse brains infected with A7(74) on post infection day (PID) 7 were compared to brains collected from L10 infected mice at the end stage of disease (between PID 5-6). Chemokine expression was measured by TLDA and double normalized to an endogenous control Eif3f and an uninfected control brain (relative quantification value=1). The y-axis represents fold changes of gene expression (values>1 upregulation, values<1 downregulation). Each column represents the mean \pm SD, n=5 for A7(74) group and n=6 for L10 group. Each sample was tested in triplicate. (Student's t-test; * p<0.05)

3.7 Expression of cytokines and genes involved in innate immune responses to viral infection during SFV encephalitis

After the characterisation of chemokines upregulated during infection with SFV, the expression of cytokines, PRRs, ISGs and other genes, involved in innate immunity, were determined following infection with A7(74) and L10 strains. These genes have been shown to be pivotal for virus clearance, such as IFNs, and induction of innate immune responses by PRRs (10, 53). Additionally ISGs are induced in the presence of IFN and are also important for effective innate immune responses to viral infections (70). Studies using WNV or other encephalitic viruses have shown that cytokines, PRRs and ISGs are highly induced during viral infection and are important for disease outcome (130, 391). Here I wanted to test whether these genes are also induced during avirulent and virulent SFV encephalitis.

3.7.1 A7(74) infection

Mice were infected with SFV A7(74) for 10 days and brains were collected on PID 3, 4, 5, 7 and 10 and from controls. Brains were analysed for the expression of inflammatory cytokines, retinoic acid-inducible gene (RIG)-I and interferon regulatory factor (IRF) 7. RIG-I and IRF7 have been shown to be important for the induction of antiviral immune responses such as the production of interferon and proinflammatory cytokines (e.g. IL-1 β , TNF) after recognition of virus (392, 393). Amongst cytokines, the expression of most IFNs (α , β , γ , ϵ and κ), TNF, IL-1 β , IL-6 and IL-10 were examined during SFV infection. In particular IFNs have been reported to play a major role during viral infections and are critically important for effective antiviral immune responses (394-396). All probes and primers for these selected cytokines and innate immune genes were included on the customised TLDA plates, used previously for the analysis of chemokine expression (see section 3.4).

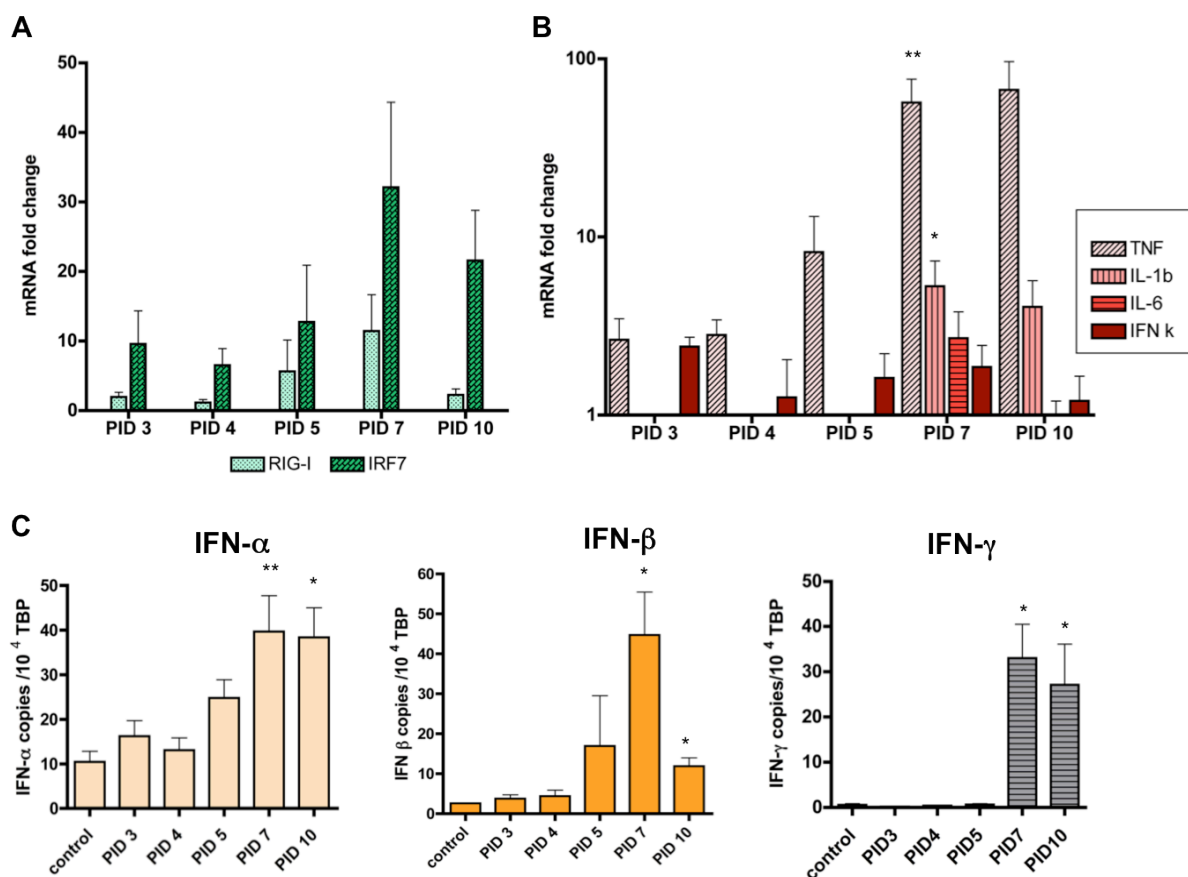


Figure 3.20 Expression of genes involved in innate immunity during viral brain infection with SFV A7(74)

Mice were infected with SFV A7(74) and brains were collected on post infection day (PID) 3, 4, 5, 7 and 10. (A and B) The expression of gene transcripts was measured by TLDA, and normalized to an endogenous control 18S and uninfected control brain (relative quantification (RQ) value=1). The fold increase is depicted on the y-axis. A Kruskal-Wallis test was performed; overall significance is shown as * $p < 0.05$ and ** $p < 0.01$. (C) Absolute copy numbers of IFN- α , β and γ were normalized to TATA binding protein (TBP). A One-Way ANOVA with Tukey's post test was performed for IFN- α samples, and a Mann-Whitney U test was performed for IFN- β and γ samples. All results represent $n=4-5$ mice per time point. Data are shown as mean \pm SD. Each gene was tested in triplicate.

The genes RIG-I and IRF7 were both upregulated during A7(74) infection with IRF7 reaching an approximately 32-fold upregulation relative to uninfected mouse brains (Fig. 3.20 A). TNF was significantly ($p < 0.01$) upregulated over the time course of infection, peaking on PID 7. On PID 7 a 60-fold upregulation was reached compared to an uninfected control brain. IL-1 β expression increased significantly ($p < 0.05$) on PID 7 relative to a control mouse brain. IL-6 and IFN- κ were not significantly upregulated, and expression was similar to that in control brains (Fig. 3.20 B). The cytokines IL-10 and IFN- ϵ were not altered during SFV infection. Unfortunately the expression of IFN- α , β and γ could not be evaluated by TLDA because the expression of these IFNs was too low in control

samples and resulted in a RQ value of zero. Therefore a comparison of IFN expression between control and SFV infected samples was not possible. To this end, the expression was assessed by QPCR (Fig. 3.20 C). IFN expression was uniformly low in all control samples with less than 10 copies per 1×10^4 TBP. The maximal expression of IFNs was reached on PID 7 and was significantly different to control samples (IFN- α : $p < 0.01$; IFN- β and IFN- γ : $p < 0.05$). On PID7 the expression of IFN- α was 4-fold, IFN- β 22-fold and IFN- γ 52 fold upregulated compared with healthy control samples.

3.7.2 L10 infection

The expression of cytokines, PRRs and ISGs was also determined by TLDA for L10 infected brains in asymptomatic and symptomatic mice. Within the PRR group, expression levels of MDA-5 and RIG-I were more than 100-fold upregulated during symptomatic infection compared to an uninfected control brain (Fig. 3.21 A). Interestingly, TLRs, known to play a major role in pathogen recognition, were only less than 10-fold upregulated relative to controls during asymptomatic and symptomatic L10 infection. In symptomatic mice all ISGs were more than 10-fold upregulated, except TLR7 (Fig. 3.21 A). All PRRs and ISGs were statistically significantly different, when comparing asymptomatic with symptomatic mouse brains, with the exception of TLR7 again.

Within the cytokine group, type-I and type-II interferons were more than 1000-fold upregulated compared to levels in healthy control brains during symptomatic stages of L10 infection. Additionally, the expression of TNF was 1636-fold and 20-fold upregulated during symptomatic and asymptomatic stages of L10 infection, respectively, compared to resting levels. Neither IL-4 nor transforming growth factor β (TGF- β) expression levels were significantly upregulated, compared to expression levels in a healthy control brain. When comparing asymptomatic with symptomatic mice, cytokine expression was always higher in samples from symptomatic mice and reached statistical significance in most of the cases (Fig. 3.21 B).

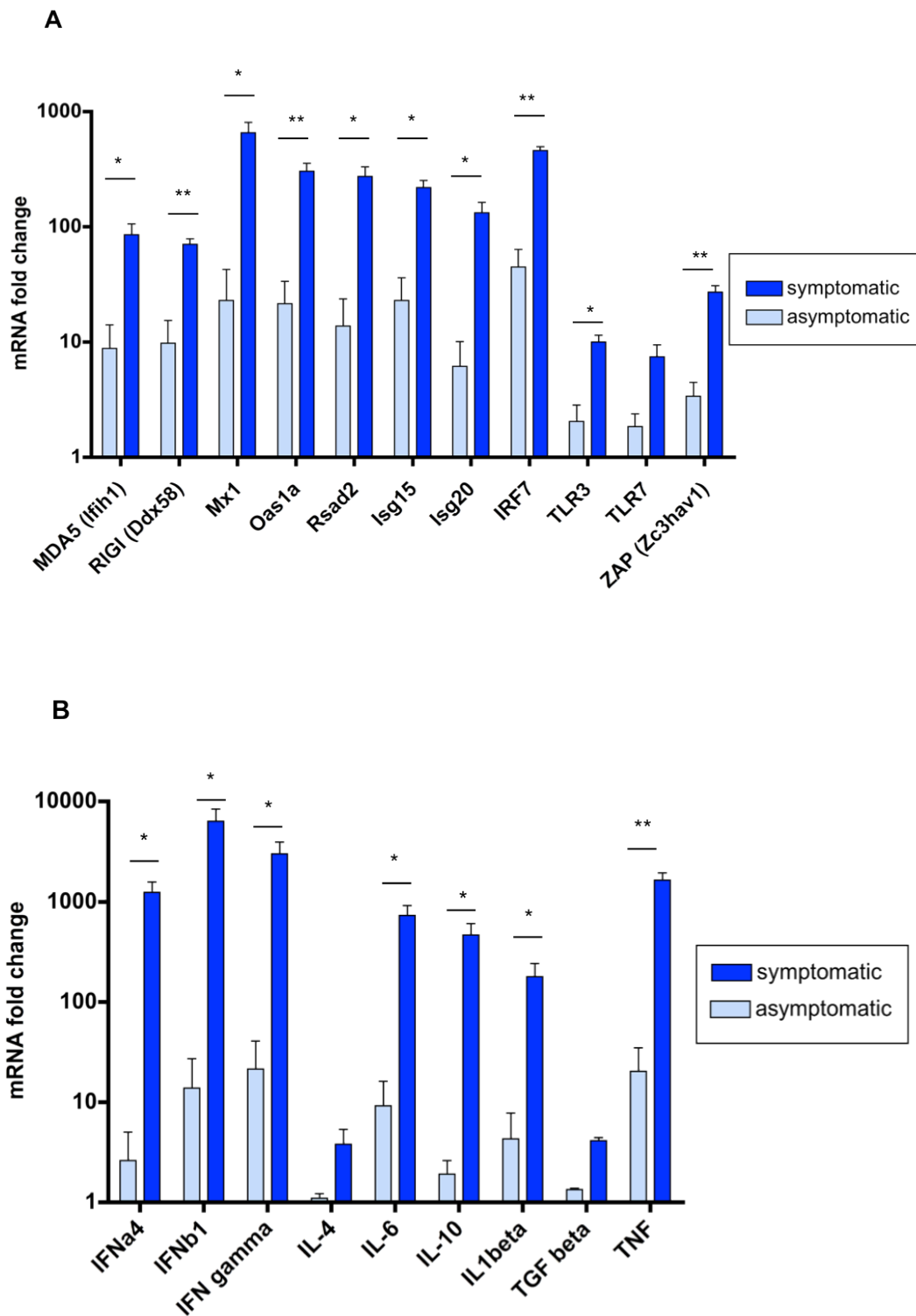


Figure 3.21 Expression of genes involved in innate immunity during viral brain infection with SFV L10

Brains from L10 infected mice were collected shortly before the onset of disease (PID 4) and at the end stage of disease, accompanied with severe neurological symptoms. (A) Fold change of interferon-stimulated genes and pattern-recognition factors, and (B) cytokines, relative to an uninfected control brain (relative quantification value=1) and normalized to an endogenous gene *Eif3f*, were measured by TLDA. Representative results of $n=3-6$ mice per group. Each gene was tested in triplicate. Results are shown as mean \pm SD. (Student's t-test; * $p < 0.05$, ** $p < 0.01$)

3.7.3 Expression of CD45 during A7(74) and L10 infection

In addition to determining the expression of cytokines and innate immune genes during SFV infection, the expression of the pan-leukocyte marker CD45 was also assessed by TLDA and QPCR, to evaluate the extent of leukocyte infiltration into the CNS. During A7(74) infection upregulation of transcript levels started between PID 5 and PID 7, reaching maximal upregulation (7-fold) by PID 7 (Fig. 3.22 A). Validation by QPCR confirmed that the expression of CD45 was maximal on PID 7 (Fig. 3.22 B). The expression of CD45 on PID 7 was highly significantly upregulated compared to controls ($p < 0.01$). Between PID 3 and PID 5, expression of CD45 was unaltered and comparable to healthy control mouse brains. The maximal expression of CD45 was reached on PID 7 and was significantly increased ($p < 0.001$) compared to controls.

For studies involving L10 infection CD45 expression was only assessed by QPCR because the CD45 gene was not part of the panel of genes, selected for TLDA analysis. CD45 was significantly ($p < 0.01$) higher in asymptomatic mice compared to healthy controls (Fig. 3.22 C). Asymptomatic mice also displayed a higher CD45 expression compared to controls but the result did not reach statistical significance ($p > 0.05$).

Taken together, the results presented in this chapter demonstrate that cytokines and innate immune genes are selectively upregulated during viral infection. Compared to chemokine expression, shown in section 3.4 and 3.5, the expression of cytokines and innate immune genes was generally lower. Major cytokines upregulated during SFV infection were type-I and type-II IFNs and TNF. CD45 was consistently and significantly ($p < 0.05$), upregulated by PID 7 suggesting infiltration of CD45⁺ leukocytes into the CNS. The infiltration of leukocytes into the CNS will be examined in great detail in chapter 4.

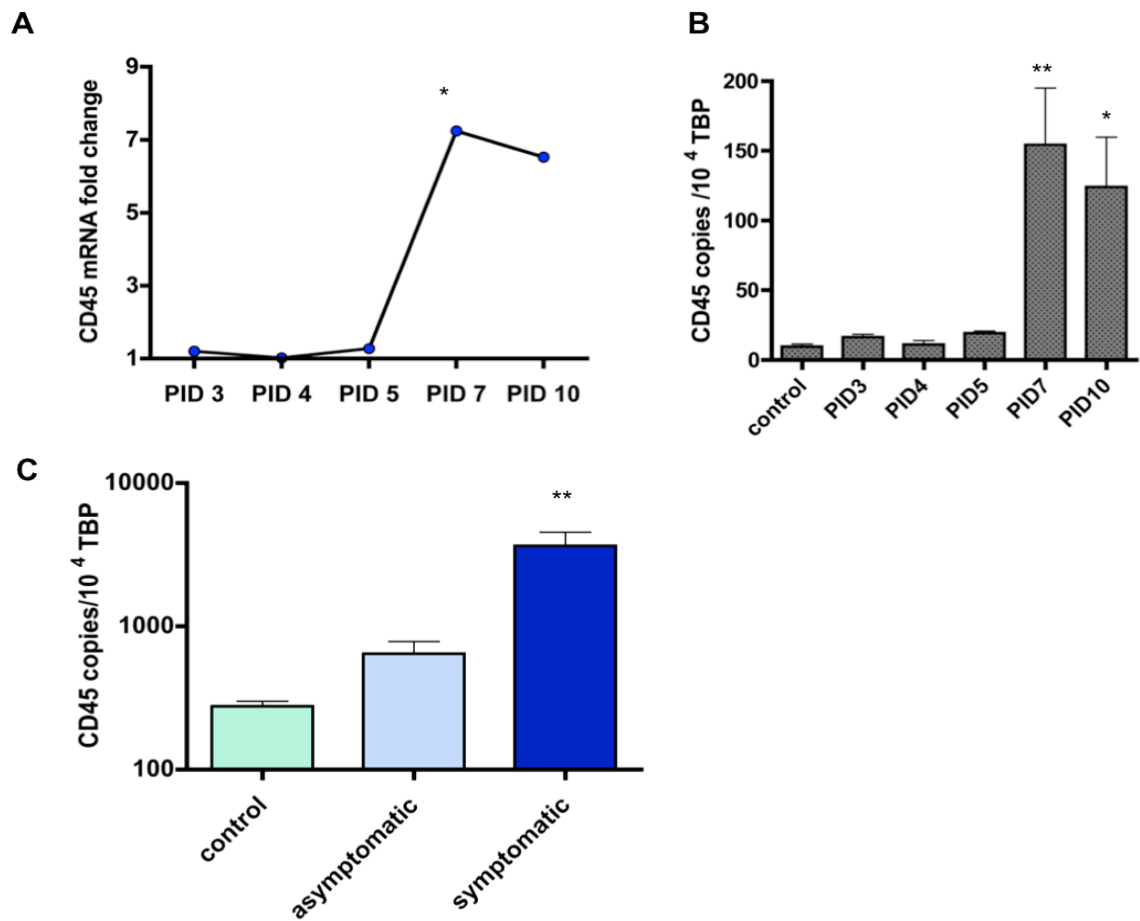


Figure 3.22 Expression of CD45 during viral infection of the brain with SFV

(A and B) Mice were infected with A7(74) and brains collected over the time course of infection. Isolated RNA was analysed for the expression of CD45. (A) TLDA analysis of relative CD45 expression over time of infection. Each sample (n=4-5 mice per time point) was double normalized to an endogenous control 18S and uninfected control brain (relative quantification value=1). Values >1 signify upregulation. Overall significance was determined using the Kruskal-Wallis test; * p<0.05. (B) Absolute copy numbers of CD45 were measured by QPCR and normalised to TATA binding protein (TBP). (C) Mice were infected with L10 and brains collected before and after the onset of symptoms. The absolute copy number of CD45 transcripts was measured by QPCR and normalized to TBP. Representative results of n=3-6 mice per group. Data shown as mean \pm SD. Each sample was tested in triplicate. (Kruskal-Wallis test with Dunn's post test; * p<0.05, ** p<0.01)

3.8 Discussion and summary

First, a model for SFV infection in C57BL/6 mice was established using avirulent and virulent strains. Infection of mice using both viral strains was successful and mice developed viral encephalitis similar to that described by Fazakerley *et al.* (298). Previous studies suggested using a dose of 5×10^4 PFU/ml of avirulent or virulent SFV strains for inoculation of BALB/c mice (298, 387). While this dose worked well for infection of C57BL/6 mice with A7(74), the dose had to be optimised for L10 infection as the C57BL/6 mice were not getting sick at the given dose. A 40-fold higher concentration of L10 was inoculated i.p. to induce sickness in the majority of C57BL/6 mice. From this it is possible that C57BL/6 mice are less susceptible to L10 infection than BALB/c mice. In support of this, previous studies by Reiner *et al.* and Liu *et al.* have shown that the two mouse strains have different immune responses to pathogenic agents due to their different genetic backgrounds making them differentially susceptible to certain diseases (397, 398). From these studies it has been shown that C57BL/6 mice induce predominantly Th1 immune responses whereas BALB/c mice induce preferentially Th2 responses. Although different pathogens were used in these studies, such as parasites and bacteria, in part this could explain the reduced susceptibility of C57BL/6 mice to L10 infection compared to infection within BALB/c mice, and would explain the requirement for a higher dose of L10 for disease induction.

It has been shown by Fazakerley *et al.* that viremia during A7(74) and L10 infection reach similar levels of viral titers (298). However, here it was shown that viremia in L10 mice was approximately 100-fold higher compared to viremia in A7(74) infected mice. This discrepancy could be explained by the use of a 40 times higher inoculation dose of L10 virus compared to the dose of A7(74) virus. The overt signs of L10 infection have been described in this study for the first time. Surprisingly, L10 infection led to different signs of disease in nearly all the mice and resulted in a broad range of symptoms. Additionally, 60%-70% of mice succumbed to death between 5-6 days post infection. BALB/c mice have been shown to get sick by PID 4, and all mice died by PID 6 (309). This again supports the hypothesis that pathogenesis might differ with mouse strains.

One of the main aims of this chapter was to define the magnitude and form of chemokine expression during SFV infection by TLDA analysis. In brief, chemokines were selectively upregulated during avirulent and virulent infection of the brain. Chemokine upregulation in infected mouse brains increased concomitantly with viral SFV titers in the brain. This increase is depicted in Figure 3.23 using the example of CCL2 and CXCL10 gene expression compared to nsp3 expression of SFV.

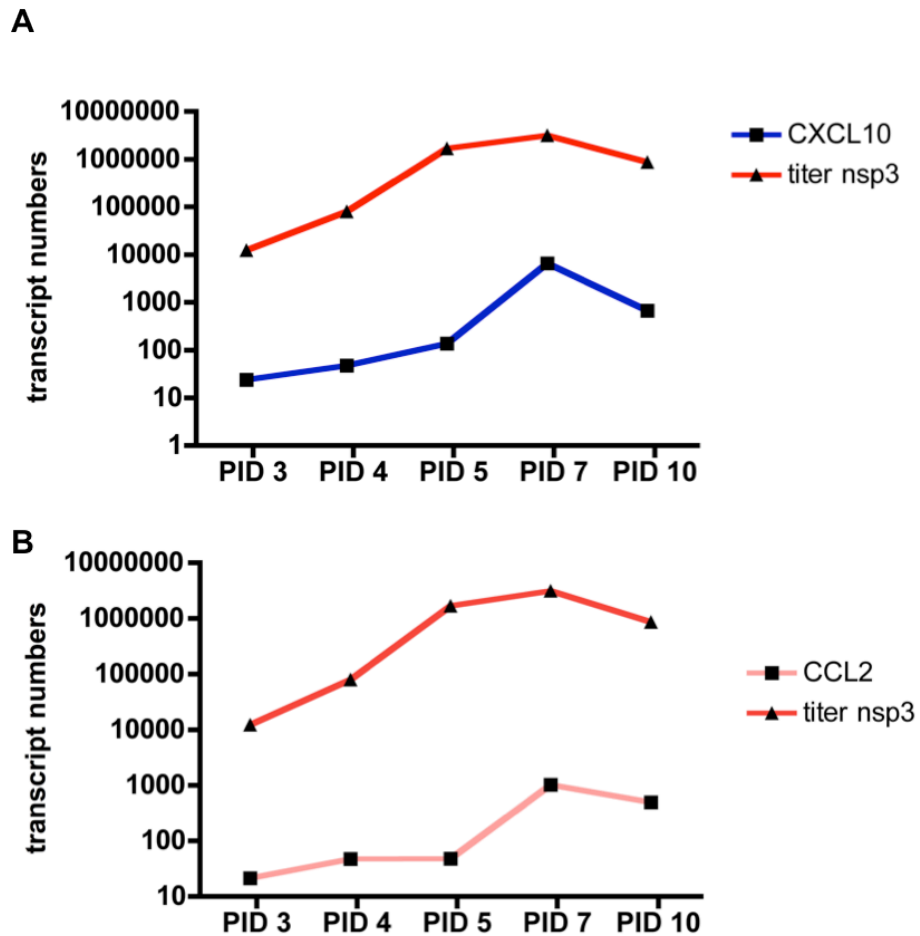


Figure 3.23 Expression of CXCL10 and CCL2 in SFV infected brains compared to viral titer

(A and B) Mice were infected with A7(74) and brains collected over the time course of infection (PID= post infection day). Isolated RNA was analysed for the expression of SFV nsp3, CXCL10 and CCL2. (A) Copy numbers of CXCL10 and SFV nsp3 per 10^4 and 10^3 TATA-binding protein (TBP), respectively. (B) Copy numbers of CCL2 and SFV nsp3 per 10^4 and 10^3 TBP, respectively.

It was noted that the magnitude of expression depends on the disease severity and viral strain used. Infection of mice with L10 induced a strong and robust upregulation of chemokines including CCL20, CXCL1, CXCL2 and CXCL3 which

were only minimally increased, or not expressed, during avirulent infection with A7(74). Shirato *et al.* have found similar results regarding chemokine expression during lethal and non-lethal infection of mice with WNV (358). They have assayed only a limited set of chemokines, but nonetheless they have demonstrated that the expression level of chemokines on PID 3 is similar following infection with both viral strains of WNV, but by PID 7, most chemokines are significantly increased during lethal WNV infection compared to non-lethal infection. Thus, this study supports those reported here that chemokines are differentially expressed in the virally infected brain, depending on the strain used and progression of the disease. Again, not all chemokines are upregulated during viral encephalitis and this suggests that induction of chemokine expression is relatively specific.

Five chemokines have been identified being highly upregulated during SFV infection, regardless of disease progression or strain used. These chemokines were CCL2, CCL5, CCL7, CXCL9 and CXCL10. During avirulent and asymptomatic L10 infection, these chemokines were more than 100-fold upregulated, and during symptomatic L10 infection these chemokines were more than 1000-fold increased, relative to controls. These chemokines have also been reported to be upregulated during other viral encephalitides, suggesting that they might be important for different types of viral encephalitis in general, and thus make them and their receptors attractive targets for therapeutic interventions (128, 129, 358).

Amongst all chemokines, CXCL9 and CXCL10 have been identified as the major upregulated chemokines during SFV infection, using both strains. It was noted that the expression of CXCL10 was upregulated as early as 3 days post infection and subsequently highlights this chemokine as being the earliest upregulated chemokine during SFV infection. Parsons *et al.* have shown that the blood brain barrier becomes leaky between PID 4 and PID 10 (399). Therefore the source of CXCL10 expression during earlier time points of SFV infection is likely to be neurons or glial cells. In support of this, Klein *et al.* have shown that CXCL10 is predominantly produced by neurons in the WNV infected CNS (153). Furthermore it has also been shown by previous studies that CXCL10 expression parallels levels of viral titers in the brain of WNV and LCMV infected mice (153, 322). CXCL9 expression was also highly upregulated very early during SFV infection but

the cellular source of this chemokine remains unclear. Some studies report that microglia are the main source of CXCL9, and expression is solely induced by IFN- γ (400). The CXCL9/CXCL10-CXCR3 axis will be explored in further detail in chapter 6.

The expression of CCL2, CCL5 and CCL7 was also strongly increased during SFV infection. The upregulation of the expression of these chemokines started by PID 5, and levels of CCL2 and CCL7 peaked on PID 7 while CCL5 levels peaked on PID 10. These findings suggest that the cellular source of CCL2, CCL5 and CCL7 might be different, or that the molecular cues required for inducing chemokine expression are distinct. It was noted that the chemokine expression pattern of these three chemokines correlated with the influx of leukocytes into the CNS (399). This result supports the hypothesis that these chemokines are predominantly expressed by infiltrating leukocytes rather than neuronal and glial cells.

CCL2 is an important chemokine expressed in the CNS of mice infected with MHV, LCMV and WNV (128, 214, 401). In these studies the CCL2-CCR2 axis has been shown to be pivotal for the migration of monocytes into the CNS, where they can differentiate into microglia during the repair phase of the brain. Furthermore Getts *et al.* have shown that a deficiency of CCL2 results in reduced mortality during WNV infection and they have proposed a pathogenic role of CCL2 during viral encephalitis (106). However the exact role of CCL2 during viral brain infection is not clear because another study linked CCL2 expression with enhanced survival during WNV infection, which suggests a beneficial role of this chemokine during viral encephalitis (346). The CCL2-CCR2 axis during SFV infection is investigated in further detail in chapter 6.

CCL5 was the only chemokine during SFV infection, whose expression peaked on PID 10 instead of PID 7. Thus, during later time points of acute infection CCL5 is likely to be expressed by cells infiltrating, or by neurons and glial cells that are induced to express CCL5. During WNV, MHV and LCMV infection, CCL5 has also been identified as a key CC-chemokine upregulated in the CNS (128, 173, 336). Therefore the expression of CCL5 in the CNS appears to be important during different types of viral brain infections. The cellular source of CCL5 was not investigated in this study but it has been proposed by previous studies that T-

cells are an important source during WNV infection (402). However astrocytes and neurons are also capable of producing CCL5 during neuroinflammation such as EAE, or in response to dsRNA viral mimics (385, 403). The CCR5 axis will be, again, investigated in more detail in chapter 6.

Of note is the differential expression of CXCL1, CXCL2 and CXCL3 during SFV infection. While these chemokines are only minimally, or not, expressed during avirulent and asymptomatic L10 infection, CXCL1-CXCL3 expression was strongly upregulated in terminally ill mice infected with the virulent strain L10. CXCL2 was the third most strongly upregulated CXC chemokine after CXCL9 and CXCL10. Since CXCL1-CXCL3 are chemoattractants for CXCR2⁺ neutrophils it was hypothesised that a large number of neutrophils might enter the CNS during later stages of L10 infection. This hypothesis will be investigated in more detail in chapter 4.

Furthermore it was shown here that the expression of CX₃CL1 in the CNS is not changed during SFV infection compared to healthy control mouse brains. Previous studies have suggested that CX₃CL1 is more implicated in neurodegenerative diseases than viral infections (404).

Analysis of the cytokine and innate immunity gene expression during SFV infection revealed that the highest upregulation occurred by PID 7. This correlates with both peak leukocyte influx and viral RNA load, suggesting that these cytokines are predominantly released by either; infiltrating leukocytes or from resident neurons and glial cells that induced to express them indirectly by leukocyte entry. The main cytokines identified during avirulent and virulent infection with SFV were type-I and type-II interferons and TNF. TNF was already upregulated by PID 3 during A7(74) infection and on PID 4 during L10 infection. As mentioned before on PID3 or PID4, the BBB is unlikely to be permeable yet (305). Therefore the source of TNF expression is most likely neurons or glia. During WNV infection of the brain, neurons have been shown to express TNF. This cytokine has been demonstrated to exert neuroprotective functions during viral encephalitis (88).

Amongst innate immunity genes, RIG-I and IRF7 were both highly upregulated during SFV infection. IRF7 expression was induced very early during A7(74)

infection, suggesting that neurons and astrocytes are capable of inducing innate immune responses. Additionally, analysis of ISGs during L10 infection revealed that almost all ISGs were highly upregulated (>100 fold) during viral encephalitis. This is in line with the high expression of interferons which induce the expression of ISGs. Interestingly, TLR3 and TLR7 expression, shown to be induced in the presence of viral dsRNA and ssRNA, respectively, was only moderately increased during L10 infection (405). This contrasts with another study, where specific TLRs were found to be highly upregulated in response to SFV infection using BABL/c and 129 mice (406). A reason for this discrepancy could be the use of different mouse strains. In this study C57BL/6 mice were used, which are genetically different from BALB/c and 129 mice (397, 398). The expression of CD45 was assessed by QPCR to determine the extent of leukocyte infiltration during SFV infection. However, the expression of CD45 has to be carefully interpreted because microglia also express CD45. Therefore the extent of leukocyte infiltration cannot be determined based on the mRNA levels of CD45 only.

In the next chapter the numbers of leukocytes entering the CNS will be assessed by flow cytometry and leukocyte subsets will be identified based on the expression of various surface markers.

Chapter 4

Identification of leukocyte subsets infiltrating the CNS during Semliki Forest virus infection

4.1 Introduction and aims

In the previous chapter, a thorough analysis of chemokine expression was conducted, identifying 5 chemokines that are highly upregulated during viral encephalitis. As discussed in the general introduction chapter, chemokines are important regulators of leukocyte trafficking, and due to the strong increase of CCL2, CCL5, CXCL9, CXCL10 it was hypothesised that many T-cells, monocytes and NK-cells infiltrate the brain during SFV infection. However other chemokines were also upregulated and therefore other leukocyte subsets might additionally enter the virally infected CNS. *To test this hypothesis I therefore sought to define the kinetics of leukocyte subsets entering the CNS during avirulent and virulent infection with SFV.*

One of the hallmarks of the healthy CNS is the low abundance of leukocytes, and most of these are in the CSF. In contrast to other organs in the body, the majority of leukocytes in the CNS are memory T-cells and predominantly CD4+ T-cells (119). An influx of leukocytes into the CNS has been observed using different types of viral infections. However what role leukocytes play in the CNS during pathogenesis remains unclear. Studies using WNV as a model of infection have shown that T-cells and monocytes are beneficial for survival and virus clearance (106, 140, 141). In contrast to this, other viral encephalitis studies using LCMV as a model of infection, have reported that monocytes and other leukocyte subsets in the CNS are pathogenic and enhance mortality (154, 367, 369).

For alphaviruses little is known about chemokine-mediated leukocyte infiltration into the CNS. Therefore defining the kinetics of leukocyte entry into the CNS during viral encephalitis could be key for the development of therapeutic interventions. One study by Parsons and Webb has demonstrated that leukocytes enter the brain and spinal cord during SFV infection, but to date, the temporal infiltration of leukocyte subsets into the infected CNS has not been examined yet (399). Furthermore the authors have shown that the BBB becomes permeable for leukocytes between PID 4 and PID 10. *Therefore in this study I investigated entry of leukocyte subsets between 3 and 10 days post infection.*

Flow cytometry was used to identify leukocyte subsets and to investigate kinetics of leukocyte entry into the CNS. For most of this study the avirulent strain A7(74) was used, because mice infected with L10 succumb before mounting an effective immune response. Therefore using strain A7(74) seems more suitable for studying leukocyte infiltration into the CNS. Some preliminary data on leukocyte entry into the brains of mice infected with the virulent strain L10 shall be presented at the end for comparison.

4.2 Optimisation of leukocyte isolation from SFV infected brains

In the previous chapter it was noted that chemokines are highly and selectively upregulated during viral encephalitis using SFV strain A7(74) and L10. To explore how this relates to infiltration of leukocytes into the brain, mice were infected with SFV strain A7(74) for 10 days, and brains were collected from control, PID 4, 5, 7 and 10, and analysed by flow cytometry. Neural tissue from mice typically contains a lot of myelin debris that can interfere with antibody binding during flow cytometry. Therefore it was necessary to remove myelin debris prior to antibody staining for flow cytometric analysis, without compromising the number of live cells. Brain cells were isolated from the CNS using two different methods: by myelin depletion or by Percoll density gradients. Both isolation techniques were tested and compared.

Initially, myelin removal beads were used to isolate leukocytes from healthy control mouse brains. This method had the advantage over the use of density gradients that the number of mice per time point could be reduced, as the yield of cells from one mouse brain was high enough to perform flow cytometry after myelin depletion. CD45^{hi} leukocytes counted before and after the use of myelin removal beads were compared by flow cytometry. Unpurified neural cells, before myelin depletion, were analysed first (Fig. 4.1 A). It was shown that the brain contained an enormous quantity of myelin debris that was defined as SSC^{hi}FSC^{lo}, and was located outside the P1 gate (see arrow Fig. 4.1 A). After exclusion of DRAQ7⁺ dead cells, live cells (P2 gate) were examined for the presence of doublets, and single cells (P3 gate) were further gated on CD45 versus SSC. According to the literature, CD45⁻ and CD45^{int} cells (P5 gate) have been described as microglia, whereas CD45^{hi} cells (P4 gate) have been

identified as leukocytes (407, 408) Most cells were CD45 low or intermediate, typical of microglial cells. After depletion of myelin from the brain sample, the amount of SSC^{hi}FSC^{lo} myelin debris was reduced and more CD45^{hi} leukocytes could be seen (Fig. 4.1 B). After dead cell exclusion, CD45^{hi} and CD45^{int} cells were identified within the P4 and P5 gate, respectively. Compared to brain samples containing myelin, samples depleted of myelin displayed higher purity of CD45^{hi} cells within the P4 and P5 gate. However the number of CD45^{hi} cells within the living cell population was still considerably low and comprised only 0.33% of total cells after using myelin removal beads.

Next, Percoll density gradients were used to isolate mononuclear cells from murine brains (Fig. 4.1 C). This method required a larger number of mice per time point because mouse brains had to be pooled, in order to achieve an adequate number of cells to perform flow cytometry. The advantage of this method was that cells were highly purified and enriched in mononuclear cells. In addition to mononuclear cells, microglia are also enriched and can be collected from the interphase of the 30%/70% Percoll layer. Due to the density gradient, myelin debris, neurons and granulocytes were largely removed from the brain samples. After gating on CD45^{hi} cells and performing dead cell exclusion, three distinct cell populations became visible based on the expression of CD45: a CD45^{hi}, CD45^{int} and CD45⁻ cell population (Fig. 4.1 C). After the use of density gradients the frequency of CD45^{hi} cells was increased from 0.33% of live cells in myelin-depleted samples to 8.73% in Percoll isolated samples. This amounts to an approximately 26-fold increase in leukocyte numbers using Percoll density gradients.

Overall, the comparison of different isolation techniques showed that the use of density gradients is the preferred method of choice for isolating mononuclear cells from the brain because these cells were highly purified and enriched and allowed a clear distinction between microglia and leukocytes based on the expression of CD45. Subsequently, this method was used for the remainder of this thesis for all flow cytometric analyses. However, one disadvantage of using the Percoll method is that neutrophils cannot be isolated from brain samples. For subsequent analyses, the dead cell marker DRAQ7 was used to select for total live cells in all samples, and doublet exclusion was performed using SSC-Area versus Height (Fig. 4.1).

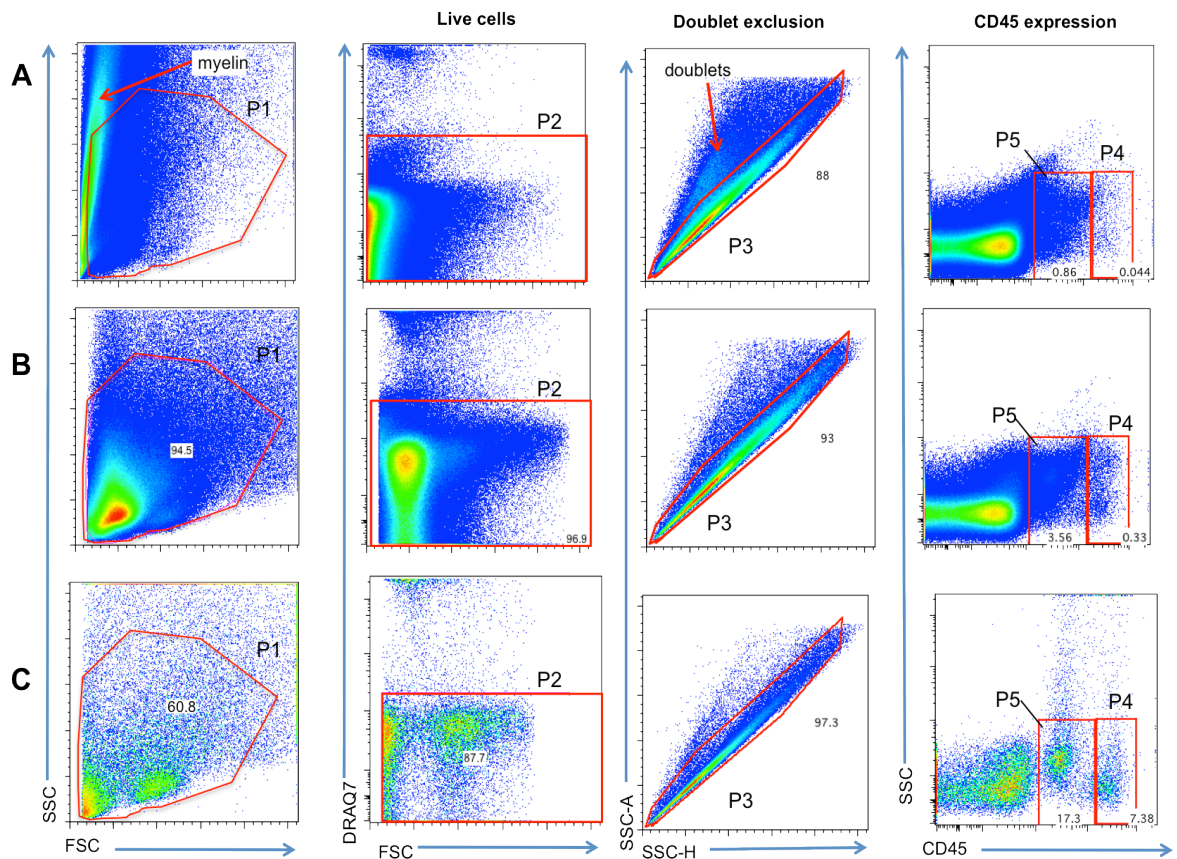


Figure 4.1. Isolation of leukocytes from SFV infected brains using myelin removal beads or density gradients

Mononuclear cells were isolated from murine brains infected with SFV A7(74) and different methods were used to isolate CD45^{hi} leukocytes for flow cytometry. The efficiency of CD45⁺ cell isolation from brains for each method was determined by flow cytometry. (A) Brain cells isolated before the use of Myelin removal beads. (B) Brain cells obtained after the use of Myelin removal beads. (C) Mononuclear cell enrichment using the Percoll method. Panels on the left identify lymphocytes and myeloid cells (gate P1), gate P2 shows total live cells, gate P3 depicts single cells, and panels on the right identify CD45^{hi} leukocytes (gate P4) and CD45^{int} microglia (gate P5).

4.3 Increase of CD45^{hi} cells within SFV A7(74) infected brains

To investigate brain leukocyte infiltration following SFV infection and to identify specific leukocyte subsets, all cells were subsequently gated on CD45^{hi} cells. It was noted that the CD45^{hi} cell population significantly increased with the duration of infection (Fig. 4.2 A-C). The increase of leukocyte numbers within the CNS first became apparent on PID 5 and reached maximal levels on PID 10, when an average of 20% of all live single cells were CD45^{hi} leukocytes (Fig. 4.2 C). The fold increases of mean leukocyte numbers in the CNS during SFV infection are shown in Table 4.1. Leukocytes were next analysed and

categorised into different subsets based on the expression of NK-cell, T-cell, B-cell and myeloid cell markers.

Table 4.1 Fold increases of leukocytes within SFV infected brains relative to healthy control mouse brains.

Mice were infected with SFV A7(74) and brain cells were isolated using Percoll density gradients. CD45^{hi} cells were counted by flow cytometry. The numbers of leukocytes in the CNS are presented as mean percentage \pm SD. Results are representative of 10 pooled mouse brains per time point and 3 individual experiments.

	Control	PID 4	PID 5	PID 7	PID 10
Mean \pm SD	2.89 \pm 0.923	2.44 \pm 0.722	4.90 \pm 1.48	13.76 \pm 2.98	20.14 \pm 4.72
Fold increase		0.9	1.8	4.9	7.2

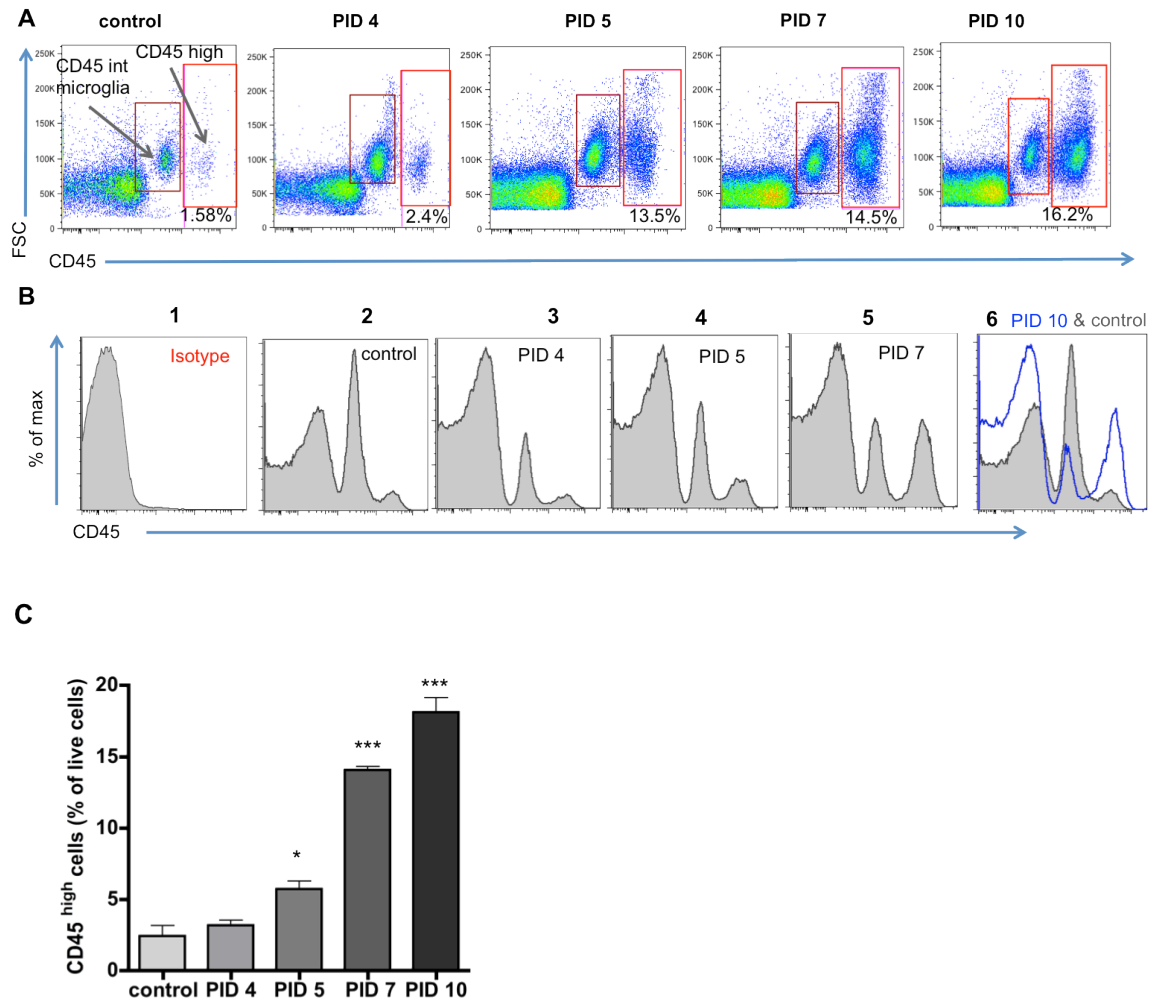


Figure 4.2. Identification of CD45^{hi} leukocytes in the brain

Mononuclear cells were isolated from murine brains infected with SFV A7(74) and analysed for the expression of CD45 by flow cytometry. Doublet exclusion was performed for all samples. (A) Expression of CD45 on total live single cells over the time course of infection. Gate 1= CD45^{int} cells and gate 2= CD45^{hi} cells. (B) Histograms: 1 = Isotype; 2-5 = differential expression of CD45 over the time course of infection; 6 = CD45 staining of cells from control (shaded) and post infection day (PID) 10 (blue) samples. (C) Proportion of CD45^{hi} leukocytes within gate 2 at each time point post infection. Results are representative of 10 pooled mouse brains per time point and 3 individual experiments. Data are presented as mean \pm SD. (One-Way ANOVA with Tukey's post test; * $p < 0.05$, *** $p < 0.001$).

4.4 NK-cells are one of the first cells infiltrating the brain during SFV infection

After the identification of CD45^{hi} cells within the brain, leukocytes were analysed for the combined expression of NK1.1 and Nkp46. Both markers together are expressed on NK-cells (409). The proportion of NK1.1⁺Nkp46⁺ cells amongst total live CD45^{hi} cells in the brain increased significantly between PID 4 and PID 5 compared to controls ($p < 0.05$), and decreased to lower levels at

later time points (Fig. 4.3 A and B). Despite the decrease of proportions of NK1.1⁺NKp46⁺ cells over time within the CD45^{hi} cell compartment, the frequencies of NK1.1⁺NKp46⁺ cells per 10⁴ isolated live brain cells reached maximal levels by PID 10 (Fig. 4.3 C) although this did not reach statistical significance. Histological analysis showed that CD49b⁺ cells were localised in cortical regions of the brain by PID 5, and infiltrated the brain parenchyma in the cortex and also appeared in meningeal areas (Fig. 4.3 D and E). CD49b is a pan NK-cell marker.

4.5 Identification of myeloid cells during SFV infection

Next, the viable CD45^{hi} cell population was examined for the presence of CD11b⁺ cells during SFV infection. Myeloid cells typically express this marker as do microglia, but microglia are not CD45^{hi} but rather CD45^{lo}-CD45^{int} (407, 410). The results demonstrate that the frequency of CD11b⁺ cells within CD45^{hi} cells increases from approximately 49% of CD45^{hi} CD11b⁺ cells in healthy control brains to approximately 64% of cells by PID 4 and PID 5, decreasing thereafter to below control levels (Fig. 4.4 A and B). However assessment of the numbers of CD11b⁺ cells per 10⁴ live brain cells showed that the number of CD11b⁺ cells increased significantly ($p < 0.05$) by PID 5 and reached maximal levels on PID 7 ($p < 0.01$) (Fig. 4.4 C). These differences in proportions and numbers reflect changes in the other leukocyte populations entering the brain during viral encephalitis.

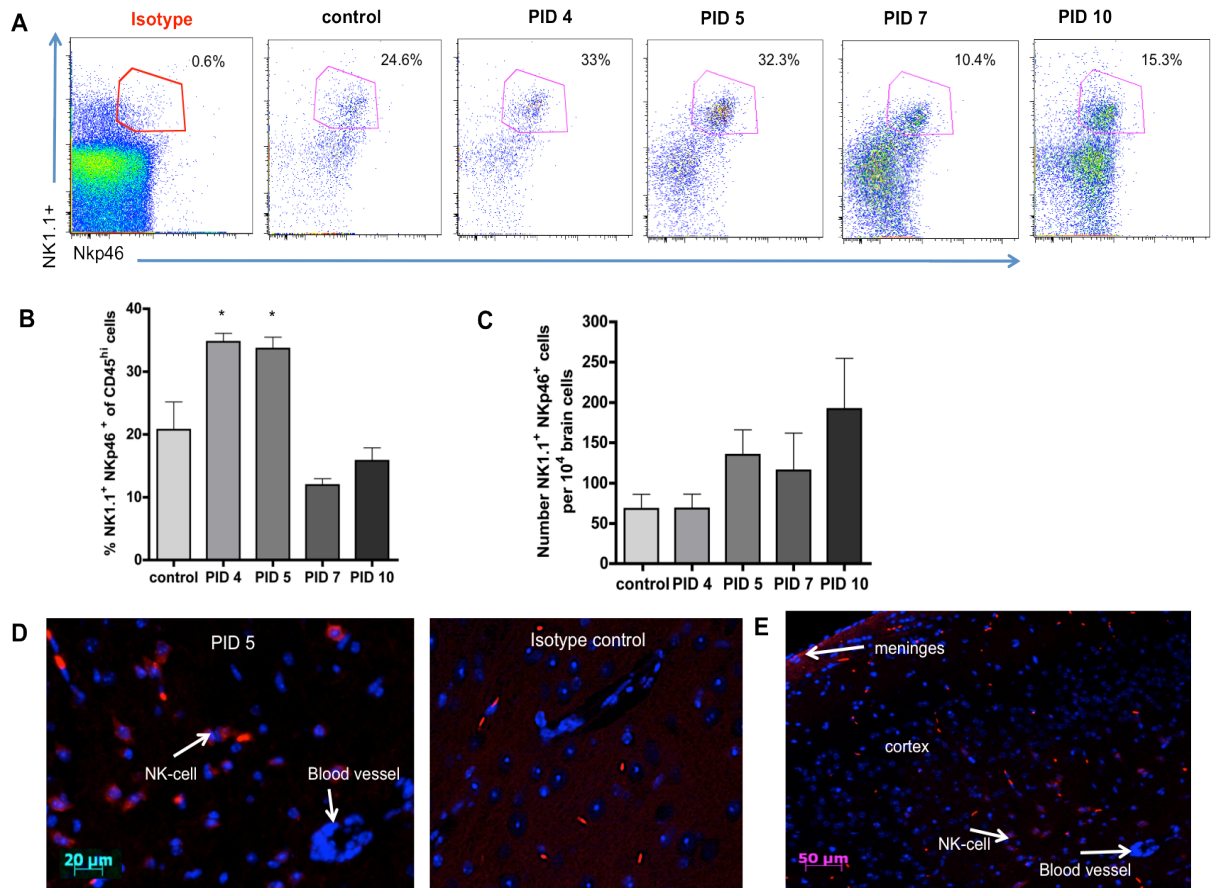


Figure 4.3. NK-cells enter the brain early during SFV infection

Mice were infected with SFV A7(74) and brains were collected on post infection day (PID) 4, 5, 7 and 10 and compared to control brains. NK-cells were identified on the basis of NK1.1 and Nkp46 expression. All cells analysed were gated on live single CD45^{hi} cells. (A) Representative dot plots of NK1.1 and Nkp46 expression within CD45^{hi} cells at each time point post infection. Isotype control is shown on the left. (B) Proportions of NK1.1⁺Nkp46⁺ cells within CD45^{hi} cells over time. (C) Number of NK1⁺Nkp46⁺ cells per 10⁴ isolated live brain cells. Data are represented as mean \pm SD of 5-10 pooled mouse brains per time point from 3 individual experiments. (D and E) Fluorescent images of brain sections from infected brain on PID5 and isotype control, stained for CD49b⁺ NK-cells, and mounted with Vectashield plus DAPI (blue cell nuclei). Magnification at (D) 10x and (E) 20x. ((B) One-way ANOVA with Dunnett's post test and (C) Kruskal-Wallis test with Dunn's post test; both * $p < 0.05$)

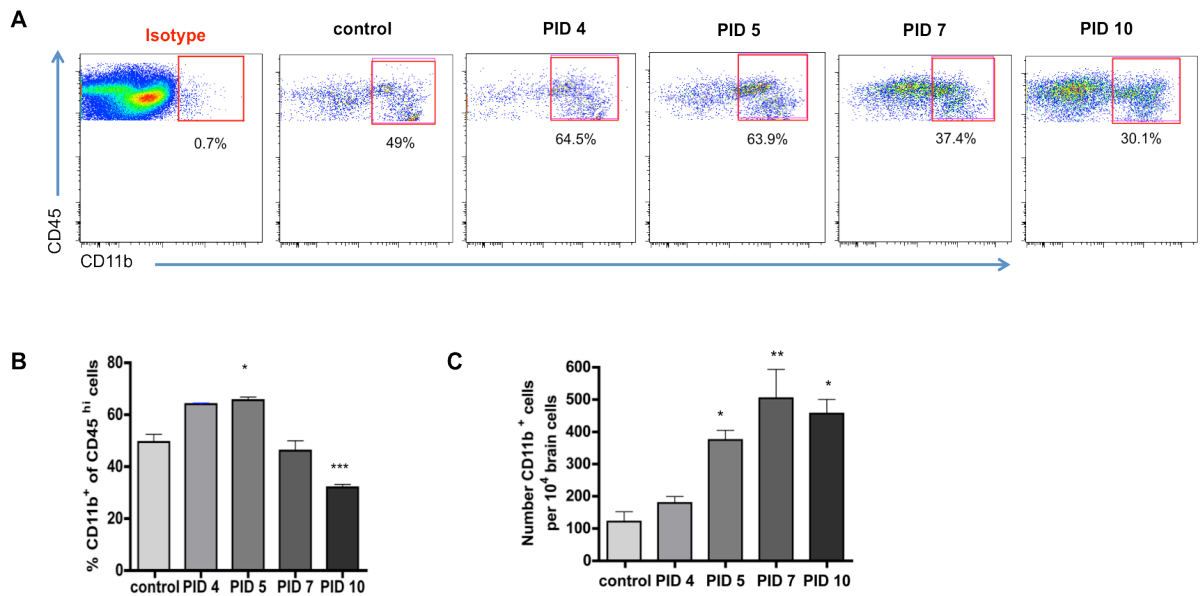


Figure 4.4. Identification of myeloid cells entering the brain during SFV infection

Mice were infected with SFV A7(74) for 10 days and the number of myeloid cells (CD11b⁺) was determined by flow cytometry on post infection day (PID) 4, 5, 7 and 10. (A) Representative dot plots of CD11b staining on live single CD45^{hi} cells. (B) Proportions of CD11b⁺ cells within total live CD45^{hi} compartment at each time point. (C) Number of CD11b⁺ cells per 10⁴ isolated live brain cells. Data are represented as mean \pm SD of 5-10 pooled mouse brains per time point from 3 individual experiments. (One-way ANOVA with Tukey's post tests; * $p < 0.05$, ** $p < 0.01$ *** $p < 0.001$)

4.5.1 Identification of residual neutrophils, and Ly6C^{hi} monocytes and Ly6C^{lo} cells in the brain during SFV infection

Following on from this the CD11b⁺ compartment was then further characterised. To that end, two markers were used to discriminate between neutrophils and monocytes/macrophages: Ly6G and Ly6C (Fig. 4.5 A). Ly6G is a marker specifically expressed on neutrophils. Amongst CD45^{hi} cells, the percentage and number per 10⁴ isolated brain cells of Ly6G⁺ cells was not significantly changed over the time course of infection (Fig. 4.5 B). Of note, Percoll density gradients remove most of the neutrophils from the sample, and the residual neutrophils shown on the dot plots represent residual neutrophils, which were not removed from the brain samples. However, the number of neutrophils was minimally increased by PID 4 similar to proportional numbers at this time point (Fig. 4.5 B). Immunohistochemical staining for myeloperoxidase, an enzyme present within granules of neutrophils, revealed that neutrophils are not apparent in the brain of infected mice at any time point analysed (data

not shown here). Therefore it is very likely that neutrophils do not, or only minimally, enter the brain during SFV infection. This will be discussed later.

The number of Ly6G⁻ cells per 10⁴ isolated brain cells significantly increased by PID 5 ($p < 0.001$), and stayed elevated until PID 10 (Fig. 4.5 C). Similar to this, the proportion of Ly6G⁻ cells was also significantly increased by PID 5 ($p < 0.05$), but proportions decreased by PID 7 to levels similar to control levels. Therefore proportions of Ly6G⁻ cells were not significantly changed by PID 7 and 10 compared to proportions in control mouse brains. Next, the Ly6G⁻ fraction within the CD45^{hi}CD11b⁺ compartment was further analysed based on intensity of Ly6C expression. The proportion of Ly6C⁻ cells within Ly6G⁻ cells was high (approximately 64% \pm 12 SD) in control samples and significantly ($p < 0.05$) decreased by PID 7 and 10 to approximately 25% (Fig. 4.5 E). Based on recent studies this cell fraction consists mainly of macrophages and DCs (24). Unfortunately a distinction between macrophages and DCs was not possible, as the staining for F4/80 did not work well. It is not clear why this antibody did not work in this study but it is possible that the enzymatic digestion of brain tissue for the isolation of mononuclear cells affects the F4/80 antibody staining. However immunohistochemical staining for MAC-2, a marker expressed on macrophages, showed that MAC-2⁺ cells, which are known as macrophages, were localised in the sulcus, meninges (Fig. 4.6 A and B) and also near blood vessels in cortical regions of SFV infected brains on PID 5 (Fig. 4.6 D). No MAC-2⁺ cells were detectable in brain sections from infected mice from PID 7 and PID 10. The appropriate isotype control was used (4.6 C).

The Ly6C^{int} cell compartment was not significantly altered during viral infection, and proportions were similar to steady state (Fig. 4.5 E). Lastly the proportion of Ly6C^{hi} cells during SFV infection was initially low (11.5% \pm 2.5 SD) in control samples but increased significantly ($p < 0.05$) by PID 4. The proportions of these cells increased even further by PID 7 and 10, reaching approximately 60% of cells within the Ly6G⁻ cell compartment. Previous studies have categorised Ly6C^{hi} cells as ‘inflammatory monocytes’ (24, 411). In support of this other studies have shown that during viral infection mostly Ly6C^{hi} monocytes enter the brain (23). Therefore it is most likely that the Ly6C^{hi} cells detected during SFV infection and shown here are ‘inflammatory’ monocytes.

4.6 Identification of plasmacytoid DCs cells during SFV infection

Expression data presented in chapter 3 showed that type-I interferon was highly induced during SFV encephalitis. pDCs are known to be a source of interferon, and therefore I wanted to test whether these cells were capable of entering the brain by using the markers CD11c and pDC (412). Previous studies have shown that during neuroinflammation such as MS or EAE, and during WNV infection pDCs infiltrate the brain during inflammation and secrete high amounts of IFN- α (93, 413). First cells were gated on CD11b⁺ and MHC-II⁺ cells (not shown here) before examining expression of CD11c and pDCA (Fig. 4.7 A and B). In control and PID 4 samples, no CD11c⁺pDCA⁺ cells could be detected. However by PID 5 a small population of CD11c⁺pDCA⁺ cells appeared in infected brains. This cell population increased further in number and proportions, and by PID 7 the number of CD11c⁺pDCA⁺ per 10⁴ isolated live brain cells was significantly increased ($p < 0.05$) compared to control mouse brains (Fig. 4.7 C). However the number of CD11c⁺pDCA⁺ cells decreased 2.8-fold by PID 10. The proportion of CD11c⁺pDCA⁺ cells was not significantly changed during SFV infection of the brain. Of note is that the number of pDCs entering the brain during infection was quite low.

Other subsets of DCs could not be identified here, as the flow cytometric staining was limited to 7 markers. Additionally the marker F4/80 did not work well, and this would make a distinction between macrophages and DCs difficult.

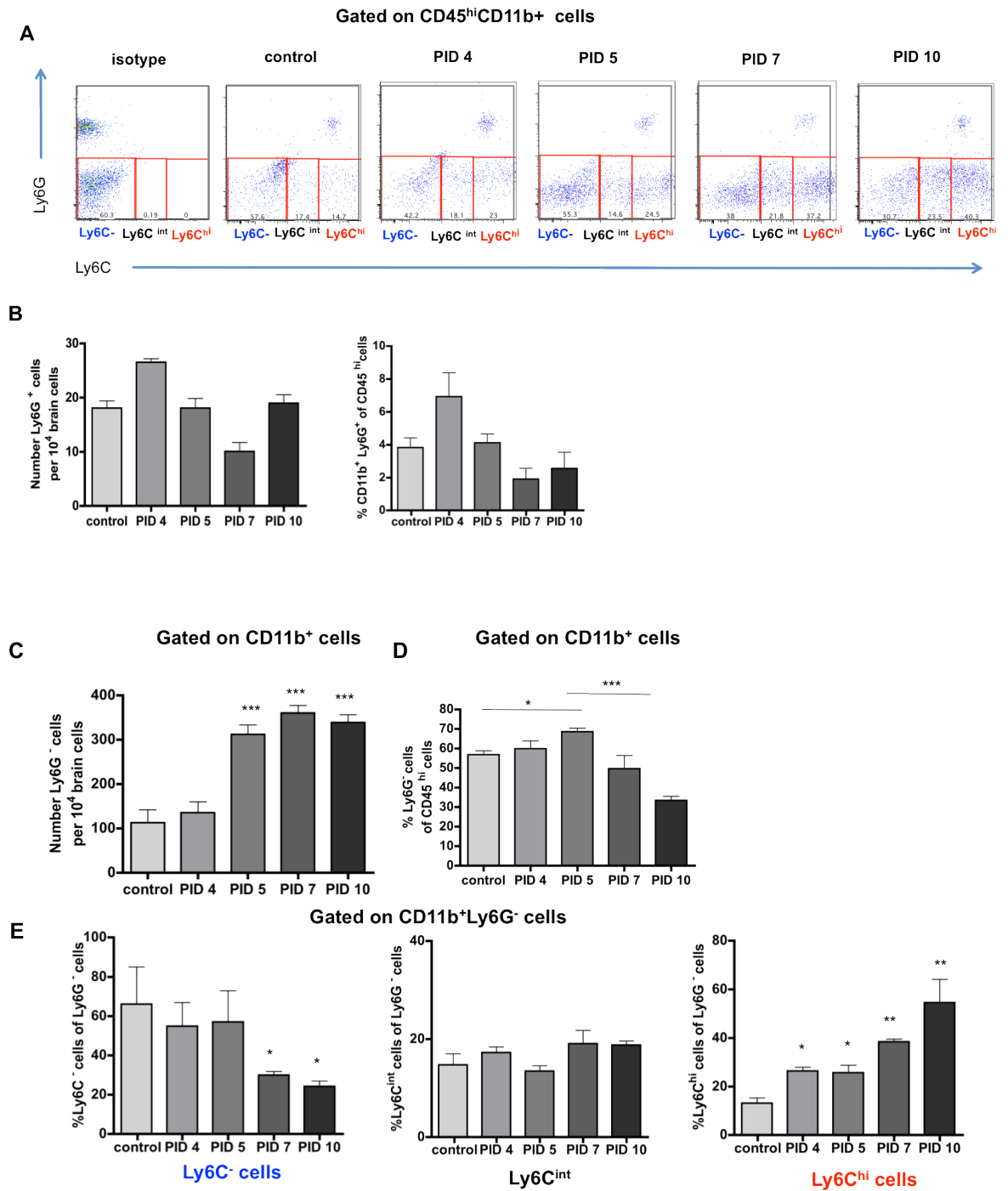


Figure 4.5. Identification of monocytes, macrophages and neutrophils in the brain during SFV infection

Mice were infected with SFV A7(74) for 10 days and the number of myeloid cells was determined by flow cytometry from controls and at 4, 5, 7 and 10 days post infection (PID). (A) Representative dot plots of Ly6G and Ly6C expression on CD11b⁺ cells gated on live CD45^{hi}CD11b⁺ cells at each time point. Appropriate Isotype control is shown in the left panel. (B) Numbers of Ly6G⁺ cells per 10⁴ isolated live brain cells, and proportions amongst CD45^{hi} cells. (C) Numbers of Ly6G⁻ cells per 10⁴ isolated live brain cells, and (D) proportions amongst total live CD45^{hi} cells. (E) Proportions of Ly6C⁻, Ly6C^{int} and Ly6C^{hi} fractions within the CD11b⁺Ly6G⁻ cell compartment. Data are represented as mean \pm SD of 5-10 pooled mouse brains per time point from 3 individual experiments. (One-way ANOVA with Tukey's post test; * $p < 0.05$, ** $p < 0.01$, *** $p < 0.001$)

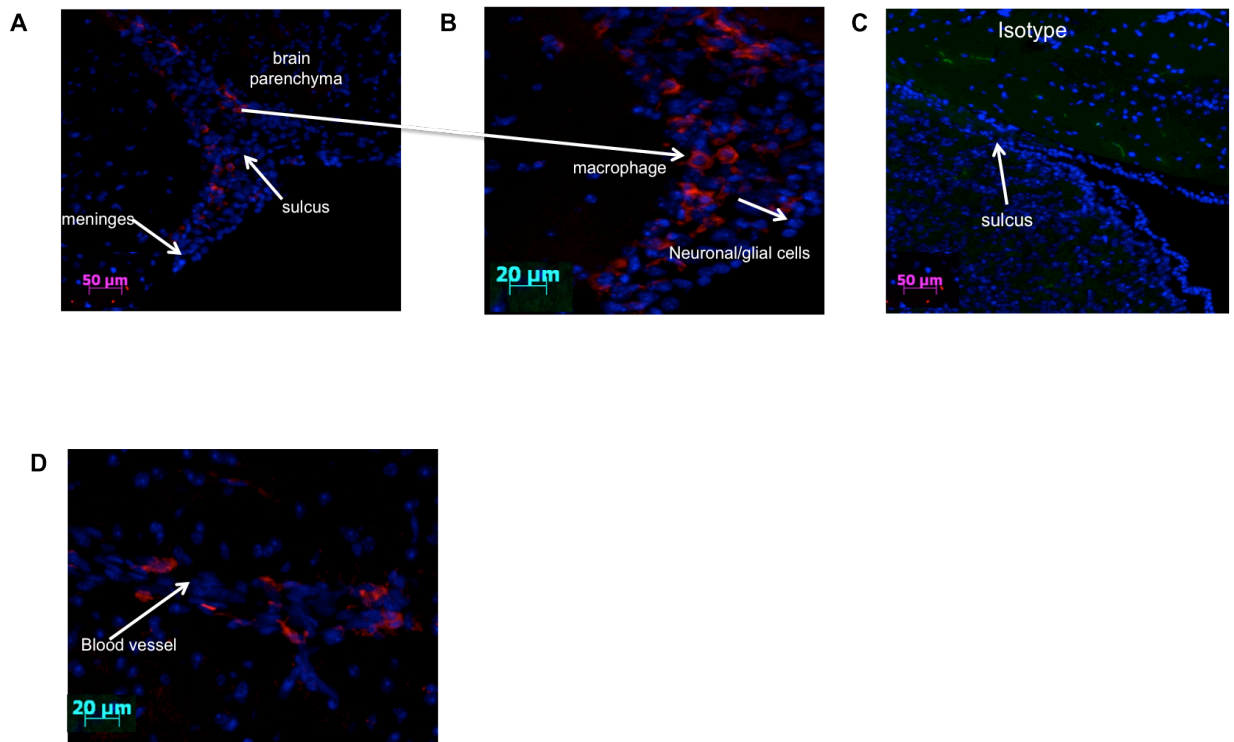


Figure 4.6. Immunohistochemical staining for macrophages within the CNS of infected mice

Mice were infected with SFV A7(74) for 5 days and brains were collected for analysis by immunohistochemistry. Brains were fixed in formalin, embedded in paraffin and cut into 6 μm thick sections for staining. (A) Fluorescent image of MAC-2 staining in an infected brain at 10x and (B) 20x magnification. (C) Isotype control staining for MAC-2 in a SFV infected mouse brain at 10x magnification. (D) Fluorescent staining of a blood vessel from infected brains for the detection of MAC-2⁺ macrophages at 20x magnification. Fluorescently stained brain sections were mounted with Vectashield plus DAPI (cell nuclei blue).

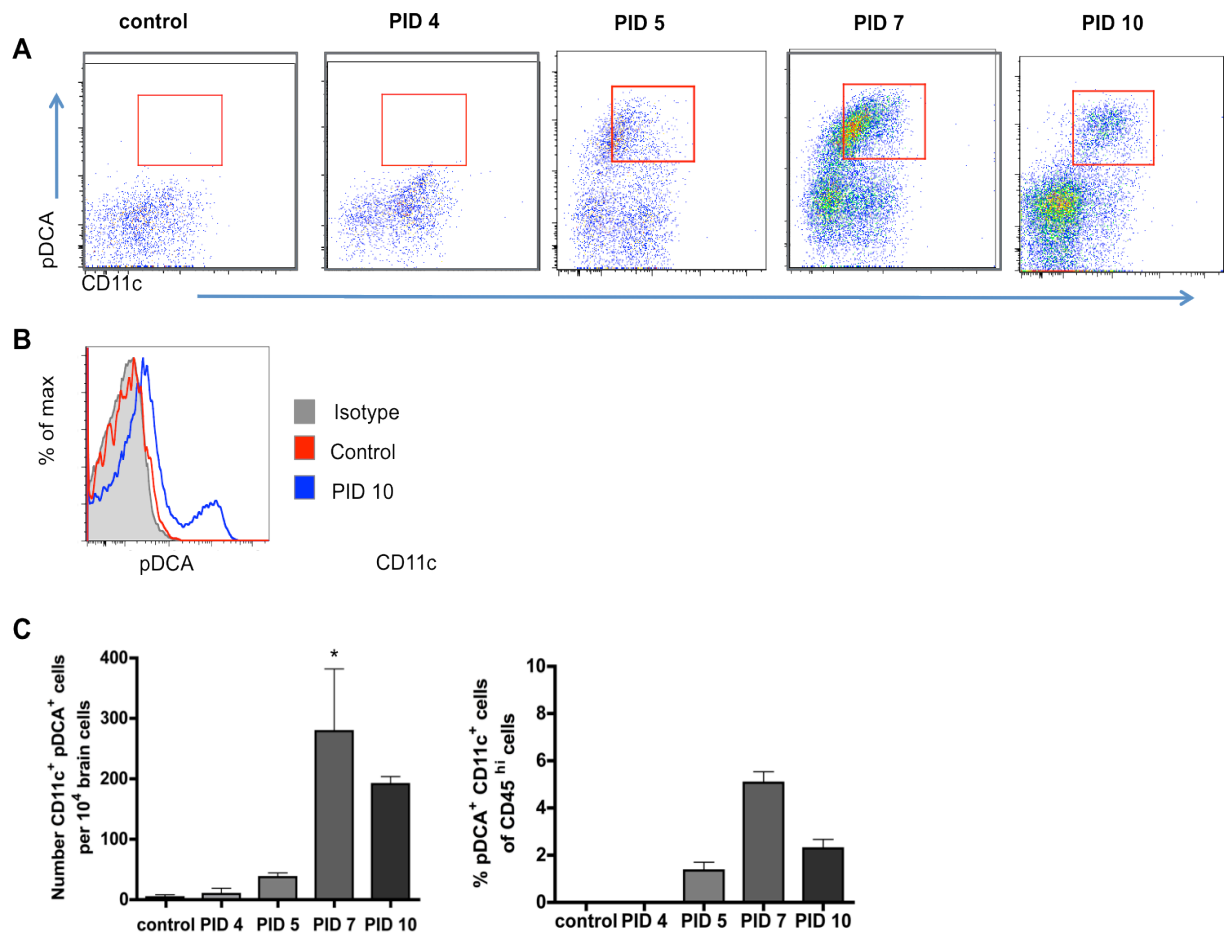


Figure 4.7. Identification of plasmacytoid DCs in SFV infected murine brains

Mice were infected with SFV A7(74) for 10 days and the number of CD11c⁺pDCA⁺ cells was determined by flow cytometry on post infection day (PID) 4, 5, 7 and 10. (A) Representative dot plots of pDCA and CD11c expression within gated live CD45^{hi}CD11b⁺ cells at each time point. (B) Histogram represents staining with the appropriate isotype control (grey), and staining of pDC in control (red) and PID 10 samples (blue). (C) Number and proportion of CD11c⁺pDCA⁺ cells per 10⁴ isolated live brain cells amongst total CD45^{hi} cells. Data are represented as mean \pm SD of 4-8 pooled mouse brains per time point from 3 individual experiments. (One-way ANOVA with Tukey's post test; * $p < 0.05$)

4.7 Identification of T-cells in SFV infected brains

Given the strong induction of CXCL9 and CXCL10, both CXCR3 ligands, following viral infection of the brain, it was hypothesised that a large number of T-cells would enter the CNS during SFV encephalitis. To test this hypothesis, CD45^{hi} leukocytes were stained for the CD3, CD4 and CD8 T-cell markers and analysed by flow cytometry. CD45^{hi} cells in control samples comprised approximately 20% CD3⁺ T-cells (Fig. 4.8 A and B). On PID 4 and PID 5 the proportions of CD3⁺ T-cells were not significantly altered compared with controls. However, on PID 7 the proportion of CD3⁺ T-cells within the CD45^{hi} cell compartment rose to

almost 40%, and increased by an additional 20% by PID 10. A significant increase ($p < 0.05$) of cell numbers of $CD3^+$ T-cells per 10^4 isolated live brain cells was seen at PID 7 and PID 10 matching the significant increase ($p < 0.05$) in proportions of $CD3^+$ T-cells within the $CD45^{hi}$ cell population at both time points (Fig. 4.8 B). Thus, a large number of T-cells enter the brain between PID 7 and PID 10.

Next, the $CD3^+$ T-cells were further analysed for the expression of CD4 or CD8 (Fig. 4.8 C). While the proportions of $CD3^+CD4^+$ T-cells did not change significantly over time, the $CD3^+CD8^+$ T-cell fraction increased approximately 2-fold by PID 7 ($p < 0.05$) and 4-fold by PID 10 ($p < 0.01$). These data suggest that $CD8^+$ T-cells preferentially accumulate in SFV infected brains. Staining by immunohistochemistry, using an antibody for CD3, revealed that T-cells were localised throughout the brain and were able to infiltrate deep into the brain parenchyma (Fig. 4.8 D). In particular, T-cells were localised in the perivascular space of capillaries, in the cortex and in the meninges (Fig. 4.8 D and E). Clusters of T-cells could also be detected in the dentate gyrus of the hippocampus, cerebellum and around ventricles (Fig. 4.8 F).

4.7.1 Phenotypic characterisation of T-cells in the brain

Next, $CD3^+$ T-cells were further phenotyped based on the expression of CD44, CD62L, CCR5 and CXCR3. Effector cells have been defined as $CD3^+CD44^{hi}CD62L^{lo}$ and memory cells as $CD3^+CD44^{hi}CD62L^{hi}$ (414). It was found that $>80\%$ of all $CD3^+$ T-cells were effector cells on PID 7 and PID 10 (Fig. 4.9 A). In control samples, a few memory T-cells were additionally found in the CNS, but this cell population was dramatically reduced within the $CD3^+$ T-cell population from 18% of memory T-cells in healthy control brains to 2.42% of cells on PID 10. A significant increase in numbers of effector cells per 10^4 isolated live brain cells was observed on PID 7 ($p < 0.01$) and PID 10 ($p < 0.001$) (Fig. 4.9 B). Within the $CD3^+$ T-cell population the proportion of $CD44^{hi}CD62L^{lo}$ cells also significantly increased by PID 7 and PID 10 (both $p < 0.001$) and matched the increase in numbers per 10^4 isolated live brain cells (Fig. 4.9 B).

Staining for the chemokine receptor CXCR3 revealed, in keeping with high expression of CXCL9 and CXCL10, that the majority of T-cells (70-80% of $CD3^+$

T-cells) expressed CXCR3 between PID 7 and PID 10 (Fig. 4.9 C). Within the CD3⁺ T-cell population the increase in proportions of CXCR3⁺ cells on PID 10 was significant ($p < 0.05$) compared to resting mice. In support of this, the number of CXCR3⁺ cells within 1×10^4 live brain cells was also significantly increased by PID 7 ($p < 0.01$) and PID 10 ($p < 0.001$).

Within the CD3⁺ T-cell compartment the proportion of CCR5⁺ cells, a receptor mainly found on inflammatory cells, was significantly increased at PID 7 and PID 10 (both $p < 0.05$) compared to controls (Fig. 4.9 D). This is in agreement with the significant increase of CCR5⁺ cell numbers within 10^4 isolated live brain cells at PID 7 ($p < 0.05$) and PID 10 ($p < 0.001$) compared with healthy control brains (Fig. 4.9 D).

Thus, CD3⁺ T-cells accumulate in the brain by PID 7 and are capable of infiltrating deep into the brain parenchyma. Most T-cells on PID 7 and 10 displayed the CD8⁺CD44^{hi}CD62L^{lo} phenotype, and most CD3⁺ cells were CXCR3⁺ and CCR5⁺.

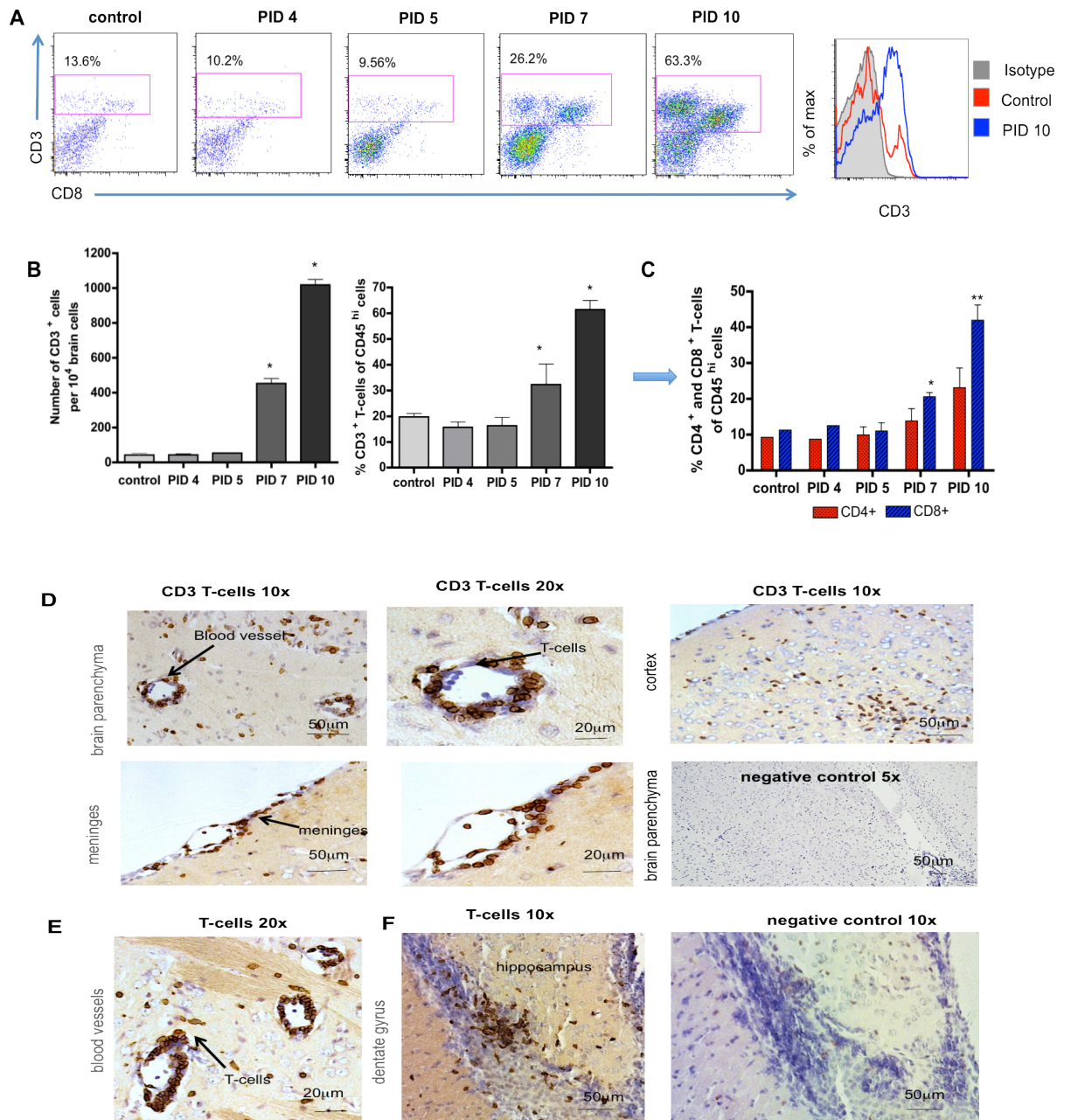


Figure 4.8. Accumulation of CD3⁺ T-cells in the brain during SFV infection

Mice were infected with SFV A7(74) for 10 days and the number of CD3⁺ T-cells was determined by flow cytometry on the days indicated. (A) Representative dot plots of CD3⁺ cells gated on live CD45^{hi} cells at each time point. A histogram (panel on the right) shows the shift of CD3 expression on cells from control (red) and PID 10 samples (blue). Shaded histogram represents staining with the appropriate isotype control. (B) Number and proportion of CD3⁺ cells amongst total CD45^{hi} cells, respectively. (C) Proportions of CD4⁺ and CD8⁺ T-cells of total live CD45^{hi} cells. (D) CD3 staining in the brain parenchyma, cortex and the meninges including negative control staining. (E) Perivascular T-cells and (F) foci of T-cells in the dentate gyrus of the hippocampus at 10x and 20x magnification, respectively. Negative control of CD3 staining is shown on the left. All immunohistochemistry images are taken from infected brains on PID 7. Cell nuclei were visualized with DAB counterstain. Flow cytometry data are represented as mean \pm SD of 5-10 pooled mouse brains per time point from 3 individual experiments. ((B) Kruskal-Wallis test with Dunn's post test and (C) two-way ANOVA with Bonferroni's post test; * $p < 0.05$, ** $p < 0.01$)

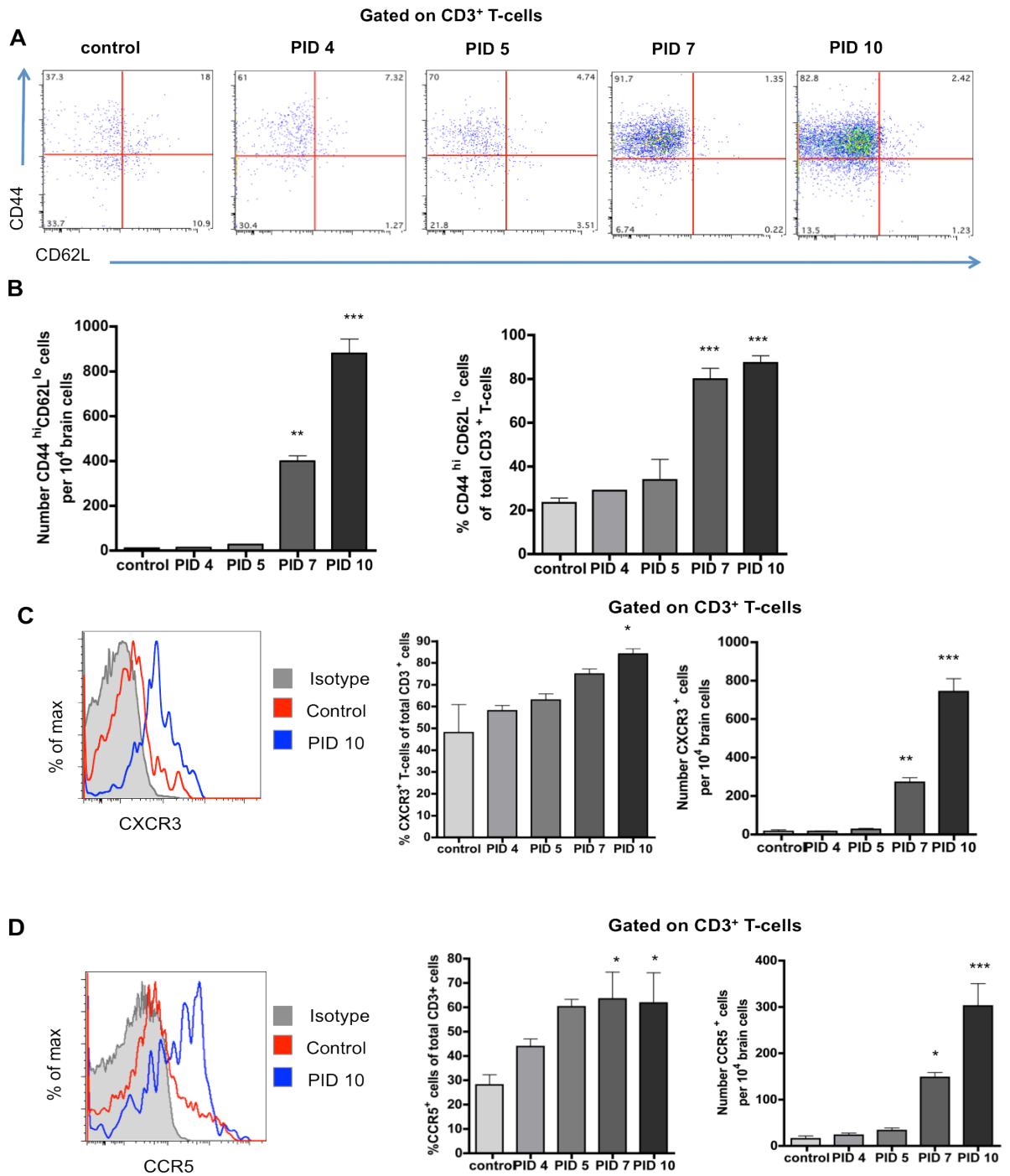


Figure 4.9. Phenotypic characterization of T-cells from the brains of SFV infected mice

Mice were infected with SFV A7(74) for 10 days and cells were isolated from the brains on post infection day (PID) 4, 5, 7, and 10 and from controls, and analysed by flow cytometry. (A) Representative dot plots of CD44 and CD62L staining of CD45^{hi}CD3⁺ cells at each time point. (B) Numbers and proportions of CD44^{hi}CD62L^{lo} cells per 10⁴ live brain cells and amongst CD3⁺ cells, respectively. (C) Histogram, showing differential expression of CXCR3 on cells of control (red) and PID10 samples (blue). Shaded histogram represents staining with the appropriate isotype control. The proportion and absolute number of CD3⁺ CXCR3⁺ cells are shown in the middle and on the left. (D) Histogram showing differential expression of CCR5 on cells of control (red), PID 10 samples (blue) and in isotype controls (shaded). The proportion of CD3⁺CCR5⁺ cells of total CD3⁺ T-cells and number of CD3⁺CCR5⁺ cells within 10⁴ live brain cells. Data are represented as mean \pm SD of 5-10 pooled mouse brains per time point from 3 individual experiments. (One-way ANOVA with Tukey's post test; * $p < 0.05$, ** $p < 0.01$, *** $p < 0.001$)

4.8 Accumulation of B-cells in the brain during later stages of SFV infection

QPCR results reported in the previous chapter revealed a significant upregulation of CXCR5 mRNA expression, a chemokine receptor predominantly expressed on B-cells. To determine whether B-cells enter the CNS during SFV infection, leukocytes were stained for CD19, a marker for B-cells, and cells were analysed by flow cytometry. The results demonstrate that B-cells infiltrate the brain during later stages of SFV infection, on PID 10 (Fig. 4.10 A). Both, cell numbers per 10^4 isolated live brain cells and proportions within the $CD45^{\text{hi}}$ cell population of $CD19^+$ cells showed a significant increase in cell numbers only at PID 10 (both $p < 0.01$) (Fig. 4.10 B).

Analysis by immunohistochemistry, using an antibody for B220, confirmed that $B220^+$ B-cells enter the brain predominantly on PID 10 (Fig. 4.10 C and D). Infected brain sections from PID 7 contained only few B-cells. Sections from control, PID 4 and PID 5 samples were negative for B220 staining. Thus, B-cells appear to infiltrate the brain during later stages of SFV infection. After infiltration, B-cells were mainly localised around ventricles and along the sulcus suggesting that B-cells possibly enter the brain via the CSF-blood barrier (Fig. 4.10 C). Double staining for $CD3^+$ T-cells and B220+ cells showed that often these cells cluster together in areas of the ventricles (Fig. 4.11 A). For instance a cluster of T- and B-cells was found in the choroid plexus of the lateral ventricle (Fig. 4.11 B, C and D). In general, T-cells seemed to be more capable of infiltrating the brain parenchyma than B-cells which were exclusively located around ventricles.

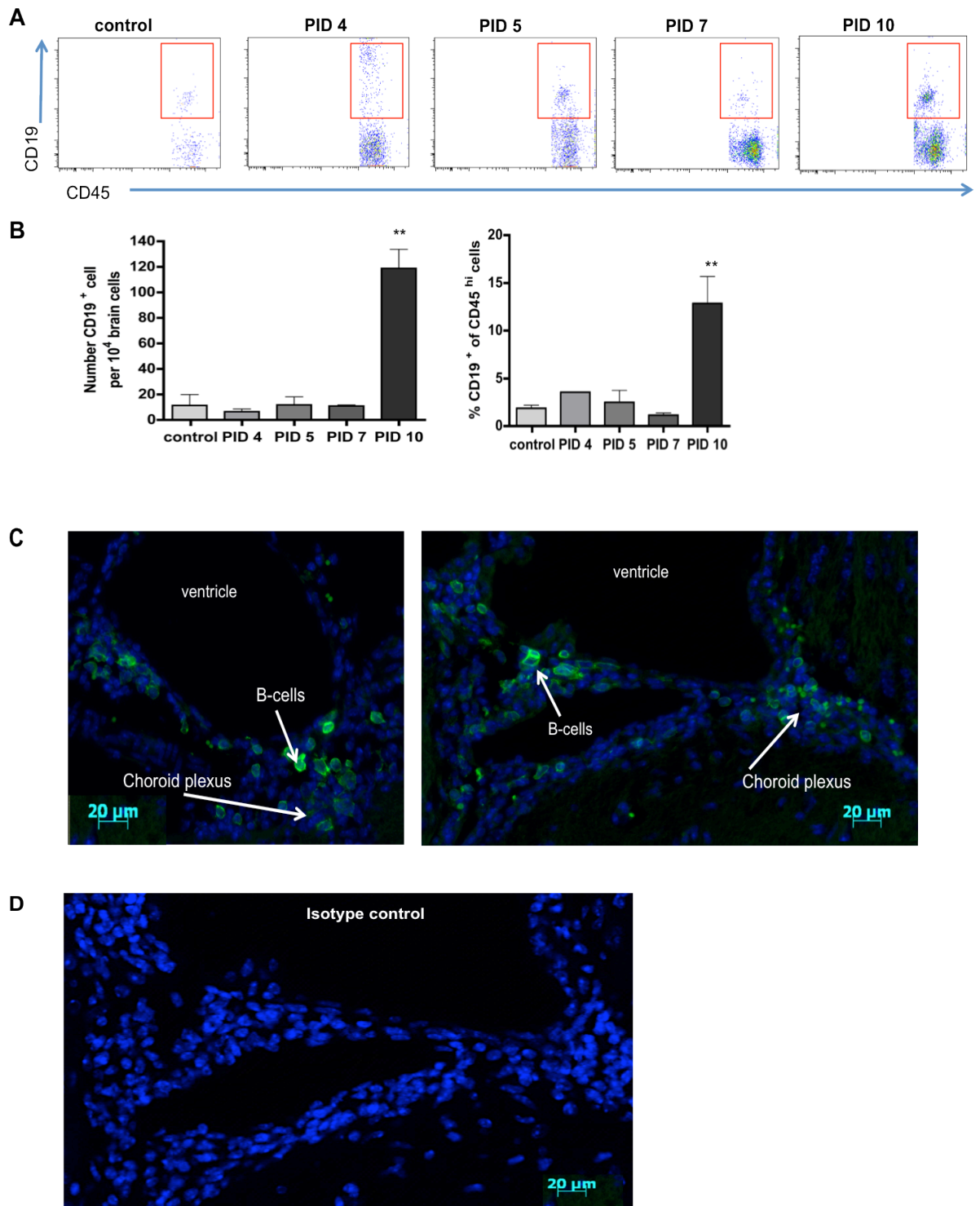


Figure 4.10. B-cells enter the brains of mice late during acute encephalitic infection with SFV

Mice were infected with SFV A7(74) for 10 days and cells were isolated from the brains on post infection day (PID) 4, 5, 7, and 10 and from controls for analysis by flow cytometry. (A) Representative dot plots of CD19 and CD45 on CD45^{hi} cells at each time point. (B) Absolute number of CD19⁺ cells per 10⁴ isolated live brain cells and proportions of CD19⁺ cells within total live CD45^{hi} cells. (C) Fluorescent staining for B220⁺ cells in SFV infected brains on PID 10. (D) Staining with appropriate isotype control. Brain sections were mounted with Vectashield plus DAPI (cell nuclei blue). Magnification at 20x. Flow cytometry data are represented as mean \pm SD of 5-10 pooled mouse brains per time point from 3 individual experiments. (One-way ANOVA with Tukey's post test; ** $p < 0.01$)

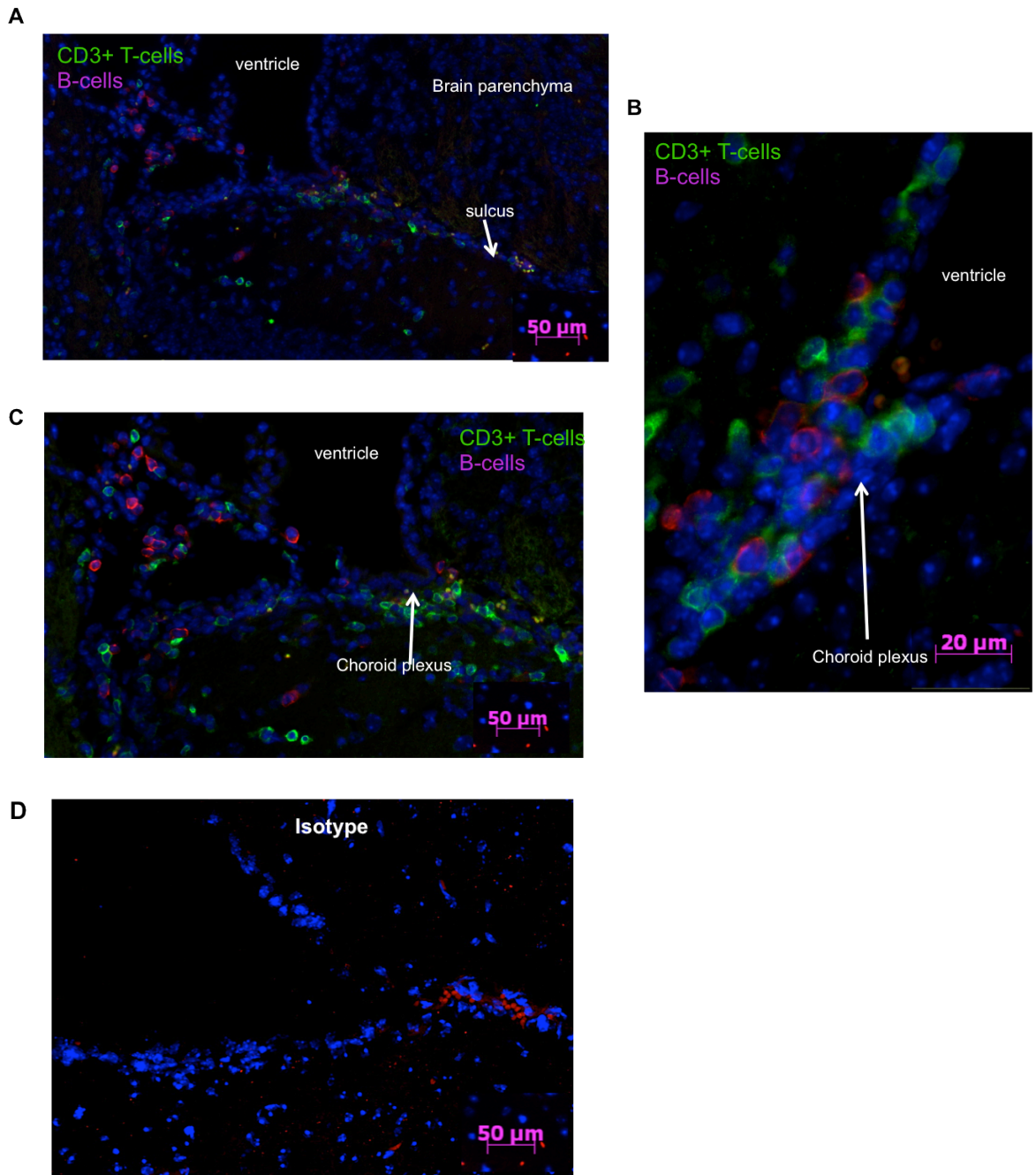


Figure 4.11. Double staining of B-cells and T-cells in SFV infected brains

Mice were infected with SFV A7(74) for 10 days and brains were collected, fixed in formalin, embedded in paraffin, and cut into 6 μm thick sections for immunohistochemistry. Brain sections from post infection day 10 were fluorescently stained with anti-mouse B220 and CD3 antibodies. (A and C) T-cells and B-cells were observed around the ventricles and the sulcus, and (B and C) in the choroid plexus. (D) Staining with the appropriate isotype control. Magnification at 10x (A, C and D) and 40x (B).

4.9 Leukocyte infiltration into the CNS during L10 infection

To date, the kinetics of leukocyte entry into the brain during L10 infection have not been determined and are examined here for the first time. Due to the strong upregulation of chemokines during L10 infection, it was expected that a large number of leukocytes would infiltrate the brain during lethal infection with SFV L10. Mice were infected and brains collected from terminally ill mice, and analysed by flow cytometry. Control mouse brains were also collected for comparison. A density gradient was used to isolate mononuclear cells from brains. For flow cytometry analysis of all L10 samples, the same gating strategy has been used, as described in section 4.2, to identify CD45^{hi} cells. The number of CD45^{hi} cells was significantly increased ($p < 0.05$) and constituted approximately 18% of all live cells compared to control samples, where leukocytes constituted approximately 1% of all live cells (Fig. 4.12 A).

4.9.1 Identification of myeloid cells in L10 infected brains

Firstly, amongst viable CD45^{hi} cells, the absolute number and proportion of CD11b⁺ cells was determined. Compared to controls, the proportion of CD11b⁺ cells within the CD45^{hi} population was increased during L10 infection but the result did not reach statistical significance. The number of CD11b⁺ cells per 10⁴ isolated live brain cells was also assessed, and the results show that the number was increased in the brains of terminally ill mice (Fig. 4.12 B) but this was not statistically significant (student's t-test). Within the CD11b⁺ cell population most cells in control and infected brain samples were Ly6G⁻Ly6C^{hi}, and less than 10% of CD11b⁺ cells were Ly6G⁻Ly6C⁻ (Fig. 4.12 C) suggesting that the majority of cells in the brain were monocytes. However numbers revealed that Ly6C^{hi} cells were much higher in infected samples compared to healthy controls. The number of Ly6C⁻ cells in both samples was similar (Fig. 4.12 C). Hardly any Ly6G⁺ cells were found in the brains of control and infected mice. A clearer examination of monocytes, macrophages and DCs was not possible as the staining was limited to 7 colours, and additionally the marker F4/80 did not work well.

4.9.2 Identification of T-cells and NK-cells in L10 infected brains

Having identified the proportion of CD11b⁺ cells in L10 infected murine brains, the number of T-cells and NK-cells was next examined due to the high upregulation of T-cell and NK-cell attracting chemokines during SFV infection (chapter 3). Amongst CD45^{hi} cells the proportion of CD3⁺ T-cells did not differ in control mice compared to L10 infected mice. However analysis of the numbers of CD3⁺ T-cells per 10⁴ isolated live brain cells showed that the number of cells was 15-fold increased in infected mice. This result could not be analysed statistically as this experiment was only performed once (Fig. 4.13 A).

The comparison of CD8⁺ T-cell and CD4⁺ T-cell numbers in L10 infected brains revealed that the proportion of CD8⁺ T-cells within the CD45^{hi} cell population in infected mice was increased compared to the proportion of CD4⁺ T-cells. In control brains both T-cell subsets were present at an almost equal ratio (Fig. 4.13 B).

NK-cells were detected in L10 infected brains, using the surface markers NK1.1 and Nkp46. The proportion of NK-cells within the CD45^{hi} cell population was increased in L10 infected brains compared to control brains (Fig. 4.13 C). This increase in NK-cells was matched by an increase in cell numbers per 10⁴ isolated live brain cells.

Taken together, a large number of CD45^{hi} cells entered the brain during L10 infection when mice became terminally ill. It appears from these data that the majority of CD45^{hi} cells are myeloid cells, and mainly Ly6C^{hi} monocytes. Additionally T-cell and NK-cell infiltration was observed but the extent of infiltration appeared to be less. The experiment needs to be repeated to achieve statistical significance and to confirm these preliminary data.

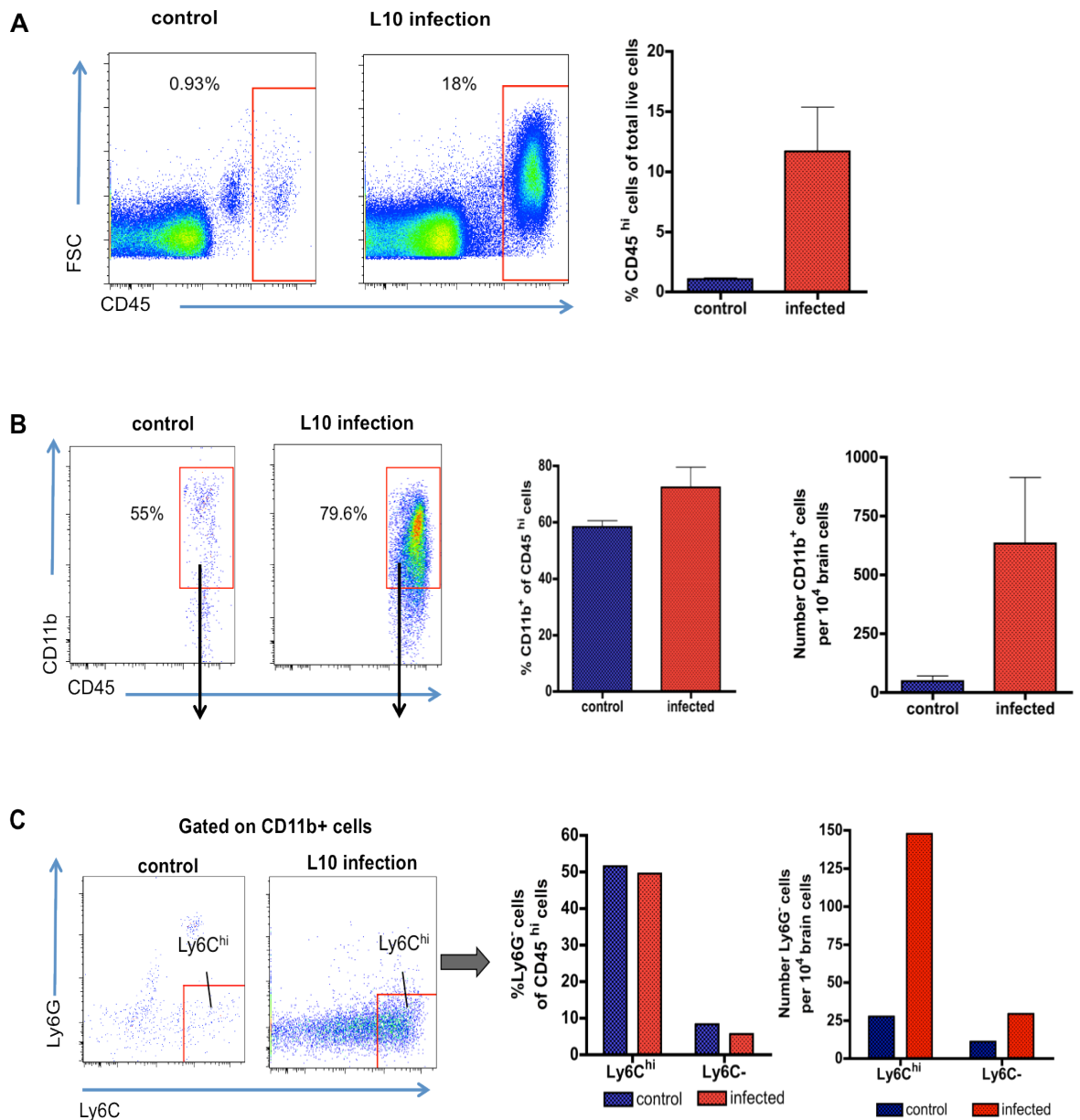


Figure 4.12. Infiltration of CD45^{hi} cells and accumulation of myeloid cells in the brains of mice infected with the virulent strain L10

Mice were infected with SFV L10 and brains cells were isolated from terminally ill mice on post infection day (PID) 5 and analysed by flow cytometry. (A) Representative dot plots of CD45 expression versus FSC on total live single cells in control (left panel) and L10 infected brains (middle panel). The proportion of CD45^{hi} cells of total live cells is shown on the right. (B) Representative dot plots of CD11b⁺ cells (left side). The proportion of CD11b⁺ amongst total CD45^{hi} cells and number per 10⁴ isolated live brain cells. (C) Dot plots of Ly6G and Ly6C by CD45^{hi}CD11b⁺ cells. The proportion of Ly6G⁻ cells in control and infected brain samples is shown on the left. Number of Ly6G⁻ cells per 1x10⁴ brain cells is shown on the right. Data are represented as mean \pm SD of 3-4 pooled mouse brains and from 1 individual experiment. (Student's t-test; all not significant)

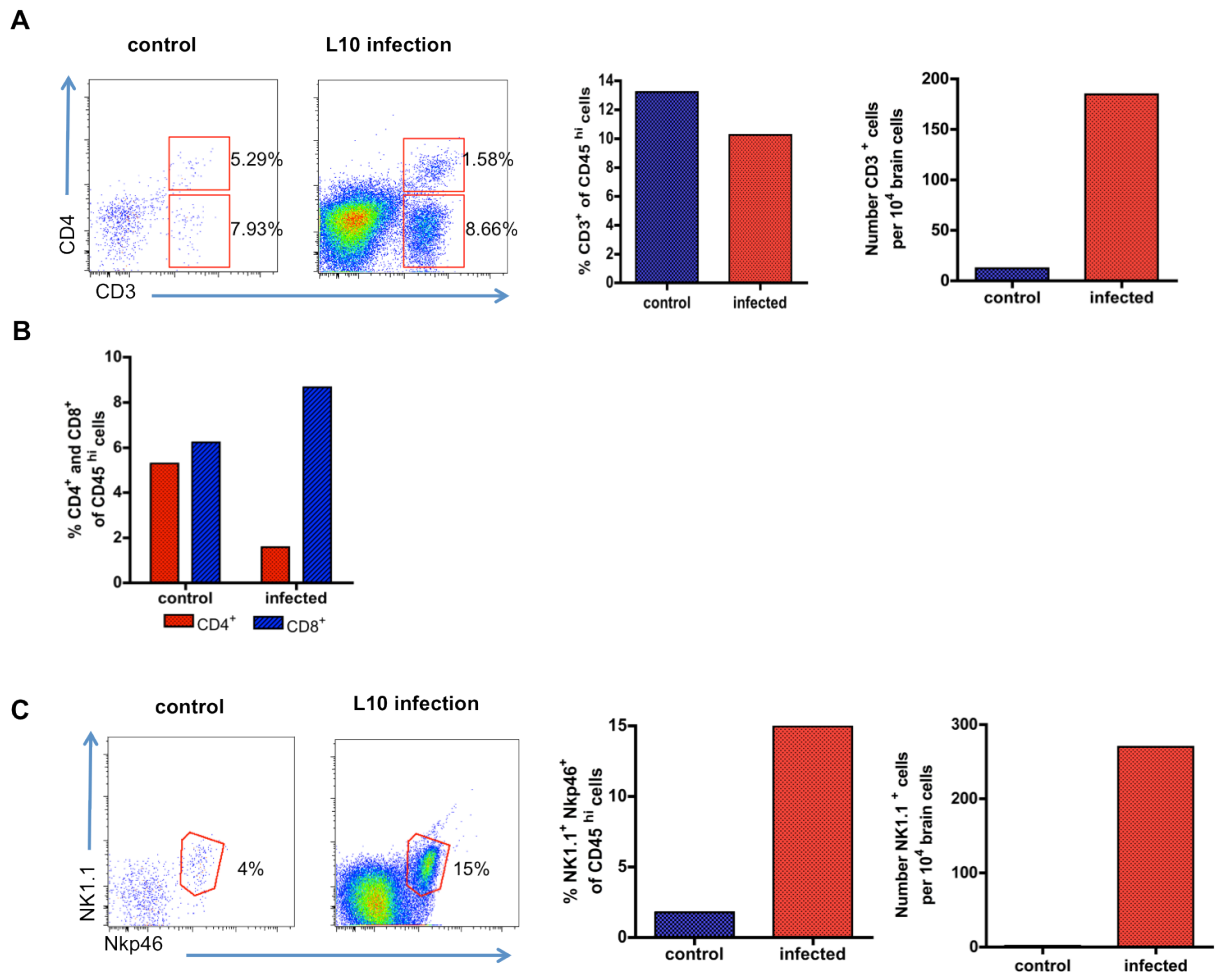


Figure 4.13. Accumulation of T-cells and NK-cells in the brains of mice infected with the virulent strain L10

Mice were infected with SFV L10 and brain cells were isolated from terminally ill mice on post infection day (PID) 5 and analysed by flow cytometry. (A) Representative dot plots of CD3 and CD4 expression on cells amongst total live CD45^{hi} cells in control (left FACS panel) and L10 infected brains (right FACS panel). The proportion of CD3⁺ cells amongst live CD45^{hi} cells and numbers per 10⁴ live brain cells was determined. (B) Proportion of CD4⁺ and CD8⁺ T-cells of total live CD45^{hi} cells. (C) Representative plots of NK1.1 and Nkp46 expression on cells amongst total live CD45^{hi} cells in control (left FACS panel) and L10 infected brains (right FACS panel). The proportion of NK1.1⁺ and Nkp46⁺ cells amongst CD45^{hi} cells and number per 10⁴ live brain cells was calculated. Data are represented as mean \pm SD of 3-4 pooled mouse brains from 1 individual experiment.

4.10 Discussion and summary

It was hypothesised that a large number of leukocytes infiltrate the CNS during lethal SFV encephalitis based on the previous findings, reported in chapter 3, that many leukocyte attracting chemokines are highly upregulated in the CNS of mice infected with SFV L10. A few studies using the avirulent strain A7(74) have shown that leukocytes enter the brain during SFV infection between 4 and

10 days post infection (307, 399). In these studies leukocyte infiltration has been observed in the CSF, brain parenchyma and spinal cord of mice. Morris *et al.* have partly characterised the cellular infiltrate within the CNS during SFV infection but only by immunohistochemistry (307). They have shown that many T-cells and F4/80⁺ macrophages are detectable in brains by 7 days post infection when infiltration was maximal.

In this chapter, for the first time, the timing of specific leukocyte subsets, entering the CNS during SFV infection, has been determined by flow cytometry. Due to the difficulty of isolating mononuclear cells from the murine CNS, brains had to be pooled to obtain sufficient numbers of cells for flow cytometry. The results demonstrate that leukocyte numbers increase almost 2-fold by PID 5 compared to resting mice. Leukocyte infiltration was maximal on PID 10. This is in contrast to previous findings where maximal leukocyte numbers were observed on PID 7 (51, 399). This discrepancy could be due to the different mouse strains used. Previous SFV studies have used BALB/c mice whereas in this study C57BL/6 mice were chosen for analysis. Furthermore the number of leukocytes entering the brain during SFV infection increased concomitantly with the upregulation of inflammatory chemokine expression. This is depicted in Figure 4.14 comparing the percentage of CD45 influx with the copy numbers of CXCL10 and CCL2 in the infected CNS. Furthermore, the high number of leukocytes in control brains most likely arises from insufficient blood perfusion, and is therefore a result of blood contamination.

One of the first leukocytes entering SFV infected mouse brains were a few Ly6G⁺ neutrophils on PID 4, and NK-cells and monocytes/macrophages on PID 5. However for the following reasons, it is most likely that these neutrophils arose in the brain due to insufficient brain perfusion and not leukocyte infiltration. Firstly, it has been reported that neutrophils enter the brain only under extreme conditions such as during severe bacterial or viral infections (415). Extravasated neutrophils in the CNS, have been associated with the break-down of the BBB and often cause severe tissue damage due to the release of cytotoxic and antimicrobial products from their granules (89, 415). Therefore neutrophils in healthy brains would be dangerous for the delicate CNS environment.

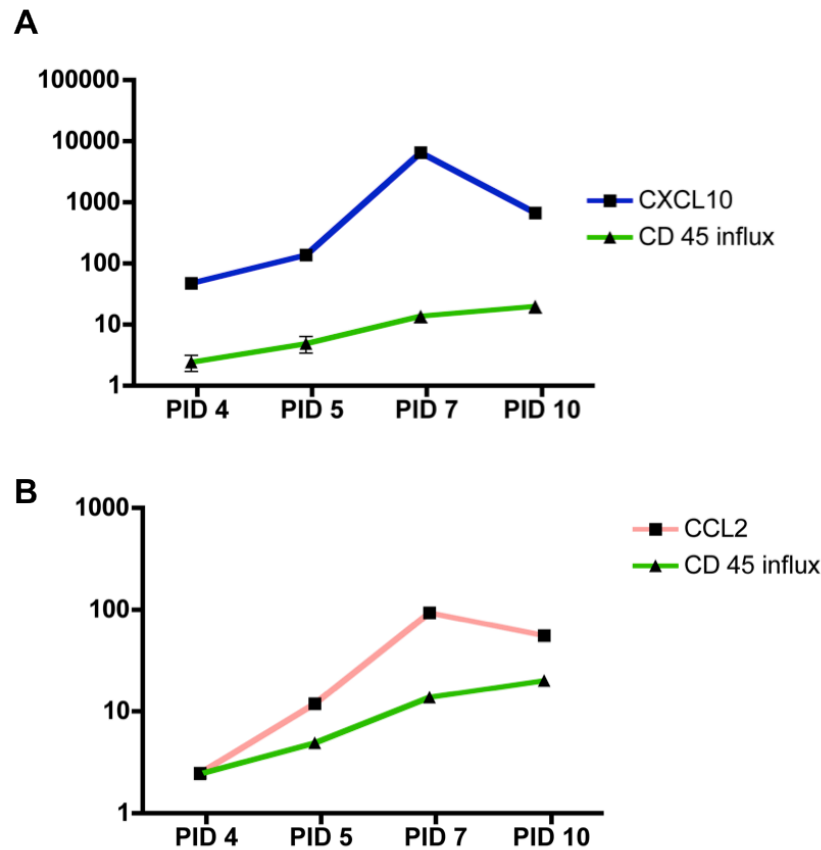


Figure 4.14. Expression of CXCL10 and CCL2 compared with CD45 influx into SFV infected mouse brains

Mice were infected with SFV A7/74 and brains were collected over the time course of infection (PID= post infection day). Isolated RNA was analysed by QPCR for the expression of CXCL10 and CCL2. The CD45 influx was measured by FACS analysis and the percentage of CD45 influx per 10^4 brain cells is depicted. (A) Transcript numbers of CXCL10 per 10^4 TATA binding protein (TBP) and percentage of CD45 influx are shown. (B) Transcript numbers of CCL2 per 10^4 TBP and percentage of CD45 influx are shown.

Secondly, the use of Percoll density gradients for the isolation of mononuclear cells from murine brains, typically leads to the loss of neutrophils within the mononuclear cell fraction at the 30% and 70% interphase, which is used for subsequent flow cytometric analysis. The residual neutrophils within the isolated mononuclear cell fraction of the brain from infected and control mice, detectable by flow cytometry, are most likely a result of blood contamination. Thus, neutrophils are usually not or only at very low levels present in isolated brain cells using this method. Thirdly, immunohistochemical staining for neutrophils in control brain sections was negative for these cells. Therefore the presence of neutrophils in healthy brains is highly unlikely. Lastly, chemokine expression in the healthy CNS revealed that neutrophil attracting chemokines

are not, or only minimally, expressed in the brain. Thus, it is unlikely that the relatively high proportions of neutrophils observed in healthy control brains are infiltrating neutrophils and it is therefore suggested that they are a result of blood contamination. This residual amount of neutrophils and possibly other leukocytes detected in SFV infected brains is taken into consideration when comparing control mouse brains with SFV infected brains. Neutrophil numbers in SFV infected brains that are significantly higher than in controls brains are considered to be entering the brain as a consequence of viral encephalitis.

Data on NK-cell trafficking into the CNS are sparse but some previous studies have shown that NK-cells enter the brain during early stages of acute viral encephalitis using WNV or VEEV as models of infection (348, 416). During SFV infection the relative proportion of NK-cells was increased as early as PID 4, when the BBB has been reported to become permeable (399). The relatively high proportion of NK-cells in control and PID 4 samples was possibly a result of blood contamination due to insufficient brain perfusion, as control brains do not contain resident NK-cells (139). Indeed, analysis of the numbers of NK1.1⁺Nkp46⁺ per 10⁴ isolated brain cells showed that NK-cells enter the brain from PID 5 onwards when leukocyte infiltration was twice as high compared to healthy control brains. These findings are also consistent with immunohistochemical analyses where NK-cells were detected in the brain by PID 5. The exact role of NK-cells in the brain is not clear but a study by Alsharifi *et al.* has shown that NK-cell depletion during SFV infection leads to a more rapid disease progression during virulent infection suggesting that NK-cells are beneficial (417). However the mortality rate in control and NK-cell depleted mice was unchanged. This is in contrast to another study by Shrestha *et al.* which has demonstrated that NK-cells do not influence WNV pathogenesis in the CNS (348). However both studies have shown that NK-cells enter the CNS during early stages of brain infection, and these observations are in agreement with my results.

The other leukocyte subsets observed on PID 4 were CD11b⁺Ly6C⁺ or Ly6C⁻ cells. Based on the expression of Ly6G, Ly6C and MHC-II, the CD11b⁺Ly6C^{hi} or CD11b⁺Ly6C⁻ cells could be defined as monocytes or macrophages, respectively. However, immunohistochemical staining specific for macrophages, using the antibody MAC-2, revealed that macrophages enter the brain during SFV

infection, and are localised mainly in meningeal areas of the brain. Of note, staining for macrophages in the CNS has to be carefully considered because microglia express similar markers as macrophages (117). This makes it difficult to distinguish between these two cell populations by immunohistochemistry. The majority of CD11b⁺ cells were Ly6C^{hi} cells. In previous studies these cells have been described as ‘inflammatory’ monocytes (24). In agreement with my results Mildner *et al.* have shown through bone marrow chimeric and adoptive transfer studies that inflammatory Ly6C^{hi}CCR2⁺ monocytes preferentially accumulate in irradiated mouse brains (33). This increase in Ly6C^{hi} monocytes seems to be a hallmark of viral brain infections (23, 106). Numerous studies using encephalitic viruses have shown that Ly6C^{hi} monocytes infiltrate the brain during infection (23). For example, during WNV infection only Ly6C^{hi} cells are recruited to the brain and it has been shown that these cells can differentiate into ‘inflammatory’ macrophages, CD11c⁺DCs and CD45^{int} microglia once they enter the CNS (106).

On PID 7 the number of leukocytes was approximately 5-fold increased. At this time point many T-cells entered the CNS during SFV infection. Histological studies by Morris *et al.* have revealed that the cellular infiltrate on PID 7 and PID 10 was mainly comprised of CD3⁺ T-cells and in particular of CD8⁺ T-cells (307). The number of CD4⁺ T-cells has been shown to be less evident in infected mouse brains. In support of this, I have found similar results in this study. The T-cell infiltration peaked on PID 10 and not PID 7, as observed in the previous study by Morris *et al.* (307). T-cells on PID 10 represented almost 64% of all leukocytes at this time point. In addition to flow cytometric results, immunohistochemistry revealed that CD3⁺ T-cells do not appear to enter SFV infected brains before PID 7. This is in agreement with data presented by Morris *et al.* who demonstrated that T-cells infiltrate the CNS mainly between PID 7 and PID 10 (307). Most T-cells were able to penetrate deep into the brain parenchyma. This is in line with studies using WNV as a model of infection where it has been shown that T-cell numbers are strongly increased in the infected brain and are localised deep in the brain parenchyma (321).

In this study CD8⁺ T-cells were significantly increased by PID 7 and 10, and were generally more abundant than CD4⁺ T-cells within the CNS of SFV infected mice. CD8⁺ T-cells appear to play important roles during viral infections of the

brain including WNV, LCMV and MHV (140, 141, 418, 419). These cells have been shown to be important for virus clearance and destruction of infected cells. Furthermore it has also been reported that the majority of T-cells during neuroinflammation are effector T-cells (420). In agreement with these previous studies, healthy brains contained few cells with the CD44⁺CD62L⁺ phenotype of effector T-cells. With disease progression the number and proportions of effector T-cells were increased by PID 7 and 10.

After further phenotyping most of the T-cells on PID 7 and PID 10 expressed the chemokine receptors CXCR3 and CCR5, confirming the presence of activated and inflammatory T-cells within the inflamed brain. CXCR3 is an important chemokine receptor during many viral infections of the brain as discussed in the general introduction. A study by Zhang *et al.* has demonstrated that CXCR3 deficient mice exhibit enhanced mortality and reduced clearance of WNV in the CNS due to a significant reduction in CD8⁺ T-cell entry into the brain (375). CCR5 has also been reported to be pivotal during WNV infection. Glass *et al.* have shown that many cell types, such as monocytes, T-cells and NK-cells, express CCR5, and CCR5 deficiency in mice results in increased mortality, reduced leukocyte infiltration and higher viral titers (173). What role CXCR3 and CCR5 play during SFV infections shall be discussed in further detail in chapter 6.

Beside the large infiltration of T-cells into the CNS on PID 7, some CD11c⁺pDCA⁺ cells entered the brain during SFV infection. There are hardly any existing data on the presence of pDCs in the brain of virally infected mice, but EAE and MS studies have shown that these cells enter the CSF during neuroinflammation, and secrete high amounts of IFN- α (413). In support of this Bailey-Bucktrout *et al.* have shown that during EAE pDCs, which enter the brain during inflammation, activate many CNS inflammation, which in turn activate inflammatory cytokines, contributing this way to neuroinflammation (421). Furthermore the authors demonstrated that pDC depleted mice display an increase in clinical EAE severity, and upon pDC reconstitution the severity of the disease is immediately ameliorated, suggesting that pDCs have regulatory effects during EAE. The role of pDCs during viral encephalitis is not yet clear and shall be addressed in the future. The identification of other DC subsets was

not possible as only a limited number of markers could be used for the 7-colour flow cytometry.

Morris *et al.* have demonstrated that B-cells enter the brain late during viral infection with SFV strain A7(74). They have demonstrated by immunohistochemistry that B-cells enter the brain on PID 7, and reach maximal levels between PID 14 and PID 21 (307). In addition to that, B-cells have been shown to be associated with inflammatory lesions and perivascular cuffs (51). These observations are in agreement with findings presented here. However B-cells entered the SFV infected brain later compared to previous studies. This is consistent with results obtained by immunohistochemistry flow cytometry. The differential use of mouse strains in this and previous studies could in part explain the temporal difference in B-cell infiltration into the CNS.

Next, the kinetics of leukocyte entry during L10 infection of mice was defined for the first time. Leukocyte numbers were 16-fold increased compared to resting mice. The fold increase during L10 infection was higher compared to avirulent infection with strain A7(74). Therefore it is possible that the extent of leukocyte infiltration depends on the virus strain used. However it is not clear whether leukocyte infiltration is a beneficial or detrimental process during viral encephalitis. Of note is the loss of the distinct CD45^{int} microglial cell population in L10 infected mice. This could be explained due to the following reasons. First, it is possible that the CD45^{int} microglial cell population was lost during the process of mononuclear cell isolation. Second, CD45^{int} microglia could have upregulated their CD45 expression and become CD45^{hi} in response to lethal infection with SFV. However this possibility seems unlikely as many studies have reported that activated microglia become only CD45^{int} and not CD45^{hi} during activation of microglia in neuroinflammation (117, 407, 410, 422). Due to time constraints the L10 experiment was only performed once, and therefore further tests are required to draw firm conclusions from these preliminary results.

There is a significant amount of knowledge regarding leukocyte trafficking during WNV infection but little is known about the detailed chemokine expression profile within the CNS of infected mice. Therefore a thorough chemokine expression analysis will be performed in the next chapter to

determine if the same chemokine pattern can also be found during brain infections using a virus from a different virus family. A common denominator with regards to chemokine expression would allow the design of appropriate intervention strategies for encephalitic processes in general.

Although I was able to localize some leukocytes subsets within the avirally infected CNS, such as NK-cells, T-cells and macrophages, co-staining with chemokines did not work. This might have been due to the fact that brain tissue was embedded in paraffin rather than snap frozen. Therefore another alternative to localize chemokine expression within the infected CNS would be to use in-situ hybridization (ISH). Due to time constrains ISH was not performed and should be used in future experiments.

Chapter 5

Characterization of chemokine and cytokine driven CNS responses in West Nile virus infection

5.1 Introduction and aims

Chemokines are important regulators of leukocyte trafficking in the body. As discussed in detail in the general introduction (chapter 1), chemokines play important roles during viral encephalitis. To date the expression and role of chemokines during viral brain infection have not been well characterised. In chapter 3 it was shown that chemokines are strongly, and selectively, upregulated in the CNS of mice infected with SFV. Concomitantly with the high expression of chemokines in the brain, it was shown that a large number of leukocytes infiltrate the infected CNS during SFV, and this is discussed in detail in chapter 4. The key chemokines upregulated during SFV infection were also found to be increased in other viral infections such as LCMV or MHV (128, 129). It was therefore hypothesised that the chemokine expression profile during viral encephalitis is similar between different pathogens. *To test this hypothesis a different model of viral encephalitis was used to investigate if the chemokine expression profile is pathogen-specific.*

WNV was chosen as a model of infection since chemokines appear to play a pivotal role in the pathogenesis of WNV encephalitis. For example, it has been demonstrated that CCR5 is important for survival during WNV infection and clearance of virus by attracting the appropriate leukocytes into the CNS (362). However chemokines in the CNS of WNV infected mice have only been partly analysed in previous studies (214, 358). In particular CCL2 and CCL5 have been identified as important chemokines during WNV encephalitis (423, 424). *To establish a detailed and clear picture of chemokine expression during WNV infection of the brain, the other aim of this chapter was to investigate the form and magnitude of chemokine expression during WNV induced encephalitis in detail.*

Furthermore cytokines and PRRs have also been shown to be involved during WNV infection (54, 72, 425). *Subsequently in this chapter, I also investigated the expression of specific cytokines, and two selected PRRs, during WNV infection of the CNS.*

5.2 Determination of viral titers in the blood and brain during West Nile virus infection

First, C57BL/6 mice were inoculated intranasally with the suggested dose of 2×10^4 PFU of WNV strain NY99 (426). Brains and blood were collected from control and infected mice at 2, 3, and 5 days post infection. The viral titers in the brain and blood were measured by QPCR to evaluate the functionality of WNV as model of infection. The viral titer in the blood reached a high titer of approximately 1×10^8 viral copies per 1 ml blood on PID 2 and stayed elevated throughout the infection until death after PID 6 (Fig. 5.1 A). The titer in the blood was slightly reduced on PID 6 but the difference was not statistically significant.

Viral titers in the brain were initially low on post infection day 2. However viral transcripts quickly increased to more than 1×10^6 viral copies per 1×10^4 housekeeping gene TATA-binding protein (TBP) by PID 4 and PID 6 (Fig. 5.1 B). The increase of viral transcripts on PID 6 was significantly different ($p < 0.01$) to uninfected control brains. When mice became critically ill after PID 6, they were euthanized according to Home Office regulations.

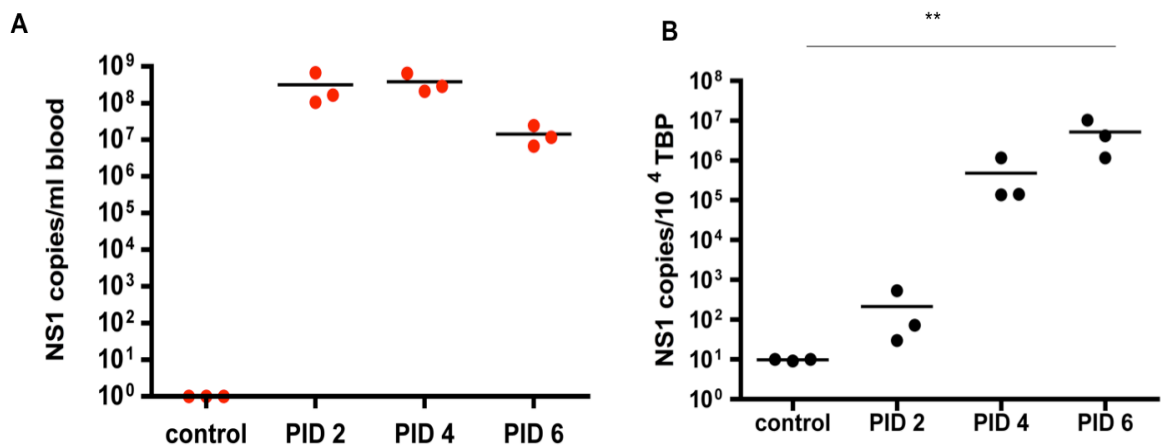


Figure 5.1 Viral titers in the blood and brain of WNV infected mice

Mice were inoculated intranasally with WNV strain NY99. Brains and blood were collected from infected mice on post infection day (PID) 2, 4 and 6, and from healthy control mice. Viral gene transcripts for NS1 were quantified by QPCR. (A) Viral titer in the blood and (B) brains of infected and healthy mice with $n=3$ mice per time point. (Kruskal Wallis test with Dunn's post test; ** $p < 0.01$)

These data demonstrate that viral transcripts can be reliably and reproducibly detected in the brain and blood of WNV infected mice and confirms the efficiency of this model of infection to study viral encephalitis.

5.3 Histological analysis of WNV infected brains

To localise virus-infected cells and to investigate pathological changes in WNV infected mouse brains, immunohistochemistry was performed. Prior to staining, infected brains were fixed in formalin, embedded in paraffin and cut into 6 μm thick sections. Histological analysis of brain sections from infected mice revealed that perivascular cuffings form around blood vessels on PID 4 and PID 6, indicating leukocyte infiltration into the perivascular space of the BBB of cerebral capillaries (Fig. 5.2 A and B). Next, brain sections from infected mice were stained for viral protein NS1. On PID 4 a few viral particles could be detected, and by PID 5 virus had spread throughout the brain (Fig. 5.3). Mice became severely ill on PID 6, displaying neurological symptoms including paralysis of fore or hind limbs, and succumbed to the disease shortly afterwards.

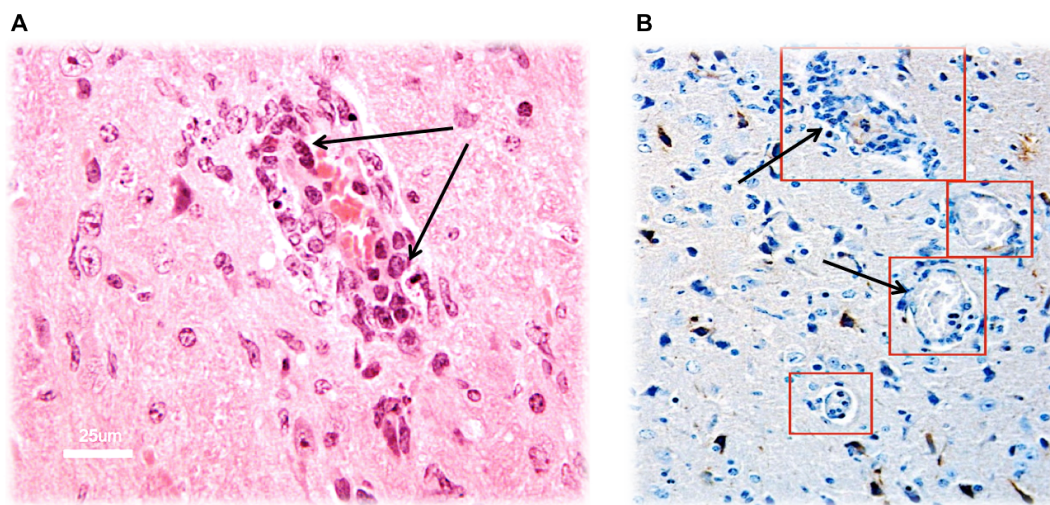


Figure 5.2 Perivascular cuffings forming around blood vessels during WNV infection

After intranasal infection of mice with WNV strain NY99, perivascular cuffings (see arrows) appeared in the brain around blood vessels. (A) Haematoxylin and Eosin staining of a brain vessel on post infection day (PID) 6. (B) Cuff development within the brain of mice on PID 6. Brown staining indicates CXCL10 immunolabelling. Other cells were counterstained with hematoxylin. All images were taken from rostral regions of the brain. (A) Magnification at 40x and (B) 20x. n=3-4 mice. Help with this staining was kindly provided by Dr Nick Johnson, AHVLA, Surrey, UK.

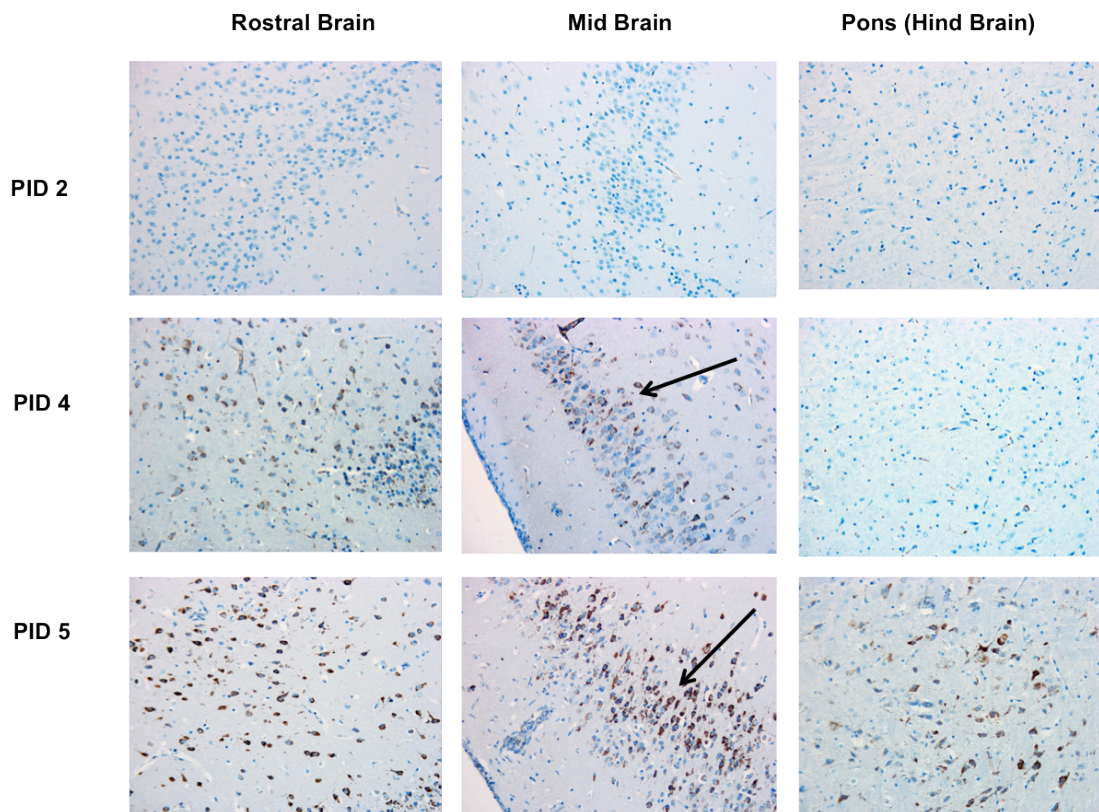


Figure 5.3 Staining for viral protein in WNV infected mouse brains

Mice were infected intranasally with WNV strain NY99, and brains were collected from infected mice on post infection day (PID) 2, 4 and 5, and from healthy control mice. Brain sections were formalin-fixed and paraffin embedded, and stained for viral protein NS1. Shown are infected neurons (brown staining, see arrows) scattered throughout the brain. Six μm thick sections were cut for immunohistochemistry. Brain sections were taken from rostral-, mid- and hind brain areas. All images are representative of 3-4 mice per time point. Magnification of all images at 20x. Help with this staining was kindly provided by Dr Nick Johnson, AHVLA, Surrey, UK.

5.4 Chemokine expression during WNV infection

After determining viral titers in mice and investigating pathological changes in the CNS during WNV infection, it was next examined which chemokines are upregulated during WNV encephalitis. In chapter 3 it was demonstrated that chemokines are highly and selectively upregulated during SFV infection. Furthermore it was also shown that the magnitude of chemokine expression was dependent on the virus strain and disease severity.

To test whether chemokines in WNV infected brains were upregulated in a similar fashion to SFV infection, brains were collected from mice infected with WNV strain NY99, which is a lethal and neuroinvasive strain of WNV. As in chapter 3 chemokine expression was measured by TLDA. To this end the same

TLDA plates as in described in chapter 3 were used for analysis of WNV infected samples. In brief, a 384-well format was selected, containing 32 genes, including most inflammatory CC- and CXC- chemokines, CX₃CL1, XCL1, and a few inflammatory cytokines and innate immune response genes, known to play a role during viral infections.

To test control and WNV infected brain samples by TLDA, the RNA quality was first assessed using the Agilent Bioanalyser. All samples were of high quality with a RIN greater than 8 (Fig. 5.4 A). The electropherogram for each sample showed a clear 18S and 28S band, which, again, is an indicator of high quality RNA. A representative electropherogram of one sample is illustrated in Fig. 5.4 B. The RIN values for each analysed sample are listed in Appendix 2 C.

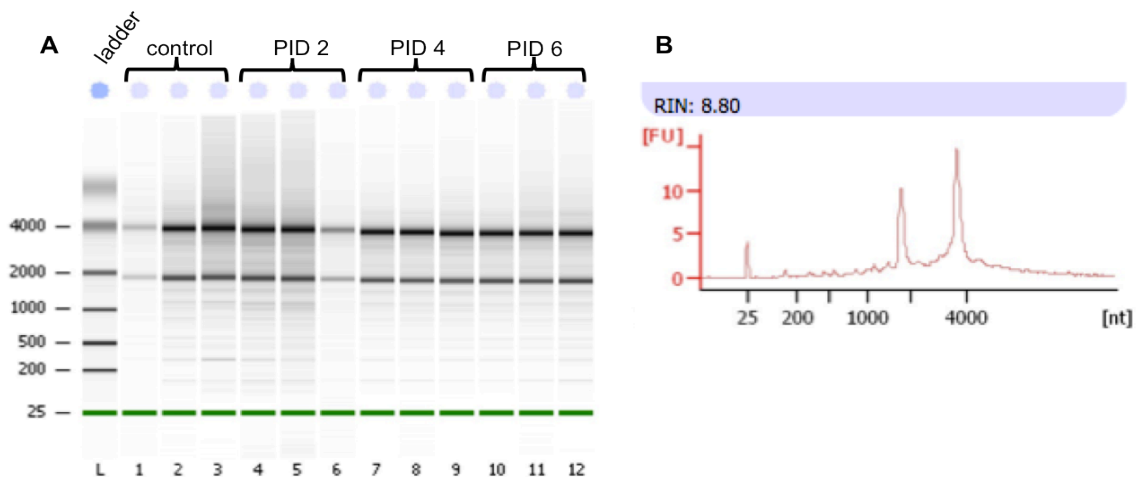


Figure 5.4 Assessment of RNA quality, isolated from WNV infection brains

Total RNA was extracted from healthy control and WNV infected brains over the time course of infection and RNA quality was assessed for TLDA analysis using the Agilent Bioanalyser. (A) Gel-like image of extracted RNA from murine brains. Lane L: size marker (number of nucleotides, nt); Lane 1-3: healthy control samples; Lane 4-6: post infection day (PID) 2 samples; Lane 7-9: PID 4 samples; Lane 10-12: PID 6 samples. (B) Representative electropherogram showing the RNA profile of a high quality RNA sample. The x-axis represents amplicon size (nt), while the y-axis represents fluorescence units (FU). The RNA integrity number (RIN) was calculated and is indicated on the upper left hand corner of the electropherogram.

5.4.1 CC-chemokine expression

Chemokine expression on PID 2 was generally very low and comparable to healthy control mouse brains. The expression of CCL2 and CCL4 was more than two-fold upregulated at this point (Fig. 5.5). The expression profile between PID

4 and PID 6 was relatively similar but the magnitude of expression was several fold higher on PID 6 when mice were terminally ill (Fig. 5.5). In summary, chemokines CCL2-CCL7 were more than 100-fold upregulated on PID 4 and more than 1000-fold upregulated on PID 6. The most upregulated CC-chemokines during WNV infection of the brain were CCL2, CCL4 and CCL5. CCL2 expression on PID 4 was upregulated on average 309-fold \pm 114 SD compared to resting mice. By PID 6 a further 8.5-fold upregulation was noticed. The expression levels of CCL4 and CCL5 on PID 4 were 724 \pm 344 SD and 377 \pm 151 SD fold increased, respectively, compared to healthy mice. By PID 6 both chemokines were more than 3000-fold upregulated compared to controls. The expression levels of CCL20 and CCL11 were only moderately upregulated compared to other CC chemokines.

To examine, if the expression of CCL2 and CCL5 is reproducibly elevated during WNV infection relative to healthy uninfected control brains, a QPCR analysis was performed to validate the results obtained from the TLDA analysis. The expression of CCL2 was significantly ($p < 0.05$) increased by PID 6 compared to controls (Fig. 5.6 A). CCL5 was also significantly upregulated by PID 4 and PID 6 (both $p < 0.05$) compared to healthy controls (Fig. 5.6 B). The expression of CCL5 was 330-fold and 1402-fold upregulated on PID 4 and 5, respectively. Thus, QPCR results are in agreement with results obtained from TLDA analysis and demonstrate strong upregulation of CCL2 and CCL5 during WNV infection.

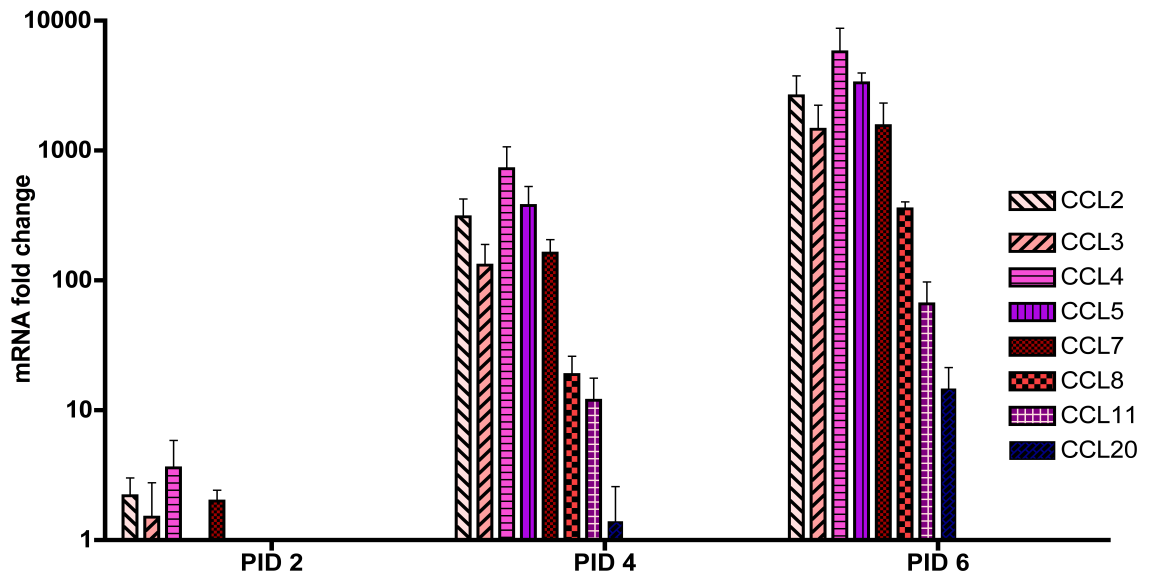


Figure 5.5 Identification of CC-chemokine expression patterns during WNV infection with strain NY99

All mice were infected with WNV intranasally, and RNA was isolated from infected brains on post infection day (PID) 2, 4 and 6, and from healthy controls. The expression of CC-chemokines was measured by TLDA. Each gene was double normalized to an endogenous control 18S and to an uninfected healthy control brain. The relative quantification (RQ) values are depicted as mRNA fold changes and are shown on the y-axis. The RQ value of an uninfected control brain was set to 1. Data are shown as mean \pm SD, n=3 mice per time point. Each gene was tested in triplicate.

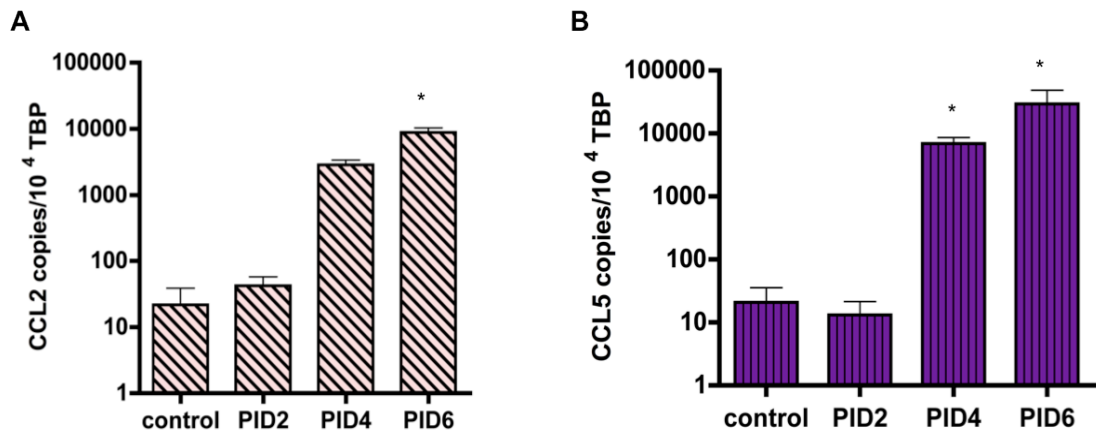


Figure 5.6 Validation of CCL2 and CCL5 expression by QPCR during WNV infection

The expression of CCL2 and CCL5 transcripts was highly upregulated during WNV infection, as shown by TLDA analysis. Therefore these genes were selected for validation by QPCR. The absolute copy number of each gene was measured and normalized to 1×10^4 copies of TATA-binding protein (TBP). Shown is the expression of (A) CCL2 and (B) CCL5. Each gene was tested in triplicate; Data presented as mean \pm SD with n=3 mice per time point; PID=post infection day; (Kruskal-Wallis test with Dunn's post test; * $p < 0.05$)

5.4.2 CXC-chemokine expression

On PID 2 CXCL9 and CXCL10 were 3- and 9-fold upregulated, respectively, while other CXC-chemokines were only minimally, or not, upregulated compared to resting mice (Fig. 5.7). On PID 4 other chemokines such as CXCL1, CXCL2 and CXCL16 were moderately upregulated compared to controls (Fig. 5.7). CXCL9 and CXCL10 levels were the earliest and highest upregulated CXC-chemokines in WNV infected brains. The expression of CXCL9 was 331-fold \pm 116 SD upregulated, and CXCL10 levels were 2350-fold \pm 671 SD increased relative to resting mouse brains, making CXCL10 the most upregulated chemokines on PID 4.

On PID 6 the chemokine expression levels were similar to that on PID 4 but generally the magnitude of expression was markedly higher. For example, levels of CXCL1 and CXCL2 were rapidly 20-fold and 89-fold upregulated, respectively, between PID 4 and PID 6. The expression of CXCL9 was 6923-fold upregulated by PID 6 compared to controls, which resulted in CXCL9 being the most upregulated chemokine on PID 6. The expression of CXCL10 was also highly, 2603-fold \pm 379 SD, upregulated on PID 4 compared to controls but the level of expression increased only minimally between PID 4 and PID 6. The expression levels of CXCL5 and CXCL12 were similar to controls.

Due to the rapid upregulation of CXCL1 and CXCL2, and the strong upregulation of CXCL10, a QPCR analysis was performed to validate the results obtained by TLDA analysis. CXCL1 was significantly upregulated by PID 4 ($p < 0.05$) and PID 6 ($p < 0.05$) compared to controls (Fig. 5.8 A). CXCL2 was significantly upregulated by PID 6, showing a 330-fold increase compared to controls (Fig. 5.8 B). CXCL10 expression was also significantly upregulated on PID 4 and PID 6 (both $p < 0.05$) (Fig. 5.8 C). Overall, these QPCR results were in agreement with the TLDA results but the magnitude of CXCL1 and CXCL2 expression was slightly lower as assessed by QPCR.

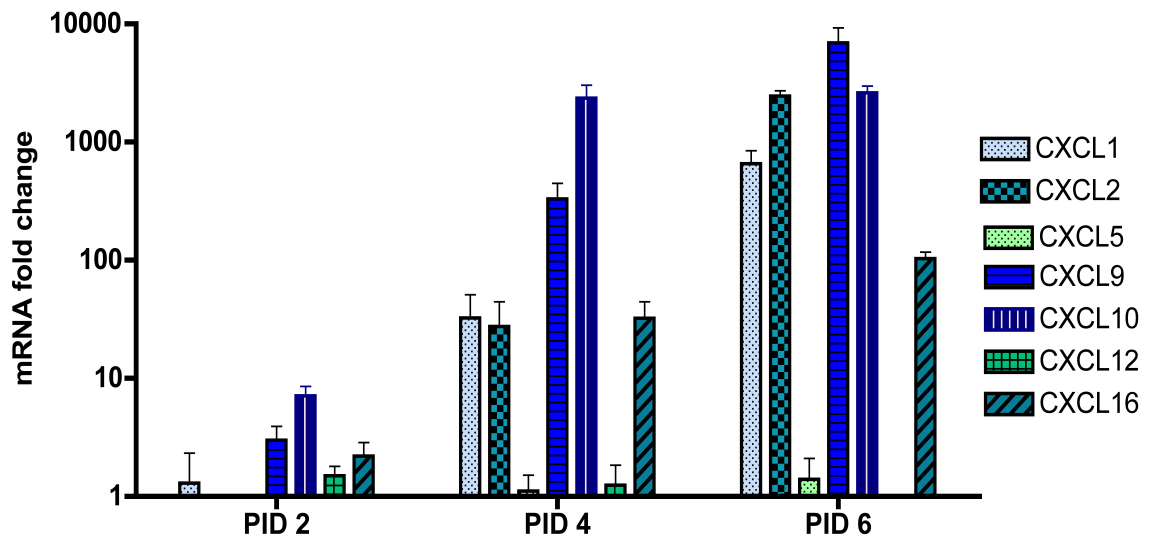


Figure 5.7 Identification of CXC chemokine expression patterns during WNV infection with strain NY99

All mice were infected intranasally with WNV, and RNA was isolated from infected brains on post infection day (PID) 2, 4 and 6, and from healthy controls. The expression of CXC-chemokines was measured by TLDA. Each gene was double normalized to an endogenous control 18S and to an uninfected healthy control brain. The relative quantification (RQ) values are depicted as mRNA fold changes and shown on the y-axis. The RQ value of an uninfected control brain is set to 1. Data are presented as mean \pm SD with n=3 mice per time point. Each gene was tested in triplicate.

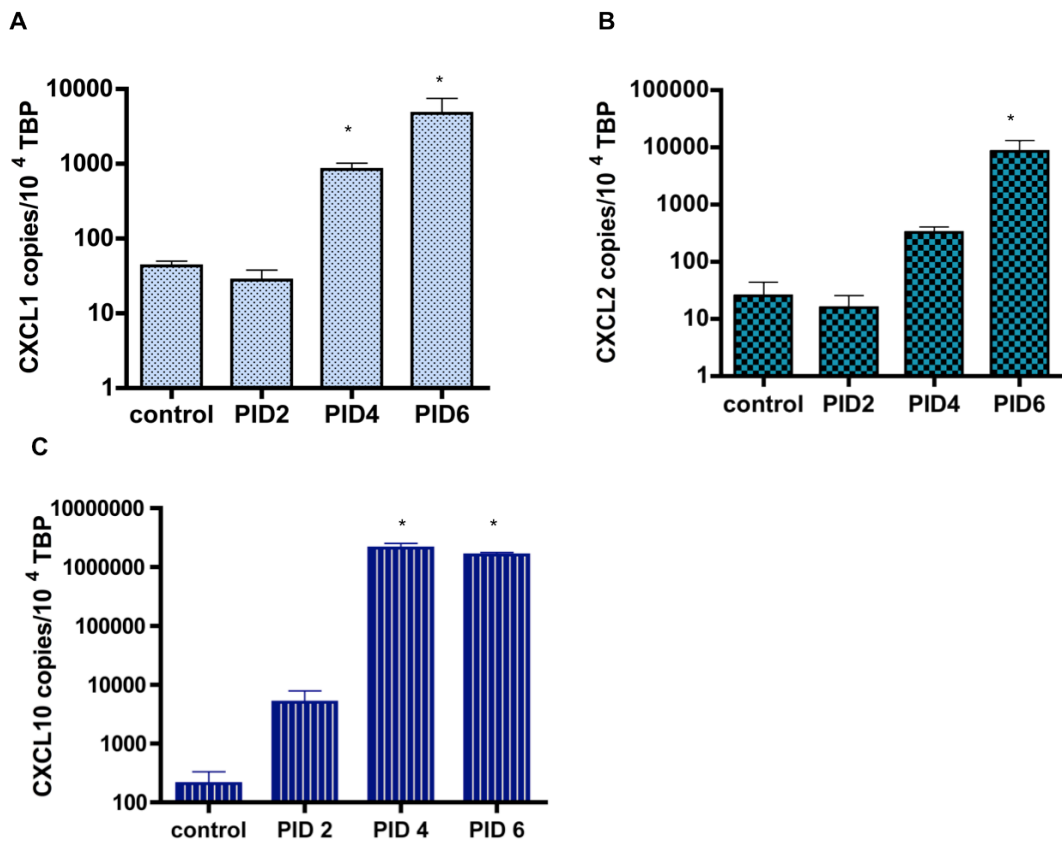


Figure 5.8 Validation of CXCL1, CXCL2 and CXCL10 expression by QPCR

The expression of CXCL1, CXCL2 and CXCL10 was highly upregulated by TLDA analysis during WNV infection and therefore these genes were selected for validation by QPCR. The absolute copy numbers of each gene were measured and normalized to 1×10^4 copies of TATA-binding protein (TBP). Shown are the expression of (A) CXCL1, (B) CXCL2 and (C) CXCL10 by QPCR. Each gene was tested in triplicate. Data are presented as mean \pm SD with $n=3-4$ mice per time point. PID=post infection day. (Kruskal-Wallis test with Dunn's post test; * $p < 0.05$)

5.4.3 CX₃CL1 and CXCR5 expression

The expression level of CX₃CL1 was similar to that in healthy control brains (Fig. 5.9). On PID 6 CX₃CL1 expression was 0.6-fold downregulated compared to expression levels at other time points but this result was not statistically significant.

CXCR5 is mainly expressed on B-cells and binds to the ligand CXCL13. The expression of CXCR5 was measured by QPCR only, since this chemokine receptor and its ligand were not included on the TLDA plates. Here we showed that CXCR5 is significantly ($p < 0.05$) upregulated on PID 6, suggesting the possibility of B-cell infiltration into the CNS of terminally ill mice infected with WNV (Fig. 5.10).

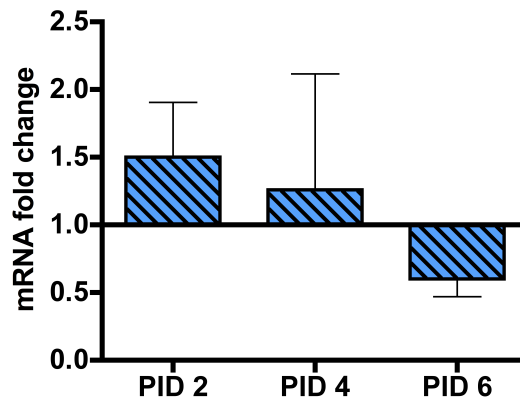


Figure 5.9 Expression of CX₃CL1 during WNV infection relative to an uninfected healthy mouse brain by TLDA

After infection of mice intranasally with WNV, RNA was isolated on post infection day (PID) 2, 4, and 6 from infected and control mice. The expression of CX₃CL1 was double normalized to an endogenous control 18S and to an uninfected healthy control brain. The relative quantification (RQ) values are depicted as mRNA fold changes and are shown on the y-axis. The RQ value of an uninfected control brain was set to 1. Data are presented as mean ± SD with n=3 mice per time point. (One-way ANOVA with Tukey's post test; results were not significant)

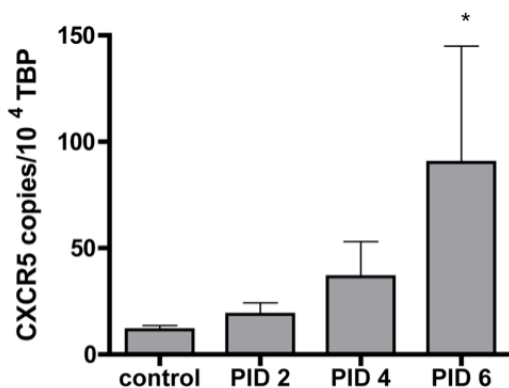


Figure 5.10 The expression of CXCR5 in WNV infected brains

Mice were infected intranasally with strain NY99. Absolute copy numbers in infected and control mouse brains were measured in control and WNV infected samples by QPCR at the time indicated on the x-axis. Data were normalized to 1×10^4 copies of TATA binding protein (TBP). Data are presented as mean ± SD with n=3 mice per time point. (Kruskal-Wallis test with Dunn's post test; * p<0.05)

5.5 Expression of cytokines and genes involved in innate immune responses to viral infection with WNV

After the characterisation of chemokine expression during WNV encephalitis, the expression of cytokines and PRRs, involved in innate immunity, was determined. On PID 2 cytokines were generally not, or minimally, upregulated. However IRF7 and RIG-I were 22-fold ± 6 SD and 132-fold ± 10 SD upregulated, respectively, compared to control brains (Fig. 5.11). These two PRRs were consistently increased during WNV infection. On PID 4 most cytokines and PRRs were more than 100-fold upregulated with the exception of TGF- β and IL-1 β (Fig. 5.11). IFN- α was the most upregulated cytokine during WNV infection, reaching a 1890-fold ± 532 SD increase on PID 4 and a 3730-fold ± 1298 SD upregulation by PID 6. On PID 6 the expression profile of PRRs and cytokines was similar to that on PID 4 but cytokine expression was several fold higher (Fig. 5.11). Most cytokines were more than 1000-fold increased compared to resting mouse brains with the exception, again, of TGF- β and IL-1 β . Thus, cytokines and PRRs, similar to chemokines, are selectively and highly upregulated in the CNS of WNV infected mice.

The result of IFN- β expression obtained by TLDA analysis was validated by QPCR. IFN- β was significantly ($p < 0.05$) and rapidly upregulated by PID 4 and PID 6. The fold increase compared to controls was calculated and amounted to a 270-fold and 350-fold upregulation by PID 4 and PID 6, respectively (Fig. 5.12 A). Unfortunately the expression of IFN- γ could not be evaluated by TLDA because the expression was too low in control samples and resulted in a RQ value of zero, which made subsequent comparisons impossible. To this end, the expression of IFN- γ was assessed by QPCR (Fig. 5.12 B). It was shown that IFN- γ levels were indeed very low in control brain samples, and the copy numbers of IFN- γ were significantly ($p < 0.05$) higher by PID 4 and PID 6. However, the maximal upregulation of IFN- γ expression was later, on PID 6, compared to maximal levels of IFN- β expression by PID 4. Fold changes between controls and infected samples were calculated. IFN- γ was 13-fold and 411-fold upregulated by PID 4 and PID 6, respectively.

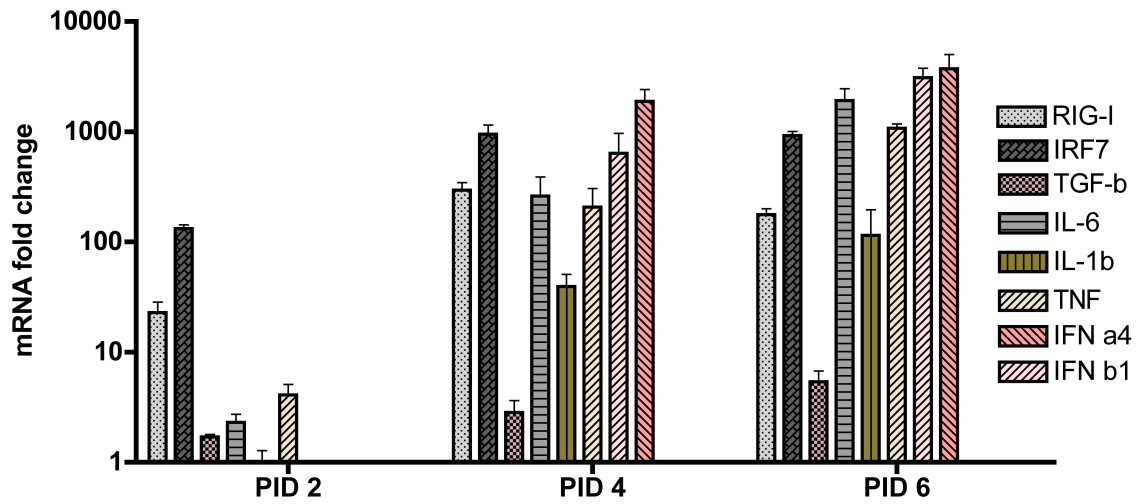


Figure 5.11 Expression of cytokines and genes involved in innate immune responses during WNV infection of the brain

Mice were infected i.n. with WNV strain NY99, and brains were collected for TLDA analysis on post infection day (PID) 2, 4, and 6 and from healthy control mice. Each gene was double normalized to an endogenous control 18S and to an uninfected healthy control brain. Changes in relative quantification (RQ) compared to controls are depicted as mRNA fold changes on the y-axis. The RQ value of an uninfected control brain equals 1. Each gene was tested in triplicate. Data are represented as mean \pm SD with n=3-4 mice per time point.

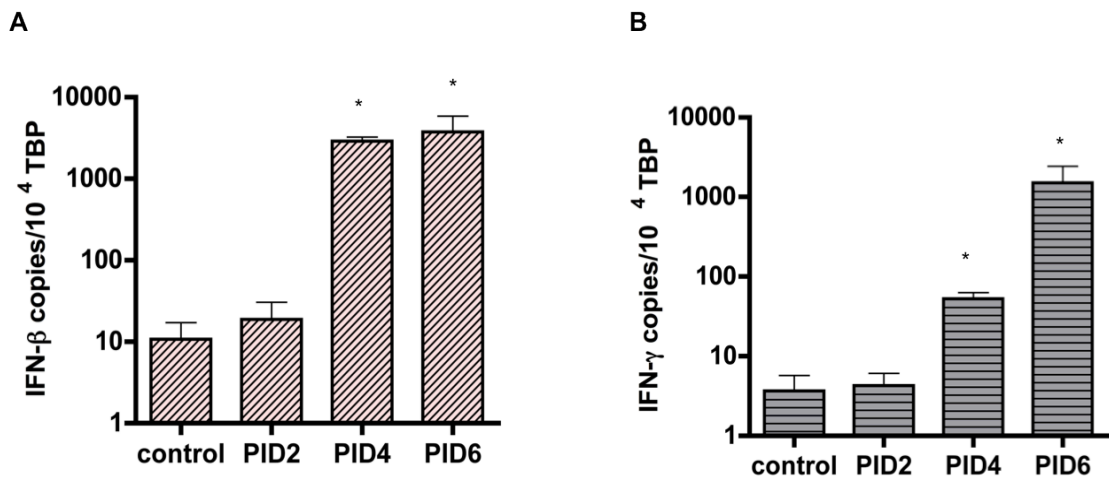


Figure 5.12 Expression of IFN- β and IFN- γ in WNV infected brains by QPCR

Mice were infected with WNV i.n. for 6 days, and brains were collected from infected and control mice. Absolute copy numbers were measured and normalized to the housekeeping gene TATA binding protein (TBP). Shown are the expression of (A) IFN- β and (B) IFN- γ . Data are presented as mean \pm SD with n=3-4 mice per time point. Each sample was tested in triplicate. (Kruskal-Wallis test with Dunn's post test; * p<0.05)

5.5.1 Expression of CD45

To evaluate the extent of leukocyte infiltration into the CNS on the mRNA level, the expression of the pan-leukocyte marker CD45 was assessed by TLDA and

QPCR. TLDA results demonstrated that CD45 is significantly upregulated by PID 4 ($p < 0.05$) and PID 6 ($p < 0.01$) compared to healthy control mouse brains (Fig. 5.13 A). Upregulation was highest on PID 6, with a 26-fold ± 5.4 SD increase compared to resting mouse brains. This result is in agreement with results obtained by QPCR (Fig. 5.13 B). CD45 was, again, significantly upregulated by PID 4 ($p < 0.05$) and PID 6 ($p < 0.01$). Absolute copy numbers of CD45 were generally low in control samples. Thus, these results suggest that a large number of leukocytes infiltrate the brain during WNV infection.

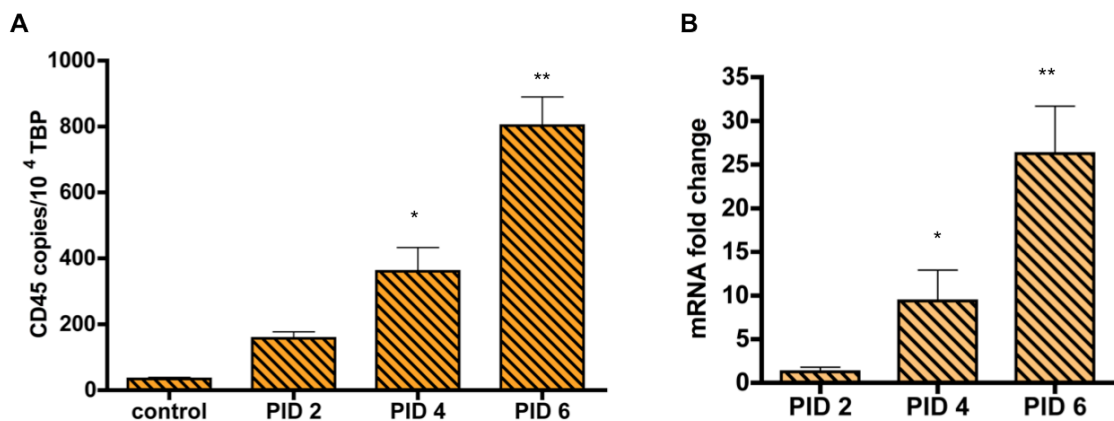


Figure 5.13 Absolute and relative expression of CD45 during WNV infection of the CNS

Mice were infected i.n. with WNV strain NY99, and brains were collected on post infection day (PID) 2, 4, and 6, and from healthy control mice. (A) Absolute copy numbers of CD45 per 1×10^4 TATA binding protein (TBP) were measured by QPCR. (B) mRNA fold changes of CD45 expression relative to the expression of an uninfected control brain were measured by TLDA. Data are presented as mean \pm SD with $n=3-4$ mice per time point. Each sample was tested in triplicate. (One-way ANOVA with Tukey's post test; * $p < 0.05$, ** $p < 0.01$)

5.6 Discussion and summary

Firstly, C57BL/6 mice were successfully infected with WNV. Similar to SFV infection, WNV infected mice developed a high viremia within 2 days of infection. Viremia remained elevated in WNV infected mice and was not cleared by PID 6. In support of this, mice infected with SFV strain L10 also had high viral titers in the blood which remained elevated throughout the course of infection while mice infected with strain A7(74) were able to clear the virus from the blood (Data shown in chapter 3). Viral titers in the brain during WNV were elevated by PID 4 and increased further by PID 6 when mice became terminally

ill. A similar result has also been observed during L10 infection where viral titers steadily rose until the death of the mice.

Klein *et al.* have reported that WNV predominantly infects neurons and spreads throughout the brain (153). Histological analysis confirmed these findings and revealed an increasing number of infected neurons throughout the brain over the course of infection. Additionally, perivascular cuffings in the infected brain became evident, indicative of leukocyte infiltration. Previous studies have shown that a large number of leukocytes enter the brain during WNV infection, and therefore these findings are in agreement with the results presented here (20, 355, 375).

One of the main aims of this study was to identify the form and magnitude of chemokine and cytokine expression during WNV infection, and to investigate whether chemokine expression was pathogen-specific. The data demonstrate that WNV infection results in a more rapid, broader based and higher-level, induction of chemokines and cytokines than avirulent SFV A7(74) infection, suggestive of a more aggressive CNS response to the virus comparable to that seen with SFV L10 infection. In brief, the following six chemokines have been identified as being highly upregulated during WNV infection: the CC-chemokines CCL2, CCL4, CCL5 and the CXC-chemokines CXCL2, CXCL9 and CXCL10. Within CC-chemokines CCL4 was the most upregulated chemokine followed by CCL5 and CCL2, and within CXC-chemokines induction of CXCL9 expression was highest followed by CXCL10 and CXCL2.

Previous studies have reported that CXCL9 and CXCL10 are the most strongly induced chemokines during other viral infections of the brain using LCMV or MHV as models of infection (154, 427). In support of this another study using WNV as a model of viral encephalitis has demonstrated that CXCL10 is one of the earliest upregulated chemokines during WNV infection of the brain. The main source of CXCL10 has been shown to be neurons, and expression of this chemokine seems to vary within different brain areas (153, 375). Data presented in this chapter confirm previous findings that CXCL10 is rapidly, and strongly, induced during WNV infection of the brain.

Of interest is that CXCL9 expression on PID 6 is higher than CXCL10 expression. However on PID 2 and PID 4 CXCL10 was the highest induced chemokine during WNV infection. It appears that once CXCL10 was upregulated by PID 4 the expression was not further increased by PID 6 whereas the expression of CXCL9 increased 20-fold between PID 4 and 6. This suggests the possibility that the cellular source and regulation of expression of CXCL9 and CXCL10 is different and dependent on distinct factors. In support of this, Klein *et al.* have shown that CXCL10 is produced earlier than CXCL9, and that levels of CXCL9 expression exceeds levels of CXCL10 later during infection with WNV (153). Studies of neuroinflammation have demonstrated that many neural cells are capable of producing CXCL10 whereas CXCL9 was shown to be predominantly expressed by microglia and mononuclear cells in the infected brain (400). Additionally some studies have demonstrated that CXCL10 expression is induced in response to type-I and type-II interferon whereas the expression of CXCL9 is induced by IFN- γ only (242, 428). In agreement with these studies the TLDA data presented here demonstrate that IFN- α is the strongest upregulated cytokine during WNV infection and transcript levels were already increased by PID 2 compared to resting mouse brains. Similar to this, IFN- β was also highly and rapidly upregulated by TLDA and QPCR. In contrast to this the QPCR results show that the expression of IFN- γ is not increased by PID 2 but is significantly upregulated by PID 4 and PID 6. From this it appears that type-I interferon expression is induced earlier than type-II interferon expression. Thus the differential expression of IFNs could explain the higher expression of CXCL9 at later time points compared to CXCL10.

Also of note is the strong upregulation of CCL4 expression during WNV infection of the brain. This result is in agreement with a previous study where CCL4, together with the other CCR5 ligands CCL3 and CCL5, was also highly upregulated during lethal WNV infection (358). Interestingly another study by Lim *et al.* has demonstrated that CCL4 is not induced by WNV infection (214). This discrepancy could be explained by the use of a different viral dose of WNV for the inoculation of mice. Lim *et al.* have used a low dose of 4×10^2 PFU of WNV whereas 2×10^4 and 1×10^5 PFU were used in this study and by Shirato *et al.*, respectively (214, 358).

The expression of the other CCR5 ligand CCL5 was also strongly induced during WNV infection. This is in agreement with previous studies, identifying CCL5 as one of the key chemokines upregulated in the CNS during WNV encephalitis (54, 197, 361). Consistent with WNV studies, CCL5 has also been shown to be strongly upregulated during other viral infections including SFV infection, as illustrated in chapter 3, as well as MHV or LCMV infection (319, 429).

The strong induction of CXCL1 and CXCL2 during lethal WNV infection is also striking. A similar result was found during SFV infection of the brain, as discussed in chapter 3. However during avirulent infection with SFV, CXCL1 and CXCL2 were not, or only minimally, upregulated relative to resting mouse brains. Thus, it is possible that the expression of CXCL1 and CXCL2 is associated with more severe disease outcomes. CXCL1 and CXCL2 are both ligands for CXCR2⁺ neutrophils. In support of my results Kim *et al.* have demonstrated that the attraction of neutrophils in response to CXCL1 and CXCL2 expression during LCMV infection leads to fatal meningoencephalitis (138). This is in contrast to another study by Hosking *et al.* who have shown that infiltration of neutrophils in response to CXCL1, CXCL2 and CXCL5 expression during MHV infection is beneficial and leads to enhanced survival, decreased viral titers in the brain and increased T-cell migration to the CNS (340). Thus, the role of CXCL1 and CXCL2 associated neutrophil attraction into the CNS during viral encephalitis is inconclusive and further studies are required to elucidate its role.

The expression of CCL2 during WNV infection was also strongly upregulated in the CNS. This result, again, is consistent with results obtained from SFV infected mouse brains using strains L10 and A7(74). In comparison to other chemokines, and their receptors, the role of the CCL2-CCR2 axis has been well described in many models of viral encephalitis. For example, in WNV infection of the CNS, CCL2 has been shown to play a pivotal role for the attraction of CCR2⁺ monocytes into the CNS (106, 214, 401). Additionally Chen *et al.* have shown that the CCL2-CCR2 axis is important for trafficking of leukocytes into the brain during MHV infection for viral clearance and enhanced survival of the host (334). However, the role of CCR2 in mediating monocyte entry into the CNS is contentious, since it is hard to evaluate the role of CCR2 in CCR2^{-/-} mice due to their monocytopenia. Therefore in chapter 6 pharmacological blockers of CCR2

are used to investigate in more detail the role of CCR2 in monocyte trafficking into the CNS.

In conclusion, the chemokine expression during WNV infection was very similar to that during SFV infection using the lethal strain L10. Chemokines were strongly upregulated compared to controls. Cytokines and PRRs were also strongly induced in WNV infection similar to that seen in L10 infection. The chemokine expression pattern during WNV differs from that seen during avirulent SFV infection in several ways. Firstly, chemokines were more rapidly and more highly increased during WNV infection. Secondly, chemokine expression was generally broader based. For example CXCL1, CXCL2 and CXCL3 were not, or only minimally, expressed during A7(74) infection. Avirulent infection of the CNS induces a highly selective, and lower level induction of chemokines compared to virulent infection of the CNS using two different viruses, SFV L10 and WNV NY99.

In the next chapter the role of key chemokines, identified through studies using SFV and WNV, shall be investigated in more detail in regard to leukocyte infiltration and pathogenesis.

Chapter 6

Pharmacological intervention using chemokine antagonists during SFV infection

6.1 Introduction and aims

Chemokine mediated influx of leukocytes into the CNS can act to clear infections but can also be responsible for deleterious bystander neuronal damage associated with morbidity and, in some cases, increased mortality. The outcome of disease depends not only on the virus strain used but also on a range of host factors, including immune status and age.

In the previous chapters 3 and 5 a thorough chemokine expression analysis in the brain was performed, and I was able to identify key chemokines upregulated during SFV and WNV infection. These key chemokines are ligands for CCR2, CCR5 and CXCR3. The role of these chemokine receptors during viral encephalitis has yet to be fully elucidated because it is not clear whether these receptors are beneficial or detrimental to disease outcome. A previous study has demonstrated that CCR2 is pivotal for the recruitment of monocytes to the brain where they play pathogenic roles during viral infection (106). This is in contrast to another study where CCR2⁺ monocytes were depleted which resulted in enhanced mortality, suggesting a protective role of CCR2⁺ monocytes during viral encephalitis (346).

Similar contradictory results were obtained using CXCR3^{-/-} mice. One study has reported that WNV or LCMV infected CXCR3^{-/-} mice display enhanced CNS viral titers and mortality, and reduced CD8⁺ T-cell recruitment to the CNS which is associated with reduced viral clearance (375, 430). Another study by Hofer *et al.* has demonstrated that CXCR3^{-/-} mice, infected with LCMV, display unaltered neurological disease and mortality, suggesting that CXCR3 is not pathogenic (431). Likewise a putative role for CCR5 has also been suggested in the context of immune responses to WNV infection, although CCR5 is dispensable for responses to LCMV (173, 319, 336). Firm conclusions on the chemotactic basis by which leukocytes enter the CNS is difficult using gene deficient mice, in which deficiency in a particular chemokine receptor may exert its influence at multiple stages including developmental and homeostatic stage, and generation of primary immune responses, in addition to the process by which leukocytes enter the CNS.

In an attempt to understand the role of the chemokine receptors CCR2, CCR5 and CXCR3 during viral encephalitis, SFV was used as a model of infection. *The main aim in this chapter was to evaluate the hierarchy and relative importance of distinct chemokine receptors for CNS leukocyte influx and pathogenesis.* This is the first time that a panel of chemokine receptor antagonists has been used in the context of viral encephalitis.

To block CCR2, the chemokine receptor blocker RS504393 was used, which binds selectively to CCR2 with high affinity (218, 432). For the blockade of CCR5, two blockers, Maraviroc and DAPTA were used as both blockers have been shown to be highly efficient in blocking CCR5 during HIV infection (198, 223). Lastly, CXCR3 was blocked using the imidazo-pyrazine derivative, referred to as compound 21, which was kindly provided by Amgen. This blocker has been shown to be highly efficient in blocking CXCR3 in a mouse model of lung inflammation (232). All antagonists are discussed in depth in section 1.3.5 of the introduction.

6.2 Characterisation of the role of CCR2 during viral encephalitis

To investigate the role of CCR2 during SFV encephalitis the chemokine blocker RS504393 was used at a concentration of 5mg/kg in 6.6% DMSO in PBS twice a day. This dose was selected based on studies by Yang and Kitagawa *et al.* (218, 432). Control mice were treated with vehicle control. This blocker has previously been shown to be efficient in blocking CCR2 recruitment to sites of inflammation in models of LPS induced lung inflammation and progressive kidney fibrosis.

Before treatment, mice were first infected with SFV strain A7(74) unless stated otherwise. The drug, or vehicle control, was administered to infected mice by oral gavage twice daily between post infection days 3-7, to prevent interfering with monocyte numbers in the blood during the first phase of infection when virus disseminates throughout the body.

6.2.1 Identification of monocytes in the blood during early stages of SFV infection

For West Nile virus infection it has been reported that monocytes are highly elevated in the blood during the first 5 days of infection (214). This monocytosis

is pivotal for the infiltration of monocytes into the virally infected CNS. To investigate whether monocytosis also occurs during SFV infection, blood was collected from SFV infected mice between 24 hours to 7 days post infection, and analysed by flow cytometry. After inoculation of mice with SFV strain A7(74), titers rose quickly to high levels within 24 hours post infection. Viremia was almost completely cleared from the blood by PID 7, when viral transcript levels for E1 or nsp3 were very low (Fig. 6.1 A and B).

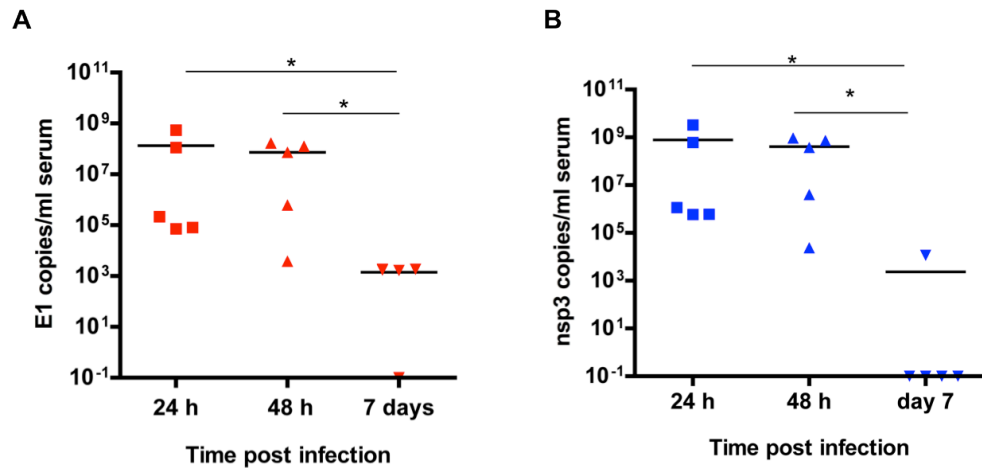


Figure 6.1 Viral titers in the serum of SFV A7(74) infected mice

Mice were inoculated i.p. with SFV strain A7(74) and serum was collected from infected mice at the time points indicated. Viral titers were measured by QPCR. (A) Copy numbers of viral genes E1 and (B) nsp3 were quantified in the serum of infected mice. n=5 mice per time point; (Kruskal-Wallis test with Dunn's post test; * p<0.05)

After analysis of viral titers in the blood of SFV infected mice, the proportion of myeloid cells in the blood was determined next. Overall, the percentage of CD11b⁺ cells was significantly elevated (p<0.05) 48 hours post infection compared to healthy controls (Fig. 6.2 A). Furthermore the level of CD11b⁺ cells in the blood significantly decreased again by PID 7 when levels of myeloid cells were similar to controls. The proportion of CD11b⁺Ly6C^{hi}CCR2⁺ cells, identified as 'inflammatory' monocytes, was already significantly (p<0.05) increased by 24 hours post infection, and returned to basal levels by PID 7 (Fig. 6.2 B and C).

Antibody staining for Ly6C and Ly6G revealed that the proportion of Ly6C⁻ and Ly6C^{hi} and Ly6C^{int} cells within the CD11b⁺ compartment increased 24 hours post infection and often reached maximal levels 48 hours post infection (Fig. 6.2 D-

G). The increase of Ly6C⁻ cells and Ly6C^{hi} cells was significant ($p < 0.05$) by 48 and 24 hours post infection, respectively, whereas the increase in Ly6C^{int} cells was not statistically significant by 24 and 48 hours post infection (Fig. 6.2 E-G). Lastly, the proportion of CD11b⁺Ly6G⁺ cells, identified as neutrophils, was not significantly changed in the blood over the time course of infection (Fig. 6.2 H). Thus, the proportions of monocytes are also elevated during SFV infection but the increase is less profound compared to WNV infection where monocyte numbers in the blood are approximately 3.5 fold higher during WNV infection compared to healthy control mice (214).

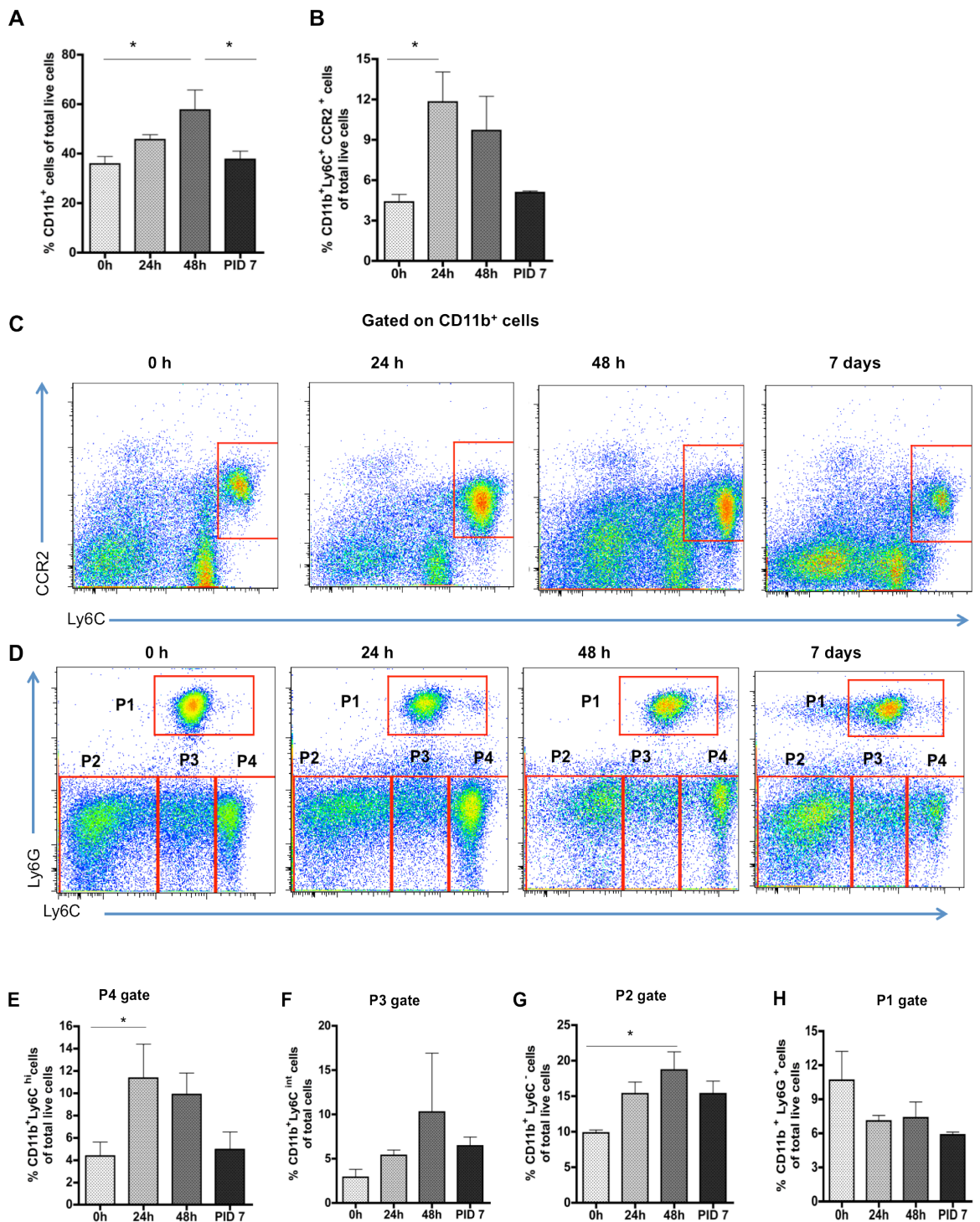


Figure 6.2 Identification of myeloid cells subsets in the blood during SFV infection

Mice were infected with SFV strain A7(74) and blood was collected at the indicated time points (PID=post infection day). The proportions of myeloid cell subsets were determined by flow cytometry. (A) Proportions of CD11b⁺ cells and (B) CD11b⁺Ly6C^{hi}CCR2⁺ monocytes within isolated leukocytes in the blood. (C) Representative dot plots of CD11b⁺Ly6C^{hi}CCR2⁺ monocytes in the blood over the time course of infection, gated on CD11b⁺ cells. (D) Representative dot plots of Ly6C and Ly6G expression by CD11b⁺ cells, revealing a distinct leukocyte population within each gate P1-P4. Proportions of (E) CD11b⁺Ly6C^{hi} monocytes within the P4 gate, (F) CD11b⁺Ly6C^{int} monocytes within the P3 gate, (G) CD11b⁺Ly6C⁻ cells within the P4 gate and (H) neutrophils (CD11b⁺Ly6G⁺) within the P1 gate amongst total live cells in the blood. Data are represented as mean \pm SD with n=5 mice per time point. (One-way ANOVA with Tukey's post test; * p<0.05)

6.2.2 Inhibition of CCR2 leads to the reduction of leukocyte accumulation in the CNS during SFV A7(74) infection

After infection of mice with SFV A7(74), and treatment of mice with vehicle or CCR2 blocker, the number of CD45^{hi} cells was determined by flow cytometry. The data demonstrate that the extent of leukocyte infiltration into the brain of WT infected mice treated with CCR2 blocker was significantly reduced ($p < 0.001$) (Fig. 6.3 A and B). Compared to untreated controls the proportion of CD45^{hi} cells in the CNS of treated mice was up to 54% reduced. To further confirm the roles of CCR2 in leukocyte accumulation in the infected CNS, I also used CCR2^{-/-} mice in this experiment in which leukocyte infiltration was significantly ($p < 0.001$) reduced (approximately 76%) to a level similar to that observed in mice treated with RS504393.

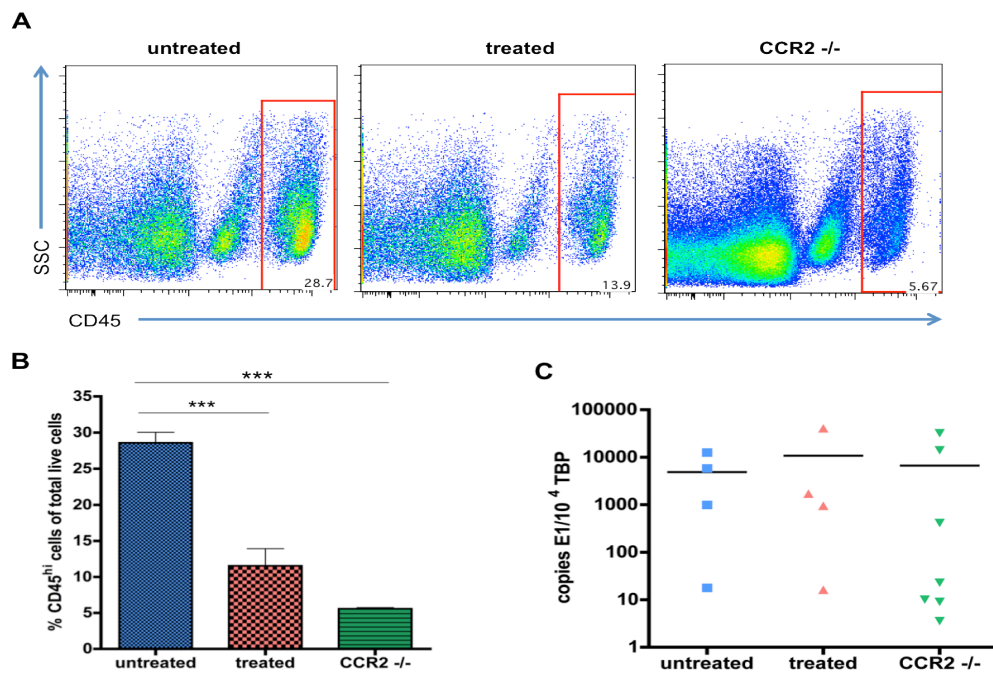


Figure 6.3 Reduction of leukocyte infiltration into the CNS during SFV infection in CCR2 deficient mice or mice treated with CCR2 blocker

Wild type and CCR2 deficient mice were infected with SFV strain A7(74) for 7 days and brains were collected for analysis. The number of CD45^{hi} leukocytes in each group was determined by flow cytometry. Mice were treated twice daily by oral gavage with vehicle (6.6% DMSO in PBS) (untreated and CCR2^{-/-} group) or 5 mg/kg RS504393 (CCR2 blocker) (treated group) between post infection days 3-7. $n = 4-7$ pooled mouse brains per group from 1-3 individual experiments. Analysis in CCR2^{-/-} mice was only performed once. (A) Representative dot plots of CD45 expression on isolated brain cells in untreated, treated and CCR2^{-/-} mice on post infection day 7. Cells were gated on CD45^{hi} cells. (B) Proportion of CD45^{hi} cells within total live brain cells. (C) Expression of the viral protein E1 in each group was measured and normalized to 1×10^4 copies of TATA-binding protein (TBP). Data are presented as mean \pm SD (One-way ANOVA with Tukey's post test; *** $p < 0.001$)

To determine if the reduction of leukocyte infiltration has an effect on viral titers in the CNS, the expression of the viral protein E1 was measured by QPCR. The results show that viral titers were not significantly changed in CCR2 blocker treated or CCR2^{-/-} mice compared to that in untreated wildtype control brains (Fig. 6.3 C).

Next the leukocyte subsets entering the brain of CCR2 treated mice during viral encephalitis were investigated in more detail to determine which leukocyte population is specifically affected by the blockade of CCR2. As mentioned in the general discussion CCR2 is predominantly expressed on monocytes but can also be found on few activated NK-cells and T-cells, although this point of view is contentious (25, 211, 212). I have therefore selected markers for monocytes such as CD11b and Ly6C, and also for T-cells and NK-cells such as CD3 and NK1.1, respectively, for subsequent flow cytometry analysis. All three leukocyte subsets have been found to infiltrate the brain during SFV infection as demonstrated in chapter 4.

6.2.2.1 T-cells and NK-cells entering the CNS during CCR2 blockade of SFV infected mice

Despite a 5.1-fold reduction of CD45^{hi} leukocytes in CCR2 deficient mouse brains, the proportion of CD3⁺ T-cells was significantly ($p < 0.01$) higher compared with proportions in brains of untreated and CCR2 blocker treated wild type mice (Fig. 6.4 A and B). This discrepancy can probably be explained by the lack of monocytic cells entering the brain in CCR2^{-/-} mice, resulting in high proportions of T-cells within the CD45^{hi} compartment. Indeed, after determining the number of CD3⁺ T-cells per 10⁵ brain cells it was demonstrated that the number of T-cells entering the brain in CCR2^{-/-} mice was significantly ($p < 0.05$) lower compared with untreated wild type mouse brains (Fig. 6.4 B). The proportion of CD3⁺ T-cells in CCR2 blocker treated mice was comparable to that of untreated mice, but the number of CD3⁺ T-cells was significantly ($p < 0.05$) reduced in treated mice. Thus, the genetic or pharmacological blockage of CCR2 results in a significant reduction of T-cell numbers within the CNS. Within the CD3⁺ cell fraction the proportion of CD4⁺ cells was significantly lower ($p < 0.05$) in control mice compared with CCR2^{-/-} mice but the percentage of CD4⁺ T-cells was highest in treated mice. The proportion of CD8⁺ cells was significantly higher in control

mice compared to CCR2 deficient mice and also higher in CCR2 blocker treated mice, but this result was not statistically significant (Fig. 6.4 C).

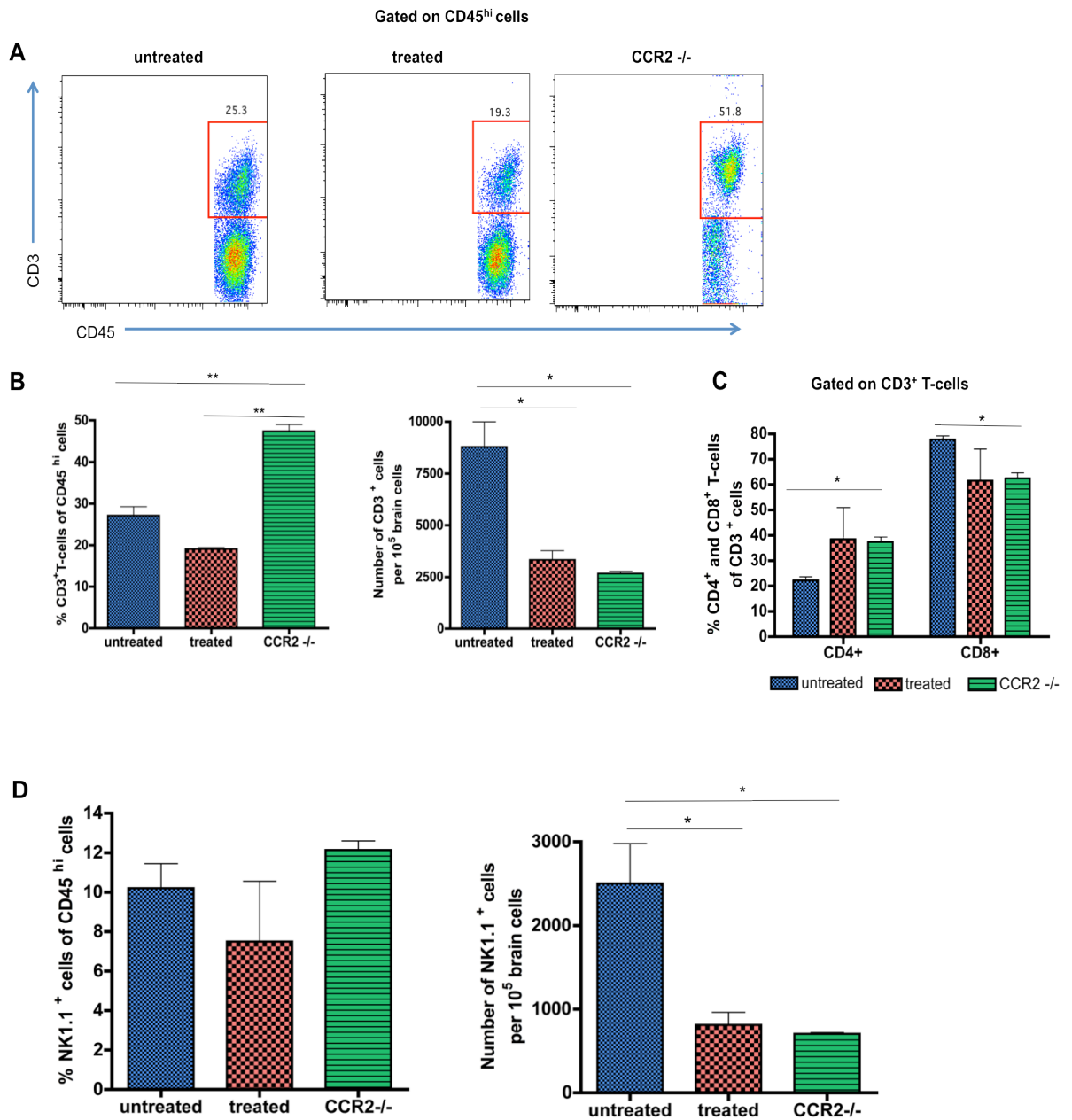


Figure 6.4 Reduction of CD3⁺ T-cells and NK-cells within the brains of SFV infected mice in CCR2 deficient or CCR2 blocker treated mice

Wild type and CCR2^{-/-} mice were infected with SFV strain A7(74) for 7 days and brains were collected for analysis. The number of CD3⁺ T-cells and NK1.1⁺ cells was assessed by flow cytometry. Mice were treated twice daily by oral gavage with vehicle (6.6% DMSO in PBS) (untreated and CCR2^{-/-} group) or 5 mg/kg RS504393 (CCR2 blocker) (treated group) between post infection days 3-7. n = 4-7 pooled mouse brains per group from 1-3 individual experiments. (A) Representative dot plots of CD3 expression on CD45^{hi} cells in the brain in untreated, treated and CCR2 deficient mice on post infection day 7. (B) Proportions and numbers of CD3⁺ T-cells in the brain within each group. (C) Proportion of CD4⁺ and CD8⁺ T-cells within the CD3⁺ cell population (D) Proportions and numbers of NK1.1⁺ cells in the CNS within each group. All cells were gated on CD45^{hi} cells. Data are presented as mean ± SD ((B and D) One-way ANOVA with Tukey's post test and (C) Two-way ANOVA with Bonferroni's post test; * p<0.05, ** p<0.01)

The proportion of NK-cells was not significantly different between untreated and CCR2 blocker treated wild type mice or CCR2 deficient mice (Fig. 6.4 D). However the number of NK-cells per 10^5 brain cells was significantly reduced in CCR2 blocker treated mice and CCR2 deficient mice (both $p < 0.05$) compared with untreated wild type counterparts.

6.2.2.2 Myeloid cells

Having analysed the effect of CCR2 blockage on T-cell and NK-cell entry into the CNS, the number of CD11b⁺ cells in the brain of untreated, treated and CCR2^{-/-} mice was determined. During SFV infection many monocytes/macrophages enter the CNS, and since CCR2 is highly expressed on these cells it was hypothesised that the number of monocytes and macrophages would be decreased. The number of CD11b⁺ cells per 10^5 isolated brain cells was significantly (both $p < 0.01$) reduced in treated and CCR2^{-/-} mice. However in CCR2^{-/-} mice also the percentage of CD11b⁺ cells was significantly reduced (both $p < 0.01$) compared with untreated mice (Fig. 6.5 A and B). Within CD11b⁺ leukocytes the proportion and number of Ly6C^{hi} cells was significantly reduced in CCR2 blocker treated and CCR2 deficient mice (both $p < 0.001$) (Fig. 6.5 C). However the proportion of Ly6C⁻ cells within the myeloid cell compartment was significantly increased ($p < 0.001$) in CCR2 blocker treated mice. These cells are probably macrophages based on their SSC and FSC properties. Contrary to this, the proportion of Ly6C⁻ cells within CCR2^{-/-} mice was significantly ($p < 0.01$) decreased compared to untreated control mice (Fig. 6.5 D). Numbers of Ly6C⁻ cells revealed similar results and show a significant reduction of Ly6C⁻ cells in CCR2^{-/-} mice compared to untreated and treated mice.

The numbers of CD11b⁺Ly6C^{hi}CCR2⁺ cells per 10^5 brain cells, previously described as 'inflammatory monocytes', were significantly reduced in CCR2 blocker treated and CCR2 deficient mice (both $p < 0.001$) compared with untreated control mice (Fig. 6.6 A and B) (106). The proportion of CD11b⁺CCR2⁺ cells was almost completely reduced in CCR2 blocker treated mice, similar to the defect seen in CCR2 deficient mice, and resulted in a significant reduction of monocytic cells within the infected brain (both $p < 0.05$). Thus, the pharmacological blockage of CCR2 with RS504393 results in the selective reduction of CCR2⁺ cells

within CD11b⁺ cells in the CNS of SFV infected mice, confirming the efficacy of this drug in blocking CCR2.

6.2.2.3 *Effect of CCR2 blocker on blood monocytes during SFV infection*

In a previous study using WNV it was reported that CCR2 plays an important role in the egress of monocytes from the bone marrow and return of monocytes from the blood to the bone marrow (214). To test the role of CCR2 in trafficking of monocytes to the CNS and to investigate if the observed reduction of monocyte numbers in the brain was due to monocytopenia, blood was taken from mice treated with RS504393 or vehicle control. The proportions of CD11b⁺ cells and CD11b⁺Ly6C^{hi}CCR2⁺ cells, also described as ‘inflammatory monocytes’, were not significantly different after treatment with CCR2 blocker suggesting that the CCR2 blocker had no effect on the number of circulating monocytes within the blood. However, 24 hours after treatment, the proportion of monocytes was slightly higher compared with untreated counterparts (Fig. 6.7 A -C). This increase was not statistically significant. Furthermore within CD11b⁺ cells the proportions of Ly6C^{hi} and Ly6C^{int} monocytes (P4 and P3 gate), Ly6C⁻ cells (P2 gate) and CD11b⁺Ly6G⁺ neutrophils (P1 gate) were not significantly different in mice treated with the CCR2 blocker compared with proportions in untreated mice (Fig. 6.7 D-H).

Thus CCR2 plays a critical role in the accumulation of monocytes/macrophages and T-cells in the CNS during viral encephalitis with no significant effect on viral titers in the CNS.

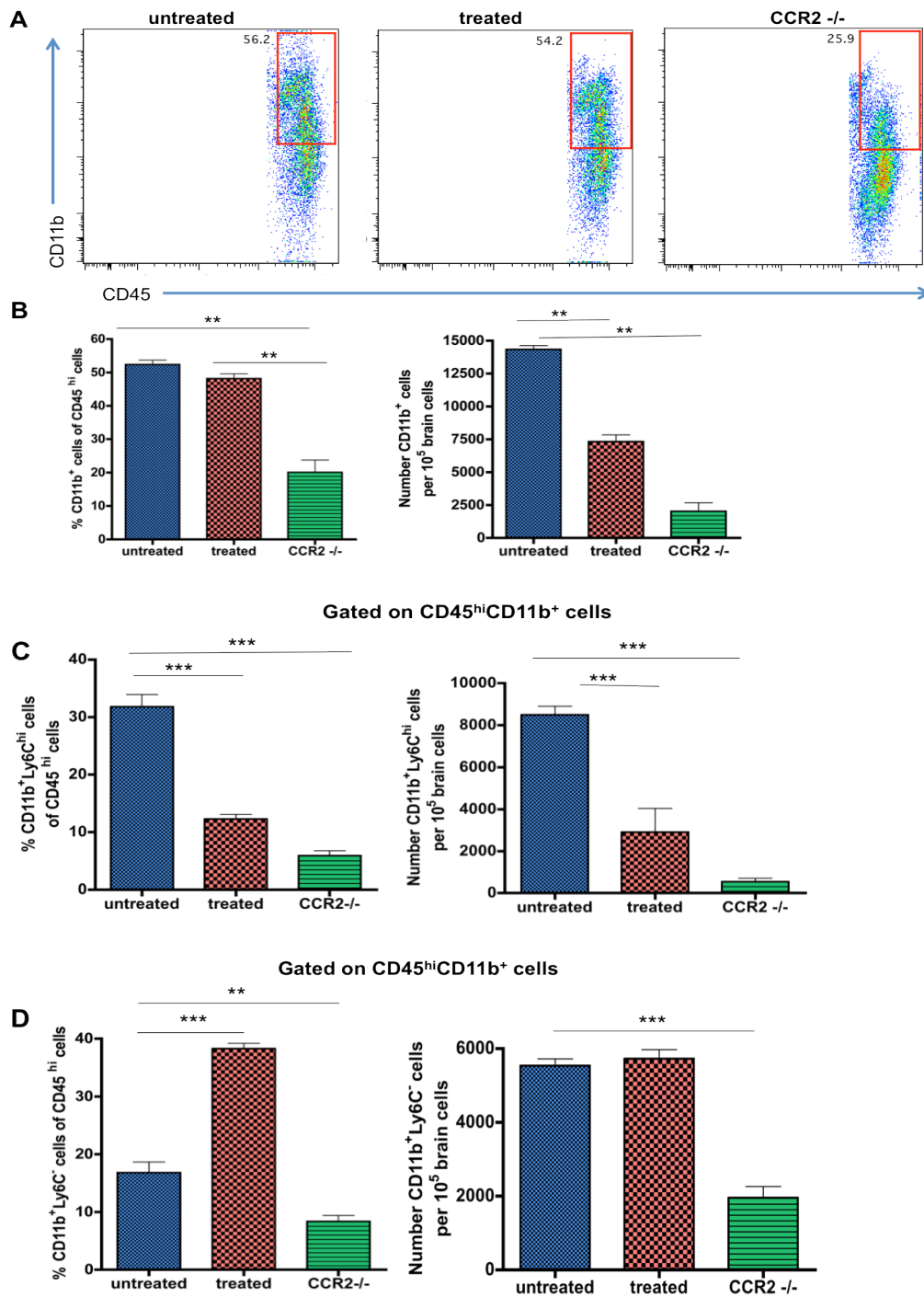


Figure 6.5 Identification of myeloid cells in the CNS during SFV infection of CCR2 deficient mice and mice treated with CCR2 blocker

Wild type and CCR2 deficient mice were infected with SFV strain A7(74) for 7 days and brains were collected for analysis. The number of CD11b⁺ cells and myelomonocytic cells was determined by flow cytometry. Mice were treated twice daily by oral gavage with vehicle (6.6% DMSO in PBS) (untreated and CCR2^{-/-} group) or 5 mg/kg R5504393 (CCR2 blocker) (treated group) between post infection days 3-7. n = 4-7 pooled mouse brains per group from 1-3 individual experiments. (A) Representative dot plot of CD11b expression on CD45^{hi} cells within the brain of untreated, treated and CCR2^{-/-} mice. (B) Proportions and numbers of CD11b⁺ cells gated on CD45^{hi} cells. (C) Proportions and numbers of CD11b⁺Ly6C⁺ and (D) CD11b⁺Ly6C⁻ cells within CD45^{hi} cells. Data are presented as mean \pm SD (One-way ANOVA with Tukey's post test; ** p<0.01, *** p<0.001)

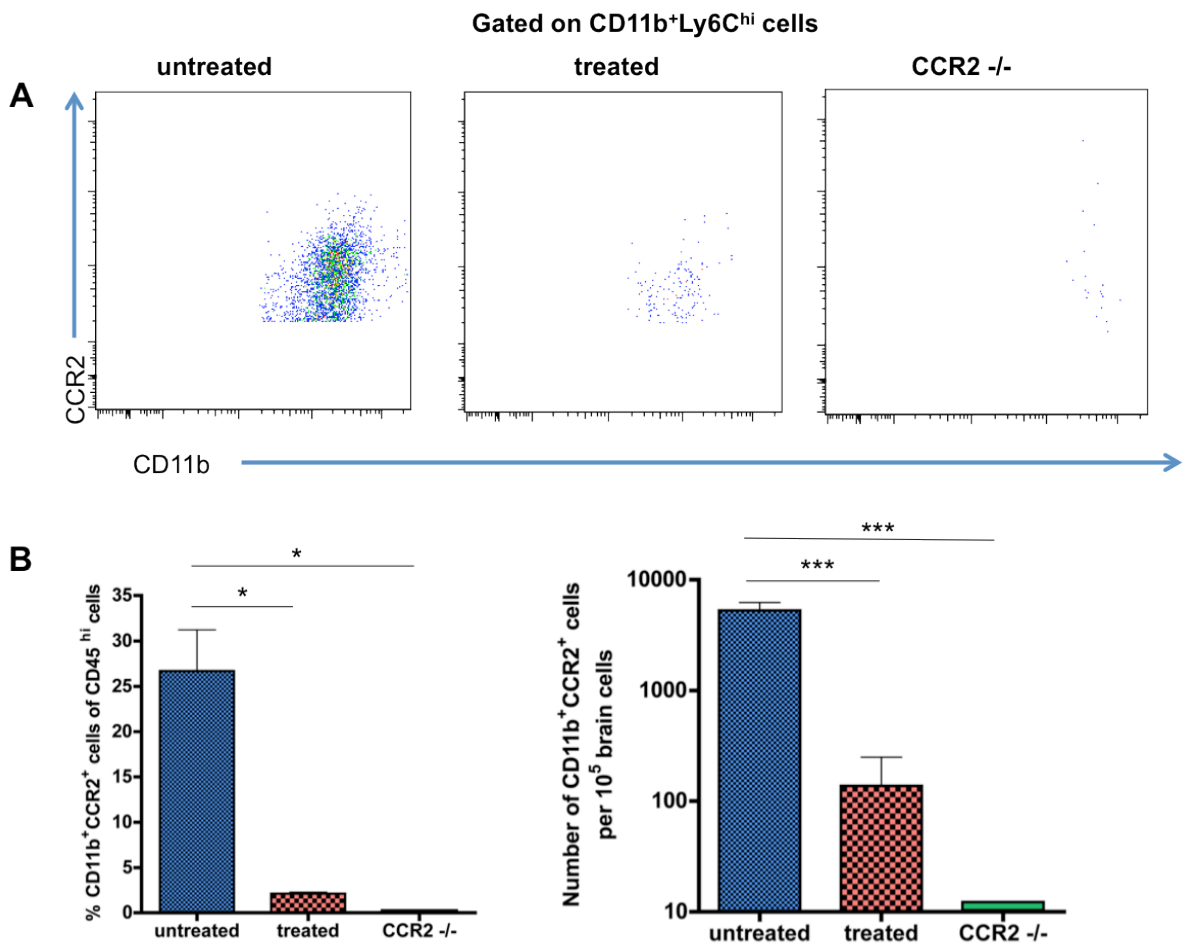


Figure 6.6 Expression of CCR2 on CD45^{hi} cells in the brain of SFV infected mice in CCR2 deficient and CCR2 blocker treated mice

Wild type and CCR2 deficient mice were infected with SFV strain A7(74) for 7 days and brains were collected for analysis. The number of CD11b⁺CCR2⁺ cells was determined by flow cytometry. Mice were treated twice daily by oral gavage with vehicle (6.6% DMSO in PBS) (untreated and CCR2^{-/-} group) or 5 mg/kg RS504393 (CCR2 blocker) (treated group) between post infection days 3-7. n= 4-7 pooled mouse brains per group from 1-3 individual experiments. (A) Representative dot plot of CCR2 expression on CD11b⁺ cells, gated on CD45^{hi} cells, in the brains of untreated, treated and CCR2^{-/-} mice. (B) Proportions and numbers of CD11b⁺CCR2⁺ cells within leukocytes. Data are represented as mean \pm SD (One-way ANOVA with Tukey's post test; * p<0.05, *** p<0.001)

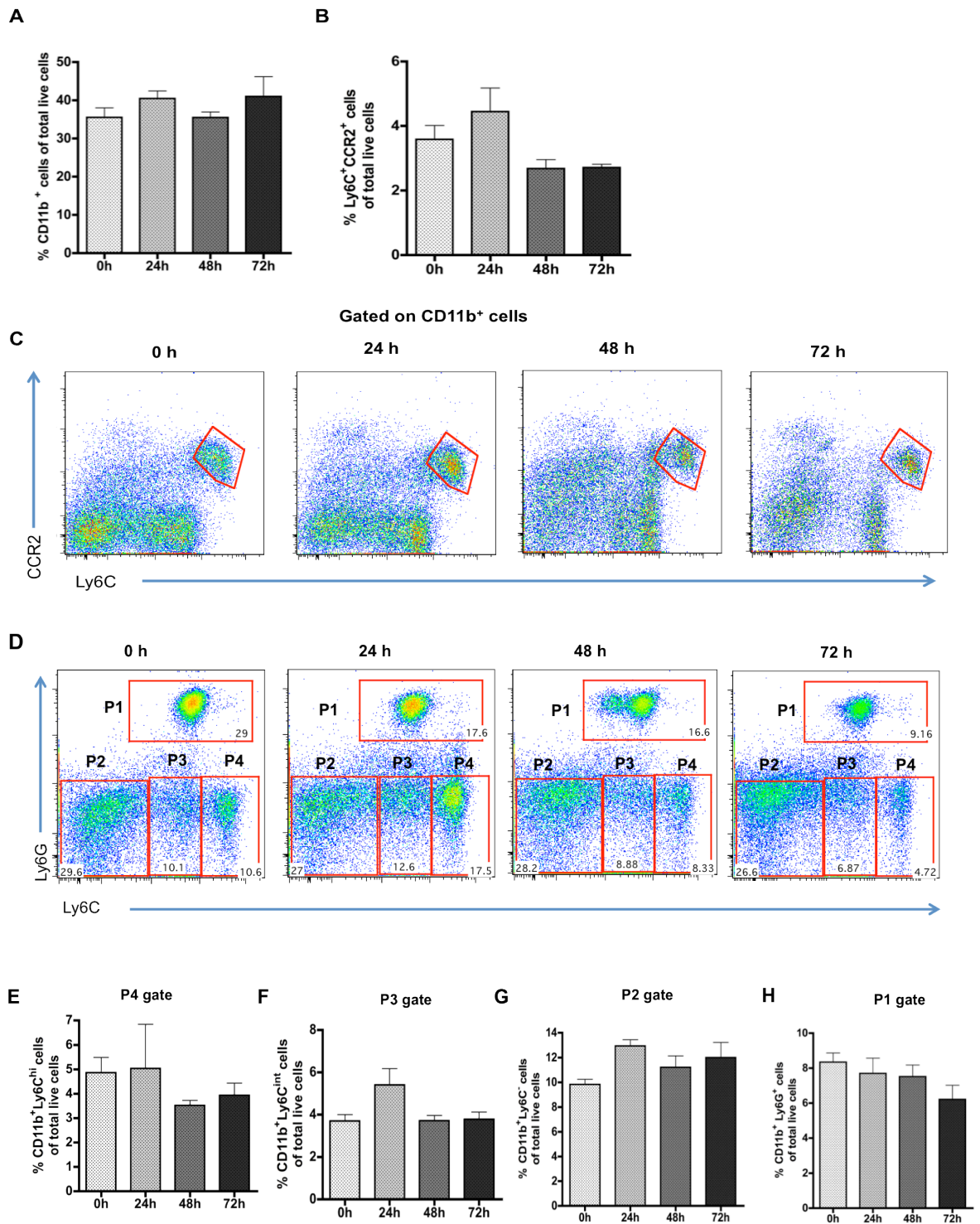


Figure 6.7 Identification of myeloid subsets in the blood of mice treated with the CCR2 blocker RS504393

Wild type mice were treated twice daily by oral gavage with 5 mg/kg RS504393 (CCR2 blocker) and blood was collected at various time points as indicated. The number of myeloid subsets in the blood was determined by flow cytometry. Data are presented as mean \pm SD with $n=5$ mice per time point. (A) Proportion of CD11b⁺ and (B) CD11b⁺Ly6C⁺CCR2⁺ cells within total live cells in the blood. (C) Representative dot plot of CCR2 and (D) Ly6C and Ly6G expression gated on CD11b⁺ leukocytes. Four distinct leukocyte populations were identified and numbered P1-P4. (E) Proportion of CD11b⁺Ly6C^{hi} (monocytes) within the P4 gate, (F) CD11b⁺Ly6C^{int} cells within the P3 gate, (G) CD11b⁺Ly6C⁻ cells within the P2 gate and (H) CD11b⁺Ly6G⁺ cells (neutrophils) within the P1 gate in the blood. (One-way ANOVA with Dunnett's post test; all data not significant)

6.2.3 Chemokine expression levels in the CNS of mice with genetic or pharmacological blockage of CCR2

A previous WNV study has proposed the idea that in $CCR5^{-/-}$ mice the reduction in leukocyte numbers in the brain might lead to different chemokine and cytokine expression patterns that recruit other leukocyte subsets (173). To test whether chemokine expression levels and in particular CCL2, a selective ligand for CCR2, were also elevated during SFV infection after treatment with CCR2 blocker, brain samples were analysed by TLDA or QPCR.

The absolute copy numbers of CCL2 transcripts were significantly ($p < 0.05$) increased in CCR2 blocker treated mice compared with untreated and $CCR2^{-/-}$ mice (Fig. 6.8). Additionally the number of CCL2 transcripts was not increased in $CCR2^{-/-}$ mice compared with untreated mice.

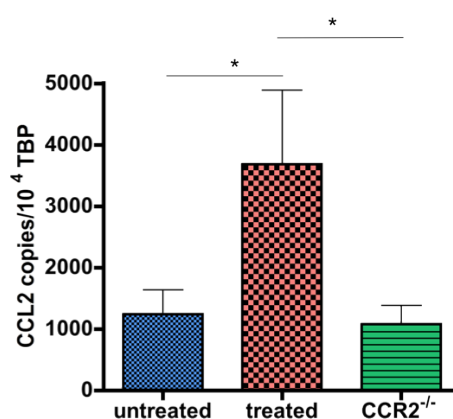


Figure 6.8 Expression of CCL2 in the CNS of CCR2 deficient mice or mice treated with the CCR2 blocker

Wild type and CCR2 deficient mice were infected with SFV strain A7(74) for 7 days and brains were collected for analysis. Mice were treated twice daily by oral gavage with vehicle (6.6% DMSO in PBS) (untreated and $CCR2^{-/-}$ group) or 5 mg/kg RS504393 (CCR2 blocker) (treated group) between post infection days 3-7. The absolute copy numbers of CCL2 was determined by QPCR and data was normalized to 1×10^4 copies of TATA-binding protein (TBP). Data are presented as mean \pm SD with $n=4-7$ mice per group. (One-way ANOVA with Tukey's post test; * $p < 0.05$)

A thorough analysis of chemokine and cytokine expression by TLDA in SFV infected and untreated, treated and CCR2 deficient mice revealed that generally most chemokines were not significantly different in treated versus untreated, and $CCR2^{-/-}$ mice versus treated mice. (Appendix 4A, B, D and E). Exceptions were the expression levels of CCL2, CCL20 and CCL28. The QPCR results for the expression levels of CCL2 were confirmed by results obtained by TLDA analysis

showing significant higher expression levels of CCL2 in CCR2 blocker treated mice compared to untreated mice or CCR2^{-/-} mice (Appendix 4). The expression level of CCL20 was significantly higher in CCR2^{-/-} mice compared to CCR2 blocker treated mice (Appendix 4). The expression of CCL28 was significantly higher expressed in CCR2 blocker treated mice compared to untreated controls.

Despite the minimal and not significant difference of most other chemokines expressed in untreated, treated and CCR2 deficient mice, in almost all cases the levels of chemokines were slightly higher in CCR2 blocker or CCR2 deficient mice. The expression levels of cytokines was, again, not significantly different between untreated, treated and CCR2^{-/-} mice (Appendix 4 C and F). Thus, these data suggest that the blockade or the deficiency of CCR2 does not result in profound alterations of the chemokine and cytokine expression profiles in the brain of SFV infected mice. Other factors seem to be involved in the control of chemokine and cytokine expression during SFV encephalitis.

6.2.4 The role of CCR2 for the pathogenesis of virulent infection of the brain with SFV strain L10

Lim *et al.* have reported that CCR2 is critical for survival during WNV infection of the brain. To examine whether CCR2 is also important for the pathogenesis of lethal SFV infection, mice were inoculated with SFV strain L10 and survival was analysed. The results demonstrate that the survival in wild type untreated mice was 50% compared with 20% in CCR2 deficient mice (Fig. 6.9). Furthermore CCR2 deficient mice died earlier compared with wild type mice but this difference was not statistically significant (Logrank test). Thus, these data suggest that CCR2 might also play a role during L10 infection. However this experiment was only performed once and this result needs to be confirmed with repeat experiments. Due to time constraints the effect of CCR2 blocker RS504393 on the survival of L10 infected mice could not be pursued further and is part of future experiments.

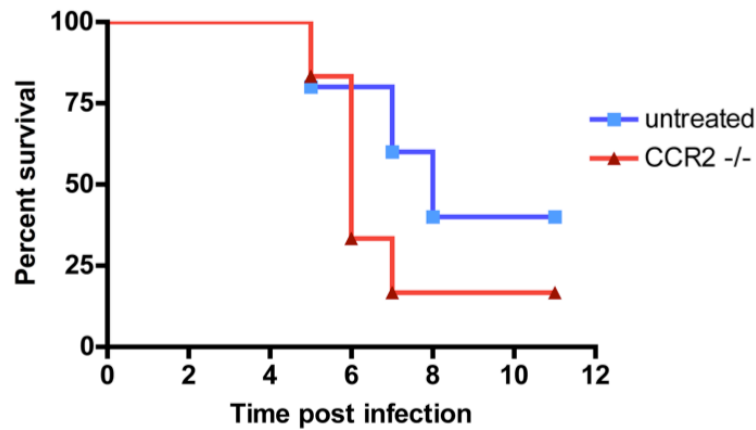


Figure 6.9 Survival of CCR2 deficient mice infected with the virulent SFV strain L10

Wild type and CCR2 deficient mice were infected i.p. with SFV strain L10 for 12 days. The survival of CCR2 deficient and wild type mice was assessed. Mice were euthanized once they became terminally ill. n=10 mice per group. (Logrank (Mantel-Cox test; not significant)

6.3 Characterisation of the role of CCR5 during viral encephalitis

CCR5 has been reported to be important for the migration of monocytes, macrophages, T-cells and NK-cells. Since CCR5 ligands were expressed in the SFV infected brain, I next examined the role of CCR5 in leukocyte accumulation during SFV-dependent encephalitis using CCR5 blockers Maraviroc and DAPTA. As discussed in detail in section 1.3.6 Maraviroc is an allosteric CCR5 inhibitor approved by the FDA, and is used for the treatment of HIV. DAPTA is another CCR5 antagonist, and is a synthetic peptide comprised of eight amino acids of the gp120 V2 region of HIV, which targets CCR5 selectively. Both blockers have been shown to be effective in blocking CCR5.

6.3.1 Antagonism of CCR5 during SFV infection using Maraviroc

Maraviroc was originally discovered after a high throughput screen by the pharmaceutical company Pfizer and is a selective imidazopyridine CCR5 ligand (198). As this drug has been shown to be a potent CCR5 blocker, this drug was used for blocking CCR5 during SFV infection with strain A7(74). A dose of 25 mg/kg/day was administered to mice by intraperitoneal injections once daily between PID 3-7. This dose has been shown to be effective in blocking CCR5⁺ cells in a breast cancer mouse model, and therefore I have used 25mg/kg

Maraviroc or vehicle control for the treatment of SFV infected mice (433). To examine the role of CCR5 during viral encephalitis, leukocyte infiltration was measured by flow cytometry.

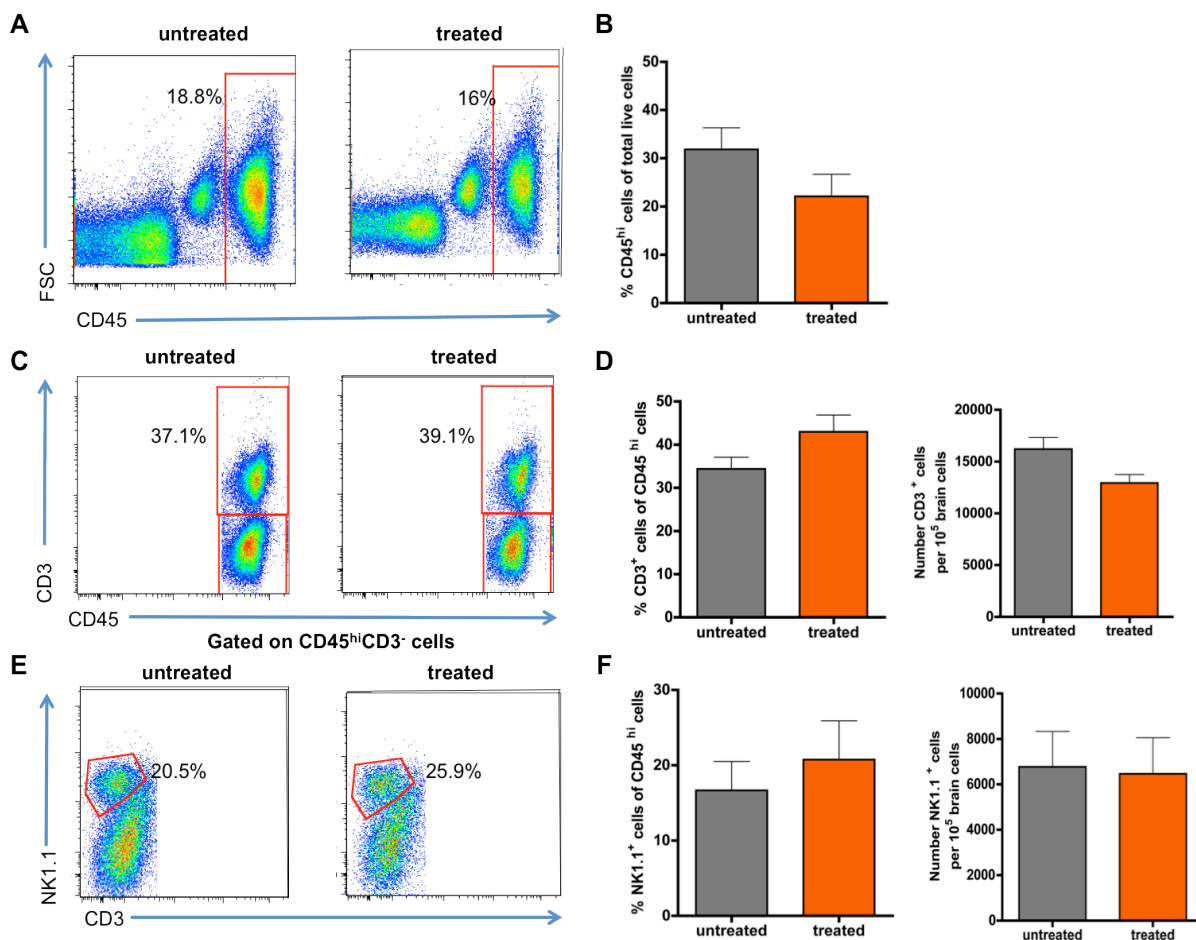


Figure 6.10 Identification of CD45^{hi}, CD3⁺ T-cells and NK-cells in SFV infected mice treated with the CCR5 blocker Maraviroc

Mice were infected with SFV strain A7(74) for 7 days and brains were collected. All mice were treated once daily by i.p. injection with vehicle (25% DMSO in PBS) or 25 mg/kg Maraviroc between post infection days 3-7. The number of CD45^{hi}, CD3⁺ and NK1.1⁺ cells in both groups was determined by flow cytometry. Data are presented as mean \pm SD with n=4-6 pooled mouse brains per group. Representative dot plots of (A) CD45^{hi} cells, (C) CD3⁺ cells within CD45^{hi} cells, and (E) NK1.1⁺ and CD3⁻ cells within CD45^{hi} cells. (B) Proportion of CD45^{hi} cells within total live brain cells in both groups. (D) Proportions and numbers of CD3⁺ T-cells within CD45^{hi} cells and 1×10^5 live brain cells in untreated and treated mice. (F) Proportions and numbers of NK1.1⁺CD3⁻ cells within CD45^{hi} cells and 1×10^5 live brain cells in untreated and treated mice. (Student's t-test; all not significant)

The proportion of CD45^{hi} cells within total live cells in Maraviroc treated mice was comparable with untreated mice (Fig. 6.10 A and B). Using further markers to identify other leukocyte subsets, the expression of CD3 and NK1.1 by CD45^{hi} cells was examined. The proportion and numbers of CD3⁺ and NK1.1⁺ cells in Maraviroc treated mice were not significantly different from untreated mice (Fig. 6.10 C-F). Finally the number and proportion of CD11b⁺ cells within CD45^{hi}

cells were determined and, again, no significant difference between untreated and treated mice could be observed (Fig. 6.11 A and B). To measure viral titers in the brain and to investigate the effect of Maraviroc on virus levels, E1 virus transcripts were measured by QPCR. The results show that viral titers were not significantly different between the groups (Fig. 6.11 C). Thus, Maraviroc did not have any effect on leukocyte infiltration and viral titer. Therefore another CCR5 blocker, DAPTA was used in subsequent experiments to investigate the role of CCR5 during viral encephalitis.

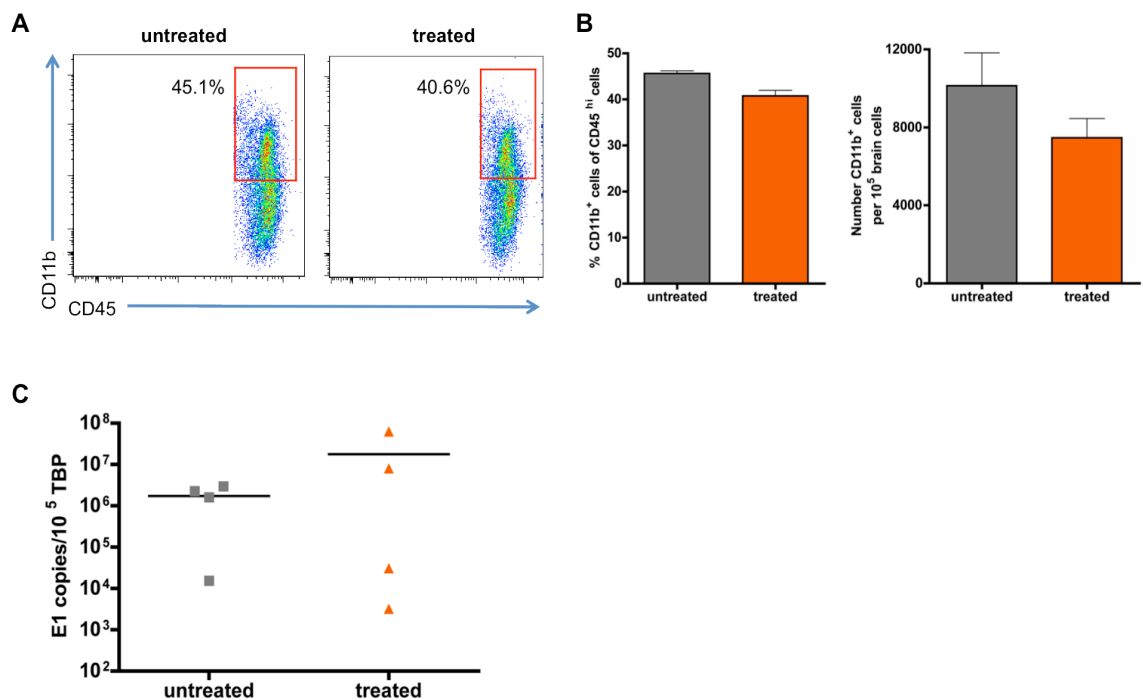


Figure 6.11 Identification of myeloid cells in the brain of SFV infected mice treated with the CCR5 blocker Maraviroc

Mice were infected with SFV strain A7(74) for 7 days and brains were collected. All mice were treated once daily by i.p. injection with vehicle (25% DMSO in PBS) or 25 mg/kg Maraviroc between post infection days 3-7. The number of CD11b⁺ cells was determined by flow cytometry. Data are presented as mean ± SD with n=4-6 pooled mouse brains per group. (A) Representative dot plot of CD11b expression on CD45^{hi} cells in treated and untreated mice. (B) Proportions and numbers of CD11b⁺ cells in the brain of untreated and treated mice within the CD45^{hi} population and 1x10⁵ live brain cell population, respectively. (C) Expression of the viral protein E1 per 1x10⁵ TATA-binding protein (TBP) in the brain of untreated and treated mice. (Student's t-test; all not significant)

6.3.2 Antagonism of CCR5 during SFV infection using DAPTA

Previous studies using rats have shown the efficacy of DAPTA in blocking CCR5 in a neuroinflammatory model of Alzheimer's disease (225). In this experiment, DAPTA was administered to mice subcutaneously at a concentration of 1 mg/kg/day between PID 3-7 as this dose has previously been shown to be

effective in blocking CCR5 in chronically LPS inflamed mice (225). The proportion of CD45^{hi} cells and the presence of leukocyte subsets in untreated and treated mice on PID 7 were determined by flow cytometry.

The treatment of mice with DAPTA resulted in a modest (approximately 50%), but not significant, reduction of leukocyte recruitment to the CNS (Fig. 6.12 A and B). The reduction of leukocytes did not lead to a change in viral titers and the number of E1 transcripts was comparable between untreated and treated mice (Fig. 6.12 C). Importantly, however, the number and proportion of CCR5⁺ leukocytes was significantly reduced (both $p < 0.01$) in DAPTA treated mice compared with untreated mice, confirming the effectiveness of DAPTA as a CCR5 blocker (Fig. 6.12 D-F). After determining the effect of CCR5 on the infiltration of CD45^{hi} cells into the CNS, I next set out to investigate the effect of CCR5 blockade on the infiltration of distinct leukocyte subsets into the virally infected CNS.

The proportion of CD3⁺ T-cells was significantly ($p < 0.05$) reduced in DAPTA treated mice (Fig. 6.13 A and B). Consistent with this, the number of CD3⁺ T-cells per 10⁵ isolated brain cells was also reduced in treated mice, but this result did not reach statistical significance. Within the CD45^{hi}CD3⁺ T-cell population, the proportion of CD4⁺ and CD8⁺ cells was also assessed. The proportion of both types of T-cells in treated mice was comparable to proportions in untreated mice, suggesting that CD4⁺ and CD8⁺ T-cells are equally reduced during CCR5 blocker treatment of SFV infected mouse brains (Fig. 6.13 C). The proportion and number of NK1.1⁺ cells was not significantly different in treated mice compared with untreated mice suggesting that another chemokine receptor is involved in the attraction of NK-cells into the brain (Fig. 6.13 D-E).

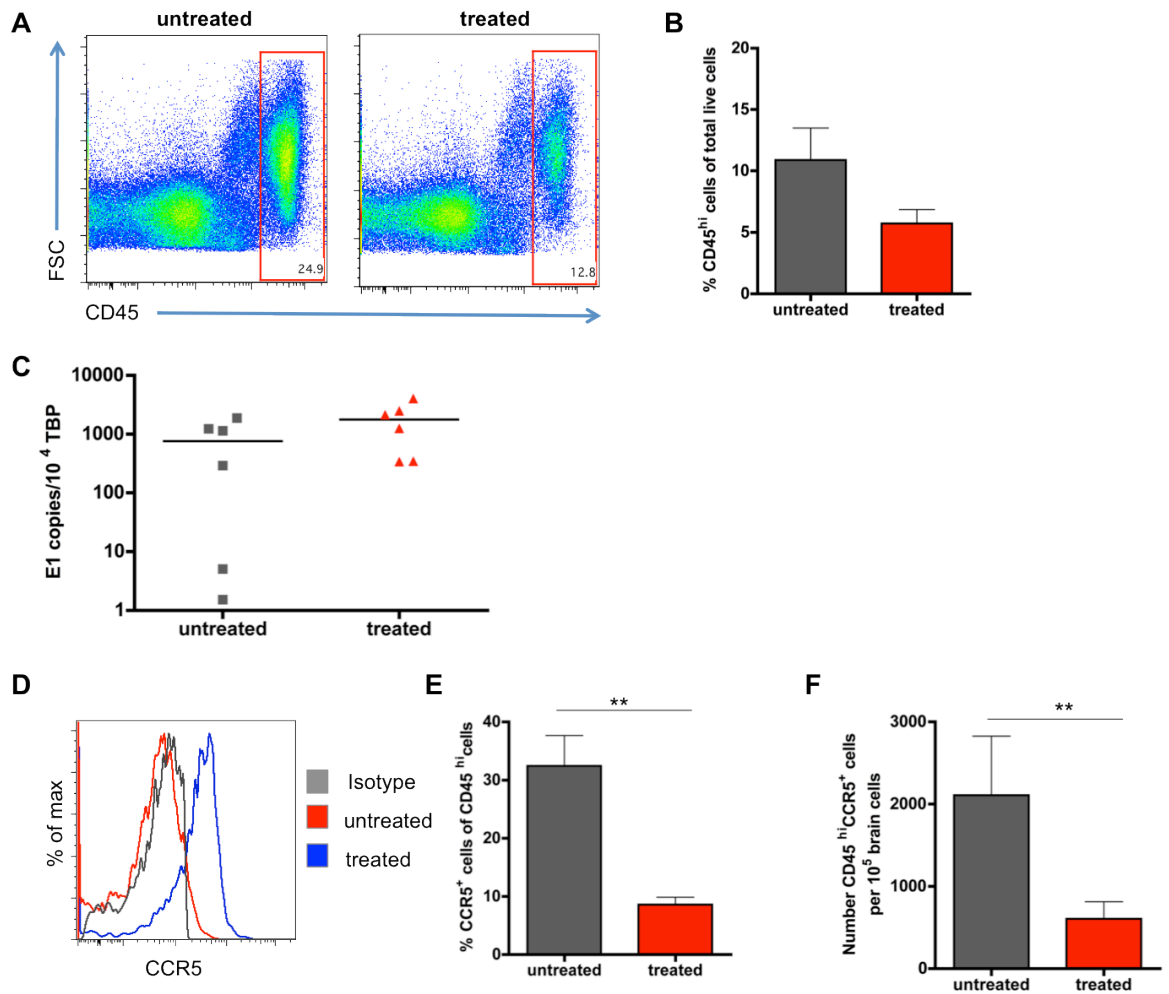


Figure 6.12 Identification of CD45^{hi} and CCR5⁺ cells in the brains of SFV infected mice treated with the CCR5 blocker DAPTA, and determination of viral titers

Mice were infected with SFV strain A7(74) for 7 days and brains were collected. All mice were treated once daily by s.c. injection with vehicle (water) or 1 mg/kg DAPTA between post infection days 3-7. The number of CD45⁺ and CCR5⁺ cells was determined by flow cytometry. Data are presented as mean \pm SD with n=4-6 pooled mouse brains per group from 2 individual experiments. (A) Representative dot plots of CD45 expression on isolated brain cells of untreated and treated mice. All cells were gated on CD45^{hi} cells. (B) Proportion of CD45^{hi} cells within total live brain cells. (C) Expression of viral protein E1 in untreated and treated mice measured by QPCR. Absolute copy numbers of E1 were normalized to 1×10^4 TATA-binding protein (TBP). (D) Histogram showing CCR5 expression on CD45^{hi} cells in isotype (grey), untreated (red) and treated (blue) murine brain samples. (E) Proportions and (F) number of CD45^{hi} CCR5⁺ cells per 10^5 isolated brain cells in untreated and treated mice. (Mann-Whitney U test; ** p<0.01)

The number and proportion of CD11b⁺ cells within the leukocyte population in treated mouse brains was, similar to NK-cells, also comparable to untreated mouse brains (Fig. 6.14 A and B). However the number of CD11b⁺ cells was slightly reduced in treated mice. Within the CD11b⁺ cell compartment, the proportion of Ly6C⁺ and Ly6C⁻ monocytes/macrophages in DAPTA treated mice

was similar to that in untreated mice but the number of Ly6C⁺ and Ly6C⁻ cells per 10⁵ isolated brain cells was slightly reduced in treated mice (Fig. 6.14 C-F). However, this result did not reach statistical significance.

Thus, CCR5 plays a role in the infiltration of leukocytes into the CNS during viral encephalitis, but the reduction of leukocytes within the CNS after treatment is less profound compared to treatment with the CCR2 blocker. The viral titer was unaffected by CCR5 blockade and the subsequent modest reduction of leukocyte subsets within the CNS.

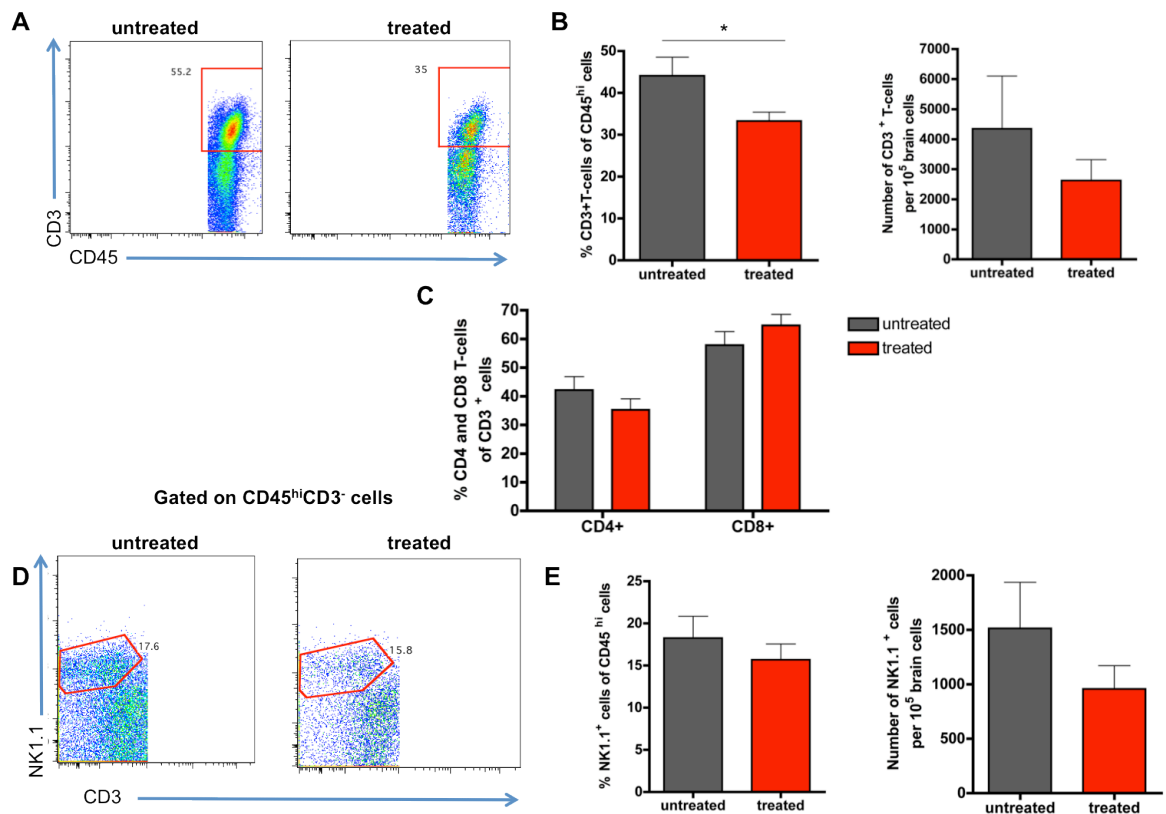


Figure 6.13 Identification of CD3⁺ T-cells and NK-cells in the brain of SFV infected mice treated with the CCR5 blocker DAPTA

Mice were infected with SFV strain A7(74) for 7 days and brains were collected. All mice were treated once daily by s.c. injection with vehicle (water) or 1 mg/kg DAPTA between post infection days 3-7. The number of CD3⁺ and NK1.1⁺ cells was determined by flow cytometry. Data are presented as mean \pm SD with n=4-6 pooled mouse brains per group from 2 individual experiments. (A) Representative dot plots of CD3 expression by CD45^{hi} cells in the brain of untreated and treated mice. (B) Proportions and absolute numbers of CD3⁺ T-cells in both groups and (C) proportions of CD4⁺ and CD8⁺ cells within CD3⁺ cells. (D) Representative dot plots of NK1.1⁺CD3⁻ cells in the brain of untreated and treated mice. Cells were gated on CD45^{hi} cells. (E) Proportions and absolute numbers of NK1.1⁺ cells in the brain of both groups. (student's t-test; * p<0.05)

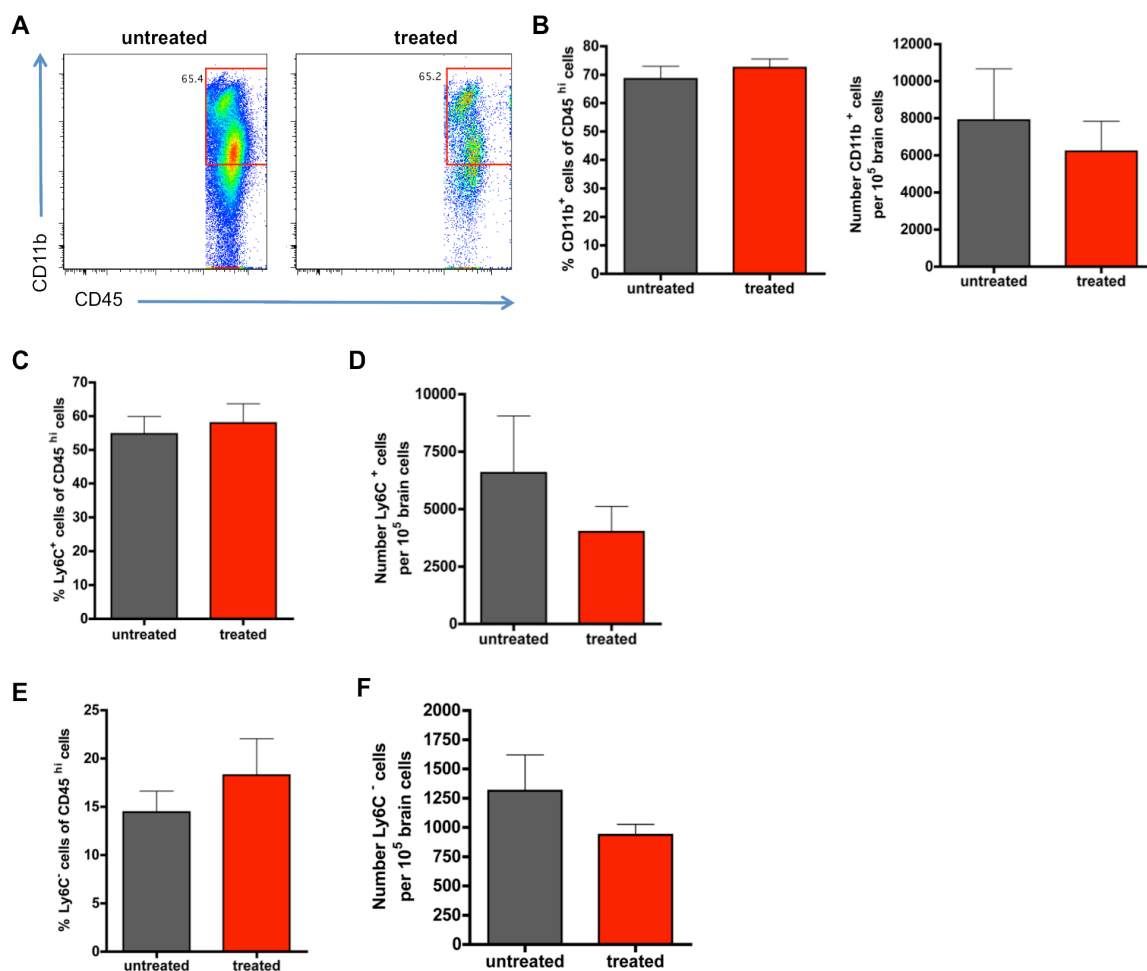


Figure 6.14 Identification of myeloid cells in the brains of SFV infected mice treated with the CCR5 blocker DAPTA

Mice were infected with SFV strain A7(74) for 7 days and brains were collected. All mice were treated once daily by s.c. injection with vehicle (water) or 1 mg/kg DAPTA between post infection days 3-7. The number of CD11b⁺ cells was determined by flow cytometry. Data are presented as mean \pm SD with $n=4-6$ pooled mouse brains per group from 2 individual experiments. (A) Representative dot plots of CD11b expression by CD45^{hi} cells in the brain of untreated and treated mice. (B) Proportions and absolute numbers of CD11b⁺ cells in the brain of both groups. (C) Proportions and (D) absolute numbers of CD11b⁺Ly6C⁺ cells in untreated and treated mice. (E) Proportions and (F) absolute numbers of CD11b⁺Ly6C⁻ cells in the CNS of both groups.

6.3.3 Chemokine expression levels in the CNS of SFV infected mice treated with the CCR5 blocker DAPTA

Analysis by TLDA revealed that only three chemokines were significantly differently expressed in treated mice compared with untreated mice. These were CCL2, CCL7 and CXCL12, which were significantly higher in SFV infected DAPTA treated mice (Appendix 5 A and B). The CCR5 ligands CCL3-5, CCL8, CCL11 and CCL20 were not significantly differently expressed after blockade of the CCR5 receptor. Of note, all the chemokine expression levels in CCR5 treated mice were generally slightly higher compared with untreated mice, but the difference did not reach statistical significance. Furthermore the expression of

cytokines was not significantly different in treated mice compared with untreated mice but, again, the cytokine levels tended to be marginally higher in treated brain samples (Appendix 5 C). The expression levels of RIG-I and IRF7 were similar to untreated mice (Appendix 5 D).

6.4 Characterisation of the role of CXCR3 during viral encephalitis

In the previous chapter I demonstrated that the CXCR3 ligands CXCL9 and CXCL10 were strongly upregulated in the brain during viral encephalitis compared with uninfected healthy control mouse brains. The CXCR3 blocker was obtained from Amgen Inc. and is referred to as 'compound 21'. The efficacy of this drug has been evaluated in a previous study using a mouse model of lung inflammation (232). Compound 21 was administered to SFV infected mice at a concentration of 10 mg/kg once daily by subcutaneous injection, a dose previously suggested by Du *et. al* (232). The drug or vehicle control was administered to SFV infected mice from PID 3 until PID 7 when mice were culled. This timing of treatment was selected, again, based on the previous study using the mouse lung inflammation model. The effect of CXCR3 blockade on leukocyte infiltration into the CNS, and in particular of T-cells, which predominantly express CXCR3, was determined by flow cytometry. Furthermore viral titers in the brain were measured by QPCR to examine the effect of this chemokine receptor on virus levels.

6.4.1 The effect of CXCR3 blockade on leukocyte infiltration into the CNS of SFV A7(74) infected mice

The accumulation of CD45^{hi} cells within the CNS of infected mice was substantially and significantly ($p < 0.01$) reduced from 17.3% in untreated mice to 2.6% in CXCR3 blocker treated mice (Fig. 6.15 A and B). This amounts to an approximately 84% reduction of leukocytes in treated mice. Consistent with this, the number and proportion of CXCR3⁺ cells within the CD45^{hi} cell population was also significantly ($p < 0.05$) reduced, confirming the efficacy of compound 21 in blocking CXCR3 (Fig. 6.15 C-E). Interestingly, despite the significant reduction of leukocyte infiltration, the number of SFV E1 transcripts in the brain was unaffected by CXCR3 blockade (Fig. 6.15 F).

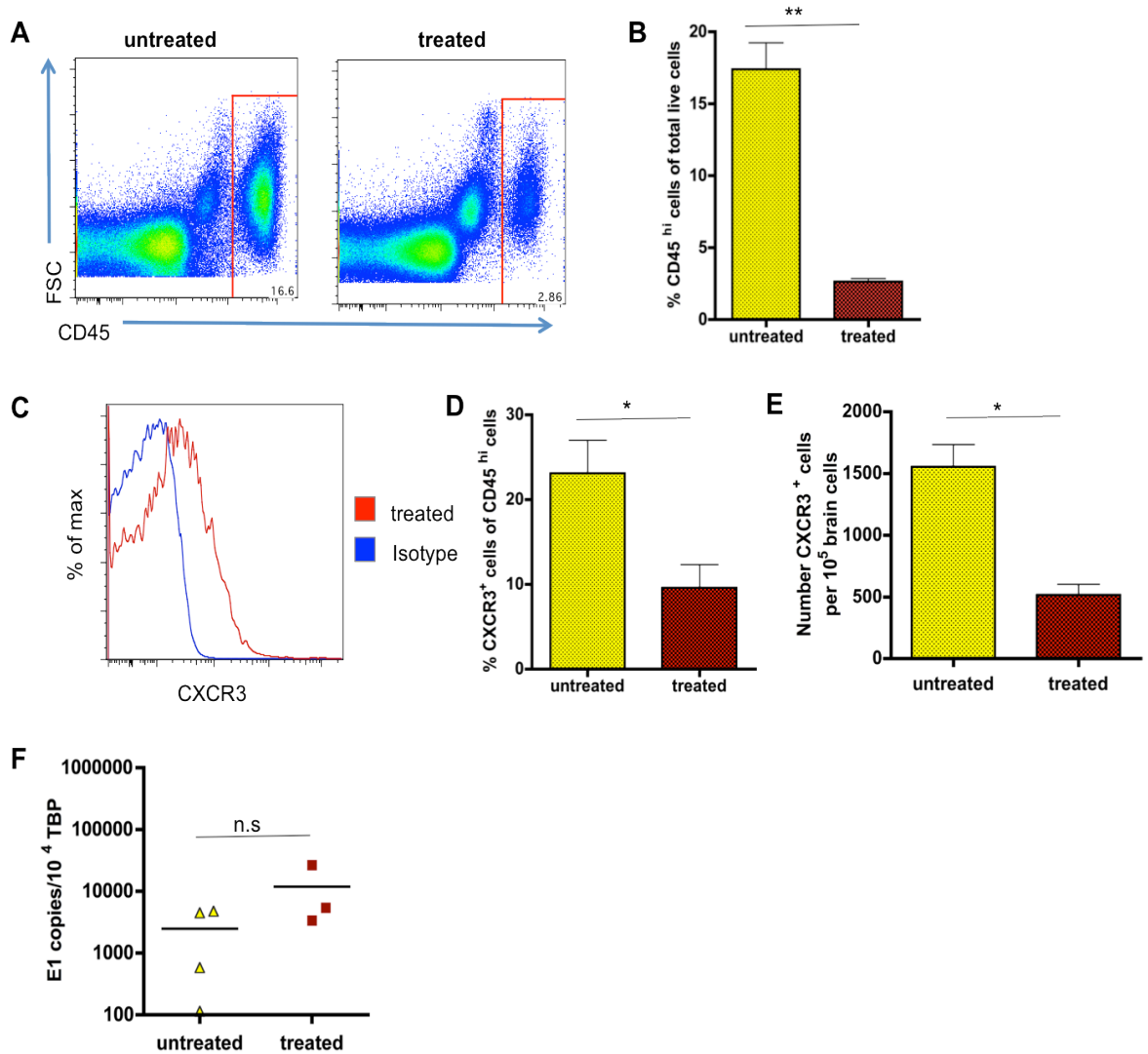


Figure 6.15 Identification of CD45^{hi} cells in the brains of SFV infected mice treated with the CXCR3 blocker compound 21, and determination of viral titers

Mice were infected with SFV strain A7(74) for 7 days and brains were collected for analysis. All mice were treated once daily by s.c. injection with vehicle (50% DMSO and 25% PEG400 in water) or 10 mg/kg compound 21 between post infection days 3-7. The number of CD45^{hi} cells infiltrating the CNS was measured by flow cytometry and viral titers were examined by QPCR. Data are presented as mean \pm SD, n=8 pooled mouse brains from 2 individual experiments. (A) Representative dot plots of CD45 expression on live brain cells in untreated and treated mice. All cells were then gated on CD45^{hi} cells. (B) Proportion of CD45^{hi} cells within total live cells. (C) Histogram showing the expression of CXCR3 by CD45^{hi} cells from isotype (blue) and treated (red) mice. (D) Proportions and (E) numbers of CD45^{hi}CXCR3⁺ per 10⁵ brain cells of treated and untreated mice. (F) Expression of E1 viral protein by QPCR. Data was normalized to 1x 10⁴ TATA-binding protein (TBP). n=3 mice per group. ((B and E) Student's t-test; * p<0.05, ** p<0.01 and (F) Mann-Whitney-U test; ns=not significant)

Within the CD45^{hi} cell population the proportion ($p < 0.05$) and number ($p < 0.01$) of CD3⁺ T-cells was significantly reduced in compound 21 treated mice compared with untreated mice (Fig. 6.16 A and B). Within the reduced T-cell population, compound 21 did not alter the proportion of CD4⁺ T-cells, although the number of CD4⁺ T-cells was significantly ($p < 0.01$) lower in treated mice compared with untreated mice. The relative percentage and number of CD8⁺ T-cells was significantly ($p < 0.01$) reduced after treatment with compound 21 (Fig. 6.16 C and D). After further analysis of CD3⁺ T-cells it was found that the number and proportion of CD44^{hi}CD61L^{lo} effector cells were significantly ($p < 0.01$ and $p < 0.05$, respectively) reduced in mice treated with the CXCR3 blocker compared with untreated mice (Fig. 6.16 E and F).

To investigate whether the blockade of CXCR3⁺ cells also affects the infiltration of other leukocyte subsets, not or only minimally, expressing CXCR3, the proportion and number of NK1.1⁺ and CD11b⁺ cells was analysed in the CNS of both untreated and treated mice. The numbers of CD45^{hi}CD11b⁺ and CD45^{hi}NK1.1⁺ cells per 10⁵ isolated brain cells were both dramatically reduced in the brain of treated mice (Fig. 6.17 A and B). However the relative percentage of both, NK1.1⁺ and CD11b⁺ cells was not different between untreated and treated mice (Fig. 6.17 C and D). A statistical significance could not be calculated as this experiment was only performed once.

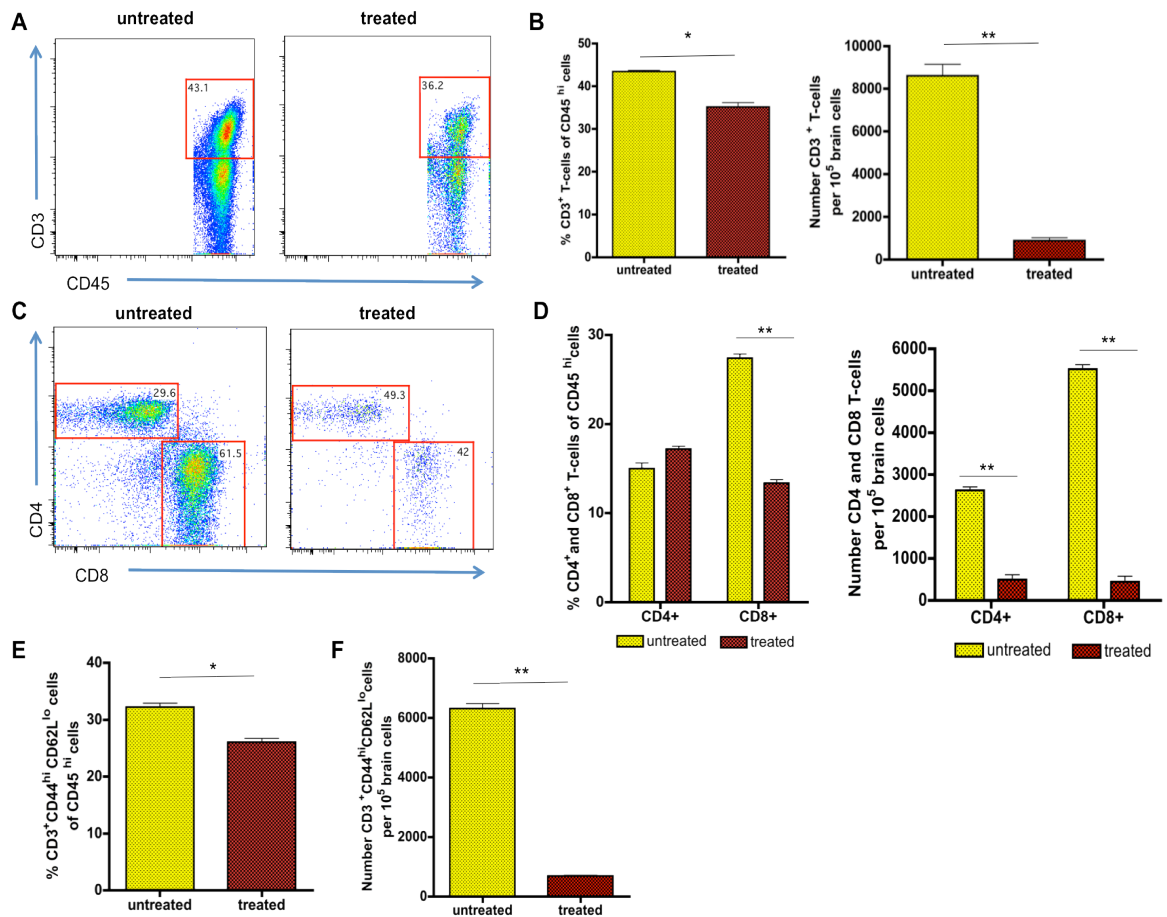


Figure 6.16 Reduction of T-cells subsets within the CNS of SFV infected mice treated with the CXCR3 blocker compound 21

Mice were infected with SFV strain A7(74) for 7 days and brains were collected for analysis. All mice were treated once daily by s.c. injection with vehicle (50% DMSO and 25% PEG400 in water) or 10 mg/kg compound 21 between post infection days 3-7. The number of CD3⁺ cells was determined by flow cytometry. Data are presented as mean \pm SD with, n=8 pooled mouse brains per group from 2 individual experiments. (A) Representative dot plots of CD3 expression by CD45^{hi} cells in the brain of untreated and treated mice. (B) Proportions and numbers of CD3⁺ T-cells in both groups. (C) Representative dot plots of CD4⁺ and CD8⁺ cells within CD3⁺ T-cells. (D) Proportions and numbers of CD3⁺CD4⁺ and CD3⁺CD8⁺ cells in the CNS in both groups. (E) Proportions and (F) numbers of CD3⁺CD44^{hi}CD62L^{lo} cells within leukocytes in the CNS of treated and untreated mice. (Student's t-test; * p<0.05, ** p<0.05)

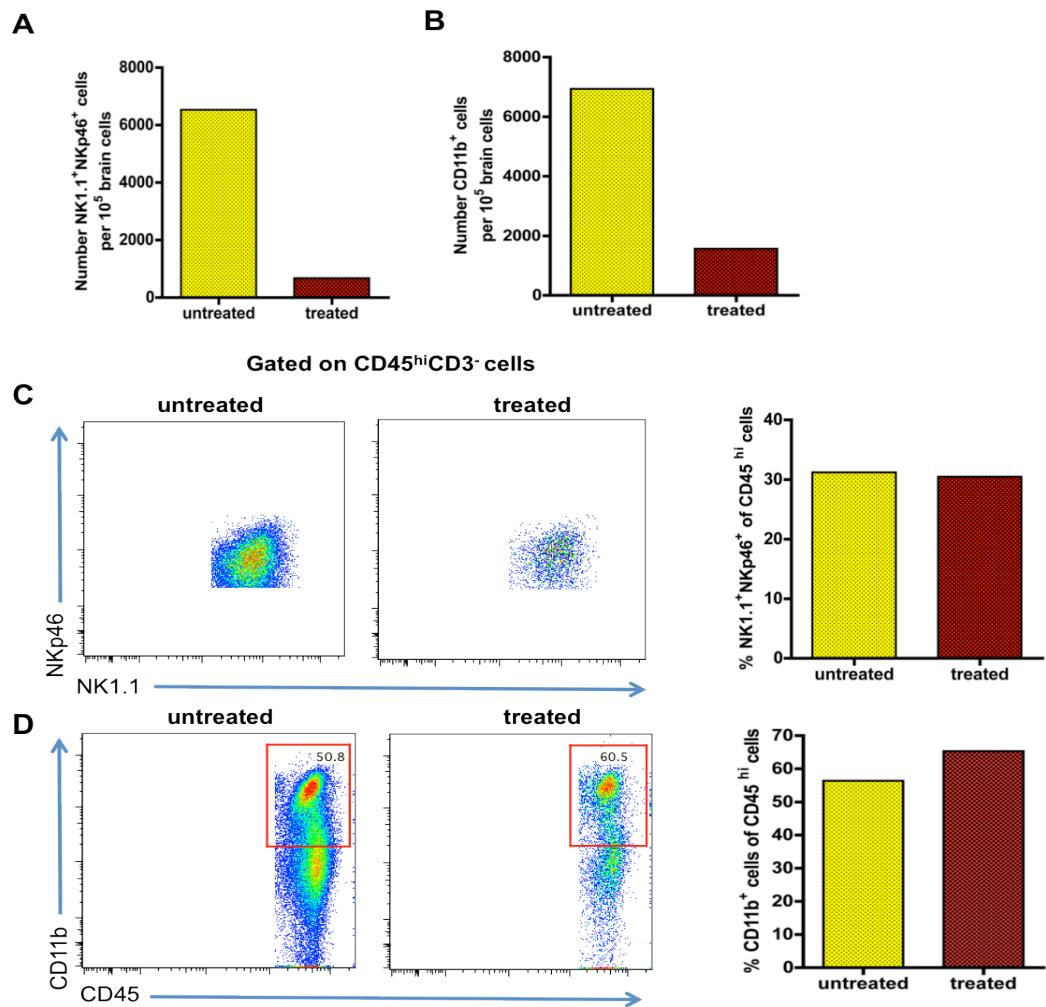


Figure 6.17 Identification of myeloid and NK-cells in the brains of SFV infected mice treated with the CXCR3 blocker compound 21

Mice were infected with SFV strain A7(74) for 7 days and brains were collected for analysis. All mice were treated once daily by s.c. injection with vehicle (50% DMSO and 25% PEG400 in water) or 10 mg/kg compound 21 between post infection days 3-7. The number of NK1.1⁺ and CD11b⁺ cells was determined by flow cytometry. Data are presented as mean \pm SD with n=8 pooled mouse brains per group from 1 individual experiment. (A) Number of NK1.1⁺NKp46⁺ cells and (B) CD11b⁺ cells per 10⁵ brain cells in both treatment groups. (C) Representative dot plots of NK1.1 and NKp46 expression by CD45^{hi} cells in the brains of untreated and treated mice, and proportions of NK1.1⁺NKp46⁺ cells in untreated and treated mice. (D) Representative dot plots of CD11b⁺ expression by CD45^{hi} cells in the CNS, and proportion of CD11b⁺ cells in the brains of both treatment groups.

6.4.2 Chemokine expression levels

In our lab I had later the opportunity to use bigger TLDA plates containing 64 genes instead of 32. This allowed me to examine the expression of more chemokines, cytokines and genes involved in innate immunity in SFV infected mice treated with compound 21 or vehicle control.

The only chemokines that were significantly differently expressed in untreated and treated mice were CCL5, CCL9, CCL17, CXCL3 and XCL1 (Appendix 6 A-D). Overall, most chemokine expression levels were reduced in compound 21 treated mice compared with untreated mice, including the CXCR3 ligands CXCL9 and CXCL10. A QPCR was performed to validate some of the results obtained by TLDA. The absolute copy numbers of CXCL9 were not different in treated mice compared with untreated mice (Fig. 6.18 A). In contrast to this, the transcript numbers of CXCL10 were minimally but not significantly reduced after treatment with compound 21 compared to untreated mice, and the levels of CXCL10 protein were unaffected (Fig. 6.18 B and C). Finally absolute copy numbers were also measured for CXCR3. The results show that CXCR3 transcript numbers are lower in treated mice compared with untreated mice but this was not statistically significant ($p > 0.05$) (Fig. 6.18 D).

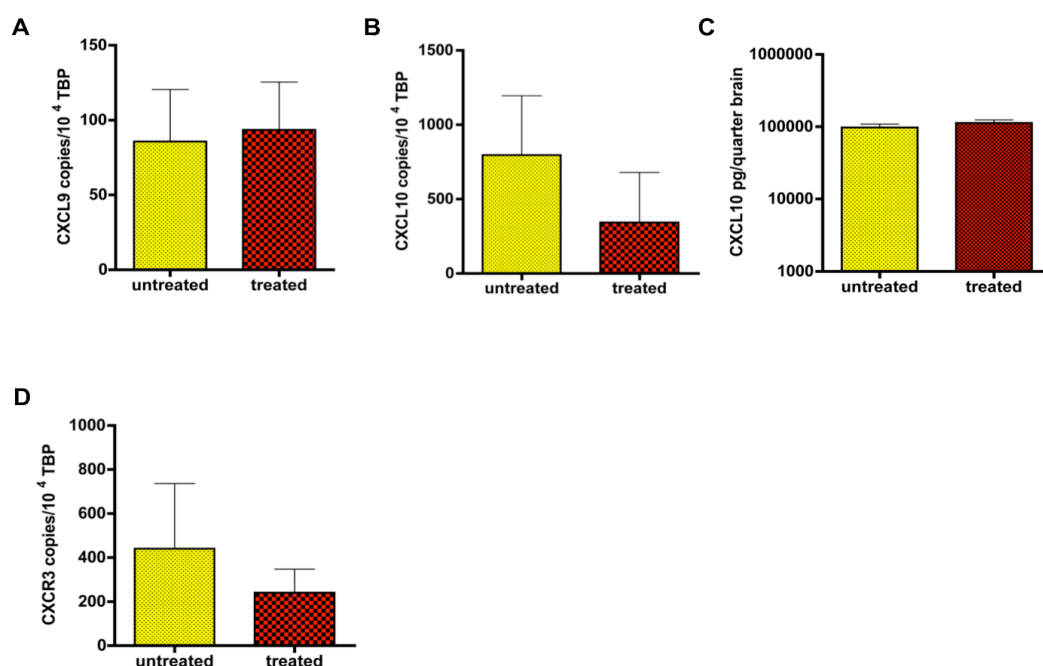


Figure 6.18 Comparison of CXC-chemokine expression pattern in untreated and CXCR3 blocker treated mice, infected with SFV strain A7(74)

Mice were infected with SFV strain A7(74) for 7 days and brains were collected for analysis. All mice were treated once daily by s.c. injection with vehicle (50% DMSO and 25% PEG400 in water) or 10 mg/kg compound 21 between post infection days 3-7. The expression of CXCL9, CXCL10 and CXCR3 was assessed by QPCR. (A and B) Absolute copy numbers of CXCL9 and CXCL10 per 1×10^4 TATA-binding protein (TBP). (C) Concentration of CXCL10 protein in the brain of untreated and treated mice measured by ELISA. (D) Absolute copy number of CXCR3 per 1×10^4 TBP. Data are presented as mean \pm SD with of $n=3-4$ mice per group. Each gene was tested in triplicate. (Student's t-test; all not significant)

The expression pattern of CX₃CL1 was not different between untreated and CXCR3 blocker treated mice. The expression level of XCL1 was significantly ($p < 0.05$) higher expressed in untreated mice compared to CXCR3 treated mice (Appendix 6 D).

The levels of cytokines and genes involved in innate immune responses were generally also lower (not significant) in compound 21 treated mice compared with untreated mice with the exception of IL-6, RIG-I and PKR where expression levels were minimally, but not significantly, higher in CXCR3 treated mice (Appendix 6 E and F). Ifit-1, an interferon inducible gene, was the only innate immune response gene that was significantly higher expressed in untreated mice compared to CXCR3 blocker treated mice.

6.4.3 Effects of blocking CXCR3 on mice infected with the virulent strain L10

Next the impact of chemokine receptor blockade on disease outcome was examined using the virulent strain L10. Due to the profound effect of CXCR3 on leukocyte recruitment into the CNS of SFV A7(74) infected mice, the effect of compound 21 was tested in a virulent model of SFV, and survival of mice was analysed. Despite the ability of compound 21 to reduce leukocyte accumulation in the CNS during SFV A7(74) infection, no survival benefit was found in L10 infected mice treated with the CXCR3 antagonist (Fig. 6.19 A).

L10 infection of the brain typically results in such a severe pathology that it is possible that the blockade of CXCR3 alone is not sufficient to see any survival benefits. In the previous section it was shown that CCR2 blocker treated mice, infected with the avirulent strain A7(74), display reduced leukocyte infiltration compared with wild type mice. Additionally CCR2^{-/-} mice infected with the virulent strain L10 died earlier compared with wild type infected mice. Therefore a combination of CCR2 and CXCR3 blockers was selected to examine the possible impact of both receptors on disease outcome. Compound 21 and RS504393 were administered to mice between PID 3-7. The results demonstrate that mice treated with both blockers had a significant survival benefit ($p < 0.05$) compared with control mice that were treated with vehicle control (Fig. 6.19 B). Unfortunately due to time constraints an experiment using the CCR2 blocker

RS504393 alone was not performed. The CXCR3 blockade experiment was only performed once, and larger experimental groups are necessary to confirm this result. Thus, these data suggest that an interventionist strategy aimed at blocking CXCR3 alone during SFV L10 infection was ineffective at ameliorating the disease but co-blocking CCR2 and CXCR3 leads to better disease outcome. Therefore it is possible that leukocyte infiltration is detrimental and results in more severe pathology during encephalitis.

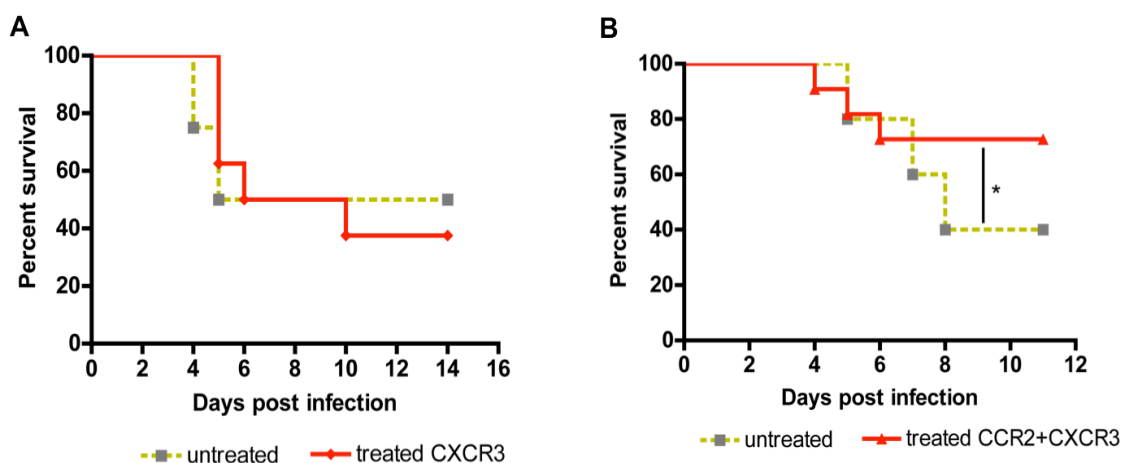


Figure 6.19 Survival of mice infected with SFV strain L10, and treated with chemokine blockers

Mice were infected with SFV strain L10 for 12-15 days and the survival of mice was determined. Mice were euthanized once they became ill. (A) Kaplan-Meier survival curve. Mice were treated once daily by s.c. injection with vehicle (50% DMSO and 25% PEG400 in water)(untreated group) or 10 mg/kg compound 21 between post infection days 3-7. (B) Kaplan-Meier survival curve. Mice were treated with compound 21 as described in (A), and twice daily by oral gavage with vehicle (6.6% DMSO in PBS) (untreated group) or 5 mg/kg RS504393 (CCR2 blocker) between post infection days 3-7. n=10 mice per group. (Logrank (Mantel- Cox) test; * p<0.05)

6.5 Discussion and summary

On the basis of the thorough chemokine expression analysis presented in chapter 3, the chemokine receptors CCR2, CCR5 and CXCR3 were identified as possible candidates for interventionist strategies. The aim of the work in this chapter was to investigate the role of these three chemokine receptors in CNS recruitment and modulation of host immune responses, which may contribute to virus-induced damage and mortality. During WNV infection it has been demonstrated that within the first 5 days post infection, monocytosis occurs which is critical for monocyte accumulation within the CNS, and this latter process of recruitment is not dependent on CCR2 (214). In contrast to this, monocytosis

itself is entirely CCR2 dependent. The results here show that circulating monocyte numbers in the blood were not affected by the CCR2 blockade and monocyte entry into the SFV infected CNS from PID 4 onwards was reduced in treated mice, suggesting that this process is dependent on CCR2 during SFV infection. Additionally monocytes increase in number in response to viral infection with SFV but the increase was less profound compared to studies using WNV as model of infection.

In chapter 4 it was shown that monocytes enter the brain early (on PID 4) during viral infection of the CNS, while simultaneously many monocyte attracting chemokines were strongly induced as described in chapter 3. The data demonstrate that blocking CCR2 results in a significant decrease in CD45^{hi} cells within the brain. Interestingly, despite decreased leukocyte numbers in the CNS, viral titers and chemokine expression patterns in the brain were not significantly changed in treated mice compared with untreated mice, suggesting that monocytes may be less critical for virus clearance, and the cellular source of chemokines is different from monocytes. This is in contrast to previous studies with WNV, which have shown that viral titers are increased in CCR2 deficient mice compared to wild type mice, suggesting a role of monocytes in virus clearance (214, 334). Furthermore it was proposed that the blockade of monocytes into the CNS of WNV infected mice results in a delay of T-cells entering the brain, and this could explain the reduced virus clearance in the CNS and higher mortality in CCR2 deficient mice (401).

After phenotyping leukocyte subsets I noticed that the number of Ly6C⁺CCR2⁺ monocytes was significantly decreased to a similar extent as in CCR2 deficient mice. In support of this Getts *et al.* have shown that CCR2 is pivotal for trafficking of Ly6C⁺ cells into the CNS where they differentiate into microglia (106). Despite the fact that CCR2 is mainly expressed on monocytes, it was noted that the number of CD3⁺ T-cells and NK-cells was also reduced. In part this can be explained by the fact that some activated T-cells and NK-cells express CCR2 (434, 435). For instance, Nansen *et al.* have shown that activated CD8⁺ T-cells express CCR2 and CCR5 during LCMV infection (319). However CCR2 is not known to be a principal regulator of T-cell migration and despite the publications by Rabin, Polentarutti and Nansen *et al.*, there are numerous other studies in which T-cell migration is unaffected in CCR2^{-/-} mice (319, 434-436).

Therefore another possible explanation for the reduction in T-cell and NK-cell number in CCR2 treated or CCR2^{-/-} mice is that recruited monocytes in the CNS have an indirect action on T-cell and NK-cells entry by secreting chemokines or cytokines which are chemoattractant for T-cells and NK-cells infiltration. Therefore a reduction in monocyte infiltration would result in reduced T- and NK-cell accumulation within the CNS. However, the TLDA analysis revealed that this is not the case, as chemokine levels were mostly unaffected by the chemokine receptor blockade. Another possibility is that the passage of monocytes leads to changes at the BBB which facilitates transmigration of T-cells and other leukocyte subsets into the brain parenchyma. Savarin *et al.* have shown that monocytes are dispensable for the migration of T-cells through the BBB during MHV infection of the CNS using CCL2 deficient mice (401). They have demonstrated that monocytes are capable of altering the BBB integrity allowing other leukocyte subsets to enter the CNS of infected mice.

During L10 infection the mortality rate in CCR2 deficient mice was higher compared with wild type mice. Of note is also that the experimental group for this survival analysis was relatively small and therefore this experiment must be repeated to draw firm conclusions from these data. However in support of my result Lim *et al.* have shown that CCR2^{-/-} mice infected with WNV exhibit a higher viral titer in the CNS due to reduced monocyte trafficking to the brain resulting in higher mortality, and Savarin *et al.* have reported that CCR2 deficient mice die earlier due to the lack of monocytes and delayed T-cell trafficking across the BBB during viral encephalitis (214, 401). However Lim *et al.* have shown that the reduction of monocytes within the CNS of WNV infected mice is a result of prior monocytopenia, and they have suggested that CCR2 is dispensable for the trafficking of monocytes into the brain during viral encephalitis. This finding is in contrast to my results which show that the temporary blockade of CCR2 did not decrease circulating monocytes in the blood, but did block monocyte entry into the CNS, suggesting that leukocytes do use this chemokine axis to enter the virus infected CNS, and is not a mere consequence of monocytopenia. Of note is that most of these studies investigating the role of CCR2 have used CCR2 deficient mice instead of using a pharmacological CCR2 blocker, as used in this study, where monocyte trafficking can be better examined. Thus, based on my preliminary data I propose that

CCR2 is crucial for the recruitment of monocytes and other CCR2 expressing leukocyte subsets into the CNS.

Two different CCR5 blockers were used in this study. Initially, the FDA approved CCR5 blocker Maraviroc was used in this study to block CCR5 during SFV infection of mice (199). However treatment with the drug did not result in a reduction of leukocyte recruitment to the CNS and did not have an effect on viral titers. Therefore another drug, referred to as DAPTA, was used. A study by Rosi *et al.* has demonstrated the efficacy of DAPTA in a chronic LPS induced inflammation model in rats (225). CCR5 blockade using DAPTA led to a reduction in leukocyte numbers in the brain, and in particular of CCR5⁺ cells, but the reduction of leukocytes was less profound than that seen with the CCR2 and CXCR3 blockers. This suggests that CCR5 plays a minor role in the pathogenesis of SFV infection of the brain.

The inefficacy of Maraviroc compared to DAPTA could be due to the following reason: Firstly, DAPTA has been shown to be 34-180 times more potent than Maraviroc in inhibiting CCR5 due to high affinity binding of DAPTA to the CCR5 binding site (198, 223). This could explain the better efficiency of DAPTA in binding CCR5 compared to Maraviroc during SFV infection. Secondly, murine CCR5 is 82% identical with the human form, and since most studies of Maraviroc have been carried out in humans and primates it is possible that Maraviroc binds to regions of CCR5 not present or less accessible in the murine form of CCR5, and this would explain why Maraviroc did not work well in the mouse model of SFV infection (437). In contrast to this, several studies have been conducted in mouse and rat models using DAPTA to block CCR5. Hence DAPTA is more suitable to block CCR5 in mice (223-225). Lastly, the dose of Maraviroc administered to mice during SFV infection might have been suboptimal. Neff *et al.* have used a dose of 62 mg/kg/ day in mice which is equivalent to the human dose of 300 mg/day (438). However in my study a dose of only 25 mg/kg/day was used, and this could explain the inefficacy of Maraviroc used here. The efficiency of Maraviroc during SFV encephalitis needs to be determined in the future, by conducting dose-dependent experiments.

This finding is in contrast to studies using WNV as a model of infection (362). CCR5 was one of the first chemokine receptors shown to play a clear role during

WNV encephalitis. CCR5 deficiency resulted in enhanced mortality and more severe pathology in the brain (197). CCR5^{-/-} mice have been shown not to be able to control viral titers in the brain (173). Furthermore the non-functional CCR5Δ32 mutation in humans was associated with more severe onset of neurological symptoms during WNV infection. Thus, the use of Maraviroc for HIV could potentially increase risks for patients to develop severe neurological forms of WNV disease. Hence, chemokines play significant roles in the pathogenesis of viral infection.

Due to high transcript levels of CXCL9 and CXCL10 in the brain of SFV infected mice and large numbers of infiltrating CD3⁺ T-cells, I next sought to determine the consequence of CXCR3 blockade on T-cell trafficking into the brain. It was demonstrated that compound 21 was highly effective at decreasing leukocyte recruitment to the CNS of infected mice. In particular T-cell numbers were strongly reduced in treated mice. Within the T-cell population the number of CD8⁺ T-cells was reduced whereas the reduction of CD4⁺ T-cells was less profound. This corresponds with results obtained from studies using WNV as a model of infection (140, 141, 375). In these studies CXCR3 was pivotal for the attraction of T-cells to the virally infected brain. Compound 21 was effective in blocking CXCR3 due to the decrease in the number and proportion of CXCR3⁺ cells within the CNS of treated mice.

The decrease in numbers of other leukocyte subsets, not or only minimally expressing CXCR3, such as CD11b⁺ cells and NK-cells suggests that the reduction of T-cells in the brain may indirectly also lead to a reduction in these cells. For instance T-cell entry could perhaps mediate permeabilisation of the BBB and facilitate entry of other leukocyte subsets. Another possibility is that chemokine and cytokine levels in treated mice are altered in a way that results in a reduction of CD11b⁺ and NK-cell entry into the CNS. However the analysis of chemokine expression patterns in untreated and treated mice revealed that chemokines were not significantly differently expressed between both groups, but generally chemokine levels tended to be lower in CXCR3 treated mice. Therefore this possibility seems unlikely. In support of my results a previous study has shown that in chemokine deficient mice the number of other leukocyte subsets, not expressing the specific chemokine receptor are also decreased

compared with wild type mice (423). The reason for this remains unknown and needs to be experimentally addressed in the future. Of note is that this experiment was only performed once and therefore needs to be repeated multiple times to confirm these findings and to obtain statistical significance.

Interestingly, while viral titers in the brain of CXCR3^{-/-} mice were increased during WNV infection the viral titer in CXCR3 blocker SFV treated mice were unaffected and similar to untreated mice. So far, none of the receptor antagonists had a significant impact on viral titres, so the reduction in leukocyte recruitment is a direct result of receptor blockade and not a result of direct or indirect virus inhibition by the antagonists.

The treatment of SFV L10 infected mice with compound 21 did not result in a significantly different disease outcome. However this is not entirely surprising as it was later noticed that the main leukocytes entering the brain of L10 infected animals were monocytes and macrophages and only few cells were T-cells. Since CXCR3 is mainly expressed on T-cells this could explain the inefficacy of compound 21 in this model of SFV infection despite high levels of CXCL9 and CXCL10 expression in the CNS of infected mice. Based on flow cytometry data a blockade of CCR2 would have been more appropriate but due to time constraints this experiments could not be conducted anymore. However CCR2^{-/-} mice were infected with L10, and the results from this experiment show that CCR2^{-/-} mice die earlier compared with wild type infected mice. Interestingly, simultaneous blockade of CXCR3 and CCR2 significantly ameliorated pathology suggesting that selective chemokine receptor blockade in combination could be used therapeutically for the treatment of viral encephalitis to overcome the redundancy of chemokine-receptor interactions. Furthermore it appears from these data that timing of therapeutic intervention is critical for survival. For instance CCR2 deficient mice die earlier compared to wild type mice whereas treatment with CCR2 and CXCR3 blocker starting on PID 3 results in enhanced survival. Importantly CXCR3 alone did not lead to a difference in survival between untreated and treated mice. Therefore it is possible that monocytes are critical in the early stages of SFV infection when the virus enters the host. In a previous study a similar trend has been observed for neutrophils during WNV infection. Bai *et al.* have shown that depletion of neutrophils prior to infection results in reduced viral titers in the blood and enhanced survival whereas

depletion shortly after WNV infection leads to increased viremia and higher mortality (350).

Of note is that L10 mice infected for more than 7 days all survived despite establishing very high virus titres in the brain, suggesting that an effective immune response, developing by PID 7, is beneficial for survival.

Overall, the results presented here demonstrate that the antagonism of CXCR3 was the most potent among all three chemokine blockers in reducing leukocyte infiltration into the CNS. Antagonism of CCR2 and CCR5 also leads to the reduction of leukocytes in response to SFV infection but the extent of leukocyte reduction was less profound than that seen with CXCR3 blockade. Thus chemokine receptors present plausible targets for viral encephalitis. The role of CCR2, CCR5 and CXCR3 in the pathogenesis of viral encephalitis will be discussed in more depth in chapter 7.

Chapter 7

General Discussion

7.1 Introduction

The infiltration of leukocytes into the ‘immune sheltered’ CNS is a hallmark of viral encephalitis. For a long time it has been assumed that leukocyte recruitment into the brain is pivotal for virus clearance and recovery of the host. However it has also been shown that leukocytes are not always beneficial for the host during viral encephalitis and may paradoxically contribute to more severe pathology, including destruction of neuronal cells (439, 440). The infiltration of leukocytes into the brain is regulated by chemokines, as discussed in more detail in section 1.3. Despite having investigated the role of some chemokines during models of viral encephalitis such as WNV, MHV or LCMV infection, a clear picture of chemokine expression during viral brain infection has not yet been established.

Therefore in an attempt to better understand the regulation of leukocyte recruitment into the virus infected brain, we have used mouse models of viral encephalitis, such as SFV and WNV, to define, in unprecedented detail, the form and magnitude of the chemotactic cues expressed by the virus infected brain, and the kinetics of entry of distinct leukocyte populations in relation to chemokine expression. Importantly, for the first time, we have utilised a panel of chemokine receptor (CKR) antagonists to evaluate the hierarchy and relative importance of distinct chemokine receptors for CNS leukocyte influx. The use of these small molecule inhibitors is particularly important because most studies have been conducted using only gene deficient mice. The deficiency of one particular chemokine receptor may exert its influence at multiple stages including during development, and during homeostatic or inflammatory immune responses, and subsequently it is difficult to draw firm conclusions from these data. Additionally, the expression of cytokines was determined during avirulent and virulent SFV infection and compared to the expression of cytokines during WNV infection.

In this chapter the main findings of this thesis will be briefly discussed and summarized, and conclusions and possible future directions presented.

7.2 Identification of chemokine expression patterns and determination of leukocyte recruitment into the CNS during viral encephalitis

Using TLDA analysis, the key chemokines identified to be highly upregulated during SFV and WNV infection were the CC-chemokines CCL2, CCL5, CCL7, and the CXC-chemokines CXCL9 and CXCL10. The results demonstrate that the chemokine expression pattern during SFV and WNV infection is remarkably similar despite using different viruses or viral strains showing varying degrees of pathogenicity. In previous studies the same chemokines have been identified to be highly upregulated in the CNS of mice infected with other encephalitic viruses such as Sindbis virus, closely related to SFV, MHV and LCMV (128, 129, 441). Thus, a certain chemokine expression pattern is evident during viral encephalitis regardless of the pathogen used.

Despite similar chemokine expression patterns during viral encephalitis using various encephalitic viruses, the magnitude of expression varies considerably depending on the degree of pathogenicity of the viral strain used. For instance chemokines were many fold more strongly induced during SFV L10 infection or virulent WNV infection compared to avirulent SFV A7(74) infection.

Importantly, some chemokines such as the neutrophil attracting chemokines CXCL1 and CXCL2 were exclusively expressed during virulent SFV infection using strain L10, and virulent WNV infection using strain NY99. In support of this, Bai *et al.* and Perry *et al.* have shown that neutrophils enter the CNS only during the onset of severe forms of viral or bacterial brain infections (350, 415, 439, 440). Furthermore, due to the toxic properties of the granules within neutrophils, the recruitment of neutrophils into the CNS has been shown to lead to severe tissue damage (18, 128, 129, 441). During SFV infection using the avirulent strain A7(74) no neutrophils were detectable by immunohistochemistry, and this result is in agreement with my results demonstrating the lack of expression of neutrophil attracting chemokines during A7(74) infection. The strong induction of CXCL1 and CXCL2 expression during virulent L10 infection suggests that neutrophils might enter the CNS and it is therefore possible that the infiltration of neutrophils is in general associated with more severe disease outcomes. Further experiments are required to investigate this possibility.

Of note, the early induction of CXCL10 and, to a lesser extent CXCL9, expression during SFV and WNV infection suggests that these chemokines are most likely expressed by cells of the CNS such as neurons and glia during very early time points of brain infection. In support of this, Klein *et al.* have demonstrated that CXCL10 is predominantly and strongly expressed in neurons while Lane *et al.* have reported that CXCL10 is mainly expressed in astrocytes during MHV infection (129, 153). From these studies it is not clear which cells of the CNS are the ultimate source of CXCL10 but the induction of CXCL10 expression appears to be localised to cells infected by the virus, suggesting that virus infected cells of the CNS are a possible source of CXCL10. In the case of SFV this would involve mainly neurons and oligodendrocytes and not astrocytes, as these are the main cells becoming infected with SFV (293).

Beyond CXCL9 and CXCL10, much chemokine expression in the brain is induced simultaneously with the appearance of viruses in the CNS, coinciding with the influx of leukocytes into the brain. This suggests that chemokines are predominantly expressed by infiltrating leukocytes. Whether leukocyte entry into the CNS is beneficial or detrimental for disease outcome is not yet clear. This is demonstrated in part by studies using WNV as a model of infection where leukocyte infiltration is pivotal for viral clearance and survival (442). In contrast to this, studies using LCMV as a model of infection have shown that leukocytes contribute to neuropathology and lead to higher mortality rates (371, 430). Fazakerley *et al.* have shown that specific leukocyte subsets such as CD4⁺ and CD8⁺ T-cells during SFV infection are pathogenic by contributing to the generation of lesions of demyelination and neuroinflammation (51, 301). In addition they have demonstrated that the presence of neutralizing IgG in the CNS of SFV infected SCID mice, devoid of B-cells and T-cells, is sufficient for viral clearance and survival of mice, suggesting that leukocytes are dispensable for survival and are mostly pathogenic (51, 443). Of note is the fact that CD45⁺ leukocyte influx in response to avirulent SFV infection was moderate compared to higher leukocyte infiltration during virulent SFV infection. Therefore it is possible that the extent of leukocyte infiltration determines whether leukocyte recruitment is pathogenic or beneficial during viral encephalitis.

The use of small molecule inhibitors for CCR2 and CXCR3, or CCR2 deficient mice, resulted in a significant decrease in leukocyte recruitment to the CNS. In

the case of combined CCR2 and CXCR3 blockade disease outcome was better with more mice surviving otherwise lethal SFV L10 infection. This suggests that reducing leukocyte infiltration in the brain is beneficial. This is in contrast to data from CCR2 deficient mice, where reduction of leukocytes within the CNS correlated with worse disease outcome, suggesting that leukocytes are beneficial. The reason for this discrepancy will be discussed in more detail in section 7.4, but at this stage no firm conclusions can be drawn from my data about the role of leukocytes during viral encephalitis. However, it appears that the role of leukocytes during viral encephalitis depends on various factors including viral strain, type of leukocytes entering the CNS and timing of infiltration.

One of the first leukocytes entering the brain during avirulent and virulent SFV infection were cells of the innate immune system such as NK-cells and CD11b⁺ myeloid cells, mainly Ly6C^{hi} and Ly6C^{lo} monocytes and macrophages, respectively. The entry of innate immune cells into the CNS correlated with entry of SFV into the brain. The recruitment of NK-cells and myeloid cells into the brain coincides with the upregulation of the appropriate chemokines during early stages of infection. For instance CXCL9 and CXCL10 expression was strongly induced during early time points of infection, and in previous studies these chemokines have been shown to attract CXCR3⁺ activated NK-cells and T-cells (379, 444). The expression of CCL2 and CCL5 was also upregulated compared to healthy controls, and these chemokines have been shown to be important for the attraction of macrophages and monocytes (445). The role of NK-cells during viral encephalitis is not yet clear, as studies have demonstrated that the depletion of NK-cells does not prevent mortality during virulent SFV or MHV infection (379, 417). NK-cells have been shown to secrete IFN- γ , and this cytokine could be partly responsible for the strong induction of CXCL9 expression and upregulation of MHC class II on myeloid cells during later time points of SFV infection. However the production of IFN- γ during early stages of brain infection can lead to the early induction of CXCL9 expression by brain endothelial cells or glial cells (242, 428).

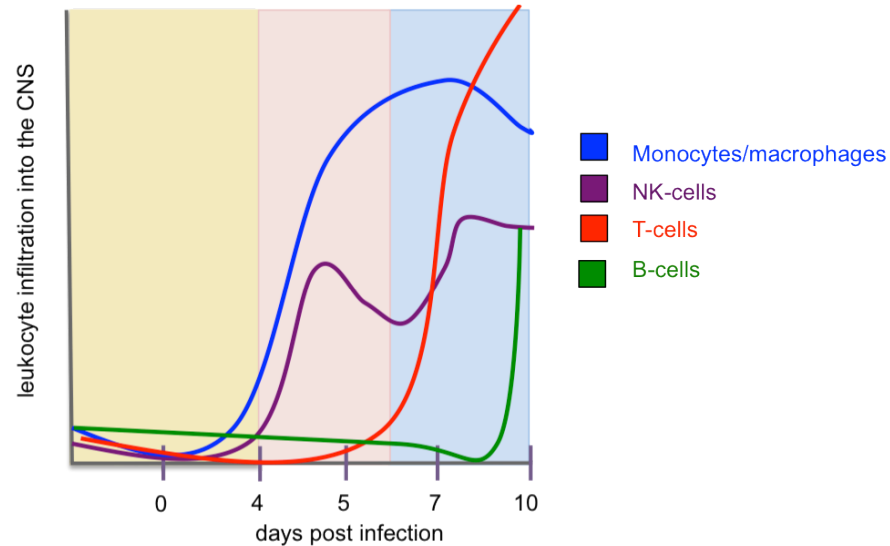


Figure 7.1. Kinetics of leukocyte entry during SFV infection

Mice were infected i.p. with SFV A7(74) for up 10 days. Diagram depicts leukocytes infiltration into the CNS

The accumulation of monocytes and macrophages within the CNS has been shown to play a paradoxical role during the pathogenesis of viral encephalitis. Savarin *et al.* have demonstrated that impaired monocyte recruitment in CCL2 deficient mice regulates trafficking of T-cells across the BBB during viral encephalitis, which subsequently leads to higher viral titers in the brains of infected mice and delays onset of disease (401). Getts *et al.* have shown that the CCL2 dependent infiltration of Ly6C^{hi} inflammatory monocytes during WNV infection is pathogenic and increases mortality (106, 446). Importantly, in many studies of viral encephalitis, the attraction of CCR2⁺Ly6C^{hi} inflammatory monocytes was dependent on CCL2 expression (23). Here it was demonstrated that a shift from Ly6C⁻ to Ly6C⁺ cells occurred between 5 and 7 days post infection, suggesting that Ly6C⁺ cells accumulate increasingly in the brain during later stages of infection. The simultaneous expression of CCL2 in SFV infected brains is in line with the recruitment of CCR2⁺ monocytes and macrophages into the CNS.

The second wave of leukocyte infiltration into the brain during avirulent SFV infection occurred after viral invasion of the brain, and comprised predominantly lymphoid cells. This second wave of leukocyte recruitment was not observed during virulent SFV infection because mice succumbed to the disease beforehand. In addition to lymphoid cells, a small increase of plasmacytoid DCs,

described as CD11b⁺CD11c⁺pDCA⁺ cells, was also observed. These cells are capable of producing large amounts of type-I IFNs (447). Type-I interferons were simultaneously upregulated with the infiltration of pDCs into the brain. Thus, it is possible that these cells contribute to high levels of type-I interferon expression in the brain at this stage of infection. Plasmacytoid DCs have also been observed in the brain during other viral encephalitic infections such as WNV infection or during autoimmune diseases such as EAE or MS (144, 413, 421).

The infiltration of T-cells coincided with high levels of CXCL9 and CXCL10 expression, both of which are ligands for CXCR3. Therefore the role of CXCR3 was investigated here and will be discussed in further detail in section 7.4. During avirulent SFV infection of the brain, a significant increase in CD8⁺ T-cell numbers was observed. However the number of CD4⁺ T-cells was also increased. In general T-cell infiltration into the CNS peaked on PID 10, concomitant with a significant reduction of viral titers and strong chemokine expression in the brain. The expression of CCL5 during SFV and WNV infection correlated with the accumulation of T-cells within the CNS. Thus, it is possible that CCL5 is predominantly expressed by T-cells. This is in agreement with a study by Lane *et al.* which revealed similar results to my findings (129). During L10 infection, T-cells also infiltrated the brain on PID 5 but the majority of the cellular infiltrate consisted mainly of innate immune cells. During A7(74) infection many T-cells were capable of infiltrating deep into the brain parenchyma. T-cell infiltration was observed throughout the brain, whereas Subak-Sharpe *et al.* have observed foci of infection mainly in the cerebellum and corpus callosum of SFV infected mice (310). In support of this, Zhang *et al.* have shown that CXCL10 is differentially expressed in the brain and results in the attraction of T-cells to particular regions of the brain including the cerebellum (375). Thus, these data suggest that different regions of the brain respond differently to viral infection and attract distinct leukocyte subsets.

Previous SFV studies have demonstrated that the T-cell response during SFV infection is pathogenic (378). CD8⁺ T-cells have been shown to be responsible for demyelination through the destruction of infected oligodendrocytes (51, 310). Furthermore it has been demonstrated that the depletion of CD4⁺ T-cells prevents the production of antiviral IgG, and results indirectly in increases of viral titer and neuroinflammation. The depletion of both CD8⁺ and CD4⁺ T-cells

in mice during SFV infection has been reported to prevent the development of CNS inflammation. Importantly, T-cells have been shown to be dispensable for viral clearance of SFV in the CNS (310). This is in contrast to studies using WNV as a model of infection where it has been demonstrated that T-cells are important for viral clearance and decrease of neuroinflammation (321). Further analysis of the data presented here revealed that most T-cells were effector T-cells, and most of the T-cells expressed the chemokine receptors CXCR3 and CCR5. This is in agreement with results obtained by TLDA, showing high expression of the appropriate ligands prior to maximal T-cell infiltration.

B-cells were detectable in the SFV infected brain by PID 10 and coincided with high expression of the chemokine receptor CXCR5 which is mainly expressed on B-cells. Before PID 10, B-cells were not detectable in the CNS. In this study mononuclear cell infiltration was not measured after PID 10 but a study by Morris *et al.* has demonstrated that B-cell numbers within the CNS of SFV infected mice were high between post infection day 14-21, although B-cells were already detectable in the brain by PID 7 (307). Immunoglobulin IgG is very important for the clearance of virus in the CNS while IgM is pivotal for the clearance of viremia (51, 298, 311). Antibody secreting cells have also been detected in the CNS during other alphavirus infections using Sindbis-virus (SINV) as a model of infection. (441).

Overall, these data suggest that chemokines are highly and selectively upregulated during viral encephalitis. The chemokine expression pattern appears to be similar regardless of the pathogen used, facilitating the identification of therapeutic targets for the treatment of viral encephalitis. Chemokine expression coincided with increase in viral titers and leukocyte recruitment to the CNS. Despite recent reports that leukocyte entry during SFV infection is pathogenic, a clear conclusion from these data cannot be drawn yet.

7.3 Cytokine expression patterns during SFV and WNV infection

The cytokine expression pattern during SFV and WNV infection was similar, suggesting that the expression of these cytokines is not pathogen or cell type specific. Studies using WNV as a model of infection have shown that cytokines

can also be expressed by cells of the CNS (54). Our results demonstrate that a few cytokines are induced early during viral infection including TNF, suggesting that neurons and glial cells are capable of producing TNF. A study by Wang *et al.* has demonstrated that the expression of TNF is mediated by TLR-3, and that this cytokine is involved in the break-down of the BBB (448). TNF is not only highly induced in SFV infected brains but also in WNV infected brains. A study conducted by Shrestha *et al.* has reported that TNF deficient mice exhibit higher mortality and increased viral titers in the brain, associated with reduced numbers of CD8⁺ T-cells and macrophages within the CNS (87). Thus, TNF is important for controlling the pathogenesis of WNV induced encephalitis. Generally most other cytokines such as IFNs, IL-1 β and IL-6 appear to be expressed concomitantly with increased infiltration of leukocytes into the CNS of A7(74) infected mice, between PID 7 and PID 10, suggesting that leukocytes are the main source of cytokines released.

The expression of IFNs was strongly induced during SFV and WNV infection. However the magnitude of IFN expression was several-fold higher during virulent infection of the CNS. Levels of IFNs were very low in control mice, and were significantly increased after virus entry into the brain. The upregulation of type-I IFN parallels the increase of viral titers within the brain, peaking by PID 7. This is agreement with previous results demonstrating that IFN-production after infection with SFV increases concomitantly with viral titers (65). SFV is highly susceptible to IFN production and it has been demonstrated that mice deficient for type-I interferon receptor succumbed to SFV infection rapidly, and displayed augmented viral titers throughout the body, suggesting that type-I interferon is protecting mice from widespread infection and reducing mortality (65). During WNV infection type-I interferons peaked on PID 6 when viral titers reached maximal levels, and this induction of expression is similar to IFN expression during SFV infection. WNV infected mice lacking the type-I interferon receptor exhibit uncontrolled viral replication, rapid entry of virus into the brain and enhanced mortality, suggesting an antiviral role of type-I interferon during WNV infection (344). As mentioned before one of the sources of type-I interferon could be pDCs which infiltrate the brain during viral encephalitis (144). Furthermore Longhini *et al.* have shown that pDCs secrete high amounts of IFN- α (413). These cells have been detected during SFV infection by PID 7. Another

increase of type-I IFN could be achieved through the activation of IRF genes within neurons and glial cells (62). For example IRF7 was induced in the SFV infected brain prior to IFN production. Other IRFs and transcription factors can also induce the production of type-I IFN. Generally IFNs are reported to be important for viral clearance and induction of CXCL9 and CXCL10 during alphavirus infection (378, 449).

IFN- γ is only upregulated during later time points correlating with the high induction of CXCL9 expression. This is in agreement with a study by Muller et al. who have shown that only IFN- γ , and not IFN α or IFN- β , induces CXCL9 expression. NK-cells and CD8⁺ T-cells produce high levels of IFN- γ , both of which infiltrate the brain during SFV and WNV infection. The depletion of IFN- γ has been shown to have no effect on the susceptibility of mice to SFV infection (66). This is in contrast to another study using IFN- γ ^{-/-} or IFN- γ receptor deficient mice infected with WNV. These mice display enhanced viral titers in the blood, widespread dissemination of virus, and exhibit more rapid entry of virus into the CNS (347). Importantly in both studies leukocyte recruitment into the CNS was not altered in SFV and WNV infected mice, suggesting that IFN- γ is not important for the migration of leukocytes but is pivotal for antiviral immune responses such as virus clearance.

In response to viral replication, the expression of ISGs was also highly induced during SFV L10 infection along with the expression of cytokines and innate immunity genes. The upregulation of ISGs during WNV infection was not assessed in this thesis but previous studies reported that ISGs are highly induced in the CNS in response to infection (72, 450). The expression of ISGs has been shown to differ within infected neurons, and the expression of OAS1 and Mx1, which were both upregulated during SFV infection, have been associated with increased risk of developing severe forms of WNV encephalitis (363).

Altogether these data suggest that cytokines and ISGs are strongly induced during SFV and WNV infection, and that they often exert antiviral functions rather than modulating the recruitment of leukocytes to the CNS. Cells of the CNS can express many cytokines but the late and strong induction of cytokines suggests that the cellular sources are probably infiltrating leukocytes.

7.4 The role of chemokine antagonists during the pathogenesis of SFV and WNV infection of the CNS

After identification of key chemokines upregulated during SFV infection, the role of the CCR2, CCR5 and CXCR3 axes during viral encephalitis was determined using small molecule inhibitors instead of gene deficient mice. The advantage of antagonists over gene deficient mice is that chemokine receptor functions can be blocked at any stage of the disease. In this thesis the antagonists were administered to mice on the day when virus started to invade the CNS, and therefore initial host immune responses to the virus were not altered using antagonists.

These three selected chemokine receptors bind the major upregulated chemokines during SFV infection. In chapters 3 and 4 it was shown that chemokine expression coincided with leukocyte recruitment within the brain, and therefore it was hypothesised that blocking one of the chemokine receptors CCR2, CCR5 or CXCR3 would result in impaired leukocyte infiltration and would change pathogenesis of virulent infection. Interestingly, viral titers were unaffected by the blockade of chemokine receptors, suggesting that viral load is not directly related to pathogenesis and cellular immune responses. The presence of IgG has been shown to be the determining factor for viral clearance during SFV infection (51). A similar result has been found during studies of SINV infection (123, 451). Christensen *et al.* have demonstrated that MHV infected mice, deficient for CXCL10 or CXCR3, experienced no reduction in viral titers despite reduced leukocyte numbers entering the brains of these mice (322).

Also of note is that chemokine expression patterns in the CNS of chemokine receptor blocker treated mice were not significantly different from untreated mouse brains. This is in contrast to a previous study which has reported that CCL2 ligands are more strongly expressed in the brains of CCR2 receptor deficient mice (214). It remains unclear why this is the case. Despite unaffected viral titers and similar chemokine expression levels in the CNS of treated and untreated mice, chemokine receptor blockers were capable of reducing the number of infiltrating leukocytes. This suggests that these antagonists specifically block recruitment of leukocyte subsets, although this does not result in antiviral properties.

The chemokine receptor CCR2 has been shown to be important for the exit of monocytes from the bone marrow (24). Furthermore ‘inflammatory’ monocytes exhibit high expression of CCR2 and are rapidly recruited to the site of inflammation during infection (20, 213). Getts *et al.* have shown that the majority of monocytes recruited to the brain during viral encephalitis are CCR2⁺ monocytes (106). Furthermore the authors have shown that the recruitment of CCR2⁺ monocytes to the brain is pathogenic, as depletion of CCL2, a specific ligand for CCR2, resulted in prolonged survival. This is in contrast to another study which has demonstrated that loss of CCR2 results in increased mortality (346). Using CCR2 deficient mice I demonstrated that mortality was not significantly different compared to wild type infected mice. Thus, from the L10 data it appears that the recruitment of CCR2⁺ monocytes to the CNS of SFV infected mice does not affect pathogenesis.

To establish a clearer picture regarding the role of monocytes during viral encephalitis, SFV infected mice, using strain A7(74), were treated with the CCR2 antagonist RS504393. The results revealed that the number of leukocytes, and in particular CCR2⁺ monocytes, was significantly reduced in CCR2 blocker treated mice. Furthermore I demonstrated that antagonism of CCR2 did not affect the number of monocytes in the blood. Thus, CCR2 is important for the trafficking of monocytes into the CNS during SFV encephalitis, and is not a consequence of prior monocytopenia. This result is in contrast to a study conducted by Lim *et al.* which has demonstrated that CCR2 is not involved in monocyte trafficking to the CNS during WNV infection, and it was suggested that another chemokine receptor such as CCR5 might be involved at this level (214). The authors have demonstrated that the main determinant for monocyte accumulation in WNV infected brains is the preceding monocytosis. A slight increase in circulating monocyte numbers was also observed in SFV infected mice but this was less profound compared to monocytosis in WNV infected mice.

The chemokine receptor CCR5 has been shown to be an important antiviral and survival determinant during WNV infection (173). In support of this another study has shown that a loss of function mutation of the CCR5 gene in humans correlates with more severe disease development and neuropathology during WNV infection (197). To investigate the role of CCR5 during SFV infection two different antagonists were used. Surprisingly the FDA approved CCR5 antagonist,

referred to as Maraviroc, did not result in a reduction of leukocyte recruitment to the CNS during SFV infection. Maraviroc is a highly efficient drug inhibiting entry of HIV into CCR5⁺ cells but from these data it appears that this drug is not efficient in reducing leukocyte recruitment during SFV encephalitis in the mouse (199). The reasons for this are discussed in chapter 6.

Using the other CCR5 blocker, referred to as DAPTA, leukocytes were only minimally reduced but the number and proportion of CCR5⁺ cells was significantly and highly reduced in DAPTA treated mice. Thus, DAPTA is efficient in blocking CCR5⁺ cell recruitment. However, it appears from my data that CCR5 plays a subordinate role in the attraction of leukocytes during SFV encephalitis. For example CCR2 and CXCR3 blockade were more efficient in reducing leukocyte recruitment compared to CCR5 blockade. In support of this, other studies using LCMV or MHV as models of infection have demonstrated that viral titers and mortality are not enhanced in CCR5 deficient mice compared to WT mice (319, 382). Thus, the role of CCR5 in the pathogenesis of viral encephalitis and antiviral host defense has only been shown so far for WNV infection (362). However, Glass *et al.* have shown that CCR5 is non-redundant during MHV infection as CCR5 has been shown to promote demyelination during MHV infection. However CCR5 is dispensable for leukocyte recruitment to the CNS during MHV infection (336, 382).

Due to the strong induction of CXCL9 and CXCL10 and high numbers of T-cells infiltrating the brain during SFV infection it was hypothesised that blockade of CXCR3, expressed mainly on T-cells and binding CXCL9 and CXCL10, would result in a significant reduction of T-cells entering the CNS, and in turn lead to more severe onsets of viral encephalitis. Using the CXCR3 antagonist, compound 21, I have demonstrated that the number of leukocytes entering the CNS is highly, and significantly, reduced in treated mice compared to untreated mice. Compared to the other antagonists used, interfering with the CXCR3 axis led to the greatest reduction in leukocyte entry into the CNS during viral encephalitis. Within leukocytes the fraction of CD3⁺ T-cells was strongly reduced after treatment with compound 21.

In particular the number of CD8⁺ T-cells was strongly reduced in treated mice. In support of this, previous studies have shown that the loss of CXCL10 or CXCR3,

using gene deficient mice, results in impaired CD8⁺ T-cell trafficking to the brain and leads to enhanced viral titers and mortality (153, 375). Surprisingly, my data demonstrate that the reduction of T-cells infiltrating the SFV infected brain of CXCR3 blocker treated mice does not reduce viral titers. In support of this, Amor *et al.* have shown that T-cells are pathogenic and are dispensable for viral clearance (51). Subak-Sharpe *et al.* have shown that CD8⁺ T-cells are pivotal for demyelination, and CD4⁺ T-cells are critical for the extent of neuroinflammation (310).

The blockade of CXCR3 also resulted in a reduction of other leukocyte subsets. For instance the number of NK-cells was reduced after treatment with compound 21. A previous study has demonstrated that activated NK-cells also express CXCR3 and are recruited to the CNS in response to viral encephalitis (379). This would explain in part why NK-cell numbers are also reduced in SFV infected mice treated with compound 21. However the antagonism of CXCR3 also resulted in the reduction of numbers of CD11b⁺ myeloid cells which do not express CXCR3. This suggests that recruited T-cells within the CNS trigger the recruitment of other leukocyte subsets that respond to distinct chemotactic cues. T-cells may do this either directly by synthesising chemokines and cytokines themselves, or indirectly by inducing chemokine expression in resident neural cells, which in turn attract leukocyte subsets into the CNS as has been suggested during LCMV infection (154).

Since compound 21 induces such a significant reduction in leukocyte recruitment, the role of this antagonist was also investigated during lethal SFV infection using strain L10. The blockade of CXCR3 did not result in an altered disease outcome, and the original hypothesis was therefore disproven. This result is in contrast to previous studies, using MHV or WNV as model of infection, which have demonstrated that CXCR3 is critical for T-cell accumulation within the infected brain parenchyma, resulting in an altered disease outcome (323, 375). For instance, during WNV infection CXCR3 deficient mice experienced significantly higher mortality compared to WT mice (153, 375). In the case of SFV infection it is possible that the blockade of T-cell entry was not enough to alter mortality. This can be explained by the fact that it was mostly cells of the innate immune response, such as myeloid and NK-cells, which infiltrated the brain prior to the death of mice. Infection with the avirulent strain A7(74)

revealed that T-cells infiltrate the brain at later time points as observed on PID 7 and PID 10. Thus, it is likely that the blockade of CXCR3 was not appropriate, and a blockade of myeloid cells or NK-cells would have been more suitable.

Importantly, the simultaneous blockade of CXCR3 and CCR2 significantly enhanced survival. However CCR2 deficient mice experienced higher mortality. This suggests that the timing of chemokine receptor blockade is important. While CCR2 deficient mice have depleted numbers of circulating monocytes, the pharmacological blockade of CCR2 does not lead to altered numbers of monocytes circulating in the blood. Schall *et al.* have proposed the idea that target selection, time of intervention and functional dose are the key determinants for the development of successful chemokine receptor drugs for treatment of inflammatory diseases (207). Furthermore they have suggested that redundancy of the chemokine network is not the main hurdle for the successful development of drugs but rather the use of ineffective dosing or inappropriate target selection.

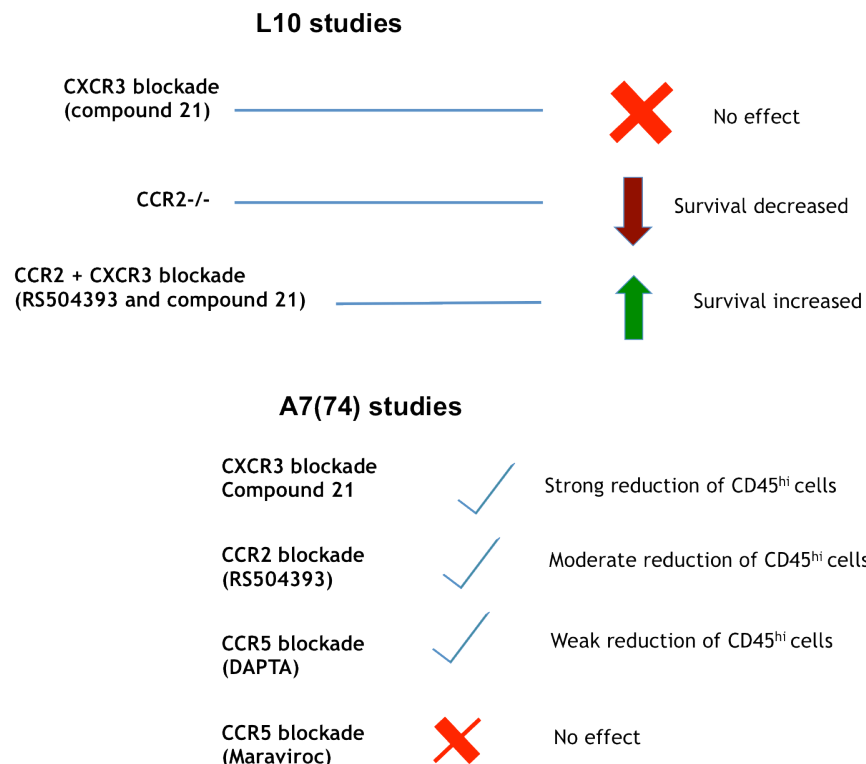


Figure 7.2. The role of chemokine receptor antagonists during SFV infection

Summary of the use of all chemokine receptor antagonists used in this thesis are shown. L10 infections were survival experiments. A7(74) infections were avirulent and the extent of leukocyte infiltration into the virally infected CNS was measured.

Based on the chemokine receptor blocker data no firm conclusions can be drawn about the role of leukocyte infiltration during viral encephalitis. While CCR2 deficient mice exhibit reduced leukocyte infiltration, mortality is not significantly different compared to wild type mice, but the combined blockade of CCR2 and CXCR3 resulted in reduced leukocyte infiltration and enhanced survival. It appears from these data that timing of blockade and target selection are indeed the main determinants, suggesting that leukocyte recruitment can be either beneficial or detrimental depending on the context.

7.5 Conclusions

The aim of this thesis was to identify chemokine receptors as plausible therapeutic targets during viral encephalitis, using SFV as a model of infection. Prior to identification of chemokine receptors as therapeutic targets an extensive analysis of chemokine expression was performed and leukocyte recruitment to the CNS was determined. Based on my data presented here, the following conclusions were reached:

1. Chemokines are selectively and highly upregulated during viral encephalitis regardless of the pathogen used, although the magnitude of chemokine expression was several fold more strongly induced during virulent brain infection. Some chemokines are exclusively upregulated during severe forms of encephalitis.
2. The extent of leukocyte recruitment is dependent on the viral strain used. During SFV infection the first cells entering the brain were cells of the innate immune system, followed by lymphoid cells. Compared to other leukocyte subsets, T-cells were capable of infiltrating deep into the brain parenchyma.
3. Chemokine receptor antagonists are efficient in reducing leukocyte recruitment and altering disease outcome despite having no effect on viral titers. The CXCR3 axis was identified as a key instigator of CNS inflammation in response to alphavirus infection, placing it at the top of a hierarchical cascade that is followed by the CCR2 and CCR5 axes.

4. Combined treatment of mice with CCR2 and CXCR3 antagonists resulted in enhanced survival compared to untreated, or CCR2 deficient, mice. Importantly, treatment with CXCR3 blocker alone did not have an effect on disease outcome. Timing, and appropriate target selection, appears to be critical for the treatment of lethal SFV encephalitis.

Overall the data presented in this thesis demonstrate that chemokines are highly, and selectively, upregulated during viral encephalitis coinciding with infiltration of leukocyte subsets, known to express the appropriate chemokine receptors. Chemokine receptor antagonists are highly efficient in reducing leukocyte recruitment and are therefore plausible therapeutic targets in viral encephalitis.

7.6 Future directions

In this thesis I was able to provide some answers regarding the identification of chemokine expression patterns and identification of chemokine receptors as therapeutic target during viral encephalitis. However, whether leukocyte recruitment into the brain is beneficial or detrimental for the pathogenesis, remains to be determined. In future experiments the role of specific leukocyte subsets should be investigated in more detail. For example, neutrophils appear to infiltrate the brain during severe forms of encephalitis, and my results have shown that neutrophil attracting chemokines are only expressed during lethal brain infection using SFV strain L10 and WNV strain NY99. Therefore it would be interesting to further investigate the role of neutrophils during viral encephalitis by depleting these cells in SFV or WNV infected mice, using antibodies or pharmacological blockers.

In chapter 4 I was able to localise some of the leukocytes in the virally infected brain. However the chemokine antibodies (CCR2, CCR5, CXCL9 and CXCL10) for immunohistochemistry using paraffin sections did not work. It would therefore be helpful to use in-situ hybridisation in future experiments to localise chemokine expression within the brain. Of particular interest is if the majority of chemokines are produced by neurons, glial cells or leukocytes entering the blood during viral encephalitis. Additionally, in future experiments I would like

to perform IHC in L10 infected brains to localise leukocytes and virus within the infected CNS.

Due to time constraints I was not able to examine the effect of CCR2 blockade alone on survival during SFV L10 infection. Although survival experiments using CCR2 deficient were conducted, it is possible that CCR2 blockade will result in a different disease outcome, as combined blocking with CXCR3 has proven to be beneficial for survival.

Since I have proposed the idea that the dose of Maraviroc in this experiment was too low during treatment of SFV infected mice, it would be interesting to test a higher dose of this drug. Maraviroc is an already approved CCR5 blocker, and therefore it would be interesting to test its effect during viral encephalitis.

Furthermore, the timing and dosing of the drug appear to be key to successful therapeutic intervention. In future experiments it should be investigated if timing is indeed such a crucial factor. Perhaps the drug could be given at various time points post infection or beforehand.

Lastly, in this study only 3 chemokine receptor antagonists have been investigated. It would be interesting to determine if other chemokine receptor antagonists display similar efficiency in reduction of leukocyte recruitment. For instance the role of CCR1, CCR3 or CXCR2, binding to major upregulated chemokines during SFV and WNV infection, could be determined. Several CCR1 antagonists have been developed and are currently tested in clinical trial for the treatment of chronic inflammatory diseases such as rheumatoid arthritis or psoriasis (452, 453). It is possible that these blockers are also efficient in the treatment of viral encephalitis. Future research will undoubtedly uncover new and exciting roles for chemokines and their receptors in the treatment of viral encephalitis.

Appendix

1 A

Gene	Accession number
CCL2	Ccl2-Mm00441242_m1
CCL3	Ccl3-Mm99999057_m1
CCL4	Ccl4-Mm00443112_m1
CCL5	Ccl5-Mm01302427_m1
CCL7	Ccl7-Mm00443113_m1
CCL8	Ccl8-Mm01297183_m1
CCL11	Ccl11-Mm00441238_m1
CCL20	Ccl20-Mm01268754_m1
CXCL1	Cxcl1-Mm00433859_m1
CXCL2	Cxcl2-Mm00436450_m1
CXCL3	Cxcl3-Mm01701838_m1
CXCL5	Cxcl5-Mm00436451_g1
CXCL9	Cxcl9-Mm00434946_m1
CXCL10	Cxcl10-Mm00445235_m1
CXCL12	Cxcl12-Mm00445553_m1
CXCL16	Cxcl16-Mm00469712_m1
CX3CL1	Cx3cl1-Mm00436454_m1
IL1- β	Il1b-Mm00434228_m1
IL-6	Il6-Mm01210733_m1
IL-10	Il10-Mm00439616_m1
IFN- α	Ifna4-Mm00833969_s1
IFN- β	Ifnb1-Mm00439552_s1
IFN- κ	Ifnk-Mm02529417_s1
IFN- ϵ	Ifne-Mm00616542_s1
TNF	Tnf-Mm00443258_m1
TGF- β	Tgfb1-Mm03024053_m1
IRF7	Irf7-Mm00516788_m1
RIG-I	Ddx58-Mm00554529_m1
FGF2	Fgf2-Mm01285715_m1
CD45	Ptprc-Mm00448490_m1
TBP	Tbp-Mm00446971_m1
18S	18S-Hs99999901_s1

1 B

Gene	Accession number
CCL1	Ccl1-Mm00441236_m1
CCL2	Ccl2-Mm00441243_g1
CCL3	Ccl3-Mm00441259_g1
CCL4	Ccl4-Mm00443111_m1
CCL5	Ccl5-Mm01302428_m1
CCL6	Ccl6-Mm01302419_m1
CCL7	Ccl7-Mm01308393_g1
CCL8	Ccl8-Mm01297184_g1
CCL9	Ccl9-Mm00441260_m1
CCL11	Ccl11-Mm00441238_m1
CCL12	Ccl12-Mm01211783_g1
CCL17	Ccl17-Mm01244826_g1
CCL19	Ccl19-Mm00839967_g1
CCL20	Ccl20-Mm01268754_m1
CCL21	Ccl21a;Ccl21b;Gm1987;Gm13304;Gm10591;Ccl21c-Mm03646971_gH
CCL22	Ccl22-Mm00436439_m1
CCL24	Ccl24-Mm00444701_m1
CCL25	Ccl25-Mm00436443_m1
CCL26	Ccl26-Mm04204096_m1
CCL27	Ccl27a;Gm2506;Ccl27b;Gm13306-Mm01215829_m1
CCL28	Ccl28-Mm00445039_m1
CX3CL1	Cx3cl1-Mm00436454_m1
CXCL1	Cxcl1-Mm00433859_m1
CXCL2	Cxcl2-Mm00436450_m1
CXCL3	Cxcl3-Mm01701838_m1
CXCL5	Cxcl5-Mm00436451_g1
CXCL9	Cxcl9-Mm00434946_m1
CXCL10	Cxcl10-Mm00445235_m1
CXCL12	Cxcl12-Mm00445553_m1
CXCL13	Cxcl13-Mm01208154_g1
CXCL14	Cxcl14-Mm00444699_m1
CXCL15	Cxcl15-Mm00441263_m1
CXCL16	Cxcl16-Mm00469712_m1
CXCL17	Cxcl17-Mm00463791_m1
XCL1	Xcl1-Mm00434772_m1
IL-1 β	Il1b-Mm00434228_m1
IL-4	Il4-Mm00445260_m1
IL-6	Il6-Mm99999064_m1
IL-10	Il10-Mm01288386_m1
IFN- α	Ifna4-Mm00833969_s1
IFN- β	Ifnb1-Mm00439552_s1
IFN- γ	Ifng-Mm01168133_g1

Gene	Accession number
TNF	Tnf-Mm00443259_g1
TGF- β	Tgfb1-Mm00441729_g1
IRF3	Irf3-Mm01203177_m1
IRF7	Irf7-Mm00516788_m1
MDA5	Ifih1-Mm00459183_m1
Ifit-1	Ifit1-Mm00515153_m1
RIG-I	Ddx58-Mm00554529_m1
PKR	Eif2ak2-Mm00440966_m1
ISG15	Isg15-Mm01705338_s1
ISG20	Isg20-Mm00469585_m1
MX-1	Mx1-Mm00487796_m1
Oas1a	Oas1a-Mm00836412_m1
Viperin	Rsad2-Mm00491265_m1
Zc3hav1	Zc3hav1-Mm00512227_m1
TLR3	Tlr3-Mm00628112_m1
TLR7	Tlr7-Mm00446590_m1
CD207	Cd207-Mm00523545_m1
CD209a	Cd209a-Mm00460067_m1
cAMP	Camp-Mm00438285_m1
Krtap	Krtap16-5-Mm00652413_s1
eIF3f	Eif3f-Mm00517953_m1
18S	18S-Hs99999901_s1

Appendix 1. Genes selected for TaqMan low density array (TLDA)

(A) 32 genes or (B) 62 genes selected for TLDA analysis. On the left: gene names; on the right: accession number taken from the gene database for the gene assayed.

2 A

sample number	virus strain used	RIN value
control 1	A7(74)	10
control 2	A7(74)	10
control 3	A7(74)	9.9
control 4	A7(74)	8.6
PID3 1	A7(74)	9.8
PID3 2	A7(74)	8.1
PID3 3	A7(74)	9.7
PID3 4	A7(74)	9.8
PID4 1	A7(74)	9.5
PID4 2	A7(74)	9.9
PID4 3	A7(74)	9.2
PID4 4	A7(74)	8.4
PID5 1	A7(74)	8.9
PID5 2	A7(74)	8.5
PID5 3	A7(74)	9.1
PID5 4	A7(74)	9.6
PID7 1	A7(74)	9.3
PID7 2	A7(74)	9.4
PID7 3	A7(74)	9.3
PID7 4	A7(74)	9.2
PID7 5	A7(74)	8.9
PID10 1	A7(74)	8.6
PID10 2	A7(74)	9.4
PID10 3	A7(74)	9.9
PID10 4	A7(74)	9.3
PID10 5	A7(74)	9.3

2 B

sample number	virus strain used	RIN value
control 1	L10	8.5
control 2	L10	8.4
control 3	L10	8.9
PID4 1	L10	9.8
PID4 2	L10	8.7
PID4 3	L10	9.4
symptomatic 1	L10	8.9
symptomatic 2	L10	8.5
symptomatic 3	L10	8.7
symptomatic 4	L10	8.6
symptomatic 5	L10	8.5
symptomatic 6	L10	9.1

2 C

sample number	virus strain used	RIN value
control 1	NY99	8.2
control 2	NY99	8.4
control 3	NY99	8.5
PID2 1	NY99	8.5
PID2 2	NY99	8.8
PID2 3	NY99	8.4
PID4 1	NY99	8.2
PID4 2	NY99	8.1
PID4 3	NY99	8.4
PID6 1	NY99	9.1
PID6 2	NY99	8.6
PID6 3	NY99	8.8

Appendix 2. RNA quality measurements from SFV A7(74) and L10, and WNV samples

Prior to TLDA analysis, the RNA quality of (A) SFV A7(74), (B) SFV L10 and (C) WNV brain samples was measured using the Agilent Bioanalyser. The sample name, virus strain and RNA integrity number (RIN) are shown in the table. RIN>8 =high quality RNA. (A and B) Mice were infected i.p. (C) Mice were infected intranasally. PID= post infection day

A7/74

L10

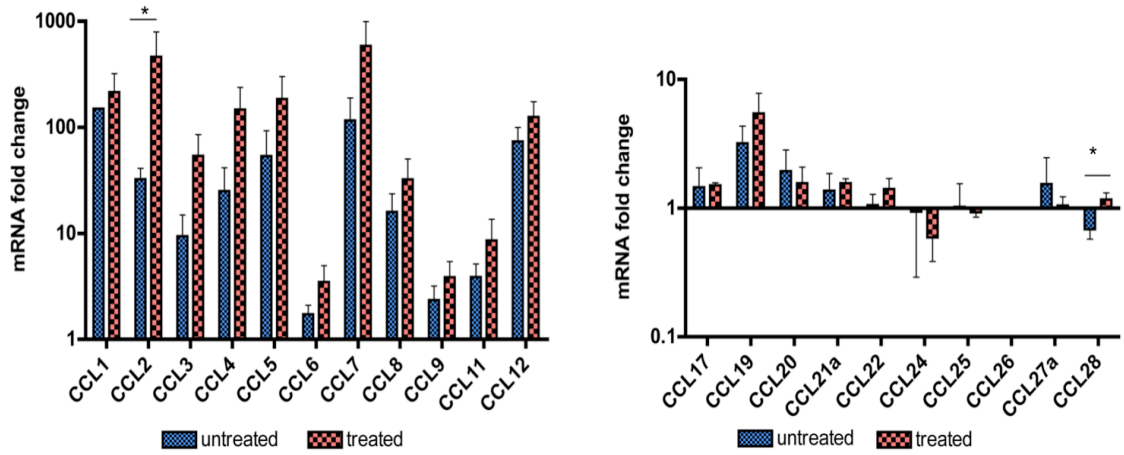
Gene	PID 3	PID 4	PID 5	PID 7	PID 10	asymptomatic	symptomatic
CCL1	ND	ND	ND	ND	ND	ND	70.321
CCL2	1.6	2.5	11.9	93.4	55.7	60.2	3094.1
CCL3	1.8	4.3	5.4	37.2	22.7	1.8	216.7
CCL4	1.6	0.5	2.6	24.4	13.5	4.6	532.9
CCL5	2.3	1.6	8.6	98.4	181.2	17.5	965.0
CCL7	1.3	1.3	5.9	42.1	33.8	47.7	2146.9
CCL8	2.0	1.3	3.5	21.2	54.4	4.7	212.7
CCL11	1.3	1.6	1.6	2.5	1.4	1.8	37.5
CCL20	ND	ND	ND	ND	ND	1.9	21.8
CXCL1	0.8	0.0	0.8	1.7	62.5	4.9	188.0
CXCL2	ND	ND	ND	ND	ND	7.4	2286.9
CXCL3	ND	ND	ND	ND	ND	3.0	215.7
CXCL5	0.7	0.4	0.7	0.9	0.8	1.3	2.6
CXCL9	1.8	3.8	12.0	301.5	211.6	44.2	3778.3
CXCL10	6.9	12.3	91.2	487.7	147.7	88.1	2683.5
CXCL12	0.8	0.7	0.8	0.6	0.8	1.0	0.9
CXCL16	1.1	1.4	1.6	8.1	11.7	2.2	26.0
CX3CL1	1.0	0.9	0.9	0.7	0.6	1.1	1.0
IL1-β	0.8	0.5	0.8	5.3	4.0	4.3	179.8
IL-6	0.5	0.2	0.9	2.7	1.0	9.2	732.1
IL-10	ND	ND	ND	ND	ND	1.9	466.1
IFN- α	ND	ND	ND	ND	ND	2.6	1237.2
IFN-β	ND	ND	ND	ND	ND	13.8	6349.0
IFN- κ	2.4	1.3	1.6	1.9	1.2	-	-
IFN- ϵ	1.7	0.1	1.0	0.7	1.0	-	-
TNF	2.6	2.8	8.2	56.9	66.9	20.3	1636.8
TGF-β	ND	ND	ND	ND	ND	1.4	4.1
IRF7	9.6	6.5	12.7	32.1	21.6	44.8	460.4
RIG-I	2.0	1.2	5.6	11.4	2.3	8.8	85.3
FGF2	0.9	0.9	0.7	0.8	0.5	-	-
CD45	1.2	1.0	1.3	7.3	6.5	-	-

Appendix 3. Comparison of gene expression in the CNS of SFV A7/74 and L10 infected mice

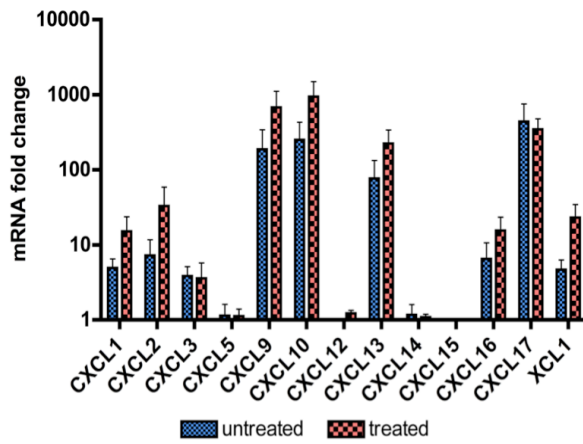
Mice were inoculated i.p with SFV strain A7/74 or L10 and RNA was isolated from infected brains at post infection day (PID) 3, 4, 5, 7 and 10 or shortly before the onset of symptoms (asymptomatic) and at the end stage of the disease (between PID 5-6). The fold change of gene expression compared to an uninfected healthy mouse brain is shown as mean of n=3-6 mice per group. Each sample was tested in triplicate. All samples were normalised to an endogenous control (TBP for A7/74 and Eif3f for L10). ND= not detectable

Appendix 4

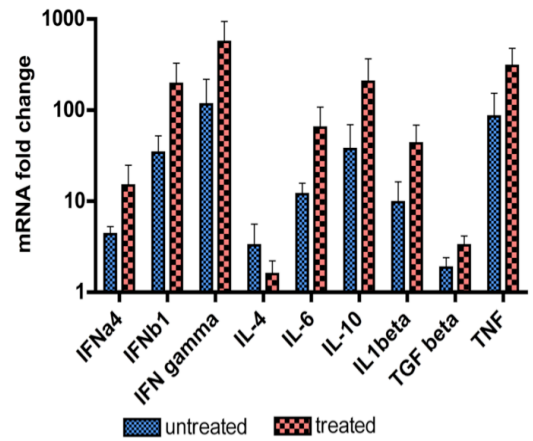
A

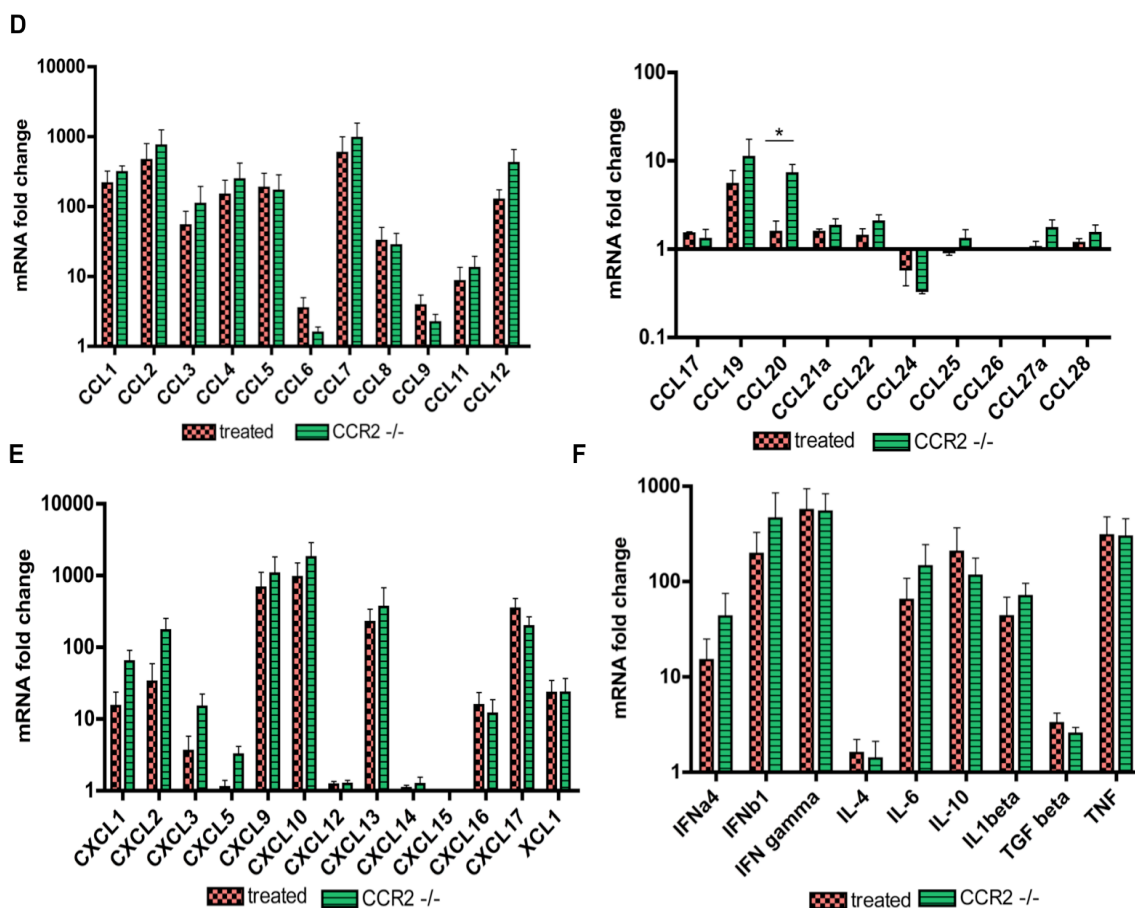


B



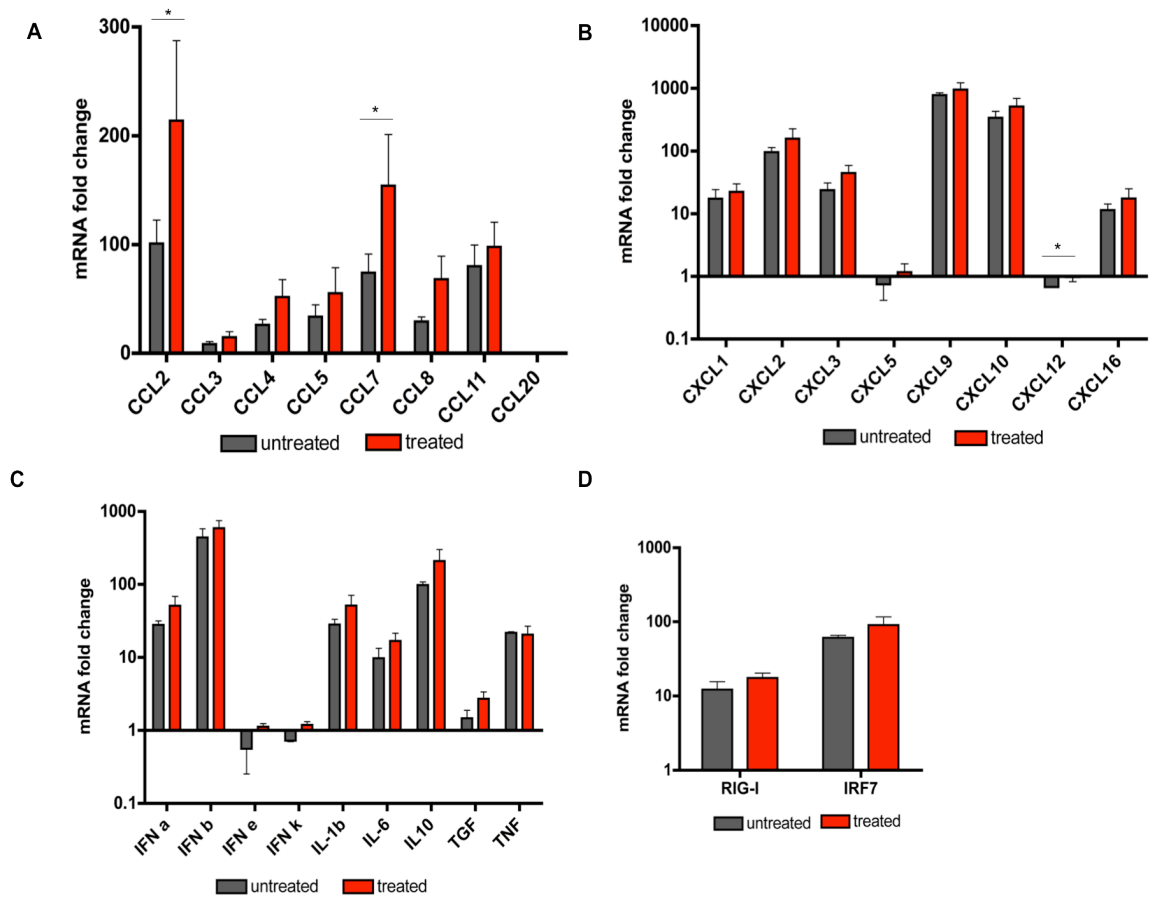
C





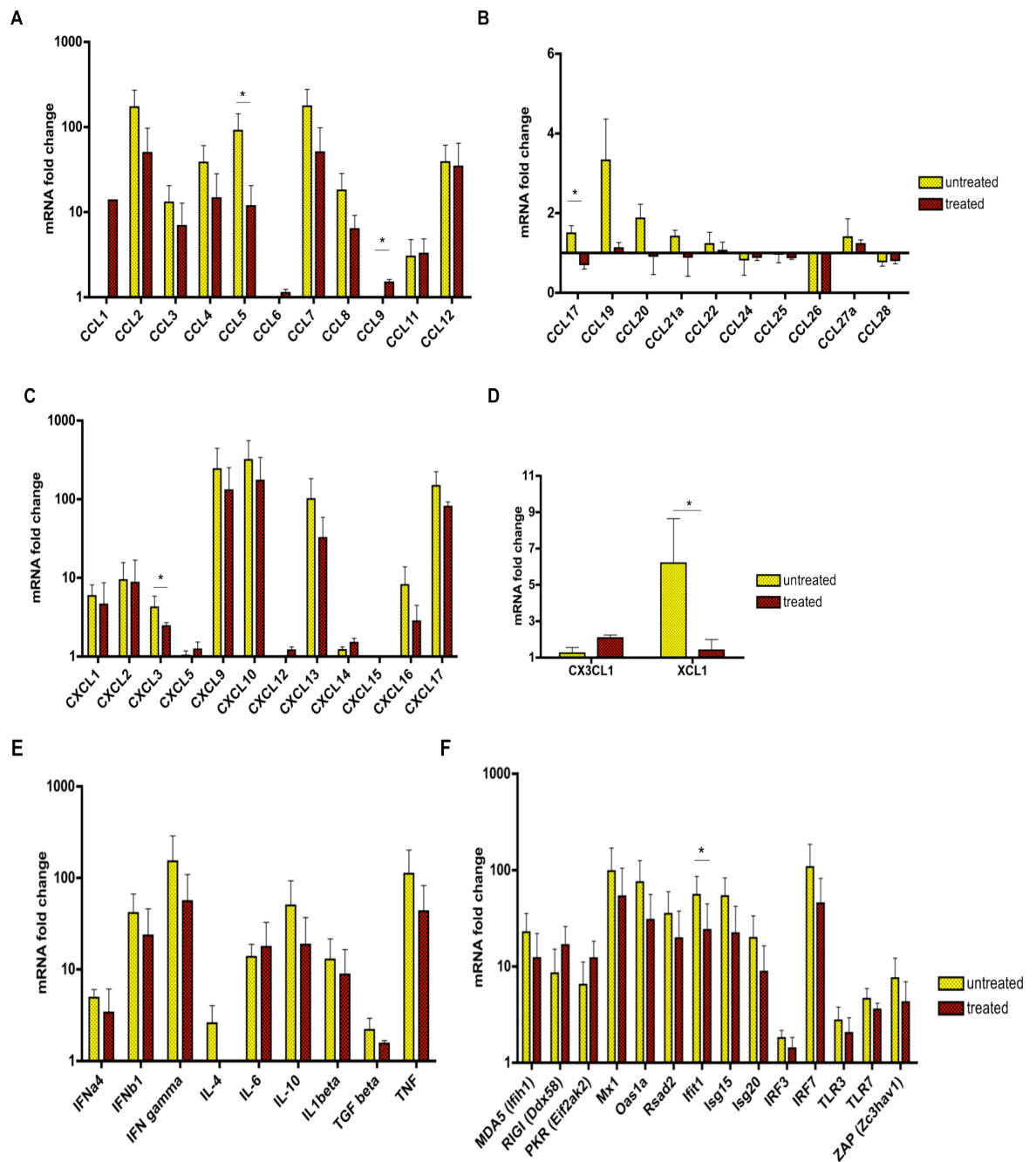
Appendix 4. Chemokine and cytokine expression levels in the CNS of mice with genetic or pharmacological blockage of CCR2

Wild type and CCR2 deficient mice were infected i.p. with SFV strain A7(74) for 7 days and brains were collected for analysis. The expression of chemokines and cytokines was measured by TLDA. Mice were treated twice daily by oral gavage with vehicle (6.6% DMSO in PBS) (untreated and CCR2^{-/-} group) or 5 mg/kg RS504393 (CCR2 blocker) (treated group) between post infection days 3-7. (A and D) CC-chemokine expression levels. (B and E) CXC-chemokine and (C and F) cytokine expression levels. Each gene was double normalised to an endogenous control Eif3f, and to an uninfected healthy control brain. The mRNA fold change compared to healthy controls is depicted on the y-axis. Data are shown as mean \pm SD, n=3 mice per time point. Each gene was tested in triplicate. (student's t-test; * p<0.05)



Appendix 5. Chemokine and cytokine expression levels in the CNS of mice after pharmacological blockage of CCR5

Mice were infected i.p. with SFV strain A7(74) for 7 days and brains were collected for analysis. The expression of chemokines and cytokines was measured by TLDA. Mice were treated once daily by s.c. injection with vehicle (water) or 1 mg/kg DAPTA between post infection days 3-7. (A) CC-chemokine and (B) CXC-chemokine expression. (C) Cytokine expression and (D) transcription factor expression levels. Each gene was double normalised to an endogenous control *Eif3f*, and to an uninfected healthy control brain. The mRNA fold change compared to healthy controls is depicted on the y-axis. Data are shown as mean \pm SD, $n=3$ mice per time point. Each gene was tested in triplicate. (student's t-test; * $p<0.05$)



Appendix 6. Chemokine and cytokine expression levels in the CNS of mice after pharmacological blockage of CXCR3

Mice were infected i.p. with SFV strain A7(74) for 7 days and brains were collected for analysis. The expression of chemokines and cytokines was measured by TLDA. Mice were treated once daily by s.c. injection with vehicle (50% DMSO and 25% PEG400 in water) or 10 mg/kg compound 21 (CXCR3 blocker) between post infection days 3-7. (A and B) CC-chemokine, (C) CXC-chemokine and (D) CX₃C and XC chemokine expression levels in the brain. (E) Cytokine expression levels. (F) Expression levels of genes involved in innate immune responses. Each gene was double normalised to an endogenous control *Eif3f*, and to an uninfected healthy control brain. The mRNA fold change compared to healthy controls is depicted on the y-axis. Data are shown as mean \pm SD, n=3 mice per time point. Each gene was tested in triplicate. (student's t-test; * p<0.05)

References

1. **Brandt E, Woerly G, Younes AB, Loiseau S, Capron M.** 2000. IL-4 production by human polymorphonuclear neutrophils. *Journal of Leukocyte Biology* **68**:125-130.
2. **Medzhitov R.** 2002. Decoding the patterns of self and nonself by the innate immune system. *Science* **296**:298-300.
3. **Medzhitov R, Janeway CAJ.** 1997. Innate immunity: the virtues of a nonclonal system of recognition. *Cell* **91**:295-298.
4. **Sunderkötter CC, Nikolic TT, Dillon MJM, Van Rooijen NN, Stehling MM, Drevets DAD, Leenen PJMP.** 2004. Subpopulations of mouse blood monocytes differ in maturation stage and inflammatory response. *J. Immunol.* **172**:4410-4417.
5. **Smet K, Contreras R.** 2005. Human Antimicrobial Peptides: Defensins, Cathelicidins and Histatins. *Biotechnol Lett* **27**:1337-1347.
6. **Ziegler-Heitbrock L, Ancuta P, Crowe S, Dalod M, Grau V, Hart DN, Leenen PJM, Liu YJ, MacPherson G, Randolph GJ, Scherberich J, Schmitz J, Shortman K, Sozzani S, Strobl H, Zembala M, Austyn JM, Lutz MB.** 2010. Nomenclature of monocytes and dendritic cells in blood. *Blood* **116**:74-80.
7. **Schlenner SM, Madan V, Busch K, Tietz A, Laufle C, Costa C, Blum C, Fehling HJ, Rodewald H-R.** 2010. Fate mapping reveals separate origins of T cells and myeloid lineages in the thymus. *Immunity* **32**:426-436.
8. **Walport MJ.** 2001. Complement. First of two parts. *N. Engl. J. Med.* **344**:1058-1066.
9. **Walport MJ.** 2001. Complement. Second of two parts. *N. Engl. J. Med.* **344**:1140-1144.
10. **Medzhitov R.** 2007. Recognition of microorganisms and activation of the immune response. *Nature* **449**:819-826.
11. **Gallucci S, Lolkema M, Matzinger P.** 1999. Natural adjuvants: endogenous activators of dendritic cells. *Nat Med* **5**:1249-1255.
12. **Mantovani B, Rabinovitch M, Nussenzweig V.** 1972. Phagocytosis of immune complexes by macrophages. Different roles of the macrophage receptor sites for complement (C3) and for immunoglobulin (IgG). *J. Exp. Med.* **135**:780-792.
13. **Chen GY, Nuñez G.** 2010. Sterile inflammation: sensing and reacting to damage. *Nat Rev Immunol* **10**:826-837.
14. **Takehita Y, Ransohoff RM.** 2012. Inflammatory cell trafficking across the blood-brain barrier: chemokine regulation and in vitro models. *Immunol Rev* **248**:228-239.
15. **Orkin SH, Zon LI.** 2002. Hematopoiesis and stem cells: plasticity versus developmental heterogeneity. *Nat Immunol* **3**:323-328.
16. **Rothenberg ME, Hogan SP.** 2006. The Eosinophil. *Annu. Rev. Immunol.* **24**:147-174.
17. **Galli SJ, Gordon JR, Wershil BK.** 1991. Cytokine production by mast cells and basophils. *Current Opinion in Immunology* **3**:865-872.
18. **Borregaard N.** 2010. Neutrophils, from marrow to microbes. *Immunity* **33**:657-670.
19. **Borregaard N, Sorensen OE, Theilgaard-Monch K.** 2007. Neutrophil granules: a library of innate immunity proteins. *Trends in Immunology* **28**:340-345.
20. **Shi C, Pamer EG.** 2011. Monocyte recruitment during infection and inflammation. *Nat Rev Immunol* **11**:762-774.
21. **Geissmann F, Manz MG, Jung S, Sieweke MH, Merad M, Ley K.** 2010. Development of Monocytes, Macrophages, and Dendritic Cells. *Science*

- 327:656-661.
22. **Iijima N, Mattei LM, Iwasaki A.** 2011. Recruited inflammatory monocytes stimulate antiviral Th1 immunity in infected tissue. *Proceedings of the National Academy of Sciences* **108**:284-289.
 23. **Terry RL, Getts DR, Deffrasnes C, van Vreden C, Campbell IL, King NJ.** 2012. Inflammatory monocytes and the pathogenesis of viral encephalitis. *Journal of Neuroinflammation* **9**:1-1.
 24. **Geissmann F, Jung S, Littman DR.** 2003. Blood Monocytes Consist of Two Principal Subsets with Distinct Migratory Properties. *Immunity* **19**:71-82.
 25. **Serbina NV, Pamer EG.** 2006. Monocyte emigration from bone marrow during bacterial infection requires signals mediated by chemokine receptor CCR2. *Nat Immunol* **7**:311-317.
 26. **Auffray C, Fogg D, Garfa M, Elain G, Join-Lambert O, Kayal S, Sarnacki S, Cumano A, Lauvau G, Geissmann F.** 2007. Monitoring of blood vessels and tissues by a population of monocytes with patrolling behavior. *Science* **317**:666-670.
 27. **Bick MJ, Carroll JWN, Gao G, Goff SP, Rice CM, MacDonald MR.** 2003. Expression of the Zinc-Finger Antiviral Protein Inhibits Alphavirus Replication. *Journal of Virology* **77**:11555-11562.
 28. **Mosser DM, Edwards JP.** 2008. Exploring the full spectrum of macrophage activation. *Nat Rev Immunol* **8**:958-969.
 29. **Gao G, Guo X, Goff SP.** 2002. Inhibition of retroviral RNA production by ZAP, a CCH-type zinc finger protein. *Science* **297**:1703-1706.
 30. **O'Shea JJ, Murray PJ.** 2008. Cytokine Signaling Modules in Inflammatory Responses. *Immunity* **28**:477-487.
 31. **Dale DC, Boxer L, Liles WC.** 2008. The phagocytes: neutrophils and monocytes. *Blood* **112**:935-945.
 32. **Gordon S.** 2003. Alternative activation of macrophages. *Nat Rev Immunol* **3**:23-35.
 33. **Mildner A, Schmidt H, Nitsche M, Merkler D, Hanisch U-K, Mack M, Heikenwalder M, Brück W, Priller J, Prinz M.** 2007. Microglia in the adult brain arise from Ly-6ChiCCR2+ monocytes only under defined host conditions. *Nat Neurosci* **10**:1544-1553.
 34. **Steinman RM.** 1991. The dendritic cell system and its role in immunogenicity. *Annu. Rev. Immunol.* **9**:271-296.
 35. **Liu K, Nussenzweig MC.** 2010. Origin and development of dendritic cells. *Immunol Rev* **234**:45-54.
 36. **Shortman K, Naik SH.** 2006. Steady-state and inflammatory dendritic-cell development. *Nature* **7**:19-30.
 37. **Iannello A, Debbeche O, Samarani S, Ahmad A.** 2008. Antiviral NK cell responses in HIV infection: I. NK cell receptor genes as determinants of HIV resistance and progression to AIDS. *Journal of Leukocyte Biology* **84**:1-26.
 38. **Ahmad A, Ahmad R.** 2003. HIV“s evasion of host”s NK cell response and novel ways of its countering and boosting anti-HIV immunity. *Curr HIV Res* **1**:295-307.
 39. **Zamai L, Ahmad M, Bennett IM, Azzoni L, Alnemri ES, Perussia B.** 1998. Natural killer (NK) cell-mediated cytotoxicity: differential use of TRAIL and Fas ligand by immature and mature primary human NK cells. *J. Exp. Med.* **188**:2375-2380.
 40. **Sun JC, Lanier LL.** 2011. NK cell development, homeostasis and function: parallels with CD8+ T cells. *Nat Rev Immunol* **11**:645-657.
 41. **Delves PJ, Roitt I.** 2000. The immune system: first of two parts. *N. Engl.*

- J. Med. **343**:37-49.
42. **Broere F, Apasov SG, Sitkovsky MV, van Eden W.** 2011. T cell subsets and T cell-mediated immunity. *Int J Immunopharmacol* **20**:15-27.
 43. **Murphy KM, Reiner SL.** 2002. Decision making in the immune system: The lineage decisions of helper T cells. *Nat Rev Immunol* **2**:933-944.
 44. **Abbas AK, Murphy KM, Sher A.** 1996. Functional diversity of helper T lymphocytes. *Nature* **383**:787-793.
 45. **Sallusto F, Impellizzeri D, Basso C, Laroni A, Uccelli A, Lanzavecchia A, Engelhardt B.** 2012. T-cell trafficking in the central nervous system. *Immunol Rev* **248**:216-227.
 46. **Kristensen NN, Madsen AN, Thomsen AR, Christensen JP.** 2004. Cytokine production by virus-specific CD8+ T cells varies with activation state and localization, but not with TCR avidity. *J. Gen. Virol.* **85**:1703-1712.
 47. **Fazakerley JK, Walker R.** 2003. Virus Demyelination. *J. of Neurovirology* **9**:148-164.
 48. **Salgame P, Abrams JS, Clayberger C, Goldstein H, Convit J, Modlin RL, Bloom BR.** 1991. Differing lymphokine profiles of functional subsets of human CD4 and CD8 T cell clones. *Science* **254**:279-282.
 49. **Allen CDC, Okada T, Cyster JG.** 2007. Germinal-center organization and cellular dynamics. *Immunity* **27**:190-202.
 50. **Kelsoe G.** 1996. The germinal center: a crucible for lymphocyte selection. *Semin. Immunol.* **8**:179-184.
 51. **Amor S, Scallan MF, Morris MM, Dyson H, Fazakerley JK.** 1996. Role of immune responses in protection and pathogenesis during Semliki Forest virus encephalitis. *J. Gen. Virol.* **77 (Pt 2)**:281-291.
 52. **Vilcek J, Feldmann M.** 2004. Historical review: Cytokines as therapeutics and targets of therapeutics. *Trends in Pharmacological Sciences* **25**:201-209.
 53. **Hertzog PJ.** 2012. Overview. Type I interferons as primers, activators and inhibitors of innate and adaptive immune responses. *Immunol. Cell Biol.* **90**:471-473.
 54. **Suthar MS, Diamond MS, Gale M.** 2013. West Nile virus infection and immunity. *Nat Rev Micro* **11**:115-128.
 55. **Cavlar T, Ablasser A, Hornung V.** 2012. Induction of type I IFNs by intracellular DNA-sensing pathways. *Immunol. Cell Biol.* **90**:474-482.
 56. **Isaacs A, Lindenmann J.** 1987. Virus interference. I. The interferon. By A. Isaacs and J. Lindenmann, 1957. *J Interferon Res* **7**:429-438.
 57. **Pestka S, Krause CD, Walter MR.** 2004. Interferons, interferon-like cytokines, and their receptors. *Immunol Rev* **202**:8-32.
 58. **Hacker H, Redecke V, Blagoev B, Kratchmarova I, Hsu L-C, Wang GG, Kamps MP, Raz E, Wagner H, Hacker G, Mann M, Karin M.** 2006. Specificity in Toll-like receptor signalling through distinct effector functions of TRAF3 and TRAF6. *Nature* **439**:204-207.
 59. **Schafer SL, Lin R, Moore PA, Hiscott J, Pitha PM.** 1998. Regulation of type I interferon gene expression by interferon regulatory factor-3. *J Biol Chem* **273**:2714-2720.
 60. **Woodward EM, Christoffersen M, Campos J, Betancourt A, Horohov D, Scoggin KE, Squires EL, Troedsson M.** 2013. Endometrial inflammatory markers of the early immune response in mares susceptible or resistant to persistent breeding-induced endometritis. *Reproduction* **145**:289-296.
 61. **Juang YT, Lowther W, Kellum M, Au WC, Lin R, Hiscott J, Pitha PM.** 1998. Primary activation of interferon A and interferon B gene

- transcription by interferon regulatory factor 3. *Proc. Natl. Acad. Sci. U.S.A.* **95**:9837-9842.
62. **Levy DE, Marie I, Smith E, Prakash A.** 2002. Enhancement and diversification of IFN induction by IRF-7-mediated positive feedback. *J Interferon Cytokine Res* **22**:87-93.
63. **Yeow WS, Au WC, Juang YT, Fields CD, Dent CL, Gewert DR, Pitha PM.** 2000. Reconstitution of virus-mediated expression of interferon alpha genes in human fibroblast cells by ectopic interferon regulatory factor-7. *J Biol Chem* **275**:6313-6320.
64. **Samuel CE.** 2001. Antiviral actions of interferons. *Clinical Microbiology Reviews* **14**:778-809.
65. **Fragkoudis R, Breakwell L, McKimmie CS, Boyd A, Barry G, Kohl A, Merits A, Fazakerley JK.** 2007. The type I interferon system protects mice from Semliki Forest virus by preventing widespread virus dissemination in extraneural tissues, but does not mediate the restricted replication of avirulent virus in central nervous system neurons. *Journal of General Virology* **88**:3373-3384.
66. **Muller U, Steinhoff U, Reis LF, Hemmi S, Pavlovic J, Zinkernagel RM, Aguet M.** 1994. Functional role of type I and type II interferons in antiviral defense. *Science* **264**:1918-1921.
67. **Collins JT, Dunnick WA.** 1993. Germline transcripts of the murine immunoglobulin gamma 2a gene: structure and induction by IFN-gamma. *Int Immunol* **5**:885-891.
68. **Boehm U, Klamp T, Groot M, Howard JC.** 1997. Cellular responses to interferon-gamma. *Annu. Rev. Immunol.* **15**:749-795.
69. **Bosselut R, Kubo S, Guintier T, Kopacz JL, Altman JD, Feigenbaum L, Singer A.** 2000. Role of CD8beta domains in CD8 coreceptor function: importance for MHC I binding, signaling, and positive selection of CD8+ T cells in the thymus. *Immunity* **12**:409-418.
70. **Schoggins JW, Wilson SJ, Panis M, Murphy MY, Jones CT, Bieniasz P, Rice CM.** 2011. A diverse range of gene products are effectors of the type I interferon antiviral response. *Nature* **472**:481-485.
71. **Schoggins JW, Rice CM.** 2011. Interferon-stimulated genes and their antiviral effector functions. *Current Opinion in Virology* **1**:519-525.
72. **Jiang D, Weidner JM, Qing M, Pan X-B, Guo H, Xu C, Zhang X, Birk A, Chang J, Shi P-Y, Block TM, Guo J-T.** 2010. Identification of five interferon-induced cellular proteins that inhibit west nile virus and dengue virus infections. *Journal of Virology* **84**:8332-8341.
73. **Zhang Y, Burke CW, Ryman KD, Klimstra WB.** 2007. Identification and Characterization of Interferon-Induced Proteins That Inhibit Alphavirus Replication. *Journal of Virology* **81**:11246-11255.
74. **Toth AM, Zhang P, Das S, George CX, Samuel CE.** 2006. Interferon action and the double-stranded RNA-dependent enzymes ADAR1 adenosine deaminase and PKR protein kinase. *Prog Nucleic Acid Res Mol Biol* **81**:369-434.
75. **Ghosh SK, Kusari J, Bandyopadhyay SK, Samanta H, Kumar R, Sen GC.** 1991. Cloning, sequencing, and expression of two murine 2'-5'-oligoadenylate synthetases. Structure-function relationships. *J Biol Chem* **266**:15293-15299.
76. **Zhou A, Hassel BA, Silverman RH.** 1993. Expression cloning of 2-5A-dependent RNAase: a uniquely regulated mediator of interferon action. *Cell* **72**:753-765.
77. **Stranden AM, Staeheli P, Pavlovic J.** 1993. Function of the mouse Mx1

- protein is inhibited by overexpression of the PB2 protein of influenza virus. *Virology* **197**:642-651.
78. Kochs G, Janzen C, Hohenberg H, Haller O. 2002. Antivirally active MxA protein sequesters La Crosse virus nucleocapsid protein into perinuclear complexes. *Proc. Natl. Acad. Sci. U.S.A.* **99**:3153-3158.
 79. Saitoh T, Satoh T, Yamamoto N, Uematsu S, Takeuchi O, Kawai T, Akira S. 2011. Antiviral protein Viperin promotes Toll-like receptor 7- and Toll-like receptor 9-mediated type I interferon production in plasmacytoid dendritic cells. *Immunity* **34**:352-363.
 80. Muller S, Moller P, Bick MJ, Wurr S, Becker S, Gunther S, Kummerer BM. 2007. Inhibition of filovirus replication by the zinc finger antiviral protein. *Journal of Virology* **81**:2391-2400.
 81. Katze MG, He Y, Gale M. 2002. Viruses and interferon: a fight for supremacy. *Nature* **2**:675-687.
 82. Goodbourn S, Didcock L, Randall RE. 2000. Interferons: cell signalling, immune modulation, antiviral response and virus countermeasures. *J. Gen. Virol.* **81**:2341-2364.
 83. Medzhitov R, Janeway CJ. 2000. Innate immunity. *N. Engl. J. Med.* **343**:338-344.
 84. Smith CA, Davis T, Anderson D, Solam L, Beckmann MP, Jerzy R, Dower SK, Cosman D, Goodwin RG. 1990. A receptor for tumor necrosis factor defines an unusual family of cellular and viral proteins. *Science* **248**:1019-1023.
 85. Schütze S, Wiegmann K, Machleidt T, Krönke M. 1995. TNF-Induced Activation of NF- κ B. *Immunobiology* **193**:193-203.
 86. Chen C-J, Ou Y-C, Chang C-Y, Pan H-C, Liao S-L, Raung S-L, Chen S-Y. 2011. TNF- α and IL-1 β mediate Japanese encephalitis virus-induced RANTES gene expression in astrocytes. *Neurochemistry International* **58**:234-242.
 87. Shrestha B, Zhang B, Purtha WE, Klein RS, Diamond MS. 2008. Tumor necrosis factor alpha protects against lethal West Nile virus infection by promoting trafficking of mononuclear leukocytes into the central nervous system. *Journal of Virology* **82**:8956-8964.
 88. Zhang B, Patel J, Croyle M, Diamond MS, Klein RS. 2010. TNF-alpha-dependent regulation of CXCR3 expression modulates neuronal survival during West Nile virus encephalitis. *Journal of Neuroimmunology* **224**:28-38.
 89. Ransohoff RM, Kivisäkk P, Kidd G. 2003. Three or more routes for leukocyte migration into the central nervous system. *Nat Rev Immunol* **3**:569-581.
 90. Rivest S. 2009. Regulation of innate immune responses in the brain. *Nat Rev Immunol* **9**:429-439.
 91. Decimo I, Fumagalli G, Berton V, Krampera M, Bifari F. 2012. Meninges: from protective membrane to stem cell niche. *Am J Stem Cells* **1**:92-105.
 92. Jacobson S, Marcus EM. 2008. Neuroanatomy. *Journal of Neuroinflammation* **23**: 186-205.
 93. Ransohoff RM, Engelhardt B. 2012. The anatomical and cellular basis of immune surveillance in the central nervous system. *Nat Rev Immunol* **12**:623-635.
 94. Jessen KR. 2004. Glial cells. *Int J Biochem Cell Biol* **36**:1861-1867.
 95. Yang N, Ng YH, Pang ZP, Südhof TC, Wernig M. 2011. Induced neuronal cells: how to make and define a neuron. *Cell Stem Cell* **9**:517-525.
 96. Crossman AR, Neary D. 2010. *Neuroanatomy*. Elsevier Churchill

- Livingstone.
97. **Nishiyama A, Komitova M, Suzuki R, Zhu X.** 2009. Polydendrocytes (NG2 cells): multifunctional cells with lineage plasticity. *Nat Rev Neurosci* **10**:9-22.
 98. **Freeman MR.** 2010. Specification and Morphogenesis of Astrocytes. *Science* **330**:774-778.
 99. **Sorg BA, Smith MM, Campagnoni AT.** 1987. Developmental expression of the myelin proteolipid protein and basic protein mRNAs in normal and dysmyelinating mutant mice. *J. Neurochem.* **49**:1146-1154.
 100. **Ginhoux F, Greter M, Leboeuf M, Nandi S, See P, Gokhan S, Mehler MF, Conway SJ, Ng LG, Stanley ER, Samokhvalov IM, Merad M.** 2010. Fate mapping analysis reveals that adult microglia derive from primitive macrophages. *Science* **330**:841-845.
 101. **Ransohoff RM.** 2007. Microgliosis: the questions shape the answers. *Nat Neurosci.* **10**; 1507-1509
 102. **David S, Kroner A.** 2011. Repertoire of microglial and macrophage responses after spinal cord injury. *Nat Rev Neurosci* **12**:388-399.
 103. **Pineau I, Lacroix S.** 2007. Proinflammatory cytokine synthesis in the injured mouse spinal cord: multiphasic expression pattern and identification of the cell types involved. *J. Comp. Neurol.* **500**:267-285.
 104. **Kaushal V, Schlichter LC.** 2008. Mechanisms of microglia-mediated neurotoxicity in a new model of the stroke penumbra. *J Neurosci* **28**:2221-2230.
 105. **Kaushal V, Koeberle PD, Wang Y, Schlichter LC.** 2007. The Ca²⁺-activated K⁺ channel KCNN4/KCa3.1 contributes to microglia activation and nitric oxide-dependent neurodegeneration. *J Neurosci* **27**:234-244.
 106. **Getts DR, Terry RL, Getts MT, Müller M, Rana S, Shrestha B, Radford J, Van Rooijen N, Campbell IL, King NJC.** 2008. Ly6c⁺ “inflammatory monocytes” are microglial precursors recruited in a pathogenic manner in West Nile virus encephalitis. *J. Exp. Med.* **205**:2319-2337.
 107. **Raivich G, Bohatschek M, Kloss CU, Werner A, Jones LL, Kreutzberg GW.** 1999. Neuroglial activation repertoire in the injured brain: graded response, molecular mechanisms and cues to physiological function. *Brain Res Brain Res Rev* **30**:77-105.
 108. **Pardridge WM.** 1999. Blood-brain barrier biology and methodology. *J. of Neurovirology.*
 109. **Tontsch U, Bauer HC.** 1991. Glial cells and neurons induce blood-brain barrier related enzymes in cultured cerebral endothelial cells. *Brain Res.* **539**:247-253.
 110. **Chaudhuri JD.** 2000. Blood brain barrier and infection. *Med Sci Monit* **6**:1213-1222.
 111. **de Boer AG, Gaillard PJ.** 2006. Blood-brain barrier dysfunction and recovery. *J Neural Transm* **113**:455-462.
 112. **Del Zoppo GJ, Milner R, Mabuchi T, Hung S, Wang X, Koziol JA.** 2006. Vascular matrix adhesion and the blood-brain barrier. *Biochem Soc Trans* **34**:1261-1266.
 113. **Abbott NJ, Rönnbäck L, Hansson E.** 2006. Astrocyte-endothelial interactions at the blood-brain barrier. *Nat Rev Neurosci* **7**:41-53.
 114. **Begley DJ, Brightman MW.** 2003. Structural and functional aspects of the blood-brain barrier. *Prog Drug Res* **61**:39-78.
 115. **Pardridge WM.** 2003. Blood-brain barrier drug targeting: the future of brain drug development. *Mol Interv* **3**:90-105- 51.
 116. **Strazielle N, Gherzi-Egea JF.** 2000. Choroid plexus in the central nervous

- system: biology and physiopathology. *J. Neuropathol. Exp. Neurol.* **59**:561-574.
117. **Ransohoff RM.** 2011. Microglia and monocytes: 'tis plain the twain meet in the brain. *Nature* **14**:1098-1100.
118. **Weller RO, Djuanda E, Yow H-Y, Carare RO.** 2008. Lymphatic drainage of the brain and the pathophysiology of neurological disease. *Acta Neuropathol* **117**:1-14.
119. **Kivisäkk P, Mahad DJ, Callahan MK, Trebst C, Tucky B, Wei T, Wu L, Baekkevold ES, Lassmann H, Staugaitis SM, Campbell JJ, Ransohoff RM.** 2003. Human cerebrospinal fluid central memory CD4⁺ T cells: evidence for trafficking through choroid plexus and meninges via P-selectin. *Proc. Natl. Acad. Sci. U.S.A.* **100**:8389-8394.
120. **Carrithers MD, Visintin I, Kang SJ, Janeway CAJ.** 2000. Differential adhesion molecule requirements for immune surveillance and inflammatory recruitment. *Brain* **123** :1092-1101.
121. **Engelhardt B, Ransohoff RM.** 2012. Capture, crawl, cross: the T cell code to breach the blood-brain barriers. *Trends in Immunology* **33**:579-589.
122. **Wekerle H, Linington C, Lassmann H, Meyermann R.** 1986. Cellular immune reactivity within the CNS. *Trends Neurosci* **9**:271-277.
123. **Griffin DE.** 2003. Immune responses to RNA-virus infections of the CNS. *Nat Rev Immunol* **3**:493-502.
124. **van Pesch V, van Eyll O, Michiels T.** 2001. The Leader Protein of Theiler's Virus Inhibits Immediate-Early Alpha/Beta Interferon Production. *Journal of Virology* **75**:7811-7817.
125. **Neumann H.** 2001. Control of glial immune function by neurons. *Glia* **36**:191-199.
126. **Neumann H, Schmidt H, Wilharm E, Behrens L, Wekerle H.** 1997. Interferon gamma gene expression in sensory neurons: evidence for autocrine gene regulation. *J. Exp. Med.* **186**:2023-2031.
127. **Harrison JK, Jiang Y, Chen S, Xia Y, Maciejewski D, McNamara RK, Streit WJ, Salafranca MN, Adhikari S, Thompson DA, Botti P, Bacon KB, Feng L.** 1998. Role for neuronally derived fractalkine in mediating interactions between neurons and CX3CR1-expressing microglia. *Proc. Natl. Acad. Sci. U.S.A.* **95**:10896-10901.
128. **Asensio VC, Campbell IL.** 1997. Chemokine gene expression in the brains of mice with lymphocytic choriomeningitis. *Journal of Virology* **71**:7832-7840.
129. **Lane TE, Asensio VC, Yu N, Paoletti AD, Campbell IL, Buchmeier MJ.** 1998. Dynamic regulation of α - and β -chemokine expression in the central nervous system during mouse hepatitis virus-induced demyelinating disease. *J. Immunol.* **160**:970-978.
130. **Wesselingh SL, Levine B, Fox RJ, Choi S, Griffin DE.** 1994. Intracerebral cytokine mRNA expression during fatal and nonfatal alphavirus encephalitis suggests a predominant type 2 T cell response. *J. Immunol.* **152**:1289-1297.
131. **Sixt M, Engelhardt B, Pausch F, Hallmann R, Wendler O, Sorokin LM.** 2001. Endothelial cell laminin isoforms, laminins 8 and 10, play decisive roles in T cell recruitment across the blood-brain barrier in experimental autoimmune encephalomyelitis. *J Cell Biol* **153**:933-946.
132. **Agrawal S, Anderson P, Durbeej M, Van Rooijen N, Ivars F, Opendakker G, Sorokin LM.** 2006. Dystroglycan is selectively cleaved at the parenchymal basement membrane at sites of leukocyte extravasation

- in experimental autoimmune encephalomyelitis. *J. Exp. Med.* **203**:1007-1019.
133. **Salinas S, Schiavo G, Kremer EJ.** 2010. A hitchhiker's guide to the nervous system: the complex journey of viruses and toxins. *Nat Rev Micro* **8**:645-655.
134. **Harling-Berg CJ, Park JT, Knopf PM.** 1999. Role of the cervical lymphatics in the Th2-type hierarchy of CNS immune regulation. This work was supported by National Institute of Health Grant (RO1 NS33070-03) and The Brain Tumor Society. *Journal of Neuroimmunology* **101**:111-127.
135. **Fischer HG, Reichmann G.** 2001. Brain dendritic cells and macrophages/microglia in central nervous system inflammation. *J. Immunol.* **166**:2717-2726.
136. **Pope JG, Vanderlugt CL, Rahbe SM, Lipton HL, Miller SD.** 1998. Characterization of and functional antigen presentation by central nervous system mononuclear cells from mice infected with Theiler's murine encephalomyelitis virus. *Journal of Virology* **72**:7762-7771.
137. **Stevenson PG, Hawke S, Sloan DJ, Bangham CR.** 1997. The immunogenicity of intracerebral virus infection depends on anatomical site. *Journal of Virology* **71**:145-151.
138. **Kim JV, Kang SS, Dustin ML, McGavern DB.** 2008. Myelomonocytic cell recruitment causes fatal CNS vascular injury during acute viral meningitis. *Nature* **457**:191-195.
139. **Hickey W.** 1999. Leukocyte traffic in the central nervous system: the participants and their roles. *Semin. Immunol.* **11**:125-137.
140. **Shrestha B, Diamond MS.** 2004. Role of CD8+ T Cells in Control of West Nile Virus Infection. *Journal of Virology* **78**:8312-8321.
141. **Sitati EM, Diamond MS.** 2006. CD4+ T-Cell Responses Are Required for Clearance of West Nile Virus from the Central Nervous System. *Journal of Virology* **80**:12060-12069.
142. **Irani DN, Lin KI, Griffin DE.** 1996. Brain-derived gangliosides regulate the cytokine production and proliferation of activated T cells. *J. Immunol.* **157**:4333-4340.
143. **Irani DN, Lin KI, Griffin DE.** 1997. Regulation of brain-derived T cells during acute central nervous system inflammation. *J. Immunol.* **158**:2318-2326.
144. **Bréhin A-C, Mouriès J, Frenkiel M-P, Dadaglio G, Desprès P, Lafon M, Couderc T.** 2008. Dynamics of immune cell recruitment during West Nile encephalitis and identification of a new CD19+B220-BST-2+ leukocyte population. *J. Immunol.* **180**:6760-6767.
145. **Ifergan I, Kebir H, Alvarez JI, Marceau G, Bernard M, Bourbonnière L, Poirier J, Duquette P, Talbot PJ, Arbour N, Prat A.** 2011. Central nervous system recruitment of effector memory CD8+ T lymphocytes during neuroinflammation is dependent on $\alpha 4$ integrin. *Brain* **134**:3560-3577.
146. **Boztug KK, Carson MJM, Pham-Mitchell NN, Asensio VCV, DeMartino JJ, Campbell ILI.** 2002. Leukocyte infiltration, but not neurodegeneration, in the CNS of transgenic mice with astrocyte production of the CXC chemokine ligand 10. *J. Immunol.* **169**:1505-1515.
147. **Zlotnik A, Yoshie O.** 2000. Chemokines: A New Classification Review System and Their Role in Immunity. *Immunity* **12**:121-127.
148. **Nomiyama H, Osada N, Yoshie O.** 2011. A family tree of vertebrate chemokine receptors for a unified nomenclature. *Developmental and*

- Comparative Immunology **35**:705-715.
149. **Rot A, Andrian von UH.** 2004. Chemokines in innate and adaptive host defense: basic chemokines grammar for immune cells. *Annu. Rev. Immunol.* **22**:891-928.
 150. **Murphy PM, Baggiolini M, Charo IF, Hebert CA, Horuk R, Matsushima K, Miller LH, Oppenheim JJ, Power CA.** 2000. International union of pharmacology. XXII. Nomenclature for chemokine receptors. *Pharmacol Rev* **52**:145-176.
 151. **Townson JR, Nibbs RJB.** 2002. Characterization of mouse CCX-CKR, a receptor for the lymphocyte-attracting chemokines TECK/mCCL25, SLC/mCCL21 and MIP-3beta/mCCL19: comparison to human CCX-CKR. *Eur. J. Immunol.* **32**:1230-1241.
 152. **Kiefer F, Siekmann AF.** 2011. The role of chemokines and their receptors in angiogenesis. *Cell Mol Life Sci* **68**:2811-2830.
 153. **Klein RS, Lin E, Zhang B, Luster AD, Tollett J, Samuel MA, Engle M, Diamond MS.** 2005. Neuronal CXCL10 Directs CD8+ T-Cell Recruitment and Control of West Nile Virus Encephalitis. *Journal of Virology* **79**:11457-11466.
 154. **Christensen JE, Simonsen S, Fenger C, Sørensen MR, Moos T, Christensen JP, Finsen B, Thomsen AR.** 2009. Fulminant lymphocytic choriomeningitis virus-induced inflammation of the CNS involves a cytokine-chemokine-cytokine-chemokine cascade. *J. Immunol.* **182**:1079-1087.
 155. **Lei Y, Takahama Y.** 2012. XCL1 and XCR1 in the immune system. *Microbes Infect* **14**:262-267.
 156. **Bazan JF, Bacon KB, Hardiman G, Wang W, Soo K, Rossi D, Greaves DR, Zlotnik A, Schall TJ.** 1997. A new class of membrane-bound chemokine with a CX3C motif. *Nature* **385**:640-644.
 157. **Combadiere C, Feumi C, Raoul W, Keller N, Rodero M, Pezard A, Lavalette S, Houssier M, Jonet L, Picard E, Debre P, Sirinyan M, Deterre P, Ferroukhi T, Cohen S-Y, Chauvaud D, Jeanny J-C, Chemtob S, Behar-Cohen F, Sennlaub F.** 2007. CX3CR1-dependent subretinal microglia cell accumulation is associated with cardinal features of age-related macular degeneration. *J. Clin. Invest.* **117**:2920-2928.
 158. **Pabon MM, Bachstetter AD, Hudson CE, Gemma C, Bickford PC.** 2011. CX3CL1 reduces neurotoxicity and microglial activation in a rat model of Parkinson's disease. *Journal of Neuroinflammation* **8**:9.
 159. **Zlotnik A, Yoshie O.** 2012. The Chemokine Superfamily Revisited. *Immunity* **36**:705-716.
 160. **Graham GJ.** 2009. D6 and the atypical chemokine receptor family: novel regulators of immune and inflammatory processes. *Eur. J. Immunol.* **39**:342-351.
 161. **Moser B.** 2004. Chemokines: role in inflammation and immune surveillance. *Annals of the Rheumatic Diseases* **63**:ii84-ii89.
 162. **Lapidot T, Dar A, Kollet O.** 2005. How do stem cells find their way home? *Blood* **106**:1901-1910.
 163. **Molyneaux KA, Zinszner H, Kunwar PS, Schaible K, Stebler J, Sunshine MJ, O'Brien W, Raz E, Littman D, Wylie C, Lehmann R.** 2003. The chemokine SDF1/CXCL12 and its receptor CXCR4 regulate mouse germ cell migration and survival. *Development* **130**:4279-4286.
 164. **Nomiyama H, Osada N, Yoshie O.** 2010. The evolution of mammalian chemokine genes. *Cytokine & Growth Factor Reviews* **21**:253-262.
 165. **Alcami A, Lira SA.** 2010. Modulation of chemokine activity by viruses.

- Current Opinion in Immunology **22**:482-487.
166. **Bodaghi B, Jones TR, Zipeto D, Vita C, Sun L, Laurent L, Arenzana-Seisdedos F, Virelizier JL, Michelson S.** 1998. Chemokine sequestration by viral chemoreceptors as a novel viral escape strategy: withdrawal of chemokines from the environment of cytomegalovirus-infected cells. *J. Exp. Med.* **188**:855-866.
 167. **Yamin R, Kaynan NS, Glasner A, Vitenshtein A, Tsukerman P, Bauman Y, Ophir Y, Elias S, Bar-On Y, Gur C, Mandelboim O.** 2013. The viral KSHV chemokine vMIP-II inhibits the migration of Naive and activated human NK cells by antagonizing two distinct chemokine receptors. *PLoS Pathog* **9**:e1003568.
 168. **Kraft K, Olbrich H, Majoul I, Mack M, Proudfoot A, Oppermann M.** 2001. Characterization of sequence determinants within the carboxyl-terminal domain of chemokine receptor CCR5 that regulate signaling and receptor internalization. *J Biol Chem* **276**:34408-34418.
 169. **Damaj BB, McColl SR, Neote K, Songqing N, Ogborn KT, Hebert CA, Naccache PH.** 1996. Identification of G-protein binding sites of the human interleukin-8 receptors by functional mapping of the intracellular loops. *FASEB J* **10**:1426-1434.
 170. **Ransohoff RM.** 2009. Chemokines and Chemokine Receptors: Standing at the Crossroads of Immunobiology and Neurobiology. *Immunity* **31**:711-721.
 171. **Mantovani A, Bonecchi R, Locati M.** 2006. Tuning inflammation and immunity by chemokine sequestration: decoys and more. *Nat Rev Immunol* **6**:907-918.
 172. **Alexander SPH, Mathie A, Peters JA.** 2008. Guide to Receptors and Channels (GRAC), 3rd edition. *Br J Pharmacol* **153**:S1-S1.
 173. **Glass WG, Lim JK, Cholera R, Pletnev AG, Gao J-L, Murphy PM.** 2005. Chemokine receptor CCR5 promotes leukocyte trafficking to the brain and survival in West Nile virus infection. *J. Exp. Med.* **202**:1087-1098.
 174. **Scott EP, Branigan PJ, Del Vecchio AM, Weiss SR.** 2008. Chemokine expression during mouse hepatitis virus-induced encephalitis: Contributions of the spike and background genes. *J. of Neurovirology* **14**:5-16.
 175. **Balkwill F.** 2004. Cancer and the chemokine network. *Nat Rev Cancer* **4**:540-550.
 176. **Raz E, Mahabaleshwar H.** 2009. Chemokine signaling in embryonic cell migration: a fisheye view. *Development* **136**:1223-1229.
 177. **Broxmeyer HE.** 2008. Chemokines in hematopoiesis. *Curr Opin Hematol* **15**:49-58.
 178. **Forster R, Sozzani S.** 2013. Emerging aspects of leukocyte migration. *Eur. J. Immunol.* **43**:1404-1406.
 179. **Alon R, Rossiter H, Wang X, Springer TA, Kupper TS.** 1994. Distinct cell surface ligands mediate T lymphocyte attachment and rolling on P and E selectin under physiological flow. *J Cell Biol* **127**:1485-1495.
 180. **Alon R, Feigelson S.** 2002. From rolling to arrest on blood vessels: leukocyte tap dancing on endothelial integrin ligands and chemokines at sub-second contacts. *Semin. Immunol.* **14**:93-104.
 181. **Handel TM, Johnson Z, Crown SE, Lau EK, Sweeney M, Proudfoot AE.** 2005. Regulation of protein function by Glycosaminoglycans-as exemplified by chemokines. *Annu. Rev. Biochem.* **74**:385-410.
 182. **Ley K, Laudanna C, Cybulsky MI, Nourshargh S.** 2007. Getting to the site of inflammation: the leukocyte adhesion cascade updated. *Nat Rev*

- Immunol 7:678-689.
183. **Vestweber D.** 2003. Lymphocyte trafficking through blood and lymphatic vessels: more than just selectins, chemokines and integrins. *Eur. J. Immunol.* **33**:1361-1364.
 184. **Moser B, Loetscher P.** 2001. Lymphocyte traffic control by chemokines. *Nat Immunol* **2**:123-128.
 185. **Luster AD, Alon R, Andrian von UH.** 2005. Immune cell migration in inflammation: present and future therapeutic targets. *Nat Immunol* **6**:1182-1190.
 186. **Worthylake RA, Burridge K.** 2001. Leukocyte transendothelial migration: orchestrating the underlying molecular machinery. *Curr Opin Cell Biol* **13**:569-577.
 187. **Gallo RC, Montagnier L.** 2003. The Discovery of HIV as the Cause of AIDS. *N. Engl. J. Med.* **349**:2283-2285.
 188. **Deng H, Liu R, Ellmeier W, Choe S, Unutmaz D, Burkhart M, Di Marzio P, Marmon S, Sutton RE, Hill CM, Davis CB, Peiper SC, Schall TJ, Littman DR, Landau NR.** 1996. Identification of a major co-receptor for primary isolates of HIV-1. *Nature* **381**:661-666.
 189. **Dragic T, Litwin V, Allaway GP, Martin SR, Huang Y, Nagashima KA, Cayanan C, Maddon PJ, Koup RA, Moore JP, Paxton WA.** 1996. HIV-1 entry into CD4+ cells is mediated by the chemokine receptor CC-CKR-5. *Nature* **381**:667-673.
 190. **Salazar-Gonzalez JF, Salazar MG, Keele BF, Learn GH, Giorgi EE, Li H, Decker JM, Wang S, Baalwa J, Kraus MH, Parrish NF, Shaw KS, Guffey MB, Bar KJ, Davis KL, Ochsenbauer-Jambor C, Kappes JC, Saag MS, Cohen MS, Mulenga J, Derdeyn CA, Allen S, Hunter E, Markowitz M, Hraber P, Perelson AS, Bhattacharya T, Haynes BF, Korber BT, Hahn BH, Shaw GM.** 2009. Genetic identity, biological phenotype, and evolutionary pathways of transmitted/founder viruses in acute and early HIV-1 infection. *J. Exp. Med.* **206**:1273-1289.
 191. **Grivel J-C, Margolis LB.** 1999. CCR5- and CXCR4-tropic HIV-1 are equally cytopathic for their T-cell targets in human lymphoid tissue. *Nat Med* **5**:344-346.
 192. **Moore JP, Kitchen SG, Pugach P, Zack JA.** 2004. The CCR5 and CXCR4 coreceptors--central to understanding the transmission and pathogenesis of human immunodeficiency virus type 1 infection. *AIDS Res. Hum. Retroviruses* **20**:111-126.
 193. **Levy JA.** 1996. Infection by human immunodeficiency virus--CD4 is not enough. *N. Engl. J. Med.* **335**:1528-1530.
 194. **Ullum H, Cozzi Lepri A, Victor J, Aladdin H, Phillips AN, Gerstoft J, Skinhøj P, Pedersen BK.** 1998. Production of beta-chemokines in human immunodeficiency virus (HIV) infection: evidence that high levels of macrophage inflammatory protein-1beta are associated with a decreased risk of HIV disease progression. *Journal of Infectious Diseases* **177**:331-336.
 195. **Liu R, Paxton WA, Choe S, Ceradini D, Martin SR, Horuk R, MacDonald ME, Stuhlmann H, Koup RA, Landau NR.** 1996. Homozygous defect in HIV-1 coreceptor accounts for resistance of some multiply-exposed individuals to HIV-1 infection. *Cell* **86**:367-377.
 196. **Novembre J, Galvani AP, Slatkin M.** 2005. The Geographic Spread of the CCR5 Δ 32 HIV-Resistance Allele. *Plos Biol* **3**:e339.
 197. **Glass WG, McDermott DH, Lim JK, Lekhong S, Yu SF, Frank WA, Pape J, Cheshier RC, Murphy PM.** 2006. CCR5 deficiency increases risk of

- symptomatic West Nile virus infection. *J. Exp. Med.* **203**:35-40.
198. **Dorr P, Westby M, Dobbs S, Griffin P, Irvine B, Macartney M, Mori J, Rickett G, Smith-Burchnell C, Napier C, Webster R, Armour D, Price D, Stammen B, Wood A, Perros M.** 2005. Maraviroc (UK-427,857), a potent, orally bioavailable, and selective small-molecule inhibitor of chemokine receptor CCR5 with broad-spectrum anti-human immunodeficiency virus type 1 activity. *Antimicrobial Agents and Chemotherapy* **49**:4721-4732.
199. **Wilkin TJ, Gulick RM.** 2012. CCR5 Antagonism in HIV Infection: Current Concepts and Future Opportunities. *Annual Review of Medicine* **63**:81-93.
200. **Schols D, Struyf S, Van Damme J, Esté JA, Henson G, De Clercq E.** 1997. Inhibition of T-tropic HIV strains by selective antagonization of the chemokine receptor CXCR4. *J. Exp. Med.* **186**:1383-1388.
201. **Liles WC, Broxmeyer HE, Rodger E, Wood B, Hübel K, Cooper S, Hangoc G, Bridger GJ, Henson GW, Calandra G, Dale DC.** 2003. Mobilization of hematopoietic progenitor cells in healthy volunteers by AMD3100, a CXCR4 antagonist. *Blood* **102**:2728-2730.
202. **Devine SM, Flomenberg N, Vesole DH, Liesveld J, Weisdorf D, Badel K, Calandra G, DiPersio JF.** 2004. Rapid mobilization of CD34+ cells following administration of the CXCR4 antagonist AMD3100 to patients with multiple myeloma and non-Hodgkin's lymphoma. *J. Clin. Oncol.* **22**:1095-1102.
203. **Sorensen TL, Tani M, Jensen J, Pierce V, Lucchinetti C, Folcik VA, Qin S, Rottman J, Sellebjerg F, Strieter RM, Frederiksen JL, Ransohoff RM.** 1999. Expression of specific chemokines and chemokine receptors in the central nervous system of multiple sclerosis patients. *J. Clin. Invest.* **103**:807-815.
204. **Cartier L, Hartley O, Dubois-Dauphin M, Krause K-H.** 2005. Chemokine receptors in the central nervous system: role in brain inflammation and neurodegenerative diseases. *Brain Res Brain Res Rev* **48**:16-42.
205. **Liu L, Graham GJ, Damodaran A, Hu T, Lira SA, Sasse M, Canasto-Chibuque C, Cook DN, Ransohoff RM.** 2006. Cutting edge: the silent chemokine receptor D6 is required for generating T cell responses that mediate experimental autoimmune encephalomyelitis. *J. Immunol.* **177**:17-21.
206. **Reboldi A, Coisne C, Baumjohann D, Benvenuto F, Bottinelli D, Lira S, Uccelli A, Lanzavecchia A, Engelhardt B, Sallusto F.** 2009. C-C chemokine receptor 6-regulated entry of TH-17 cells into the CNS through the choroid plexus is required for the initiation of EAE. *Nat Immunol* **10**:514-523.
207. **Schall TJ, Proudfoot AEI.** 2011. Overcoming hurdles in developing successful drugs targeting chemokine receptors. *Nat Rev Immunol* **11**:355-363.
208. **Gerard C, Rollins BJ.** 2001. Chemokines and disease. *Nat Immunol* **2**:108-115.
209. **Wells TNC, Power CA, Shaw JP, Proudfoot AEI.** 2006. Chemokine blockers - therapeutics in the making? *Trends in Pharmacological Sciences* **27**:41-47.
210. **Liang M, Mallari C, Rosser M, Ng HP, May K, Monahan S, Bauman JG, Islam I, Ghannam A, Buckman B, Shaw K, Wei GP, Xu W, Zhao Z, Ho E, Shen J, Oanh H, Subramanyam B, Vergona R, Taub D, Dunning L, Harvey S, Snider RM, Hesselgesser J, Morrissey MM, Perez HD.** 2000. Identification and characterization of a potent, selective, and orally active antagonist of the CC chemokine receptor-1. *J Biol Chem*

- 275:19000-19008.
211. **Saederup N, Cardona AE, Croft K, Mizutani M, Cottle AC, Tsou C-L, Ransohoff RM, Charo IF.** 2010. Selective Chemokine Receptor Usage by Central Nervous System Myeloid Cells in CCR2-Red Fluorescent Protein Knock-In Mice. *PLoS ONE* **5**:e13693.
 212. **Mack M, Cihak J, Simonis C, Luckow B, Proudfoot AE, Plachý J, Brühl H, Frink M, Anders HJ, Vielhauer V, Pfirstinger J, Stangassinger M, Schlöndorff D.** 2001. Expression and characterization of the chemokine receptors CCR2 and CCR5 in mice. *J. Immunol.* **166**:4697-4704.
 213. **Tsou C-L, Peters W, Si Y, Slaymaker S, Aslanian AM, Weisberg SP, Mack M, Charo IF.** 2007. Critical roles for CCR2 and MCP-3 in monocyte mobilization from bone marrow and recruitment to inflammatory sites. *J. Clin. Invest.* **117**:902-909.
 214. **Lim JK, Obara CJ, Rivollier A, Pletnev AG, Kelsall BL, Murphy PM.** 2011. Chemokine receptor *Ccr2* is critical for monocyte accumulation and survival in West Nile virus encephalitis. *J. Immunol.* **186**:471-478.
 215. **Gaupp S, Pitt D, Kuziel WA, Cannella B, Raine CS.** 2003. Experimental autoimmune encephalomyelitis (EAE) in CCR2(-/-) mice: susceptibility in multiple strains. *Am J Pathol* **162**:139-150.
 216. **Mirzadegan T, Diehl F, Ebi B, Bhakta S, Polsky I, McCarley D, Mulkins M, Weatherhead GS, Lapierre JM, Dankwardt J, Morgans D, Wilhelm R, Jarnagin K.** 2000. Identification of the binding site for a novel class of CCR2b chemokine receptor antagonists: binding to a common chemokine receptor motif within the helical bundle. *J Biol Chem* **275**:25562-25571.
 217. **Furuichi K, Wada T, Iwata Y, Kitagawa K, Kobayashi K-I, Hashimoto H, Ishiwata Y, Asano M, Wang H, Matsushima K, Takeya M, Kuziel WA, Mukaida N, Yokoyama H.** 2003. CCR2 signaling contributes to ischemia-reperfusion injury in kidney. *Journal of the American Society of Nephrology* **14**:2503-2515.
 218. **Kitagawa K, Wada T, Furuichi K, Hashimoto H, Ishiwata Y, Asano M, Takeya M, Kuziel WA, Matsushima K, Mukaida N, Yokoyama H.** 2004. Blockade of CCR2 ameliorates progressive fibrosis in kidney. *Am J Pathol* **165**:237-246.
 219. **Zhou Y, Kurihara T, Ryseck RP, Yang Y, Ryan C, Loy J, Warr G, Bravo R.** 1998. Impaired macrophage function and enhanced T cell-dependent immune response in mice lacking CCR5, the mouse homologue of the major HIV-1 coreceptor. *J. Immunol.* **160**:4018-4025.
 220. **Aliberti J, Reis e Sousa C, Schito M, Hieny S, Wells T, Huffnagle GB, Sher A.** 2000. CCR5 provides a signal for microbial induced production of IL-12 by CD8 α ⁺ dendritic cells. *Nat Immunol* **1**:83-87.
 221. **Andres PG, Beck PL, Mizoguchi E, Mizoguchi A, Bhan AK, Dawson T, Kuziel WA, Maeda N, MacDermott RP, Podolsky DK.** 2000. Mice with a selective deletion of the CC chemokine receptors 5 or 2 are protected from dextran sodium sulfate-mediated colitis: lack of CC chemokine receptor 5 expression results in a NK1. 1⁺ lymphocyte-associated Th2-type immune response in the intestine. *J. Immunol.* **164**:6303-6312.
 222. **Ochoa-Callejero LL, Pérez-Martínez LL, Rubio-Mediavilla SS, Oteo JAJ, Martínez AA, Blanco JRJ.** 2013. Maraviroc, a CCR5 antagonist, prevents development of hepatocellular carcinoma in a mouse model. *PLoS ONE* **8**:e53992-e53992.
 223. **Polianova MT, Ruscetti FW, Pert CB, Ruff MR.** 2005. Chemokine receptor-5 (CCR5) is a receptor for the HIV entry inhibitor peptide T (DAPTA). *Antiviral Research* **67**:83-92.

224. Pollicita M, Ruff MR, Pert CB, Polianova MT, Schols D, Ranazzi A, Perno C-F, Aquaro S. 2007. Profound anti-HIV-1 activity of DAPTA in monocytes/macrophages and inhibition of CCR5-mediated apoptosis in neuronal cells. *Antivir. Chem. Chemother.* **18**:285-295.
225. Rosi S, Pert CB, Ruff MR, McGann-Gramling K, Wenk GL. 2005. Chemokine receptor 5 antagonist D-Ala-peptide T-amide reduces microglia and astrocyte activation within the hippocampus in a neuroinflammatory rat model of Alzheimer's disease. *Neuroscience* **134**:671-676.
226. Hu JK, Kagari T, Clingan JM, Matloubian M. 2011. Expression of chemokine receptor CXCR3 on T cells affects the balance between effector and memory CD8 T-cell generation. *Proc. Natl. Acad. Sci. U.S.A.* **108**:E118-E127.
227. Qin S, Rottman JB, Myers P, Kassam N, Weinblatt M, Loetscher M, Koch AE, Moser B, Mackay CR. 1998. The chemokine receptors CXCR3 and CCR5 mark subsets of T cells associated with certain inflammatory reactions. *J. Clin. Invest.* **101**:746-754.
228. Lazzeri E, Romagnani P. 2005. CXCR3-binding chemokines: novel multifunctional therapeutic targets. *Curr. Drug Targets Immune Endocr. Metabol. Disord.* **5**:109-118.
229. Mahad DJ, Howell SJL, Woodroffe MN. 2002. Expression of chemokines in the CSF and correlation with clinical disease activity in patients with multiple sclerosis. *J. Neurol. Neurosurg. Psychiatr.* **72**:498-502.
230. Gottlieb AB, Luster AD, Posnett DN, Carter DM. 1988. Detection of a gamma interferon-induced protein IP-10 in psoriatic plaques. *J. Exp. Med.* **168**:941-948.
231. Patel DD, Zachariah JP, Whichard LP. 2001. CXCR3 and CCR5 Ligands in Rheumatoid Arthritis Synovium. *Clin Immunol* **98**:7-7.
232. Du X, Gustin DJ, Chen X, Duquette J, McGee LR, Wang Z, Ebsworth K, Henne K, Lemon B, Ma J, Miao S, Sabalan E, Sullivan TJ, Tonn G, Collins TL, Medina JC. 2009. Imidazo-pyrazine derivatives as potent CXCR3 antagonists. *Bioorganic & Medicinal Chemistry Letters* **19**:5200-5204.
233. Rostène W, Kitabgi P, Parsadaniantz SM. 2007. Opinion - Chemokines: a new class of neuromodulator? *Nat Rev Neurosci* **8**:895-904.
234. Ambrosini E, Aloisi F. 2004. Chemokines and glial cells: A complex network in the central nervous system. *Neurochem Res* **29**:1017-1038.
235. Tham TN, Lazarini F, Franceschini IA, Lachapelle F, Amara A, Dubois-Dalcq M. 2001. Developmental pattern of expression of the alpha chemokine stromal cell-derived factor 1 in the rat central nervous system. *Eur J Neurosci* **13**:845-856.
236. Cardona AE, Piro EP, Sasse ME, Kostenko V, Cardona SM, Dijkstra IM, Huang D, Kidd G, Dombrowski S, Dutta R, Lee J-C, Cook DN, Jung S, Lira SA, Littman DR, Ransohoff RM. 2006. Control of microglial neurotoxicity by the fractalkine receptor. *Nat Neurosci* **9**:917-924.
237. Banisadr G, Gosselin R-D, Mechighel P, Rostène W, Kitabgi P, Mélik Parsadaniantz S. 2005. Constitutive neuronal expression of CCR2 chemokine receptor and its colocalization with neurotransmitters in normal rat brain: functional effect of MCP-1/CCL2 on calcium mobilization in primary cultured neurons. *J. Comp. Neurol.* **492**:178-192.
238. Rezaie P, Male D. 1999. Colonisation of the developing human brain and spinal cord by microglia: a review. *Microsc Res Tech* **45**:359-382.
239. Hughes PM, Botham MS, Frentzel S, Mir A, Perry VH. 2002. Expression

- of fractalkine (CX3CL1) and its receptor, CX3CR1, during acute and chronic inflammation in the rodent CNS. *Glia* **37**:314-327.
240. **Banisadr G, Fontanges P, Haour F, Kitabgi P, Rostène W, Mélik Parsadaniantz S.** 2002. Neuroanatomical distribution of CXCR4 in adult rat brain and its localization in cholinergic and dopaminergic neurons. *Eur J Neurosci* **16**:1661-1671.
241. **Ubogu E, Cossoy M, Ransohoff R.** 2006. The expression and function of chemokines involved in CNS inflammation. *Trends in Pharmacological Sciences* **27**:48-55.
242. **Müller M, Carter S, Hofer MJ, Campbell IL.** 2010. Review: The chemokine receptor CXCR3 and its ligands CXCL9, CXCL10 and CXCL11 in neuroimmunity - a tale of conflict and conundrum. *Neuropathology and Applied Neurobiology* **36**:368-387.
243. **Baggiolini M, Loetscher P, Moser B.** 1995. Interleukin-8 and the chemokine family. *Int J Immunopharmacol* **17**:103-108.
244. **Savarin-Vuillat C, Ransohoff RM.** 2007. Chemokines and chemokine receptors in neurological disease: raise, retain, or reduce? *Neurotherapeutics* **4**:590-601.
245. **Grainger JR, Wohlfert EA, Fuss IJ, Bouladoux N, Askenase MH, Legrand F, Koo LY, Brenchley JM, Fraser IDC, Belkaid Y.** 2013. Inflammatory monocytes regulate pathologic responses to commensals during acute gastrointestinal infection. *Nat Med* **19**:713-721.
246. **Rottman JB, Slavin AJ, Silva R, Weiner HL, Gerard CG, Hancock WW.** 2000. Leukocyte recruitment during onset of experimental allergic encephalomyelitis is CCR1 dependent. *Eur. J. Immunol.* **30**:2372-2377.
247. **Tran EH, Kuziel WA, Owens T.** 2000. Induction of experimental autoimmune encephalomyelitis in C57BL/6 mice deficient in either the chemokine macrophage inflammatory protein-1alpha or its CCR5 receptor. *Eur. J. Immunol.* **30**:1410-1415.
248. **Kleinewietfeld M.** 2005. CCR6 expression defines regulatory effector/memory-like cells within the CD25+CD4+ T-cell subset. *Blood* **105**:2877-2886.
249. **Pötzl J, Botteron C, Tausch E, Pedré X, Mueller AM, Männel DN, Lechner A.** 2008. Tracing Functional Antigen-Specific CCR6+ Th17 Cells after Vaccination. *PLoS ONE* **3**:e2951.
250. **Kivisäkk P, Imitola J, Rasmussen S, Elyaman W, Zhu B, Ransohoff RM, Houry SJ.** 2009. Localizing central nervous system immune surveillance: meningeal antigen-presenting cells activate T cells during experimental autoimmune encephalomyelitis. *Ann. Neurol.* **65**:457-469.
251. **Liu L, Huang D, Matsui M, He TT, Hu T, Demartino J, Lu B, Gerard C, Ransohoff RM.** 2006. Severe disease, unaltered leukocyte migration, and reduced IFN-gamma production in CXCR3-/- mice with experimental autoimmune encephalomyelitis. *J. Immunol.* **176**:4399-4409.
252. **Müller M, Carter SL, Hofer MJ, Manders P, Getts DR, Getts MT, Dreykluft A, Lu B, Gerard C, King NJC, Campbell IL.** 2007. CXCR3 signaling reduces the severity of experimental autoimmune encephalomyelitis by controlling the parenchymal distribution of effector and regulatory T cells in the central nervous system. *J. Immunol.* **179**:2774-2786.
253. **Arimilli S, Ferlin W, Solvason N, Deshpande S, Howard M, Mocchi S.** 2000. Chemokines in autoimmune diseases. *Immunol Rev* **177**:43-51.
254. **Kohler RE, Comerford I, Townley S, Haylock-Jacobs S, Clark-Lewis I, McColl SR.** 2008. Antagonism of the chemokine receptors CXCR3 and

- CXCR4 reduces the pathology of experimental autoimmune encephalomyelitis. *Brain Pathol* **18**:504-516.
255. **Campbell GL, Hills SL, Fischer M, Jacobson JA, Hoke CH, Hombach JM, Marfin AA, Solomon T, Tsai TF, Tsu VD, Ginsburg AS.** 2011. Estimated global incidence of Japanese encephalitis: a systematic review. *Bull World Health Organ* **89**:766-74.
256. **Samuel MA, Wang H, Siddharthan V, Morrey JD, Diamond MS.** 2007. Axonal transport mediates West Nile virus entry into the central nervous system and induces acute flaccid paralysis. *Proc. Natl. Acad. Sci. U.S.A.* **104**:17140-17145.
257. **Henderson BE, Metselaar D, Kirya GB, Timms GL.** 1970. Investigations into yellow fever virus and other arboviruses in the northern regions of Kenya. *Bull World Health Organ* **42**:787-795.
258. **Center for Disease Control.** 2012. West Nile virus disease and other arboviral diseases - United States, 2011. *MMWR Morb Mortal Wkly Rep* **61**:510-514.
259. **Jones KE, Patel NG, Levy MA, Storeygard A, Balk D, Gittleman JL, Daszak P.** 2008. Global trends in emerging infectious diseases. *Nature* **451**:990-993.
260. **Zacks MA, Paessler S.** 2010. Encephalitic alphaviruses. *Veterinary Microbiology* **140**:281-286.
261. **Hollidge BS, González-Scarano F, Soldan SS.** 2010. Arboviral encephalitides: transmission, emergence, and pathogenesis. *J Neuroimmune Pharmacol* **5**:428-442.
262. **Strauss JH, Strauss EG.** 1994. The alphaviruses: gene expression, replication, and evolution. *Microbiol. Rev.* **58**:491-562.
263. **Paupy C, Delatte H, Bagny L, Corbel V, Fontenille D.** 2009. *Aedes albopictus*, an arbovirus vector: from the darkness to the light. *Microbes Infect* **11**:1177-1185.
264. **Bonn D.** 2006. How did chikungunya reach the Indian Ocean? *Lancet Infect Dis* **9**: 543-559
265. **Panning M, Grywna K, van Esbroeck M, Emmerich P, Drosten C.** 2008. Chikungunya fever in travelers returning to Europe from the Indian Ocean region, 2006. *Emerg Infect Dis* **14**:416-422.
266. **Nicoletti L, Ciccozzi M, Marchi A, Fiorentini C, Martucci P, D'Ancona F, Ciofi degli Atti M, Pompa MG, Rezza G, Ciufolini MG.** 2008. Chikungunya and dengue viruses in travelers. *Emerg Infect Dis* **14**:177-178.
267. **Atkins GJ.** 2013. The Pathogenesis of Alphaviruses. *ISRN Virology* **2013**:1-22.
268. **Rico-Hesse R, Weaver SC, de Siger J, Medina G, Salas RA.** 1995. Emergence of a new epidemic/epizootic Venezuelan equine encephalitis virus in South America. *Proc. Natl. Acad. Sci. U.S.A.* **92**:5278-5281.
269. **Casals J.** 1964. Antigenic variants of eastern equine encephalitis virus. *J. Exp. Med.* **1**:547-565.
270. **Hahn CS, Lustig S, Strauss EG, Strauss JH.** 1988. Western equine encephalitis virus is a recombinant virus. *Proc. Natl. Acad. Sci. U.S.A.* **85**:5997-6001.
271. **Frolov I, Schlesinger S.** 1996. Translation of Sindbis virus mRNA: analysis of sequences downstream of the initiating AUG codon that enhance translation. *Journal of Virology* **70**:1182-1190.
272. **Myles KM, Kelly CLH, Ledermann JP, Powers AM.** 2006. Effects of an opal termination codon preceding the nsP4 gene sequence in the O'Nyong-Nyong virus genome on *Anopheles gambiae* infectivity. *Journal of*

- Virology **80**:4992-4997.
273. **Li L, Jose J, Xiang Y, Kuhn RJ, Rossmann MG.** 2010. Structural changes of envelope proteins during alphavirus fusion. *Nature* **468**:705-708.
274. **Bonsdorff von CH, Harrison SC.** 1975. Sindbis virus glycoproteins form a regular icosahedral surface lattice. *Journal of Virology* **16**:141-145.
275. **Kielian M.** 2010. Structural biology: An alphavirus puzzle solved. *Nature* **468**:645-646.
276. **White J, Helenius A.** 1980. pH-dependent fusion between the Semliki Forest virus membrane and liposomes. *Proc. Natl. Acad. Sci. U.S.A.* **77**:3273-3277.
277. **Strauss EG, Stec DS, Schmaljohn AL, Strauss JH.** 1991. Identification of antigenically important domains in the glycoproteins of Sindbis virus by analysis of antibody escape variants. *Journal of Virology* **65**:4654-4664.
278. **Helenius A, Morein B, Fries E, Simons K, Robinson P, Schirmacher V, Terhorst C, Strominger JL.** 1978. Human (HLA-A and HLA-B) and murine (H-2K and H-2D) histocompatibility antigens are cell surface receptors for Semliki Forest virus. *Proc. Natl. Acad. Sci. U.S.A.* **75**:3846-3850.
279. **Klimstra WB, Nangle EM, Smith MS, Yurochko AD, Ryman KD.** 2003. DC-SIGN and L-SIGN can act as attachment receptors for alphaviruses and distinguish between mosquito cell- and mammalian cell-derived viruses. *Journal of Virology* **77**:12022-12032.
280. **Wang KS, Kuhn RJ, Strauss EG, Ou S, Strauss JH.** 1992. High-affinity laminin receptor is a receptor for Sindbis virus in mammalian cells. *Journal of Virology* **66**:4992-5001.
281. **Gibbons DL, Vaney M-C, Roussel A, Vigouroux A, Reilly B, Lepault J, Kielian M, Rey FA.** 2004. Conformational change and protein-protein interactions of the fusion protein of Semliki Forest virus. *Nature* **427**:320-325.
282. **Helenius A, Kartenbeck J, Simons K, Fries E.** 1980. On the entry of Semliki forest virus into BHK-21 cells. *J Cell Biol* **84**:404-420.
283. **Pathak S, Webb HE, Oaten SW, Bateman S.** 1976. An electron-microscopic study of the development of virulent and avirulent strains of Semliki forest virus in mouse brain. *J. Neurol. Sci.* **28**:289-300.
284. **Smithburn KC, Haddow A, Mahaffy AF.** 1946. A neurotropic virus isolated from *Aedes* mosquitoes caught in the Semliki forest. *Am. J. Trop. Med. Hyg.* **26**:189-208.
285. **Seamer J, Fitzgeorge R, Smith CE.** 1967. Resistance of the short-tailed vole *Microtus agrestis* (L.) to infection with two arboviruses. *Br J Exp Pathol* **48**:463-467.
286. **Bradish CJ, Allner K, Maber HB.** 1971. The virulence of original and derived strains of Semliki forest virus for mice, guinea-pigs and rabbits. *J. Gen. Virol.* **12**:141-160.
287. **Robin Y, Bourdin P, Le Gonidec G, Heme G.** 1974. Semliki forest virus and equine encephalomyelitis in Senegal. *Ann Microbiol (Paris)* **125A**:235-241.
288. **Mathiot CC, Grimaud G, Garry P, Bouquety JC, Mada A, Daguisy AM, Georges AJ.** 1990. An outbreak of human Semliki Forest virus infections in Central African Republic. *Am. J. Trop. Med. Hyg.* **42**:386-393.
289. **Willems W, Kaluza G, Boschek C, Bauer H.** 1979. Semliki forest virus: cause of a fatal case of human encephalitis. *Science.*
290. **Casadevall A, Pirofski L.** 2001. Host-pathogen interactions: the attributes of virulence. *Journal of Infectious Diseases* **184**:337-344.
291. **Glasgow GM, Sheahan BJ, Atkins GJ, Wahlberg JM, Salminen A,**

- Liljestrom P. 1991. Two mutations in the envelope glycoprotein E2 of Semliki Forest virus affecting the maturation and entry patterns of the virus alter pathogenicity for mice. *Virology* **185**:741-748.
292. McIntosh BM, Worth CB, Kokernot RH. 1961. Isolation of Semliki Forest virus from *Aedes (Aedimorphus) argenteopunctatus* (Theobald) collected in Portuguese East Africa. *Transactions of the Royal Society of Tropical Medicine and Hygiene* **55**:192-198.
293. Balluz IM, Glasgow GM, Killen HM, Mabruk MJ, Sheahan BJ, Atkins GJ. 1993. Virulent and avirulent strains of Semliki Forest virus show similar cell tropism for the murine central nervous system but differ in the severity and rate of induction of cytolytic damage. *Neuropathology and Applied Neurobiology* **19**:233-239.
294. Soilu-Hänninen M, Erälinna JP, Hukkanen V, Røyttä M, Salmi AA, Salonen R. 1994. Semliki Forest virus infects mouse brain endothelial cells and causes blood-brain barrier damage. *Journal of Virology* **68**:6291-6298.
295. Tuittila MT, Santagati MG, Røyttä M, Maatta JA, Hinkkanen AE. 2000. Replicase Complex Genes of Semliki Forest Virus Confer Lethal Neurovirulence. *Journal of Virology* **74**:4579-4589.
296. Santagati MG, Maatta JA, Itaranta PV, Salmi AA, Hinkkanen AE. 1995. The Semliki Forest virus E2 gene as a virulence determinant. *J. Gen. Virol.* **76** (Pt 1):47-52.
297. Tarbatt CJ, Glasgow GM, Mooney DA, Sheahan BJ, Atkins GJ. 1997. Sequence analysis of the avirulent, demyelinating A7 strain of Semliki Forest virus. *J. Gen. Virol.* **78**:1551-1557.
298. Fazakerley JK, Pathak S, Scallan M, Amor S, Dyson H. 1993. Replication of the A7(74) strain of Semliki Forest Virus is restricted in neurons. *Virology* **195**:627-637.
299. Oliver KR, Scallan MF, Dyson H, Fazakerley JK. 1997. Susceptibility to a neurotropic virus and its changing distribution in the developing brain is a function of CNS maturity. *J. of Neurovirology* **3**:38-48.
300. Allsopp TE, Scallan MF, Williams A, Fazakerley JK. 1998. Virus infection induces neuronal apoptosis: A comparison with trophic factor withdrawal. *Cell Death Differ* **5**:50-59.
301. Fazakerley JK, Webb HE. 1987. Semliki Forest virus-induced, immune-mediated demyelination: adoptive transfer studies and viral persistence in nude mice. *J. Gen. Virol.* **68** (Pt 2):377-385.
302. Oliver K, Fazakerley J. 1998. Transneuronal spread of Semliki Forest virus in the developing mouse olfactory system is determined by neuronal maturity. *Neuroscience* **82**:867-877.
303. Scallan M, Fazakerley J. 1999. Aurothiolates enhance the replication of Semliki Forest virus in the CNS and the exocrine pancreas. *J. of Neurovirology* **5**:392-400.
304. Allner K, Bradish CJ, Fitzgeorge R, Nathanson N. 1974. Modifications by sodium aurothiomalate of the expression of virulence in mice by defined strains of Semliki Forest virus. *J. Gen. Virol.* **24**:221-228.
305. Parsons LM, Webb HE. 1982. Blood brain barrier disturbance and immunoglobulin G levels in the cerebrospinal fluid of the mouse following peripheral infection with the demyelinating strain of Semliki Forest virus. *J. Neurol. Sci.* **57**:307-318.
306. Donnelly SM, Sheahan BJ, Atkins GJ. 1997. Long-term effects of Semliki Forest virus infection in the mouse central nervous system. *Neuropathology and Applied Neurobiology* **23**:235-241.

307. **Morris M, Dyson H, Baker D, Harbig L, Fazakerley J, Amor S.** 1997. Characterization of the cellular and cytokine response in the central nervous system following Semliki Forest virus infection. *Journal of Neuroimmunology* **74**:185-197.
308. **Fazakerley JK, Boyd A, Mikkola ML, Kaariainen L.** 2002. A Single Amino Acid Change in the Nuclear Localization Sequence of the nsP2 Protein Affects the Neurovirulence of Semliki Forest Virus. *Journal of Virology* **76**:392-396.
309. **Fazakerley JK.** 2004. Semliki forest virus infection of laboratory mice: a model to study the pathogenesis of viral encephalitis. *Arch. Virol. Suppl.* 179-190.
310. **Subak-Sharpe I, Dyson H, Fazakerley J.** 1993. In vivo depletion of CD8+ T cells prevents lesions of demyelination in Semliki Forest virus infection. *Journal of Virology* **67**:7629-7633.
311. **Suckling AJ, Jagelman S, Webb HE.** 1982. Immunoglobulin synthesis in nude (nu/nu), nu/+ and reconstituted nu/nu mice infected with a demyelinating strain of Semliki Forest virus. *Clin. Experimental Immunology* **47**:283-288.
312. **Fazakerley JK.** 2005. Semliki Forest Virus Induced Demyelination. *Br J Exp Pathol* 861-870.
313. **Fazakerley JK, Cotterill CL, Lee G, Graham A.** 2006. Virus tropism, distribution, persistence and pathology in the corpus callosum of the Semliki Forest virus-infected mouse brain: a novel system to study virus-oligodendrocyte interactions. *Neuropathology and Applied Neurobiology* **32**:397-409.
314. **Smyth JM, Sheahan BJ, Atkins GJ.** 1990. Multiplication of virulent and demyelinating Semliki Forest virus in the mouse central nervous system: consequences in BALB/c and SJL mice. *J. Gen. Virol.* **71 (Pt 11)**:2575-2583.
315. **Atkins GJ, Sheahan BJ, Dimmock NJ.** 1985. Semliki Forest virus infection of mice: a model for genetic and molecular analysis of viral pathogenicity. *J. Gen. Virol.* **66 (Pt 3)**:395-408.
316. **Brinton MA.** 2002. The molecular biology of West Nile Virus: a new invader of the Western Hemisphere. *Annu. Rev. Microbiol.* **56**:371-402.
317. **Turell MJ, O'Guinn ML, Dohm DJ, Jones JW.** 2001. Vector competence of North American mosquitoes (Diptera: Culicidae) for West Nile virus. *J Med Entomol* **38**:130-134.
318. **Smithburn KC, Hughes TP, Burke AW, Paul JH.** 1940. A Neurotropic Virus Isolated from the Blood of a Native of Uganda. *Am. J. Trop. Med. Hyg.* **s1-20**:471-492.
319. **Nansen A, Christensen JP, Andreasen SO, Bartholdy C, Christensen JE, Thomsen AR.** 2002. The role of CC chemokine receptor 5 in antiviral immunity. *Blood* **99**:1237-1245.
320. **Allan JE, Dixon JE, Doherty PC.** 1987. Nature of the inflammatory process in the central nervous system of mice infected with lymphocytic choriomeningitis virus. *Curr. Top. Microbiol. Immunol.* **134**:131-143.
321. **Cho H, Diamond M.** 2012. Immune Responses to West Nile Virus infection in the central nervous system. *Viruses* **4**:3812-3830.
322. **Christensen JE, de Lemos C, Moos T, Christensen JP, Thomsen AR.** 2006. CXCL10 is the key ligand for CXCR3 on CD8+ effector T cells involved in immune surveillance of the lymphocytic choriomeningitis virus-infected central nervous system. *J. Immunol.* **176**:4235-4243.
323. **Christensen JE, Nansen A, Moos T, Lu B, Gerard C, Christensen JP,**

- Thomsen AR. 2004. Efficient T-cell surveillance of the CNS requires expression of the CXC chemokine receptor 3. *Journal of Neuroscience* **24**:4849-4858.
324. Hayes EB, Komar N, Nasci RS, SP M, O'Leary DR, GL C. 2005. Epidemiology and Transmission Dynamics of West Nile Virus Disease. *Emerg Infect Dis* **11**:1167-1173.
325. Fischer SA. 2008. Emerging viruses in transplantation: there is more to infection after transplant than CMV and EBV. *Transplantation* **86**:1327-1339.
326. Lane TE, Liu MT, Chen BP, Asensio VC, Samawi RM, Paoletti AD, Campbell IL, Kunkel SL, Fox HS, Buchmeier MJ. 2000. A Central Role for CD4+ T Cells and RANTES in Virus-Induced Central Nervous System Inflammation and Demyelination. *Journal of Virology* **74**:1415-1424.
327. Andrade CC, Maharaj PD, Reisen WK, Brault AC. 2011. North American West Nile virus genotype isolates demonstrate differential replicative capacities in response to temperature. *Journal of General Virology* **92**:2523-2533.
328. Houtman JJ, Fleming JO. 1996. Dissociation of demyelination and viral clearance in congenitally immunodeficient mice infected with murine coronavirus JHM. *J. of Neurovirology* **2**:101-110.
329. Wang FI, Stohlman SA, Fleming JO. 1990. Demyelination induced by murine hepatitis virus JHM strain (MHV-4) is immunologically mediated. *Journal of Neuroimmunology* **30**:31-41.
330. Williamson JS, Sykes KC, Stohlman SA. 1991. Characterization of brain-infiltrating mononuclear cells during infection with mouse hepatitis virus strain JHM. *Journal of Neuroimmunology* **32**:199-207.
331. Mackenzie JM, Westaway EG. 2001. Assembly and maturation of the flavivirus Kunjin virus appear to occur in the rough endoplasmic reticulum and along the secretory pathway, respectively. *Journal of Virology* **75**:10787-10799.
332. Hunsperger EA, Roehrig JT. 2006. Temporal analyses of the neuropathogenesis of a West Nile virus infection in mice. *J. of Neurovirology* **12**:129-139.
333. Monath TP, Cropp CB, Harrison AK. 1983. Mode of entry of a neurotropic arbovirus into the central nervous system. Reinvestigation of an old controversy. *Lab Invest* **48**:399-410.
334. Chen BP, Kuziel WA, Lane TE. 2001. Lack of CCR2 results in increased mortality and impaired leukocyte activation and trafficking following infection of the central nervous system with a neurotropic coronavirus. *J. Immunol.* **167**:4585-4592.
335. Kramer-Hammerle S, Rothenaigler I, Wolff H, Bell JE, Brack-Werner R. 2005. Cells of the central nervous system as targets and reservoirs of the human immunodeficiency virus. *Virus Res* **111**:194-213.
336. Glass WG, Lane TE. 2003. Functional analysis of the CC chemokine receptor 5 (CCR5) on virus-specific CD8+ T cells following coronavirus infection of the central nervous system. *Virology* **312**:407-414.
337. Garcia-Tapia D, Loiacono CM, Kleiboeker SB. 2006. Replication of West Nile virus in equine peripheral blood mononuclear cells. *Vet Immunol Immunopathol* **110**:229-244.
338. Wang P, Dai J, Bai F, Kong KF, Wong SJ, Montgomery RR, Madri JA, Fikrig E. 2008. Matrix metalloproteinase 9 facilitates West Nile virus entry into the brain. *Journal of Virology* **82**:8978-8985.
339. Chambers TJ, Diamond MS. 2003. Pathogenesis of flavivirus encephalitis.

- Adv Virus Res **60**:273-342.
340. **Hosking MP, Liu L, Ransohoff RM, Lane TE.** 2009. A Protective Role for ELR+ Chemokines during Acute Viral Encephalomyelitis. *PLoS Pathog* **5**:1000648.
341. **Omalu BI, Shakir AA, Wang G, Lipkin WI, Wiley CA.** 2003. Fatal fulminant pan-meningo-polioencephalitis due to West Nile virus. *Brain Pathol* **13**:465-472.
342. **Kumar M, Verma S, Nerurkar VR.** 2010. Pro-inflammatory cytokines derived from West Nile virus (WNV)-infected SK-N-SH cells mediate neuroinflammatory markers and neuronal death. *Journal of Neuroinflammation* **7**:73.
343. **Halevy M, Akov Y, Ben-Nathan D, Kobiler D, Lachmi B, Lustig S.** 1994. Loss of active neuroinvasiveness in attenuated strains of West Nile virus: pathogenicity in immunocompetent and SCID mice. *Arch Virol* **137**:355-370.
344. **Samuel MA, Diamond MS.** 2005. Alpha/Beta Interferon Protects against Lethal West Nile Virus Infection by Restricting Cellular Tropism and Enhancing Neuronal Survival. *Journal of Virology* **79**:13350-13361.
345. **Pierson TC, Diamond MS, Ahmed AA, Valentine LE, Davis CW, Samuel MA, Hanna SL, Puffer BA, Doms RW.** 2005. An infectious West Nile virus that expresses a GFP reporter gene. *Virology* **334**:28-40.
346. **Ben-Nathan D, Huitinga I, Lustig S, Van Rooijen N, Kobiler D.** 1996. West Nile virus neuroinvasion and encephalitis induced by macrophage depletion in mice. *Arch Virol* **141**:459-469.
347. **Shrestha B, Wang T, Samuel MA, Whitby K, Craft J, Fikrig E, Diamond MS.** 2006. Gamma Interferon Plays a Crucial Early Antiviral Role in Protection against West Nile Virus Infection. *Journal of Virology* **80**:5338-5348.
348. **Shrestha B, Samuel MA, Diamond MS.** 2005. CD8+ T cells require perforin to clear West Nile virus from infected neurons. *Journal of Virology* **80**:119-129.
349. **Wang T, Scully E, Yin Z, Kim JH, Wang S, Yan J, Mamula M, Anderson JF, Craft J, Fikrig E.** 2003. IFN-gamma-producing gamma delta T cells help control murine West Nile virus infection. *J. Immunol.* **171**:2524-2531.
350. **Bai F, Kong KF, Dai J, Qian F, Zhang L, Brown CR, Fikrig E, Montgomery RR.** 2010. A paradoxical role for neutrophils in the pathogenesis of West Nile virus. *Journal of Infectious Diseases* **202**:1804-1812.
351. **Diamond MS, Shrestha B, Marri A, Mahan D, Engle M.** 2003. B cells and antibody play critical roles in the immediate defense of disseminated infection by West Nile encephalitis virus. *Journal of Virology* **77**:2578-2586.
352. **Diamond MS, Sitati EM, Friend LD, Higgs S, Shrestha B, Engle M.** 2003. A critical role for induced IgM in the protection against West Nile virus infection. *J. Exp. Med.* **198**:1853-1862.
353. **Wang Y, Lobigs M, Lee E, Müllbacher A.** 2003. CD8+ T cells mediate recovery and immunopathology in West Nile virus encephalitis. *Journal of Virology* **77**:13323-13334.
354. **Lanteri MC, O'Brien KM, Purtha WE, Cameron MJ, Lund JM, Owen RE, Heitman JW, Custer B, Hirschkorn DF, Tobler LH, Kiely N, Prince HE, Ndhlovu LC, Nixon DF, Kamel HT, Kelvin DJ, Busch MP, Rudensky AY, Diamond MS, Norris PJ.** 2009. Tregs control the development of

- symptomatic West Nile virus infection in humans and mice. *J. Clin. Invest.* **119**:3266-3277.
355. **Kelley TW, Prayson RA, Ruiz AI, Isada CM, Gordon SM.** 2003. The neuropathology of West Nile virus meningoencephalitis. A report of two cases and review of the literature. *Am J Clin Pathol* **119**:749-753.
356. **Hosking MP, Lane TE.** 2010. The role of chemokines during viral infection of the CNS. *PLoS Pathog* **6**:1-6.
357. **Prehaud C, Megret F, Lafage M, Lafon M.** 2005. Virus infection switches TLR-3-positive human neurons to become strong producers of beta interferon. *Journal of Virology* **79**:12893-12904.
358. **Shirato K, Kimura T, Mizutani T, Kariwa H, Takashima I.** 2004. Different chemokine expression in lethal and non-lethal murine west nile virus infection. *J. Med. Virol.* **74**:507-513.
359. **Tobler LH, Cameron MJ, Lanteri MC, Prince HE, Danesh A, Persad D, Lanciotti RS, Norris PJ, Kelvin DJ, Busch MP.** 2008. Interferon and interferon-induced chemokine expression is associated with control of acute viremia in West Nile virus-infected blood donors. *Journal of Infectious Diseases* **198**:979-983.
360. **Cheeran MC-J, Hu S, Sheng WS, Rashid A, Peterson PK, Lokensgard JR.** 2005. Differential responses of human brain cells to West Nile virus infection. *J. of Neurovirology* **11**:512-524.
361. **Lim JK, McDermott DH, Lisco A, Foster GA, Krysztof D, Follmann D, Stramer SL, Murphy PM.** 2010. CCR5 deficiency is a risk factor for early clinical manifestations of West Nile virus infection but not for viral transmission. *Journal of Infectious Diseases* **201**:178-185.
362. **Lim JK, Glass WG, McDermott DH, Murphy PM.** 2006. CCR5: no longer a "good for nothing" gene--chemokine control of West Nile virus infection. *Trends in Immunology* **27**:308-312.
363. **Bigham AW, Buckingham KJ, Husain S, Emond MJ, Bofferding KM, Gildersleeve H, Rutherford A, Astakhova NM, Perelygin AA, Busch MP, Murray KO, Sejvar JJ, Green S, Kriesel J, Brinton MA, Bamshad M.** 2011. Host genetic risk factors for West Nile virus infection and disease progression. *PLoS ONE* **6**:e24745.
364. **Loeb M, Eskandarian S, Rupp M, Fishman N, Gasink L, Patterson J, Bramson J, Hudson TJ, Lemire M.** 2011. Genetic variants and susceptibility to neurological complications following West Nile virus infection. *Journal of Infectious Diseases* **204**:1031-1037.
365. **Tachibana K, Hirota S, Iizasa H, Yoshida H, Kawabata K, Kataoka Y, Kitamura Y, Matsushima K, Yoshida N, Nishikawa S, Kishimoto T, Nagasawa T.** 1998. The chemokine receptor CXCR4 is essential for vascularization of the gastrointestinal tract. *Nature* **393**:591-594.
366. **McCandless EE, Zhang B, Diamond MS, Klein RS.** 2008. CXCR4 antagonism increases T cell trafficking in the central nervous system and improves survival from West Nile virus encephalitis. *Proc. Natl. Acad. Sci. U.S.A.* **105**:11270.
367. **Ceredig R, Allan JE, Tabi Z, Lynch F, Doherty PC.** 1987. Phenotypic analysis of the inflammatory exudate in murine lymphocytic choriomeningitis. *J. Exp. Med.* **165**:1539-1551.
368. **Christensen JP, Andersson EC, Scheynius A, Marker O, Thomsen AR.** 1995. Alpha 4 integrin directs virus-activated CD8+ T cells to sites of infection. *J. Immunol.* **154**:5293-5301.
369. **Christoffersen PJ, Volkert M, Rygaard J.** 1976. Immunological unresponsiveness of nude mice to LCM virus infection. *Acta Pathol*

- Microbiol Scand C **84C**:520-523.
370. **Leist TP, Cobbold SP, Waldmann H, Aguet M, Zinkernagel RM.** 1987. Functional analysis of T lymphocyte subsets in antiviral host defense. *J. Immunol.* **138**:2278-2281.
371. **Buchmeier MJ, Welsh RM, Dutko FJ, Oldstone MB.** 1980. The virology and immunobiology of lymphocytic choriomeningitis virus infection. *Adv Immunol* **30**:275-331.
372. **Jacobson S, Friedman RM, Pfau CJ.** 1981. Interferon induction by lymphocytic choriomeningitis viruses correlates with maximum virulence. *J. Gen. Virol.* **57**:275-283.
373. **Sandberg K, Eloranta ML, Campbell IL.** 1994. Expression of alpha/beta interferons (IFN-alpha/beta) and their relationship to IFN-alpha/beta-induced genes in lymphocytic choriomeningitis. *Journal of Virology* **68**:7358-7366.
374. **Madsen AN, Nansen A, Christensen JP, Thomsen AR.** 2003. Role of macrophage inflammatory protein-1alpha in T-cell-mediated immunity to viral infection. *Journal of Virology* **77**:12378-12384.
375. **Zhang B, Chan YK, Lu B, Diamond MS, Klein RS.** 2008. CXCR3 mediates region-specific antiviral T cell trafficking within the central nervous system during West Nile virus encephalitis. *J. Immunol.* **180**:2641-2649.
376. **Lane TE, Buchmeier MJ.** 1997. Murine coronavirus infection: a paradigm for virus-induced demyelinating disease. *Trends Microbiol* **5**:9-14.
377. **Lin MT, Stohlman SA, Hinton DR.** 1997. Mouse hepatitis virus is cleared from the central nervous systems of mice lacking perforin-mediated cytotoxicity. *Journal of Virology* **71**:383-391.
378. **Fazakerley J.** 2002. Pathogenesis of Semliki Forest Virus Encephalitis. *J. of Neurovirology* **8**:66-74.
379. **Trifilo MJ, Montalto-Morrison C, Stiles LN, Hurst KR, Hardison JL, Manning JE, Masters PS, Lane TE.** 2003. CXC Chemokine Ligand 10 Controls Viral Infection in the Central Nervous System: Evidence for a Role in Innate Immune Response through Recruitment and Activation of Natural Killer Cells. *Journal of Virology* **78**:585-594.
380. **Dufour JH, Dziejman M, Liu MT, Leung JH, Lane TE, Luster AD.** 2002. IFN-gamma-inducible protein 10 (IP-10; CXCL10)-deficient mice reveal a role for IP-10 in effector T cell generation and trafficking. *J. Immunol.* **168**:3195-3204.
381. **Stiles LN, Hosking MP, Edwards RA, Strieter RM, Lane TE.** 2006. Differential roles for CXCR3 in CD4+ and CD8+ T cell trafficking following viral infection of the CNS. *Eur. J. Immunol.* **36**:613-622.
382. **Glass WG, Liu MT, Kuziel WA, Lane TE.** 2001. Reduced Macrophage Infiltration and Demyelination in Mice Lacking the Chemokine Receptor CCR5 Following Infection with a Neurotropic Coronavirus. *Virology* **288**:8-17.
383. **Boehm T.** 2011. Design principles of adaptive immune systems. *Nat Rev Immunol* **11**:307-317.
384. **Streit WJ.** 2002. Microglia as neuroprotective, immunocompetent cells of the CNS. *Glia* **40**:133-139.
385. **McKimmie CS, Graham GJ.** 2010. Astrocytes modulate the chemokine network in a pathogen-specific manner. *Biochemical and Biophysical Research Communications* **394**:1006-1011.
386. **McKimmie CS, Roy D, Forster T, Fazakerley JK.** 2006. Innate immune response gene expression profiles of N9 microglia are pathogen-type specific. *Journal of Neuroimmunology* **175**:128-141.

387. **Gates MC, Sheahan BJ, O'Sullivan MA, Atkins GJ.** 1985. The pathogenicity of the A7, M9 and L10 strains of Semliki Forest virus for weanling mice and primary mouse brain cell cultures. *J. Gen. Virol.* **66** (Pt 11):2365-2373.
388. **Goazigo AR-L, Van Steenwinckel J, Rostène W, Parsadaniantz SM.** 2013. Current status of chemokines in the adult CNS. *Progress in Neurobiology* **104**:67-92.
389. **McCandless EE, Piccio L, Woerner BM, Schmidt RE, Rubin JB, Cross AH, Klein RS.** 2008. Pathological expression of CXCL12 at the blood-brain barrier correlates with severity of multiple sclerosis. *Am J Pathol* **172**:799-808.
390. **Forster R, Mattis AE, Kremmer E, Wolf E, Brem G, Lipp M.** 1996. A putative chemokine receptor, BLR1, directs B cell migration to defined lymphoid organs and specific anatomic compartments of the spleen. *Cell* **87**:1037-1047.
391. **Diamond MS, Farzan M.** 2012. The broad-spectrum antiviral functions of IFIT and IFITM proteins. *Nat Rev Immunol* **13**:46-57.
392. **Takeuchi O, Akira S.** 2009. Innate immunity to virus infection. *Immunol Rev* **227**:75-86.
393. **Akira S, Uematsu S, Takeuchi O.** 2006. Pathogen Recognition and Innate Immunity. *Cell* **124**:783-801.
394. **Sen GC.** 2001. Viruses and interferons. *Annu. Rev. Microbiol.* **55**:255-281.
395. **Liang TJ, Ghany MG.** 2013. Current and Future Therapies for Hepatitis C Virus Infection. *N. Engl. J. Med.* **368**:1907-1917.
396. **Perkins DJ, Polumuri SK, Pennini ME, Lai W, Xie P, Vogel SN.** 2013. Reprogramming of Murine Macrophages through TLR2 Confers Viral Resistance via TRAF3-Mediated, Enhanced Interferon Production. *PLoS Pathog* **9**:e1003479.
397. **Reiner SL, Locksley RM.** 1995. The Regulation of Immunity to *Leishmania* Major. *Annu. Rev. Immunol.* **13**:151-177.
398. **Liu T, Matsuguchi T, Tsuboi N, Yajima T, Yoshikai Y.** 2002. Differences in expression of toll-like receptors and their reactivities in dendritic cells in BALB/c and C57BL/6 mice. *Infect Immun* **70**:6638-6645.
399. **Parsons LM, Webb HE.** 1982. Virus titres and persistently raised white cell counts in cerebrospinal fluid in mice after peripheral infection with demyelinating Semliki Forest virus. *Neuropathology and Applied Neurobiology* **8**:395-401.
400. **Carter SL, Müller M, Manders PM, Campbell IL.** 2007. Induction of the genes for Cxcl9 and Cxcl10 is dependent on IFN- γ but shows differential cellular expression in experimental autoimmune encephalomyelitis and by astrocytes and microglia in vitro. *Glia* **55**:1728-1739.
401. **Savarin C, Stohlman SA, Atkinson R, Ransohoff RM, Bergmann CC.** 2010. Monocytes Regulate T Cell Migration through the Glia Limitans during Acute Viral Encephalitis. *Journal of Virology* **84**:4878-4888.
402. **Crawford A, Angelosanto JM, Nadwodny KL, Blackburn SD, Wherry EJ.** 2011. A Role for the Chemokine RANTES in Regulating CD8 T Cell Responses during Chronic Viral Infection. *PLoS Pathog* **7**:e1002098.
403. **Bajetto A, Bonavia R, Barbero S, Schettini G.** 2002. Characterization of chemokines and their receptors in the central nervous system: physiopathological implications. *J. Neurochem.* **82**:1311-1329.
404. **Mizuno T, Kawanokuchi J, Numata K, Suzumura A.** 2003. Production and neuroprotective functions of fractalkine in the central nervous system. *Brain Res.* **979**:65-70.

405. Akira S, Takeda K. 2004. Toll-like receptor signalling. *Nat Rev Immunol* 4:499-511.
406. McKimmie CS, Johnson N, Fooks AR, Fazakerley JK. 2005. Viruses selectively upregulate Toll-like receptors in the central nervous system. *Biochemical and Biophysical Research Communications* 336:925-933.
407. Sedgwick JD, Schwender S, Imrich H, Dörries R, Butcher GW, Meulenter V. 1991. Isolation and direct characterization of resident microglial cells from the normal and inflamed central nervous system. *Proc. Natl. Acad. Sci. U.S.A.* 88:7438-7442.
408. Cardona AE, Huang D, Sasse ME, Ransohoff RM. 2006. Isolation of murine microglial cells for RNA analysis or flow cytometry. *Nat Protoc* 1:1947-1951.
409. Waggoner SN, Cornberg M, Selin LK, Welsh RM. 2011. Natural killer cells act as rheostats modulating antiviral T cells. *Nature* 1:1-6.
410. Zhang G-X, Li J, Ventura E, Rostami A. 2002. Parenchymal microglia of naive adult C57BL/6J Mice express high levels of B7.1, B7.2, and MHC Class II. *Experimental and Molecular Pathology* 73:35-45.
411. Auffray C, Sieweke MH, Geissmann F. 2009. Blood Monocytes: Development, Heterogeneity, and Relationship with Dendritic Cells. *Annu. Rev. Immunol.* 27:669-692.
412. Naik SH, Corcoran LM, Wu L. 2005. Development of murine plasmacytoid dendritic cell subsets. *Immunol. Cell Biol.* 83:563-570.
413. Longhini ALF, Glehn von F, Brandão CO, de Paula RFO, Pradella F, Moraes AS, Farias AS, Oliveira EC, Quispe-Cabanillas JG, Abreu CH, Damasceno A, Damasceno BP, Balashov KE, Santos LMB. 2011. Plasmacytoid dendritic cells are increased in cerebrospinal fluid of untreated patients during multiple sclerosis relapse. *Journal of Neuroinflammation* 8:2-4.
414. Wang X-J, Ye M, Zhang Y-H, Chen S-D. 2007. CD200-CD200R Regulation of Microglia Activation in the Pathogenesis of Parkinson's Disease. *J Neuroimmune Pharmacol* 2:259-264.
415. Perry VH, Andersson PB. 1992. The inflammatory response in the CNS. *Neuropathology and Applied Neurobiology* 18:454-459.
416. Taylor K, Kolokoltsova O, Patterson M, Poussard A, Smith J, Estes DM, Paessler S. 2012. Natural killer cell mediated pathogenesis determines outcome of central nervous system infection with Venezuelan equine encephalitis virus in C3H/HeN mice. *Vaccine* 30:4095-4105.
417. Alsharifi M, Lobigs M, Simon MM, Kersten A, Müller K, Koskinen A, Lee E, Müllbacher A. 2006. NK cell-mediated immunopathology during an acute viral infection of the CNS. *Eur. J. Immunol.* 36:887-896.
418. McGavern DB, Homann D, Oldstone MBA. 2002. T cells in the central nervous system: the delicate balance between viral clearance and disease. *J Infect Dis* 182:145-151.
419. Glass WG, Chen BPB, Liu MTM, Lane TET. 2002. Mouse hepatitis virus infection of the central nervous system: chemokine-mediated regulation of host defense and disease. *Viral Immunol* 15:261-272.
420. Engelhardt B. 2010. T cell migration into the central nervous system during health and disease: Different molecular keys allow access to different central nervous system compartments. *Clin. Exp. Immunol.* 1:79-93.
421. Bailey-Bucktrout SL, Caulkins SC, Goings G, Fischer JA, Dzionek A, Miller SD. 2008. Cutting edge: central nervous system plasmacytoid dendritic cells regulate the severity of relapsing experimental

- autoimmune encephalomyelitis. *J. Immunol.* **180**:6457-6461.
422. **Carson MJ, Reilly CR, Sutcliffe JG, Lo D.** 1998. Mature microglia resemble immature antigen-presenting cells. *Glia* **22**:72-85.
423. **Lim JK, Murphy PM.** 2011. Chemokine control of West Nile virus infection. *Experimental Cell Research* **317**:569-574.
424. **Bardina SV, Lim JK.** 2012. The role of chemokines in the pathogenesis of neurotropic flaviviruses. *Immunol Res* **54**:121-132.
425. **Ramos HJ, Lanteri MC, Blahnik G, Negash A, Suthar MS, Brassil MM, Sodhi K, Treuting PM, Busch MP, Norris PJ, Gale M.** 2012. IL-1 β Signaling Promotes CNS-Intrinsic Immune Control of West Nile Virus Infection. *PLoS Pathog* **8**:e1003039.
426. **Mansfield KL, Johnson N, Cosby SL, Solomon T, Fooks AR.** 2010. Transcriptional upregulation of SOCS 1 and suppressors of cytokine signaling 3 mRNA in the absence of suppressors of cytokine signaling 2 mRNA after infection with West Nile virus or tick-borne encephalitis virus. *Vector Borne Zoonotic Dis.* **10**:649-653.
427. **Tsunoda I, Lane TE, Blackett J, Fujinami RS.** 2004. Distinct roles for IP-10/CXCL10 in three animal models, Theiler's virus infection, EAE, and MHV infection, for multiple sclerosis: implication of differing roles for IP-10. *Multiple Sclerosis* **10**:26-34.
428. **Ghera P, Gelati M, Colinge J, Feger G, Power C, Ghera P, Gelati M, Colinge J, Feger G, Power C, Papoian R, Salmaggi A.** 2002. MIG-- differential gene expression in mouse brain endothelial cells. *Neuroreport* **13**:9-14.
429. **Glass WG, Lane TE.** 2003. Functional Expression of Chemokine Receptor CCR5 on CD4+ T Cells during Virus-Induced Central Nervous System Disease. *Journal of Virology* **77**:191-198.
430. **Doherty PC, Allan JE, Lynch F, Ceredig R.** 1990. Dissection of an inflammatory process induced by CD8+ T cells. *Immunology Today* **11**:55-59.
431. **Hofer MJ, Carter SL, Müller M, Campbell IL.** 2008. Unaltered Neurological Disease and Mortality in CXCR3-Deficient Mice Infected Intracranially with Lymphocytic Choriomeningitis Virus-Armstrong. *Viral Immunol* **21**:425-433.
432. **Yang D, Tong L, Wang D, Wang Y, Wang X, Bai C.** 2010. Roles of CC chemokine receptors (CCRs) on lipopolysaccharide-induced acute lung injury. *Respiratory Physiology & Neurobiology* **170**:253-259.
433. **Velasco-Velazquez M, Jiao X, La Fuente De M, Pestell TG, Ertel A, Lisanti MP, Pestell RG.** 2012. CCR5 Antagonist Blocks Metastasis of Basal Breast Cancer Cells. *Cancer Res* **72**:3839-3850.
434. **Rabin RL, Park MK, Liao F, Swofford R, Stephany D, Farber JM.** 1999. Chemokine receptor responses on T cells are achieved through regulation of both receptor expression and signaling. *J. Immunol.* **162**:3840-3850.
435. **Polentarutti N, Allavena P, Bianchi G, Giardino G, Basile A, Sozzani S, Mantovani A, Introna M.** 1997. IL-2-regulated expression of the monocyte chemotactic protein-1 receptor (CCR2) in human NK cells: characterization of a predominant 3.4-kilobase transcript containing CCR2B and CCR2A sequences. *J. Immunol.* **158**:2689-2694.
436. **Yamasaki R, Liu L, Lin J, Ransohoff RM.** 2012. Role of CCR2 in immunobiology and neurobiology. *Clinical and Experimental Neuroimmunology* **3**:16-29.
437. **Atchison RE, Gosling J, Monteclaro FS, Franci C, Digilio L, Charo IF, Goldsmith MA.** 1996. Multiple extracellular elements of CCR5 and HIV-1

- entry: dissociation from response to chemokines. *Science* **274**:1924-1926.
438. **Neff CP, Ndolo T, Tandon A, Habu Y, Akkina R.** 2010. Oral Pre-Exposure Prophylaxis by Anti-Retrovirals Raltegravir and Maraviroc Protects against HIV-1 Vaginal Transmission in a Humanized Mouse Model. *PLoS ONE* **5**:e15257 1-6.
439. **Wilson EH, Weninger W, Hunter CA.** 2010. Trafficking of immune cells in the central nervous system. *J. Clin. Invest.* **120**:1368-1379.
440. **McGavern DB, Kang SS.** 2011. Illuminating viral infections in the nervous system. *Nat Rev Immunol* **11**:318-329.
441. **Metcalfe TU, Baxter VK, Nilaratanakul V, Griffin DE.** 2013. Recruitment and Retention of B Cells in the Central Nervous System in Response to Alphavirus Encephalomyelitis. *Journal of Virology* **87**:2420-2429.
442. **Samuel MA, Diamond MS.** 2006. Pathogenesis of West Nile Virus Infection: a Balance between Virulence, Innate and Adaptive Immunity, and Viral Evasion. *Journal of Virology* **80**:9349-9360.
443. **Boere WA, Benaissa-Trouw BJ, Harmsen M, Kraaijeveld CA, Snippe H.** 1983. Neutralizing and non-neutralizing monoclonal antibodies to the E2 glycoprotein of Semliki Forest virus can protect mice from lethal encephalitis. *J. Gen. Virol.* **64**:1405-1408.
444. **Liu MTM, Armstrong DD, Hamilton TAT, Lane TET.** 2001. Expression of Mig (monokine induced by interferon-gamma) is important in T lymphocyte recruitment and host defense following viral infection of the central nervous system. *J. Immunol.* **166**:1790-1795.
445. **Bergmann CC, Lane TE, Stohlman SA.** 2006. Coronavirus infection of the central nervous system: host-virus stand-off. *Nat Rev Micro* **4**:121-132.
446. **Getts DR, Terry RL, Getts MT, Müller M, Rana S, Deffrasnes C, Ashhurst TM, Radford J, Hofer M, Thomas S, Campbell IL, King NJC.** 2012. Targeted blockade in lethal West Nile virus encephalitis indicates a crucial role for very late antigen (VLA)-4-dependent recruitment of nitric oxide-producing macrophages. *Journal of Neuroinflammation* **9**:246.
447. **Swiecki M, Wang Y, Vermi W, Gilfillan S, Schreiber RD, Colonna M.** 2011. Type I interferon negatively controls plasmacytoid dendritic cell numbers in vivo. *J. Exp. Med.* **208**:2367-2374.
448. **Wang T, Town T, Alexopoulou L, Anderson JF, Fikrig E, Flavell RA.** 2004. Toll-like receptor 3 mediates West Nile virus entry into the brain causing lethal encephalitis. *Nat Med* **10**:1366-1373.
449. **Burdeinick-Kerr R, Govindarajan D, Griffin DE.** 2009. Noncytolytic Clearance of Sindbis Virus Infection from Neurons by Gamma Interferon Is Dependent on Jak/Stat Signaling. *Journal of Virology* **83**:3429-3435.
450. **Cho H, Proll SC, Szretter KJ, Katze MG, Gale M, Diamond MS.** 2013. Differential innate immune response programs in neuronal subtypes determine susceptibility to infection in the brain by positive-stranded RNA viruses. *Nat Med* **19**:458-464.
451. **Griffin DE, Metcalfe T.** 2011. Clearance of virus infection from the CNS. *Current Opinion in Virology* **1**:216-221.
452. **Horuk R.** 2009. Chemokine receptor antagonists: overcoming developmental hurdles. *Nat Rev Drug Discov* **8**:23-33.
453. **Dairaghi DJ, Oyajobi BO, Gupta A, McCluskey B, Miao S, Powers JP, Seitz LC, Wang Y, Zeng Y, Zhang P, Schall TJ, Jaen JC.** 2012. CCR1 blockade reduces tumor burden and osteolysis in vivo in a mouse model of myeloma bone disease. *Blood* **120**:1449-1457.